2023-08-01

Advances In One-Electron Self-Interaction-Correction Methods For Accurate And Efficient Self-Interaction-Free Density Functional Calculations

Selim Romero
University of Texas at El Paso

ADVANCES IN ONE-ELECTRON SELF-INTERACTION-CORRECTION METHODS FOR ACCURATE AND EFFICIENT SELF-INTERACTION-FREE DENSITY FUNCTIONAL CALCULATIONS

SELIM SABAG ROMERO GONZALEZ

Doctoral Program in Computational Science

APPROVED:

Rajendra R. Zope, Ph.D., Chair

Tunna Baruah, Ph.D., Co-Chair

Mark Pederson, Ph.D.

Ming Ying Leung, Ph.D.

Lela Vukovic, Ph.D.

Stephen L. Crites, Jr., Ph.D.
Dean of the Graduate School

DEDICATION

I dedicate this writing to my family, and wife. They helped me along my Ph.D. journey with love and support.

EFFICIENT AND ACCURATE SELF-INTERACTION CORRECTION IMPLEMENTATIONS TOWARD REALISTIC APPLICATIONS

by

SELIM SABAG ROMERO GONZALEZ

DISSERTATION

Presented to the Faculty of the Graduate School of

The University of Texas at El Paso

in Partial Fulfillment

of the Requirements

for the Degree of

DOCTOR OF PHILOSOPHY

Department of Computational Science

THE UNIVERSITY OF TEXAS AT EL PASO

December 2023

ACKNOWLEDGEMENTS

I am pleased to acknowledge my advisor, Dr. Rajendra Zope, for encouraging and guiding me through my academic journey. I would like to express my gratitude to my co-advisor Dr. Tunna Baruah, for sharing her expertise and providing valuable suggestions for the development of my science career.

I am immensely grateful to Drs. Yoh Yamamoto and Po-Hao Chang for their friendship and invaluable life advice. Much of my knowledge and skills acquired during my Ph.D. were imparted by both. I would also like to thank Dr. Luis Basurto for introducing me into the electronic structure lab and helping me in learning good coding practices. I extend my appreciation to Dr. Carlos Diaz for his assistance in developing new subroutines and his support.

This work was partially supported by the US Department of Energy, Office of Science, Office of Basic Energy Sciences, as part of the Computational Chemical Sciences Program under Award No. DE-SC0018331. Support for computational time at the Texas Advanced Computing Center through NSF Grant No. TG-DMR090071 and at NERSC are gratefully acknowledged. Also, my deepest gratitude to Gobierno de Mexico, CONACyT.

ABSTRACT

Density functional theory (DFT) is a widely used computational method for studying electronic structures of atoms, molecules, and solids. It provides an exact theory for obtaining ground state energy from the ground state density. However, since the exact exchange-correlation functional remains unknown, approximate exchange-correlation functionals called approximate density approximations (DFAs) are used.

The foundation of many DFAs is the local spin density approximation (LSDA). It serves as the starting point for constructing various DFAs. However, DFAs are prone to self-interaction errors (SIE) due to the improper cancellation of the approximate exchange energy and the Coulomb energy. This issue impacts the accuracy of the results obtained with DFAs. One way to address this issue is using one-electron self-interaction correction (SIC) methods. A well-known example of the one-electron SIC methods is the Perdew and Zunger SIC (PZSIC). The one-electron SIC schemes require localized orbitals to avoid the size-extensivity problem, and one choice of such orbitals is the Fermi Löwdin orbitals (FLOs). The Fermi Löwdin orbital SIC (FLOSIC) code is an implementation of various SIC schemes using FLOs, allowing researchers to utilize SIC methods. This dissertation provides an overview of DFT and SIC methods, development of new SIC schemes, and evaluates the performance of these methods using standard benchmarks datasets and different applications. This thesis introduces simplification of FLOSIC scheme to expedite SIC calculations by performing SIC calculations on a select set of orbitals. This approach, which we called vSOSIC, provides comparable performance to PZSIC that applies SIC to all orbitals for a wide range of properties. We conducted a study on the effect of SIE in the spin-state gaps of four octahedral Fe(II) complexes. The removal of self-interaction was found to be crucial for obtaining accurate spin-state gaps as regular DFA calculations perform poorly in this context. The locally scaled SIC method (LSIC) demonstrated good performance, exhibiting a mean absolute error comparable to CCSD(T) when compared to diffusion Monte-Carlo (DMC) data. Accurately describing spin-state gaps through efficient computations is valuable for modelling novel devices in technology, such as molecular switches.

Furthermore, the initial LSIC calculations were perturbatively on top of optimal PZSIC calculations. Subsequently, the full self-consistency of the LSIC method was developed, and it was demonstrated that LSIC's good performance is maintained in the full self-consistency method.

This confirms that the LSIC method exhibits comparable accuracy to higher-level density functionals.

TABLE OF CONTENTS

LIST OF TABLES

LIST OF FIGURES

CHAPTER 1: INTRODUCTION TO BACKGROUND THEORY

Chapter 1 mainly introduces Density Functional Theory (DFT), starting with the Schrödinger equation, which describes the single-electron behavior in quantum mechanics (QM). QM in real applications requires the many-body description of the electrons. This subchapter provides a brief introduction to two approaches that are used to study many-electron systems: the first theory is the Hartree-Fock (HF), and the second is Kohn-Sham (KS) DFT. KS-DFT reduces the cost of the N electron problem to $N * M^3$ grids. These theories provide a reasonable balance between accuracy and computational cost for atoms, molecules, and solids.

1.1 SCHRÖDINGER EQUATION

The Schrödinger equation holds fundamental importance in describing the quantum mechanical behavior of particles in analogous to how Newton's equations of motion describe the behavior of particles in classical mechanics. Measurable properties in classical mechanics include position, velocity, momentum, kinetic energy, potential energy, total energy, and force. To determine these properties, one must solve the differential equations derived from Newton's laws. In the case of quantum mechanics, the Schrödinger equation must be solved, yielding the system's wave function (WF). The WF provides information on properties such as total energy, kinetic energy and some others [1]. The one-particle time-independent Schrödinger equation is expressed as follows,

$$-\frac{\hbar^2}{2m}\nabla^2\phi(\vec{r}) + V(\vec{r})\phi(\vec{r}) = E\phi(\vec{r}), \tag{1.1.1}$$

$\hbar$ is Planck's constant, m is the particle mass, $V(\vec{r})$ is the potential, and $\phi(\vec{r})$ is the WF of a particular system (e.g., electron). Eq. (1.1.1) is an eigenvalue problem with a constant energy E, which is composed of eigenenergies that correspond to electronic structure of the system at a given

energy state. Eq. (1.1.1) represents the time-independent Schrödinger equation whose Hamiltonian operator is constructed as follows,

$$\widehat{H} = -\frac{\hbar^2}{2m}\nabla^2 + V(\vec{r}), \tag{1.1.2}$$

Eq (1.1.4) involves the components such as the kinetic energy (KE) operator ($\widehat{T}$) and potential operator (V). $\widehat{H}$ operator provides the total energy of the system based on its WF. According to the uniqueness theorem, a given differential equation will have a unique solution. Therefore, each atom, molecule or solid will have a unique electronic configuration that corresponds to a specific WF. Observables can be obtained by the expectation value as $\langle\phi|\,\widehat{H}\,|\phi\rangle = E$ in bra-ket notation.

1.1.1 MANY-BODY SCHRÖDINGER EQUATION

A quantum system description depends on the number of nuclei and electrons [2]. The simplest example is the hydrogen atom which has one electron and one proton. Using Eq. (1.1.2) for hydrogen provides,

$$\widehat{H} = -\frac{\hbar^2}{2m_n}\nabla_n^{\,2} - \frac{\hbar^2}{2m_e}\nabla_e^{\,2} - \frac{e^2}{4\pi\epsilon_0}\frac{1}{|\vec{r}_n-\vec{r}_e|}, \tag{1.1.1.1}$$

the last term of Eq. (1.1.1.1) is an attractive potential between proton-electron ($V_{en}(\vec{r}) = -\frac{e^2}{4\pi\epsilon_0}\frac{1}{|\vec{r}_n-\vec{r}_e|}$). Generally, a system contains M nuclei with mass M_I at position $\vec{R}_I$, and N electrons with mass m_e at position $\vec{r}_i$. The Hamiltonian for a collection of non-interacting electrons and protons is,

$$\widehat{T} = -\sum_I^N \frac{\hbar^2}{2M_I}\nabla_I^{\,2} - \sum_i^N \frac{\hbar^2}{2m_e}\nabla_i^{\,2}, \tag{1.1.1.2}$$

$$V(\vec{r}) = V_{ee} + V_{nn} + V_{en}\,, \tag{1.1.1.3}$$

V_{ee} represents the Coulomb interaction among electrons, V_{en} denotes the Coulomb interaction between electrons and nuclei, and V_{nn} corresponds to the nuclei-nuclei Coulomb interaction. These are defined as follows,

$$V_{ee} = \frac{1}{2}\sum_{i \neq j}^{N} \frac{e^2}{4\pi\epsilon_0}\frac{1}{|\vec{r}_i - \vec{r}_j|}, \tag{1.1.1.4}$$

$$V_{nn} = \frac{1}{2}\sum_{I \neq J}^{M} \frac{e^2}{4\pi\epsilon_0}\frac{Z_I Z_J}{|\vec{R}_I - \vec{R}_J|}, \tag{1.1.1.5}$$

$$V_{en} = -\sum_{i,I}^{N,M} \frac{e^2}{4\pi\epsilon_0}\frac{Z_I}{|\vec{r}_i - \vec{R}_I|}, \tag{1.1.1.6}$$

V_{ee} and V_{nn} are repulsive potentials, and V_{en} is an attractive potential. By utilizing Eqs. (1.1.1.4), (1.1.1.5), (1.1.1.6), (1.1.1.3) and (1.1.1.2) in Eq. (1.1.4), we obtain,

$$\left[-\sum_{I}^{M}\frac{\hbar^2}{2M_I}\nabla_I^2 - \sum_{i}^{N}\frac{\hbar^2}{2m_e}\nabla_i^2 + \frac{1}{2}\sum_{i \neq j}^{N}\frac{e^2}{4\pi\epsilon_0}\frac{1}{|\vec{r}_i - \vec{r}_j|} + \frac{1}{2}\sum_{I \neq J}^{M}\frac{e^2}{4\pi\epsilon_0}\frac{Z_I Z_J}{|\vec{R}_I - \vec{R}_J|} + \sum_{i,I}^{N,M}\frac{e^2}{4\pi\epsilon_0}\frac{Z_I}{|\vec{r}_i - \vec{R}_I|}\right]\psi = E_{total}\,\psi, \tag{1.1.1.7}$$

Eq. (1.1.1.7) is the Schrödinger equation for the i-th electron and I-th nucleus, with Z_I protons, providing the total energy of the system. The WF depends on the positions of all electrons and nuclei:

$$\psi = \psi(\vec{r}_1, \ldots, \vec{r}_N, \vec{R}_1, \ldots, \vec{R}_M), \tag{1.1.1.8}$$

describing the probability of finding electron $\vec{r}_1$ in $\vec{r}$ is given by,

$$P(\vec{r}_1 = \vec{r}) = \int \psi^*(\vec{r}, \vec{r}_2 \ldots, \vec{r}_N, \vec{R}_1, \ldots, \vec{R}_M)\psi(\vec{r}, \vec{r}_2 \ldots, \vec{r}_N, \vec{R}_1, \ldots, \vec{R}_M)d\vec{r}, \tag{1.1.1.9}$$

since electrons are indistinguishable particles, Eq. (1.1.1.9) becomes N times the same probability distribution, represented as,

$$\rho(\vec{r}) = \sum_{i=1}^{N} P(\vec{r}_i = \vec{r}) = N\,P(\vec{r}), \tag{1.1.1.10}$$

$$\rho(\vec{r}) = N\int \psi^*\left(\vec{r}, \vec{r}_2 \dots, \vec{r}_N, \vec{R}_1, \dots, \vec{R}_M\right)\psi\left(\vec{r}, \vec{r}_2 \dots, \vec{r}_N, \vec{R}_1, \dots, \vec{R}_M\right) d\vec{r}_1 \dots d\vec{r}_N d\vec{R}_1 \dots d\vec{R}_M, \tag{1.1.1.11}$$

the integral of the electron density over all space yields the total number of electrons,

$$\int \rho(\vec{r}) d\vec{r} = N. \tag{1.1.1.12}$$

A common practice is to utilize atomic units [2] to simplify Eq. (1.1.1.7) by setting $a_0 = 1$, $m_e = 1$, $E_{Ha} = 1$ and $e = 1$ in Eq. (1.1.1.7), resulting in,

$$\left[-\sum_{I}^{M} \frac{1}{2M_I} \nabla_I^2 - \sum_{i}^{N} \frac{1}{2}\nabla_i^2 + \frac{1}{2}\sum_{i \neq j}^{N} \frac{1}{\left|\vec{\mathrm{r}}_i - \vec{\mathrm{r}}_j\right|} + \frac{1}{2}\sum_{I \neq J}^{M} \frac{Z_I Z_J}{\left|\vec{\mathrm{R}}_I - \vec{\mathrm{R}}_J\right|} + \sum_{i,I}^{N,M} \frac{Z_I}{\left|\vec{\mathrm{r}}_i - \vec{R}_I\right|}\right] \Psi = E_{total}\Psi, \tag{1.1.1.13}$$

E_{total} is expressed in Hartree energy units and M_I is expressed in atomic mass units.

1.1.2 BORN-OPPENHEIMER APPROXIMATION

The Hamiltonian presented in Eq. (1.1.1.13) provides a comprehensive description of electronic interactions; however, it is not computationally feasible for molecular applications. To address this challenge, the Bohr-Oppenheimer approximation was introduced. This approximation assumes that the nuclei can be treated as fixed entities due to their significantly larger mass

compared to electrons ($m_p \gg m_e$), implying that the electrons move at much higher speeds compared to nuclei. Therefore, in Born-Oppenheimer approximation, the nuclear coordinates are approximated as fixed, and we treat the nuclear WF and electron WF separately. This approximation allows for the separation of nuclear and electron coordinates. In the Born-Oppenheimer approximation, the nuclei-nuclei Coulomb interaction in Eq. (1.1.1.13) becomes a constant term. The Hamiltonian now consists solely of electron contributions and incorporates the nuclei as parametric dependent coordinates:

$$\widehat{H}_{elec} = -\sum_i^N \frac{1}{2}\nabla_i{}^2 + \frac{1}{2}\sum_{i\neq j}^N \frac{1}{|\vec{r}_i - \vec{r}_j|} - \sum_{i,I}^{N,M} \frac{Z_I}{|\vec{r}_i - \vec{R}_I|}, \tag{1.1.2.1}$$

N is the number of electrons in the system, and M is the number of protons in the nuclei. Eq. (1.1.2.1) reveals that the WF solely depends on the electron coordinates ($\Psi(\vec{r}_1, \dots, \vec{r}_N) \equiv \Psi_{elec}$), and the Hamiltonian becomes only electron-dependent. For a simplified version Eq. (1.1.2.1) in terms of only electron indices, we have,

$$\widehat{H}_{elec} = -\sum_i^N \frac{1}{2}\nabla_i{}^2 + \frac{1}{2}\sum_{i\neq j}^N \frac{1}{|\vec{r}_i - \vec{r}_j|} - \sum_i^N V_{en}(\vec{r}_i)\,, \tag{1.1.2.2}$$

the term $V_{en}(\vec{r}_i)$ incorporates the parametric equations associated with all the nuclei terms. Alternatively, Eq. (1.1.2.2) can be expressed in terms of the single-electron Hamiltonian $\widehat{H}_0(\vec{r}) = -\frac{1}{2}\nabla^2 + V_{en}(\vec{r})$, where the electron coordinates $\vec{r}$ are replaced with $\vec{r}_i$. By utilizing $\widehat{H}_0$ into Eq. (1.1.2.2), we obtain a simplified electronic Hamiltonian as follows,

$$\widehat{H}_{elec} = \sum_i^N \widehat{H}_0(\vec{r}_i) + \frac{1}{2}\sum_{i\neq j}^N \frac{1}{|\vec{r}_i - \vec{r}_j|}\,. \tag{1.1.2.3}$$

While the nuclei interaction remains stationary, the electrons continue to interact with the nuclei and their associated parametric coordinates.

1.1.3 INDEPENDENT ELECTRON APPROXIMATION

The quantum mechanics problem described in Eq. (1.1.2.3) remains complicated due to the electron-electron Coulomb interaction. However, ignoring the electron-electron Coulomb repulsion leads to a simplified equation where the electrons do not interact or electron-electron interaction is small and can be represented by an approximate effective potential, known as the independent electron approximation. In this approximation, the WF can be separated into independent electron probabilities ($\phi_i(\vec{r}_i)$) as follows,

$$\psi(\vec{r}_1, \vec{r}_2 \dots, \vec{r}_N) = \phi_1(\vec{r}_1)\phi_2(\vec{r}_2) \dots \phi_N(\vec{r}_N). \tag{1.1.3.1}$$

The single-electron Hamiltonian ($\widehat{H}_0$) operates on the separable WF (Eq. (1.1.3.1)) as follows,

$$\sum_i^N \widehat{H}_0(\vec{r}_i)\{\phi_1(\vec{r}_1)\phi_2(\vec{r}_2) \dots \phi_N(\vec{r}_N)\} = E\{\phi_1(\vec{r}_1)\phi_2(\vec{r}_2) \dots \phi_N(\vec{r}_N)\}, \tag{1.1.3.2}$$

Eq. (1.1.3.2) operates only on the corresponding *i*-th electron, leaving the other electrons unaffected. Thus, the electron coordinates $\vec{r}_{N-1}$ become unit integrals, and each independent electron problem is represented by,

$$\widehat{H}_0(\vec{r})\ \phi_i(\vec{r}) = \epsilon_i\phi_i(\vec{r}), \tag{1.1.3.3}$$

Eq. (1.1.3.3) represents the one-electron eigenvalue problem, and summing up all the eigenvalues provides the total energy within this approximation. However, this theory has two main flaws: it does not incorporate Pauli's exclusion principle in the WF, and ignoring the electron-electron interaction undermines the accuracy of the independent electron approximation.

1.1.4 ANTISYMMETRY PRINCIPLE

The independent electron approximation does not include Pauli's exclusion principle, which states that any electron (fermion) with an opposite spin must change of sign. Eq. (1.1.3.1) does not exhibit such behavior. However, the interchange of electrons in the same orbital follows the antisymmetry principle, which causes a change in the sign of the WF. An example of a WF that adheres to the exclusion principle is defined as,

$$\psi(\vec{r}_1,\vec{r}_2) = \frac{1}{\sqrt{2}}[\phi_1(\vec{r}_1)\phi_2(\vec{r}_2) - \phi_1(\vec{r}_2)\phi_2(\vec{r}_1)]. \tag{1.1.4.1}$$

Eq. (1.1.4.1) exemplifies the antisymmetry principle $\psi(\vec{r}_1,\vec{r}_2) = -\psi(\vec{r}_2,\vec{r}_1)$, and yields a total energy of $E = \epsilon_1 + \epsilon_2$ through the Hamiltonian operator. This WF is known as the Slater determinant for two electrons, and its determinant form is,

$$\psi(\vec{r}_1,\vec{r}_2) = \begin{vmatrix} \phi_1(\vec{r}_1) & \phi_1(\vec{r}_2) \\ \phi_2(\vec{r}_1) & \phi_2(\vec{r}_2) \end{vmatrix}. \tag{1.1.4.2}$$

In the determinant form, orbitals are represented along the rows, and electrons are represented along the columns. A more generalized Slater determinant is defined as follows,

$$\psi(\vec{r}_1,\dots,\vec{r}_N) = \frac{1}{\sqrt{N!}}\begin{bmatrix} \phi_1(\vec{r}_1) & \cdots & \phi_1(\vec{r}_N) \\ \vdots & \ddots & \vdots \\ \phi_N(\vec{r}_1) & \cdots & \phi_N(\vec{r}_N) \end{bmatrix}, \tag{1.1.4.3}$$

Eq. (1.1.4.3) involves N electrons and N occupied orbitals, and this WF provides a total energy of $E = \sum_i^{OCC} \epsilon_i$ and a total density of $\rho(\vec{r}) = \sum_{i=1}^{Nocc} |\phi_i(\vec{r})|^2$.

1.2 MEAN-FIELD APPROXIMATION

The independent electron approximation and the exclusion principle results in a separable WF, where the separated WF ($\phi_i(\vec{r}_i)$) represents an electron state. However, these theories neglect electron-electron interaction. To incorporate the classical electron-electron Coulomb interaction, we can use the mean-filed approximation [3]. This approach considers a Coulomb electrostatic potential that depends on the electron density and requires solving Poisson's equation:

$$\nabla^2\varphi(\vec{r}) = 4\pi\rho(\vec{r}). \tag{1.2.1}$$

Electrons subjected to the electrostatic potential $\varphi(\vec{r})$ experience a potential energy $V_H(\vec{r}) = -\varphi(\vec{r})$, known as the Hartree potential. The Hartree potential also satisfies $\nabla^2 V_H(\vec{r}) = -4\pi\rho(\vec{r})$, and its established solution is given by,

$$V_H(\vec{r}) = \frac{1}{2}\int \frac{\rho(\vec{r})d\vec{r}'}{|\vec{r}-\vec{r}\prime|}, \tag{1.2.2}$$

by substituting $\frac{1}{2}\sum_{i\neq j}^{N}\frac{1}{|\vec{r}_i-\vec{r}_j|}$ with Eq. (1.2.2) in Eq (1.1.2.2), the mean-field approximation approach is defined as,

$$\left[-\frac{1}{2}\nabla^2 + V_n(\vec{r}) + V_H(\vec{r})\right]\phi_i(\vec{r}) = \epsilon_i\phi_i(\vec{r}). \tag{1.2.3}$$

The mean-field approach considers an “average” potential field interaction among the electrons. However, Eq. (1.2.2) and Eq. (1.2.3) must be solved simultaneously, and the solution must be consistent with the electron density ($\rho(\vec{r}) = \sum_{i=1}^{Nocc}|\phi_i(\vec{r})|^2$). This iterative process is known as the self-consistent field (SCF) method. Despite its usefulness, Eq. (1.2.3) still neglects important quantum mechanical behavior such as electron exchange and correlation effects.

1.3 THE VARIATIONAL PRINCIPLE

The previous subchapters introduced the simplified many-electron problem, and its solution relies on obtaining the expectation value of operator, such as Hamiltonian, using the WF. The variation principle states that any trial WF is an upper bound of the ground state energy,

$$E[\psi] \geq E_0, \tag{1.3.1}$$

where E represents the total energy and E_0 is the ground state energy. The total energy can be equal to the ground state energy if and only if the WF is equal to the ground state WF,

$$E = E_0 \Leftrightarrow |\psi\rangle = |\psi_0\rangle. \tag{1.3.1}$$

Eq. (1.3.1) implies that the energy functional $E[\psi]$ can be minimized from an initial guess WF to the ground state WF.

1.4 HARTREE-FOCK THEORY OVERVIEW

The Hartree-Fock (HF) method utilizes a Slater determinant WF and the Born-Oppenheimer approximation to solve the many-electron problem for the system's total energy. In this theory, we will use an HF WF denoted as ψ^{HF} [4]. The total energy within the HF method is given by the expectation value of the Hamiltonian operator $\hat{H}$ using the HF WF,

$$E^{HF} = \langle \psi^{HF} | \hat{H} | \psi^{HF} \rangle, \tag{1.4.1}$$

the HF method employs the Eq. (1.2.3) in spirit to obtain the total energy, but it includes electron exchange interactions. The HF energy expression can be written as,

$$E^{HF} = \sum_{i=1}^{N} \langle i | \hat{h} | i \rangle + \frac{1}{2} \sum_{i,j}^{N} ([ii|jj] - [ij|ji]). \tag{1.4.2}$$

Here, i and j are orbital WFs, $\langle i|\hat{h}|i\rangle$ represents the expectation value of the single non-interacting electron Hamiltonian, $[ii|jj]$ is a four-center electron integral, and $[ij|ji]$ is the electron-exchange integral, which is purely mathematical in nature. The $[ii|jj]$ integral is equivalent to Eq. (1.2.2). For convenience, we will utilize a simplified notation of the Coulomb electron-electron ($\hat{V}_{ee}$) as,

$$V_{ij} = \frac{1}{|\vec{r}_i - \vec{r}_j|} = \frac{1}{r_{ij}}, \tag{1.4.3}$$

where r_{ij} represents the distance between a pair of electrons used in the Coulomb potential (V_{ij}). The Coulomb potential can be represented as a four-electron integral,

$$[ik|jl] = \langle ij|kl\rangle \equiv \int d\vec{x}_1 \int d\vec{x}_2 \; \phi_i^*(\vec{x}_1)\phi_j^*(\vec{x}_2) r_{12}^{-1} \phi_k(\vec{x}_1)\phi_l(\vec{x}_2). \tag{1.4.4}$$

Here, $\vec{x}_1$ and $\vec{x}_2$ are dummy indexes representing electron coordinates, and $\langle ij|kl\rangle$ is represented in physics notation, while $[ik|jl]$ in chemist notation.

1.4.1 SELF-CONSISTENCY OF HARTREE-FOCK THEORY

The HF self-consistent field (SCF) method assumes a WF approximated as a single Slater determinant. The SCF procedure involves the use of undetermined multipliers to enforce orthonormality of orbitals and minimize the HF energy,

$$\mathcal{L}[\{\phi_i\}] = E^{HF}[\{\phi_i\}] - \sum_{i,j}^{N} \varepsilon_{ij}\big(\langle i|j\rangle - \delta_{ij}\big), \tag{1.4.1.1}$$

ε_{ij} are the Lagrange multipliers that ensure orthonormality, and the variational form of Eq. (1.4.1.1) can be written as follows,

$$\delta\mathcal{L} = \delta E^{HF}[\{\phi_i\}] - \sum_{i,j}^{N} \varepsilon_{ij}\, \delta\langle i|j\rangle. \tag{1.4.1.2}$$

Where $\delta\langle i|j\rangle$ represents the variations within two overlapping orbitals,

$$\delta\langle i|j\rangle = \langle\delta\phi_i|\phi_j\rangle + \langle\phi_i|\delta\phi_j\rangle. \quad (1.4.1.3)$$

Expressing the HF variation from Eq. (1.4.1.2) in terms of Eqs. (1.4.1.1) and (1.4.2) yields,

$$\delta\mathcal{L} = \sum_i^N \left[\langle\delta\phi_i|\hat{h}|\phi_i\rangle + \langle\phi_i|\hat{h}|\delta\phi_i\rangle\right] + \sum_{i,j}^N \left(\left[\delta\phi_i\phi_i|\phi_j\phi_j\right] + \left[\phi_i\delta\phi_i|\phi_j\phi_j\right]\right) - \sum_{i,j}^N \left(\left[\delta\phi_i\phi_j|\phi_j\phi_i\right] + \left[\phi_i\delta\phi_j|\phi_j\phi_i\right]\right) - \sum_{i,j}^N \varepsilon_{ij}\left(\langle\delta\phi_i|\phi_j\rangle + \langle\phi_i|\delta\phi_j\rangle\right), \quad (1.4.1.4)$$

Eq. (1.4.1.4) incorporates twice the Coulomb and exchange variations, which is included in the property $\langle\phi_i|\hat{h}|\delta\phi_i\rangle = \left(\langle\delta\phi_i|\hat{h}|\phi_i\rangle\right)^*$, thus simplify the HF method. The minimum energy in the HF method is found by setting the variation to zero,

$$\delta\mathcal{L} = \sum_i^N \left(\langle\delta\phi_i|\hat{h}|\phi_i\rangle\right) + \sum_{i,j}^N \left(\left[\delta\phi_i\phi_i|\phi_j\phi_j\right]\right) - \sum_{i,j}^N \left(\left[\delta\phi_i\phi_j|\phi_j\phi_i\right]\right) - \sum_{i,j}^N \varepsilon_{ij}\left(\langle\delta\phi_i|\phi_i\rangle\right) + complex\ conjugate = 0. \quad (1.4.1.5)$$

Eq. (1.4.1.5) defines the HF eigenvalue problem $\left(\frac{\delta\mathcal{L}}{\delta\phi_i}\right)$ for each orbital as,

$$\hat{h}(\vec{x}_1)\phi_i(\vec{x}_1) + \sum_{i\neq j}^N \phi_i(\vec{x}_1)\left[\int d\vec{x}_2\left|\phi_j(\vec{x}_2)\right|^2 r_{12}^{-1}\right] - \sum_{i\neq j}^N \phi_j(\vec{x}_1)\left[\int d\vec{x}_2\phi_j^*(\vec{x}_2)\phi_i(\vec{x}_2)r_{12}^{-1}\right] = \sum_j^N \varepsilon_{ij}\phi_j(\vec{x}_1), \quad (1.4.1.6)$$

Eq. (1.4.1.6) is a set of linear equations that can be diagonalized using standard linear algebra libraries such as LAPACK. The SCF cycle aims to find the set of orbitals that minimizes this

eigenvalue problem and solves self-consistently for the density, Coulomb energy, and total energy simultaneously.

1.5 DENSITY FUNCTIONAL THEORY

Hohenberg and Kohn's (HK) density functional theory (DFT) [5] originally proposed that the ground state properties depend on the electron density, which can be described by 3 coordinates. Kohn and Sham (KS) DFT [6,7] further developed this theory by introducing a framework where the interacting many-electron system is mapped onto a non-interacting electron system with an effective potential. The KS effective potential comprises the external potential, the mean-field theory (Hartree potential), and the exchange-correlation (XC) potential. The XC potential encapsulates all the quantum effects in DFT, although its exact mathematical form remains unknown. Approximating the XC potential is an active area of research, and early density functional approximations (DFAs) are based on the simplest local-spin density (LSDA). The LSDA functional will be discussed in subsequent subchapters.

1.5.1 KOHN-SHAM FORMALISM

KS formalism is established for the energy functional of the electron density (obtained from WF) and employs an effective potential. KS-DFT provides an exact theory for solving the ground state energy ($E = \mathcal{F}[\psi]$), but the exact XC functional remains unknown. The XC potential captures the quantum effects, and over a hundred approximated forms of XC functionals have been proposed to date. The simplest LSDA functional describes the electron exchange as a homogeneous electron gas. Using an approximation in XC functional, DFT can describe various properties of atoms, molecules and solids, such as total energy, polarizability, dipole-moment, and other quantities. HK theorem [5] states that the WF must be used for exited states, while the electron density is utilized for the ground state, as shown below,

$$E = \begin{cases} F[\rho(\vec{r})] & ground\ state \\ \mathcal{F}[\psi(\vec{r}_1, \dots, \vec{r}_n)] & exited\ state \end{cases}. \qquad (1.5.1.1)$$

The HK theorem defines $E[\rho]$ for a ground state system. However, since the exact energy functional is unknown, approximations are employed. The energy functional can be expressed as,

$$E[\rho] = \int d\vec{r}\rho(\vec{r})V_n(\vec{r}) + \langle\psi[\rho] \mid \hat{T} + \widehat{W} \mid \psi[\rho]\rangle, \tag{1.5.1.2}$$

where $\widehat{W}$ contains the electron-electron Coulomb potential (V_{ee}) and external potentials, and $\int d\vec{r}\rho(\vec{r})V_n(\vec{r})$ represents the electron-nuclei Coulomb energy. In KS theory, an effective potential, denoted as V_{eff}, is introduced and consists of the external, Coulomb and XC potentials. The DFT formulation uses the independent electron approximation for kinetic energy, and an effective potential $V_{eff} = V_H + V_{en} + V_{XC} + V_{ext}$, where all terms are treated as a mean-field theory (Hartree potential) except for V_{XC}.

$$E = F[\rho] = \int d\vec{r}\rho(\vec{r})V_n(\vec{r}) - \sum_i \int d\vec{r}\phi_i^*(\vec{r})\left(\frac{\nabla^2}{2}\right)\phi_i(\vec{r}) + \frac{1}{2}\int d\vec{r}\rho(\vec{r})V_H(\vec{r}) + E_{XC}[\rho] \tag{1.5.1.3}$$

$$V_H(\vec{r}) = \int d\vec{r}' \frac{\rho(\vec{r}')}{|\vec{r}-\vec{r}'|} \tag{1.5.1.4}$$

$$E_{XC}[\rho] = \int d\vec{r}\rho(\vec{r})\left(\frac{\delta E_{XC}}{\delta\rho}\right) = \int d\vec{r}\rho(\vec{r})V_{XC}[\rho(\vec{r})] \tag{1.5.1.5}$$

The term E_{XC} incorporates the quantum effects of electrons and is approximated in practice.

1.5.2 VARIATIONAL FORM OF THE KS-DFT

The minimization of the energy functional leads to the mere definition of the ground state density (ρ_0) through the variational principle,

$$\frac{\delta E[\rho]}{\delta\rho}\Big|_{\rho_0} = 0 \tag{1.5.2.1}$$

Eq. (1.5.2.1) is equivalent to the variational form of HF, but in the case of KS-DFT, it yields the KS orbitals $\phi_i(\vec{r})$ with the additional introduction of orthogonality constraints on the orbitals. The variational KS equation is given by,

$$\left[-\frac{1}{2}\nabla^2 + V_n(\vec{r}) + V_H(\vec{r}) + V_{xc}(\vec{r})\right]\phi_i(\vec{r}) = \epsilon_i\phi_i(\vec{r}), \tag{1.5.2.2}$$

where V_n represents the nuclear potential, V_H is the Hartree potential, the Laplacian term corresponds to the kinetic energy, and V_{xc} denotes the exchange-correlation potential defined as follows,

$$V_{xc}(\vec{r}) = \frac{\delta E_{xc}[\rho]}{\delta\rho}|_{\rho(\vec{r})}. \tag{1.5.2.3}$$

Eq. (1.5.2.2) is the variational form of the KS method, which is computationally inexpensive compared to HF method. The KS method provides reasonable accuracy, making it a suitable choice for calculating physical/chemical properties. The $E_{XC}[\rho]$ is available in various approximated forms with different degrees of accuracy, as described by Jacob's ladder [8], but higher accuracy comes at the expense of increased computational cost.

1.6 DENSITY FUNCTIONAL APPROXIMATIONS

DFAs are computationally more efficient than the HF method. Among the DFA functional families, LSDA is the simplest because it only relies on spin density. Generalized gradient approximations (GGAs) include both spin density and spin density gradient for the XC energy functional. Meta-GGAs (MGGAs) go a step further by incorporating spin density, spin density gradient, and density Laplacian or kinetic energy density, thereby enhancing the accuracy of the XC energy functional.

1.6.1 LOCAL SPIN DENSITY APPROXIMATION

LSDA is a fundamental DFA that serves as a building block for superior functionals [9,10]. It is derived from the homogeneous electron gas model commonly used in solid-state physics textbooks [11]. LSDA assumes non-interacting electrons in the presence of constant nuclear potential. Within this model, the WF in terms of N electrons within a volume V as follows,

$$\phi_{\vec{k}}(\vec{r}) = \frac{1}{\sqrt{V}} \exp(i\vec{k} \cdot \vec{r}), \tag{1.6.1.1}$$

$$\epsilon_{\vec{k}} = \frac{|\vec{k}|^2}{2}, \tag{1.6.1.2}$$

Eqs. (1.6.1.1) and (1.6.1.2) represent the stationary WF with wavevectors $\vec{k}$ and $\epsilon_{\vec{k}}$ eigenvalues. Among these states, the highest occupied state is associated with the Fermi level $\vec{k}_F$, which corresponds to the E_F Fermi energy. Fermi level state is defined as,

$$\vec{k}_F = (3\pi\rho)^{\frac{1}{3}}. \tag{1.6.1.3}$$

The exchange energy is constructed from the Fermi level and plane waves, resulting in the following expression,

$$E_X[\rho] = -\frac{3}{4}\left(\frac{3}{\pi}\right)^{\frac{1}{3}} \rho^{\frac{4}{3}} V. \tag{1.6.1.4}$$

This approximation neglects correlation effects. However, correlation energy can be obtained directly by directly solving the many-body Schrödinger equation using stochastic numerical methods [10]. The correlation energy approximation for the electron gas was developed by Perdew and Zunger (1981) [9], and it is expressed as follows:

$$E_C[\rho] = \rho V \begin{cases} -0.048 + 0.0311 \ln r_s + 0.002 r_s \ln r_s - 0.0116 r_s & if\ r_s < 1 \\ -\dfrac{0.1423}{1 + 1.0529\sqrt{r_s} + 0.3334 r_s} & if\ r_s \geq 1 \end{cases}$$

, (1.6.1.5)

r_s is the Wigner-Seitz radius, which is the average occupied sphere of an electron.

1.6.2 GENERALIZED GRADIENT APPROXIMATION

The LSDA functional, although simple, fails to accurately describe inhomogeneous electron density. To overcome this limitation, researchers have introduced the reduced gradient [12-15] in semilocal functional approximations. The general form of the generalized gradient approximation (GGA) semilocal energy functional is as follows,

$$E_{XC}^{GGA}[\rho_\uparrow, \rho_\downarrow] = \int d\vec{r}\, f\left(\rho_\uparrow, \rho_\downarrow, \vec{\nabla}\rho_\uparrow, \vec{\nabla}\rho_\downarrow\right), \tag{1.6.2.1}$$

Semilocal GGA are typically derived from density-gradient expansion for the exchange-correlation hole and enforces exact conditions for exchange-correlation energy such as the uniform electron gas limit and the second-order gradient expansion in the slowly varying limit. One commonly used semilocal functional is the Perdew-Burke-Ernzerhof (PBE) [12], defined as,

$$E_X^{PBE}[\rho] = \int d\vec{r}\, \rho(\vec{r})\, \epsilon_X^{unif}[\rho]\, F_X(s). \tag{1.6.2.2}$$

Here, $\epsilon_X^{unif}[\rho] = -\frac{3}{4\pi}(3\pi^2\rho)^{1/3}$ is the LSDA exchange energy density. The dimensionless density gradient s is defined as $s = \left|\vec{\nabla}\rho\right|/(2\rho(3\pi^2\rho)^{1/3})$. The enhancement factor $F_X(s)$ is described by,

$$F_X(s) = 1 + \kappa - \frac{\kappa}{1 + \mu\, s^2/\kappa}, \tag{1.6.2.3}$$

with $\kappa = 0.804$ and $\mu = 0.21951$ as constants. The enhancement factor obeys the uniform electron gas density limit $F_X(0) = 1$, and the Lieb-Oxford lower bound given by $F_X(s) \leq 1.804$. The correlation energy expression is given by,

$$E_C^{PBE}[\rho_\uparrow, \rho_\downarrow] = \int d\vec{r}\, \rho(\vec{r}) \left[\epsilon_c^{unif}(r_s, \zeta, \mathrm{t}) + H(r_s, \zeta, \mathrm{t})\right], \tag{1.6.2.4}$$

where $t = \left|\vec{\nabla}\rho\right|/(2\phi k_s \rho)$ is another dimensionless density gradient, $k_s = \sqrt{4k_F/\pi a_0}$ is the Thomas-Fermi screening wavevector, $\zeta = \frac{\rho_\uparrow + \rho_\downarrow}{\rho}$ is the relative spin polarization, and $\phi(\zeta) = \left[(1+\zeta)^{\frac{2}{3}} + (1-\zeta)^{\frac{2}{3}}\right]/2$ is the spin scaling factor. The H function of Eq. (1.6.2.4) is defined as follows,

$$H(r_s, \zeta, t) = \gamma\phi^3 \ln\left[1 + \frac{\beta}{\gamma} t^2 \cdot \frac{1 + At^2}{1 + At^2 + A^2 t^4}\right]. \tag{1.6.2.5}$$

The constant values are $\beta = 0.066725$, $\gamma = 0.031091$. A is defined as,

$$A = \frac{\beta}{\gamma}\left(\exp\left[-\frac{\epsilon_c^{unif}}{\gamma\phi^3}\right] - 1\right)^{-1}. \tag{1.6.2.6}$$

In the limit of $t \to 0$, the H function simplifies to $\beta\phi^3 t^2$, which corresponds to the slow-varying limit that describes the second-order gradient expansion. In the rapidly varying limit of $t \to \infty$, H approaches $-\epsilon_c^{unif}$, effectively reducing the correlation energy to zero in Eq. (1.6.2.4). When the electron density is high and r_s approaches 0, the correlation energy becomes constant.

Besides the popular PBE GGA functional, PBEsol and SOGGA [34] are designed with the correct coefficient in the second-order term in the density-gradient expansion and show good performance for certain properties.

1.6.3 META-GENERALIZED GRADIENT APPROXIMATION

Meta-generalized gradient approximation (meta-GGA) [16] is a further improvement that incorporates the kinetic energy density or density Laplacian to enhance the accuracy of chemical properties compared to LSDA or GGA functionals. The kinetic energy density base XC energy description is described as follows,

$$E_{XC}^{MGGA}[\rho_\uparrow, \rho_\downarrow] = \int d\vec{r}\, \rho(\vec{r}) \epsilon_{XC}(\rho_\uparrow, \rho_\downarrow, \vec{\nabla}\rho_\uparrow, \vec{\nabla}\rho_\downarrow, \tau_\uparrow, \tau_\downarrow). \quad (1.6.3.1)$$

Here, $\tau_\sigma = \frac{1}{2}\sum_i^{N_{occ}} \left|\vec{\nabla}\psi_{i\sigma}\right|^2$ represents the non-interacting kinetic energy density of the KS orbitals with spin σ. The second-order gradient expansion for τ_σ makes it possible to recover the condition set by the fourth-order gradient expansion in the enhancement factor F_x in the slow-varying density limit. There are numerous meta-GGA functionals described in literature [17-23], but we will focus on one of the most successful meta-GGAs, the Strongly Constrained and Appropriately Normed (SCAN) functional [16]. The exchange energy of spin unpolarized SCAN is denoted as follows,

$$E_X[\rho] = \int d\vec{r}\, \rho(\vec{r}) \epsilon_X^{unif} F_x(s, \alpha), \quad (1.6.3.2)$$

in this equation, $\alpha = \frac{\tau - \tau^w}{\tau^{unif}}$ is a dimensionless variable. Here, $\tau^W = \frac{\left|\vec{\nabla}\rho\right|^2}{8\rho}$ represents the Von-Weizsäcker kinetic energy density, which is equal to τ for the single orbital density limit. Additionally, $\tau^{unif} = \frac{3}{10}(3\pi^2)^{2/3}\rho^{5/3}$ is the Thomas-Fermi kinetic energy density or the uniform kinetic energy density limit. The quantity α describes chemical bonding, $\alpha \sim 0$ defines a single covalent bond, $\alpha \sim 1$ describes a metallic bond, and $\alpha \gg 1$ indicates a weak interaction. The enhancement factor for Eq. (1.6.3.2) is defined as follows,

$$F_x(s, \alpha) = (h_x^1(s, \alpha) + f_x(\alpha)[h_x^0 - h_x^1(s, \alpha)])\, g_x(s), \quad (1.6.3.3)$$

with

$$f_x(\alpha) = \exp\left[-\frac{c_{1x}\alpha}{1-\alpha}\right]\theta(1-\alpha) - d_x \exp\left[\frac{c_{2x}}{1-\alpha}\right]\theta(\alpha-1), \quad (1.6.3.4)$$

$$g_x(s) = 1 - \exp\left[-a_1 s^{-1/2}\right]. \quad (1.6.3.5)$$

The parameters for the above equations are $h_x^0 = 1.174$, $a_1 = 1.4979$, $c_{1x} = 0.667$, $c_{2x} = 0.8$ and $d_x = 1.24$. $\theta(x)$ is a step function. The enhancement factor becomes $F_x(s,\alpha) = h_x^1(s,\alpha)$ when $\alpha \approx 1$, similar to PBE, which recovers the slow-varying limit. However, Eq (1.6.3.3) satisfies the fourth-order gradient approximation. The expression for h_x^1 is given by,

$$h_x^1(s,\alpha) = 1 + \kappa_1 - \frac{\kappa_1}{1+\mu x^2/\kappa_1}, \quad (1.6.3.6)$$

and x is defined as follows,

$$x = \mu_{AK} s^2 \left[1 + \left(\frac{b_4 s^2}{\mu_{AK}}\right)\exp\left(-\frac{|b_4| s^2}{\mu_{AK}}\right)\right] + [b_1 s^2 + b_2(1-\alpha)\exp(-b_3(1-\alpha)^2)]^2. \quad (1.6.3.7)$$

The constant values are $\mu_{AK} = 10/11$, $b_2 = (5913/405000)^{1/2}$, $b_1 = (511/13500)/(2b_2)$, $b_3 = 0.5$, $b_4 = \mu_{AK}/\kappa_1 - 1606/18225 - b_1^2$, and $\kappa_1 = 0.065$. It is worth noting that SCAN satisfies the tight-bound condition $F_x \leq 1.174$ [24], which is also satisfied by LDA. On the other hand, the correlation energy is given by,

$$E_C[\rho_\uparrow, \rho_\downarrow] = \int d\vec{r}\, \rho(\vec{r})\left(\epsilon_c^{unif}(r_s, \zeta, s, \alpha)\right), \quad (1.6.3.8)$$

where Eq. (1.6.3.8) components are,

$$\epsilon_c = \epsilon_c^1 + f_c^1(\alpha)[\epsilon_c^0 - \epsilon_c^1] \quad (1.6.3.9)$$

$$f_c(\alpha) = \exp\left[-\frac{c_{1c}\alpha}{1-\alpha}\right]\theta(1-\alpha) - d_c \exp\left[\frac{c_{2c}}{1-\alpha}\right]\theta(\alpha-1) \quad (1.6.3.10)$$

Eqs. (1.6.3.9) and (1.6.3.10) represent terms analogous to exchange energy in SCAN functional. The coefficients for these terms are $c_{1c} = 0.64$, $c_{2c} = 1.5$, and $d_c = 0.7$. The SCAN functional Has shown superiority over several other GGAs and meta-GGAs in various applications. It has been successful in accurately describing properties of liquid and ice water [31], metal surfaces [32], and some others [33].

1.7 GAUSSIAN BASIS SET AND BASIS FUNCTIONS

The solution of the KS equation involves a basis set representation, where the molecular orbitals (MOs) are constructed as linear combination of atomic orbitals (AOs) using either plane waves [25] or Gaussian [4] basis functions. The molecular orbitals are represented as follows,

$$\psi_i(\vec{r}) = \sum_{\mu=1}^{N_{Basis}} C_{\mu i}\chi_\mu(\vec{r}). \quad (1.7.1)$$

Eq. (1.7.1) describes the orbital WF as a linear combination of its Gaussian basis functions (χ_μ) and its canonical eigenvectors ($C_{\mu i}$). The given Gaussian basis set remains fixed through the entire calculation, and the accuracy of the solution depends on the completeness of the basis set. More detailed information about Gaussian basis sets can be found in Zachary J. Buschmann thesis [71]. The MO coefficients $C_{\mu i}$ are the canonical molecular orbitals (CMOs) or molecular eigenvectors determined during the SCF calculation. Gaussian basis sets became popular due to their efficient integration scheme, making them computationally advantageous for first principle electronic structure methods. The present work utilizes the primitive Gaussian type orbitals (GTOs), and its cartesian definition is as follows,

$$g_\mu(\vec{r}) = A_\mu(x-x_0)^k(y-y_0)^m(z-z_0)^n e^{-\alpha_\mu\left((x-x_0)^2+(y-y_0)^2+(z-z_0)^2\right)}, \quad (1.7.2)$$

where x_0, y_0 and z_0 are the center of Gaussian, A_μ and α_μ represent the Gaussian height and width, respectively. Usually, the Gaussian is centered in an atomic position. A contracted Gaussian for an atom is $\sum_\mu g_\mu(\vec{r})$.

The definition of a Gaussian basis set is not trivial, although, there are numerous basis sets available at https://www.basissetexchange.org/. The minimal basis set is STO-2G, and there exists other choices such as 4-31G and 6-31G*, which provide more complete basis sets. The calculations in this work were achieved with the FLOSIC code, which can be accessed through https://github.com/FLOSIC/PublicRelease_2020. The FLOSIC code employs a default basis set for the NRLMOL code optimized for PBE functional [26]. For the computations in this work, the NRLMOL default basis set is utilized unless otherwise specified.

1.8 SELF-INTERACTION OF ELECTRONS

In this subsection, I will discuss some common KS-DFA limitations and brief description of methods that address this problem. DFAs especially the local and semi-local functionals while successfully at describing complex behavior of system, fail to correctly describe the simple one electron system such as hydrogen atom and a cation of hydrogen molecule. Approximate functionals (DFAs) present self-interaction error (SIE), this comes from the improper cancellation of the one-electron Coulomb and Exchange energy. As a note, HF method does not show this behavior because of its exact exchange electron description. The presence of self-interaction error (SIE) limits DFAs' accuracy for charge transfer, transition barriers and stretched bond description.

1.8.1 SELF-INTERACTION ERROR

KS-DFT employs the classical Hartree description to model the Coulomb repulsion energy term in Eq. (1.5.1.3), which accounts for the repulsion between electrons. This Hartree or mean-field represents an average Coulomb interaction arising directly from the all-electron density, allowing electrons to repeal each other and itself. Thus, it contains spurious self-repulsion. This phenomenon is commonly known as self-interaction (SI). Theoretically, the exact, yet unknown, exchange functional should nullify this residual self-interaction. However, since we lack the exact exchange-correlation functional, the self-interaction error of electrons persists.

We can describe a one-electron system, such as hydrogen atom in an exact form, where no correlation is needed. The DFA energy of the system is,

$$E^{DFA} = E^{ne}[\rho] + E^{Kin}[\rho] + E^{ee}[\rho] + E_X[\rho] \tag{1.8.1.1}$$

where E^{ne} represents the electron-nuclei Coulomb energy, E^{kin} represents the electron kinetic energy, E^{ee} represents the electron-electron Coulomb energy, and E_X is the electron exchange energy. ρ is the total electron density. The physical interaction E^{ee} of the one-electron density must be zero, but the self-Hartree energy does not vanish. Thus, the self E_X term is required to cancel that residual energy. DFAs do not properly cancel ($E^{ee} + E_X \neq 0$) for the one-electron density. This residual self-interaction error (SIE) can be removed using a correction of the type:

$$E^{1elecSIC} = E^{ne}[\rho] + E^{Kin}[\rho] + E^{ee}[\rho] + E_X[\rho] - E^{ee}[\rho_1] - E_X[\rho_1], \tag{1.8.1.2}$$

where ρ_1 is the one-electron density and equal to the total density for one-electron systems such as H_2^+. Thus, the self-interaction corrected energy is,

$$E^{1elecSIC} = E^{ne}[\rho] + E^{Kin}[\rho]. \tag{1.8.1.3}$$

The one-electron effective potential is described only by the exact asymptotic potential $V_{en}(\vec{r}) = 1/|\vec{r} - \vec{R}_n|$ with $\vec{R}_n$ as the nuclear position, and the nucleus-electron energy corresponds to $E^{ne}[\rho] = \int \rho(\vec{r}) V_{en}(\vec{r}) d\vec{r}$.

The presence of SIE results in an incorrect description of dissociation of a molecule. Simple examples where an inaccurate description of stretched bonds occurs are the He_2^+ and H_2^+ systems. With DFA-LSDA, in the dissociation limit, both the hydrogens have $1/2$ of an electron which is an unphysical result. Another problem, known as delocalization error, arises when the energy of the system is lowered for fractional occupancy which shows up in the total energy curve in the asymptotic limit where the dissociated fragments are well separated. Fig. 1.1 shows the H_2^+ dissociation energy for different methods, illustrating that DFA-LSDA incorrectly predicts lower energies for the dissociated hydrogen ion.

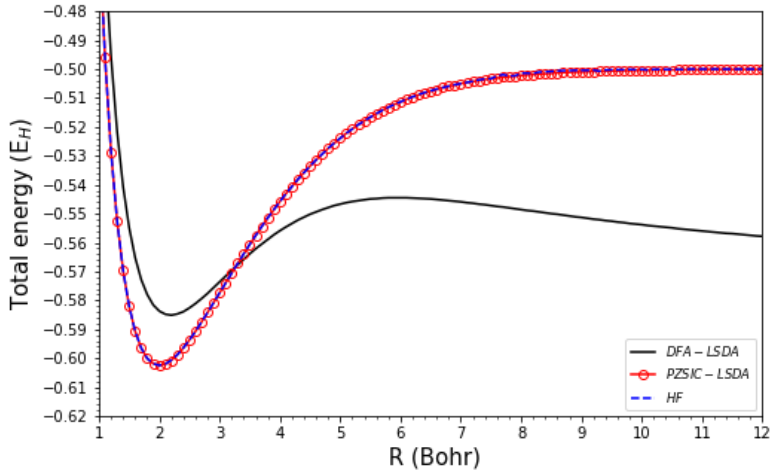

Fig. 1.1. Dissociation energy for H_2^+ compared using the DFA-LSDA, PZSIC-LSDA and HF methods with an integer occupation, calculated with the FLOSIC code.

He_2^+ molecule also exhibits SI of electrons (three electron problem). The dissociation energy curve is poorly described due to the approximate energy functional, and the HF method is no longer exact as it requires correlation effects to be accounted for.

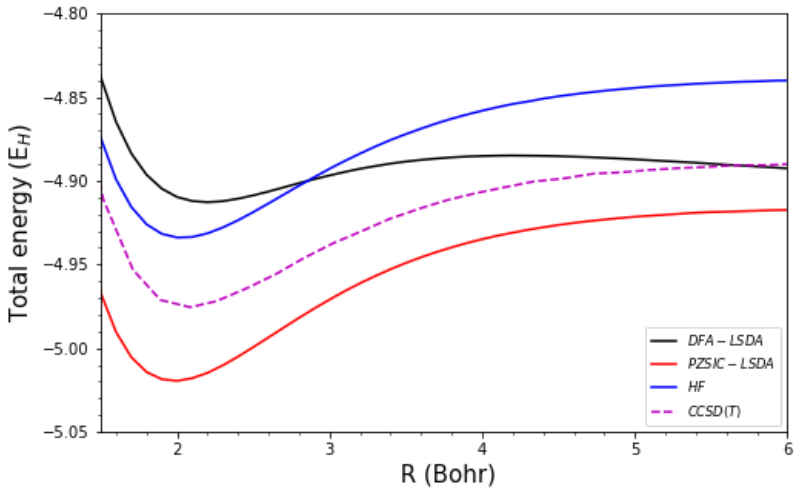

Fig. 1.2. Dissociation energy limit for He_2^+ compared using the DFA-LSDA, PZSIC-LSDA and HF methods with an integer occupation, calculated with the FLOSIC code. CCSD(T) was retrieved from [34].

Fig. 1.2 presents the dissociation energy curve for DFA-LSDA, PZSIC-LSDA, HF and CCSD(T) methods [34]. The CCSD(T) dissociation energy is considered the most accurate curvature. Interestingly, the PZSIC, HF and CCSD(T) methods show a similar behavior for the dissociation energy curve with an almost constant energy shift.

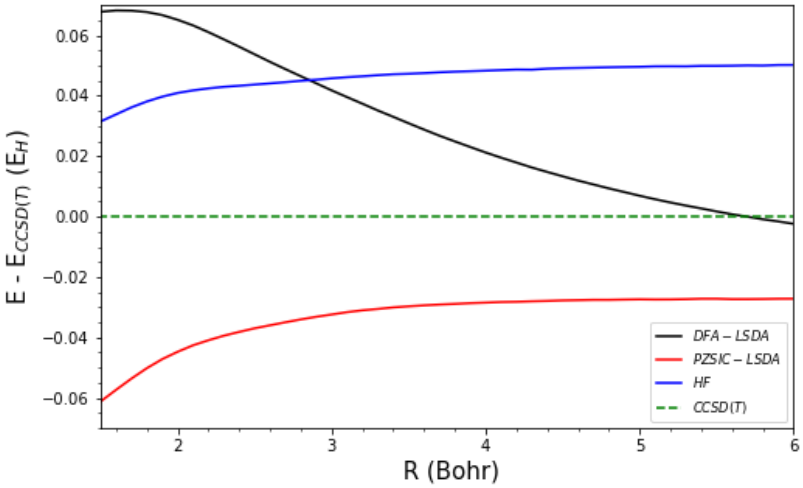

Fig. 1.3. Dissociation energy limit for He_2^+ compared to CCSD(T) [34].

Fig. 1.3 illustrates the energy difference of each method compared to CCSD(T) energy, showing an almost constant line, especially after 4 Bohr. The DFA performance is lowering the dissociation energy when He^+ and He are separate with an integer occupation ($f_i = 1$). This behavior of incorrectly obtaining lower energy is also noted in spurious fractional occupation ($0 < f_i < 1$) states [34], where total energies are too low in comparison to integer occupation states.

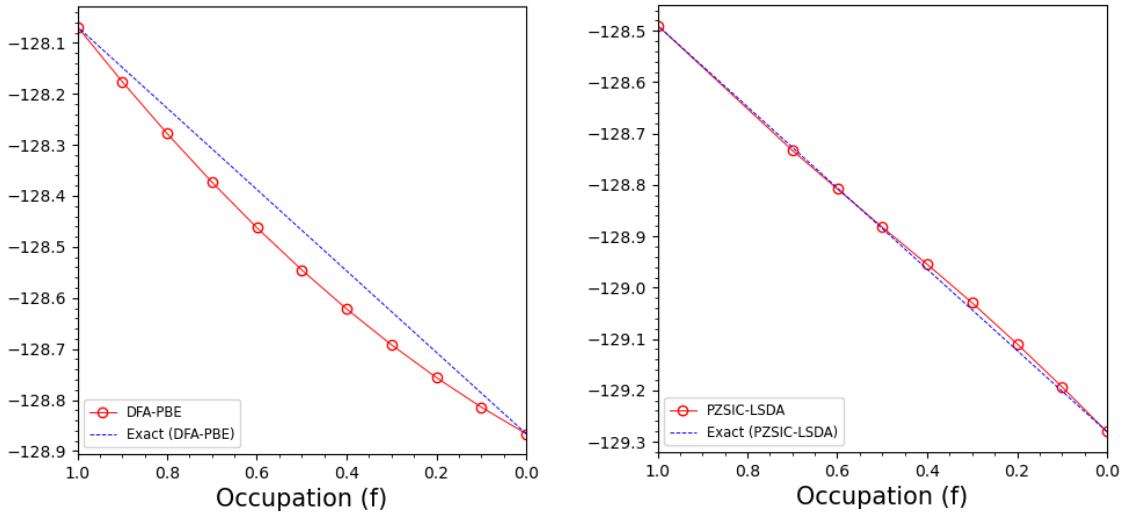

Fig. 1.4. Occupation limit derivative $\epsilon_i = \frac{\partial E}{\partial f_i}$ compared to Janak's theorem.

The reason for this fractional occupation energy resides in the exchange-correlation hole density. For dissociation fragments (e.g. H_2^+ and He_2^+), the exchange-correlation hole integrates to -1 for integer occupation of electrons, and it becomes a less negative quantity for non-integer electron occupation, as pointed out in Ref. 34.

1.8.2 ADDRESSING SELF-INTERACTION WITH DIFFERENT METHODS

There are some approaches that address the SIE and attempts to diminish or eliminate the SI. Hybrid functionals combine a fraction of exact exchange from HF method and includes a fraction of the DFA exchange-correlation. By including this exact exchange amount, the SIE is partially corrected. Some examples of popular hybrid functionals are PBE0 [37] and HSE [38] and B3LYP [39,40,41,42].

Range-separated functionals split the electron-electron interaction into short-range and long-range components. This approach considers the short-range description as semi-local functional, while the long-range component incorporates nonlocal exchange contributions. Examples of range-separated functionals include the Coulomb-attenuating method (CAM) [43], Minnesota functional

(Mn) [44], one-parameter progressive (OP) with Becke88 exchange correlation [58] functionals (LC-BOP) [59,60], and strongly constrained and appropriately normed (SCAN) functional [16]. Exact exchange and correlation potentials can be determined by different procedures, one approximation to optimized effective potential (OEP) is the Krieg-Li-Iafrate (KLI) method [46]. Multireference configuration interaction DFT (MRCI-DFT) combines elements of both DFT and wavefunction-based methods. Some examples of MR-DFT methods are the complete active space DFT (CAS-DFT) [48], density matrix embedding theory (DMET) [49], and multiconfigurational pair-density theory (MC-PDFT) [65].

Gaussian and plane-wave embedding methods combine DFT calculations with higher-level methods, such as wavefunction-based methods [50] or quantum Monte Carlo [51] computations to correct the SIE. Typically, a small part of the system is treated with higher level of theory, while the rest of the system is described using DFT. Hubbard-corrected DFT methods such as DFT+U [52,53] and DFT+DMFT [54] introduce a Hubbard-like term to include localized electron interactions, this is especially important for strongly correlated materials. These methods correct the SIE and captures correlation effects that standard DFT does not capture.

The GW approximation is a many-body perturbation theory method widely used in condensed matter physics and materials science. It combines the Green's function (G) and the screened Coulomb interaction (W) to improve the description of electron-electron interactions. The GW approximation is particularly valuable for obtaining quasiparticle energies, which play a crucial role in understanding electronic band structures, band gaps, and excitations in solids. By incorporating many-body effects and considering electron screening, the GW approximation offers a more accurate description than DFAs, especially for systems with strong correlation effects or materials characterized by narrow or localized bands. Its application has proven successful in providing improved insights into electronic properties, including optical properties, electronic excitations, and band structures in a wide range of materials [55,56,57].

This thesis is focused on one-electron self-interaction correction (SIC) methods that explicitly correct the SIE by removing spurious SI terms on an orbital by orbital basis. The Perdew and Zunger SIC (PZSIC) method [9] is an example of one-electron SIC. More details about SIC methods and current research are presented in the following subsubsections.

1.8.3 ONE-ELECTRON SELF-INTERACTION CORRECTION APPROACHES

As mentioned earlier, SIE arises due to the improper cancellation between the exchange functional and the Hartree term for the one-electron limit. When considering the exchange energy of a pair of electrons in the HF description, we obtain,

$$E_X = \frac{1}{2}\sum_\sigma \sum_{i,j} \int d\vec{r} \int d\vec{r}\prime \frac{\psi_{i\sigma}(\vec{r})\psi_{j\sigma}(\vec{r}\prime)\psi_{j\sigma}(\vec{r})\psi_{i\sigma}(\vec{r}\prime)}{|\vec{r}-\vec{r}\prime|}. \quad (1.8.3.1)$$

In the case of $i = j$, the expression in Eq. (1.8.3.1) represents the self-exchange energy, which is appropriately cancelled out for HF method. However, approximate XC functionals are typically density-dependent and may not fully capture the essence of Eq. (1.8.3.1). The SIE arises from the poor description of the one-electron limit provided by the DFAs, resulting in SI. This misdescription leads to significant shortcomings in accurately describing stretched bonds and reaction barrier heights. The SIE stems from the improper cancellation between the self-Coulomb energy and the approximate self-exchange energy in DFA calculations.

1.8.3.1 PERDEW AND ZUNGER SELF-INTERACTION CORRECTION

In 1981, Perdew and Zunger [9] proposed a one-electron SIC method known as PZSIC, which removes the SIE from a DFA functional in an orbital-by-orbital basis from the total DFA energy,

$$E^{PZSIC-DFA}[\rho_\uparrow, \rho_\downarrow] = E^{DFA}[\rho_\uparrow, \rho_\downarrow] - \sum_{i\sigma}(U[\rho_{i\sigma}] + E_{XC}^{DFA}[\rho_{i\sigma}, 0]). \quad (1.8.3.2)$$

The self-Coulomb and the self-exchange-correlation energies are given by,

$$U[\rho_{i\sigma}] = \frac{1}{2}\int d\vec{r}\rho_{i\sigma}(\vec{r}) \int d\vec{r}\prime \frac{\rho_{i\sigma}(\vec{r}\prime)}{|\vec{r}-\vec{r}\prime|}, \quad (1.8.3.3)$$

$$E_{XC}^{DFA}[\rho_{i\sigma}, 0] = \int d\vec{r}\rho_{i\sigma}(\vec{r})\epsilon_{XC}^{DFA}([\rho_{i\sigma}, 0], \vec{r}). \quad (1.8.3.4)$$

In a traditional PZSIC approach, the orbitals used in Eqs. (1.8.3.3) and (1.8.3.4) are required to satisfy the Pederson equation or localization equation (LE) [27,28]. LE aims to find the minimum energy according to the variational method. The LE is a pairwise condition for the orbitals ($\phi_{i\sigma}$), expressed as,

$$\langle \phi_{i\sigma} | V_{i\sigma}^{SIC} - V_{j\sigma}^{SIC} | \phi_{j\sigma} \rangle = 0. \tag{1.8.3.5}$$

The Eq. (1.8.3.5) requires solving N^2 parameters and it is computationally expensive. For this reason, earlier applications of PZSIC were limited to atoms and small molecules.

1.8.3.2 FERMI LÖWDIN ORBITAL SELF-INTERACTION CORRECTION

An alternative approach to solving the PZSIC Eq. (1.8.3.2) is by using Fermi-Löwdin orbitals (FLOs), as introduced by Pederson, Perdew and Ruzsinszky [29]. Yang, Pederson and Perdew introduced self-consistency for FLO-PZSIC or FLOSIC method in 2017 [35] with a Jacobi like iterative approach. The construction of FLOs involves the Löwdin orthogonalization of the Fermi orbitals (FOs). FOs are unitary and localized orbitals but are not orthogonal, and Löwdin orthogonalization is employed to achieve orthogonalization. The FO ($\boldsymbol{\phi}^{FO}$) construction requires the Fermi orbital descriptors (FODs), which are parameters in space. The FOs are defined as follows,

$$\phi_i^{FO}(\vec{r}) = \sum_j^{N_{occu}} \frac{\psi_j(\vec{a}_i)\psi_j(\vec{r})}{\sqrt{\rho(\vec{a}_i)}}. \tag{1.8.3.6}$$

Here, i and j are the orbital indices, ψ_j refers to the KS orbital, ρ represents the electron spin density, and $\vec{a}_i$ denotes the FOD position. The Löwdin orthogonalization is computed by diagonalizing the FO overlap matrix ($\boldsymbol{S}_{FO}$) and obtaining the $\boldsymbol{S}_{FO}^{-1/2}$ transformation matrix. The FLOs are then constructed using the equation $|\phi^{FLO}\rangle = \boldsymbol{S}_{FO}^{-1/2}|\phi^{FO}\rangle$. These orbitals ensure a unitarily invariant total energy. The FLOSIC approach offers a computational advantage over traditional PZSIC as it requires the optimization of $3N$ variables instead of N^2 parameters involved

in the LE [30,36]. The optimization process for the FODs can be viewed as analogous to a molecular geometry optimization process, Fig 1.5 shows a sample of the FOD structure for $[Fe(CO)_6]^{2+}$.

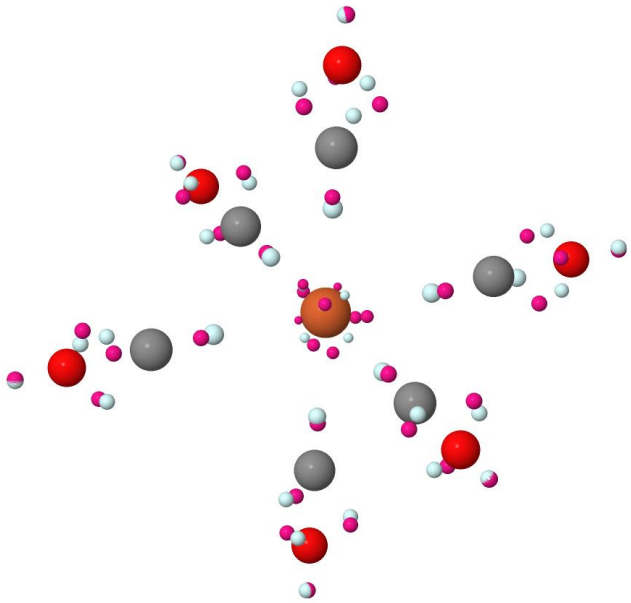

Fig. 1.5. FOD structure for $[Fe(CO)_6]^{2+}$ in the high spin state with 56 up and 52 down electrons.

The problem of obtaining the optimal set of FLOs is mapped to the problem of obtaining the optimal set of FODs. To achieve FOD optimization, we require the energy derivatives with respect to FOD positions to obtain the optimal FODs. Pederson obtained the FOD forces using energy derivatives [30,36] for FOD optimization as follows,

$$\frac{dE^{SIC}}{d\boldsymbol{a}_i} = \sum_{kl} \epsilon_{kl}^{k} \left\{ \left\langle \frac{d\phi_k^{FLO}}{d\boldsymbol{a}_m} \middle| \phi_l^{FLO} \right\rangle - \left\langle \frac{d\phi_l^{FLO}}{d\boldsymbol{a}_m} \middle| \phi_k^{FLO} \right\rangle \right\} \equiv \sum_{kl} \epsilon_{kl}^{k} \Delta_{lk,m}. \qquad (1.8.3.7)$$

The FLOSIC method is orbital-dependent, and to avoid orbital-dependent Hamiltonian matrix, an approximated Hamiltonian [35] is used in the FLOSIC code as follows,

$$\hat{H}_{mn\sigma} = \langle \phi_{m\sigma} | H_{\sigma}^{KS} + V_{m\sigma}^{SIC} | \phi_{n\sigma} \rangle. \qquad (1.8.3.8)$$

The Jacobi-like iterative procedure (hereon Jacobi rotation) is used to diagonalize the Hamiltonian in Eq. (1.8.3.8) [35]. The FLOSIC approach uses FLOs as localized orbitals and can be used in any one-electron SIC scheme. Most FLOSIC applications are performed using the PZSIC method, but there are a few other one-electron SIC approaches, such as orbital scaling SIC (OSIC) [66], locally scaled SIC (LSIC) [67], selective orbital SIC (SOSIC) [68], regional SIC (rSIC) [69], and global scaling SIC [70]. Any of these methods can utilize the FLO localization scheme to achieve the SIC.

1.8.3.3 SCALED SELF-INTERACTION CORRECTION METHODS

The PZSIC method is effective in accurately describing stretched bonds, anionic systems, and reaction barrier heights. However, PZSIC tends to overcorrect the SIE, which can lead to inaccuracies in energetic and density properties. To address this overcorrection, researchers have developed various scaling approaches that modify the correction applied by PZSIC to the density functional approximation (DFA). These scaling methods aim to strike a better balance between correcting the SIE and avoiding excessive overcorrection.

OSIC method propose to scale down the PZSIC energy functional by a constant orbital dependent value as follows [66],

$$E_{XC}^{OSIC-DFA} = E_{XC}^{DFA}[\rho_\uparrow, \rho_\downarrow] - \sum_{i\sigma}^{N_{OCC}} \chi_{i\sigma}^{k}\{U[\rho_{i\sigma}] + E_{XC}^{DFA}[\rho_{i\sigma}, 0]\}. \qquad (1.8.3.9)$$

The scaling factor is defined as $\chi_{i\sigma}^{k} = \int z_\sigma^k(\vec{r})\rho_{i\sigma}(\vec{r})d\vec{r}$. $\rho_{i\sigma}$ represents the orbital density, z_σ is the iso-orbital indicator, k is a constant value defined as $0 \leq k < \infty$ for tunning the scaling effects, and σ is the spin index. When k is sufficiently large, the DFA is recovered because z_σ is defined within 0 and 1. On the other hand, when $k = 0$, the PZSIC performance is recovered. Self-Coulomb and self-exchange-correlation terms are same as PZSIC in Eqs. (1.8.3.3) and (1.8.3.4). As mentioned before, the iso-orbital indicator z_σ is defined as $0 \leq z_\sigma \leq 1$. It is expressed as follows,

$$z_\sigma(\vec{r}) = \frac{\tau_\sigma^W(\vec{r})}{\tau_\sigma(\vec{r})}, \tag{1.8.3.10}$$

Eq. (1.8.3.10) represents the rational of the von Weiszäcker kinetic energy density $\tau_\sigma^W = \left|\vec{\nabla}\rho_\sigma(\vec{r})\right|^2/(8\rho_\sigma(\vec{r}))$ and the non-interacting kinetic energy density $\tau_\sigma = \frac{1}{2}\sum_i \left|\vec{\nabla}\psi_{i\sigma}(\vec{r})\right|^2$. In regions with single electron, τ_σ approaches τ_σ^W, resulting in a unity value for z_σ. On the other hand, for uniform electron density, τ_σ^W approaches zero, leading to $z_\sigma = 0$. The iso-orbital indicator plays a crucial role in controlling the scaling factor $\chi_{i\sigma}^k$, as it interpolates and balances the orbital electron density-dependent scaling factor.

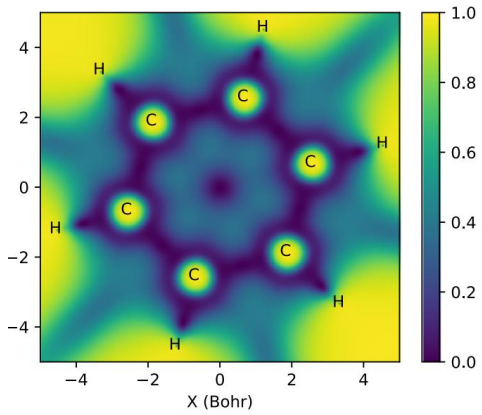

Fig. 1.6. Iso-orbital indicator represented as a 2D iso surface plot for benzene molecule, where single electron regions are represented by yellow and uniform electron density by blue.

In Fig. 1.6, the single electron regions are represented by yellow, while the uniform electron density regions are represented in blue. The locally scaled SIC (LSIC) method was invented in 2019, and this work was led by R. Zope in collaboration with the FLOSIC center, representing the of University of Texas at El Paso electronic structure lab, Central Michigan University, and Temple University. The LSIC method has shown remarkable performance for certain properties when compared either to experimental data or standard benchmarking datasets using the simplest LSDA functional. LSIC provides the correct $-1/r$ asymptotic potential, whereas the OSIC

provides an incorrect $-\epsilon_{HOMO}/r$ asymptotic potential. LSIC recovers the correct uniform gas limit description of the underlying DFA, while the PZSIC performs poorly (c.f. section 5.4.4). LSIC total energy is defined as follows,

$$E^{LSIC-DFA} = E^{DFA}[\rho_\uparrow, \rho_\downarrow] - \sum_{i\sigma}^{OCC}\{U^{LSIC}[\rho_{i\sigma}] + E_{XC}^{LSIC}[\rho_{i\sigma}, 0]\}, \quad (1.8.3.11)$$

where,

$$U^{LSIC}[\rho_{i\sigma}] = \frac{1}{2}\int d\vec{r}\, z_\sigma(\vec{r})\, \rho_{i\sigma}(\vec{r}) \int d\overrightarrow{r'}\, \frac{\rho_{i\sigma}(\overrightarrow{r'})}{|\vec{r}-\overrightarrow{r'}|}, \quad (1.8.3.12)$$

$$E_{XC}^{LSIC}[\rho_{i\sigma}, 0] = \int d\vec{r}\, z_\sigma(\vec{r})\, \rho_{i\sigma}(\vec{r})\, \epsilon_{XC}^{DFA}([\rho_{i\sigma}, 0], \vec{r}), \quad (1.8.3.13)$$

Eqs. (1.8.3.12) and (1.8.3.13) represent the LSIC self-Coulomb and self-exchange-correlation energies, respectively. The accurate description of LSIC is achieved by scaling down the self-Coulomb and self-exchange-correlation energy densities, interpolating within the single electron regions and the uniform electron regions (see Fig. 1.6).

1.9 REFERENCES OF CHAPTER 1

[1] D. Griffiths: Introduction to quantum mechanics (Prentice Hall, 1995).

[2] F. Giustino: Materials Modeling using Density Functional Theory (Oxford university press,2014).

[3] J. D. Jackson, Classical electrodynamics, 3rd ed. (Wiley, New York, NY, 1999).

[4] A. Szabo, and N. Ostlund, Modern Quantum Chemistry: Introduction to Advanced Electronic Structure Theory (Macmillan, 1982)

[5] T. L. Gilbert, "Hohenberg-kohn theorem for nonlocal external potentials," Phys. Rev. B 12, 2111–2120 (1975).

[6] W. Kohn and L. J. Sham, "Self-consistent equations including exchange and correlation effects," Phys. Rev. 140, A1133 (1965).

[7] R. O. Jones, “Density functional theory: Its origins, rise to prominence, and future,” Rev. Mod. Phys. 87, 897–923 (2015).
[8] R. Car, “Fixing Jacob's ladder”, Nature Chemistry 8, 820 (2016) .
[9] J. P. Perdew and A. Zunger, “Self-interaction correction to density-functional approximations for many-electron systems,” Phys. Rev. B 23, 5048 (1981).
[10] D. M. Ceperley and B. J. Alder, “Ground state of the electron gas by a stochastic method,” Phys. Rev. Lett.45, 566–569 (1980).
[11] C. Kittel, Introduction to Solid State Physics, 8th ed. (Wiley, 2004).
[12] J. P. Perdew, K. Burke, and M. Ernzerhof, “Generalized gradient approximation made simple,” Phys. Rev. Lett. 77, 3865 (1996).
[13] David C Langreth and MJ Mehl. “Beyond the local-density approximation in calculations of ground-state electronic properties,” Physical Review B, 28(4):1809,1983.
[14] John P Perdew and Wang Yue. “Accurate and simple density functional for the electronic exchange energy: Generalized gradient approximation,” Physical review B, 33(12):8800, 1986.
[15] Axel D Becke. “Density functional calculations of molecular bond energies,” The Journal of Chemical Physics, 84(8):4524-4529, 1986.
[16] J. Sun, A. Ruzsinszky, and J. P. Perdew, “Strongly constrained and appropriately normed semilocal density functional,” Phys. Rev. Lett. 115, 036402 (2015).
[17] J. Tao, J. P. Perdew, V. N. Staroverov, and G. E. Scuseria, “Climbing the density functional ladder: Nonempirical meta–generalized gradient approximation designed for molecules and solids,” Phys. Rev. Lett. 91, 146401 (2003).
[18] John P Perdew, Stefan Kurth, Aleˇs Zupan, and Peter Blaha. “Accurate density functional with correct formal properties: A step beyond the generalized gradient approximation,” Physical review letters, 82(12):2544, 1999.
[19] John P Perdew, Jianmin Tao, Viktor N Staroverov, and Gustavo E Scuseria. ”Meta-generalized gradient approximation: Explanation of a realistic nonempirical density functional,” The Journal of chemical physics, 120(15):6898{6911, 2004.
[20] Adrienn Ruzsinszky, Jianwei Sun, Bing Xiao, and Gbor I. Csonka. “A meta-gga made free of the order of limits anomaly,” Journal of Chemical Theory and Computation, 8(6):2078{2087, 2012. PMID: 26593840.
[21] Jianwei Sun, Bing Xiao, and Adrienn Ruzsinszky. “Communication: Effect of the orbital-

overlap dependence in the meta generalized gradient approximation,"2012.
[22] Jianwei Sun, Robin Haunschild, Bing Xiao, Ireneusz W Bulik, Gustavo E Scuseria, and John P Perdew. "Semilocal and hybrid meta-generalized gradient approximations based on the understanding of the kinetic-energy-density dependence," The Journal of chemical physics, 138(4):044113, 2013.
[23] Jianwei Sun, John P Perdew, and Adrienn Ruzsinszky. "Semilocal density functional obeying a strongly tightened bound for exchange," Proceedings of the National Academy of Sciences, 112(3):685-689, 2015.
[24] M. Ernzerhof and G. E. Scuseria, "Assessment of the Perdew-Burke-Ernzerhof exchange-correlation functional," J. Chem. Phys. 110, 5029 (1999).
[25] A. Dal Corso, "A pseudopotential plane waves program (pwscf) and some case studies," in Quantum-Mechanical Ab-initio Calculation of the Properties of Crystalline Materials, edited by C. Pisani (Springer Berlin Heidelberg, Berlin, Heidelberg, 1996) pp. 155–178.
[26] D. Porezag and M. R. Pederson, "Optimization of Gaussian basis sets for density-functional calculations," Phys. Rev. A 60, 2840–2847 (1999).
[27] M. R. Pederson, R. A. Heaton, and C. C. Lin, "Local-density Hartree-Fock theory of electronic states of molecules with self-interaction correction," J. Chem. Phys. 80, 1972 (1984).
[28] M. R. Pederson, R. A. Heaton, and C. C. Lin, "Density-functional theory with self-interaction correction: Application to the lithium molecule," J. Chem. Phys. 82, 2688 (1985).
[29] M. R. Pederson, A. Ruzsinszky, and J. P. Perdew, "Communication: Self-interaction correction with unitary invariance in density functional theory," J. Chem. Phys. 140, 121103 (2014).
[30] M. R. Pederson and T. Baruah, "Chapter eight - self-interaction corrections within the fermi-orbital-based formalism," (Academic Press, 2015) pp. 153 – 180.
[31] M. Chen, H.-Y. Ko, R. C. Remsing, M. F. Calegari Andrade, B. Santra, Z. Sun,A. Selloni, R. Car, M. L. Klein, J. P. Perdew, and X. Wu, "Ab initio theory and modeling of water," Proc. Natl. Acad. Sci. (2017), 10.1073/pnas.1712499114, https://www.pnas.org/content/early/2017/09/19/1712499114.full.pdf.
[32] R. C. Remsing, M. L. Klein, and J. Sun, "Dependence of the structure and dynamics of liquid silicon on the choice of density functional approximation," Phys. Rev. B96, 024203(2017).

[33] Sun, J., Remsing, R., Zhang, Y. et al. "Accurate first-principles structures and energies of diversely bonded systems from an efficient density functional." Nature Chem 8, 831–836 (2016). https://doi.org/10.1038/nchem.2535.

[34] Y. Zhao, D. G. Truhlar, "Construction of a generalized gradient approximation by restoring the density-gradient expansion and enforcing a tight Lieb–Oxford bound ", *J. Chem. Phys.* 128, 184109 (2008).

[35] Z.-h. Yang, M. R. Pederson, and J. P. Perdew, "Full self-consistency in the Fermi-orbital self-interaction correction," Phys. Rev. A 95, 052505 (2017).

[36] M. R. Pederson, "Fermi orbital derivatives in self-interaction corrected density functional theory: Applications to closed shell atoms," J. Chem. Phys. 142, 064112 (2015), https://doi.org/10.1063/1.4907592.

[37] C. Adamo and V. Barone, "Toward reliable density functional methods without adjustable parameters: The PBE0 model", J. Chem. Phys. 110, 6158–6170 (1999), https://doi.org/10.1063/1.478522.

[38] J. Heyd, G. E. Scuseria, and M. Ernzerhof, "Hybrid functionals based on a screened Coulomb potential", J. Chem. Phys. 118, 8207–8215 (2003), https://doi.org/10.1063/1.1564060.

[39] A.D. Becke, "Density-functional thermochemistry. III. The role of exact exchange" J.Chem.Phys. 98 5648-5652 (1993).

[40] C. Lee, W. Yang, R.G. Parr, "Development of the Colle-Salvetti correlation-energy formula into a functional of the electron density", Phys. Rev. B 37 785-789 (1998).

[41] S.H. Vosko, L. Wilk, M. Nusair, "Accurate spin-dependent electron liquid correlation energies for local spin density calculations: a critical analysis", Can. J. Phys. 58 1200-1211(1980).

[42] P.J. Stephens, F.J. Devlin, C.F. Chabalowski, M.J. Frisch, "Ab Initio Calculation of Vibrational Absorption and Circular Dichroism Spectra Using Density Functional Force Fields", J.Phys.Chem. 98 45 11623-11627 (1994).

[43] T. Yanai, D. P. Tew, N. C. Handy, "A new hybrid exchange–correlation functional using the Coulomb-attenuating method (CAM-B3LYP) " , Chem. Phys. Lett. Vol. 393, 1-3, 51-57 (2004).

[44] Y. Liu, C. Zhang, Z. Liu, D. G. Truhlar, Y. Wang, and X. He, "Supervised Learning of a Chemistry Functional with Damped Dispersion", Nat. Comp. Sci., 3, 48–58 (2023).

[45] T. Körzdörfer, S. Kümmel, and M. Mundt, Self-interaction correction and the optimized effective potential, J. Chem. Phys. 129, 014110 (2008).

[46] J. B. Krieger, Y. Li, and G. J. Iafrate, Systematic approximations to the optimized effective potential: Application to orbital-density-functional theory, Phys. Rev. A 46, 5453 (1992).
[47] Jiachen Li, Zehua Chen, and Weitao Yang, “Multireference Density Functional Theory for Describing Ground and Excited States with Renormalized Singles”, J. Phys. Chem. Lett. 13, 3, 894–903 (2022).
[48] Jürgen Gräfenstein, Dieter Cremer, “The combination of density functional theory with multi-configuration methods – CAS-DFT”, Chem. Phys. Lett., Volume 316, 5–6, 21, 569-577 (2000).
[49] Gerald Knizia and Garnet Kin-Lic Chan, “Density Matrix Embedding: A Simple Alternative to Dynamical Mean-Field Theory”, Phys. Rev. Lett. 109, 186404 (2012).
[50] Sebastian Wouters, Carlos A. Jiménez-Hoyos, Qiming Sun, and Garnet K.-L. Chan, “A Practical Guide to Density Matrix Embedding Theory in Quantum Chemistry”, J. Chem. Theory Comput. 12, 6, 2706–2719 (2016).
[51] Gubernatis, J., Kawashima, N., and Werner, P. (2016). “Quantum Monte Carlo Methods: Algorithms for Lattice Models”, Cambridge: Cambridge University Press. doi:10.1017/CBO9780511902581.
[52] E. R. Ylvisaker, W. E. Pickett, and K. Koepernik, “Anisotropy and magnetism in the LSDA+U method” Phys. Rev. B 79, 035103 (2009).
[53] B. Himmetoglu, A. Floris, S. de Gironcoli, and M. Cococcioni, Int. J. Quantum Chem. 114. 14 (2014).
[54] A. Georges, G. Kotliar, W. Krauth, and M. J. Rozenberg, “Dynamical mean-field theory of strongly correlated fermion systems and the limit of infinite dimensions”, Rev. Mod. Phys. 68, 13 (1996).
[55] Lars Hedin , “New Method for Calculating the One-Particle Green's Function with Application to the Electron-Gas Problem”, Phys. Rev. 139, A796 (1965).
[56] W. G. Aulbur, L. Jönsson, and J. W. Wilkins. "Quasiparticle calculations in solids", Sol. state Phys. 54, 1-218 (2000).
[57] F. Aryasetiawan, O. Gunnarsson, "The GW method", Rep. on Prog. in Phys. 61 237 (1998).
[58] A. D. Becke, “Density-functional exchange-energy approximation with correct asymptotic behavior ”, Phys. Rev. A 38, 3098 (1988).
[59] T. Tsuneda, and K. Hirao, “A new spin-polarized Colle-Salvetti-type correlation energy functional”, Chem. Phys. Lett. 268, 5, 510-520 (1997).

[60] T. Tsuneda , T Suzumura, and K. Hirao, “A new one-parameter progressive Colle–Salvetti-type correlation functional” , J. Chem. Phys. 110, 10664–10678 (1999).

[61] J. C. Slater, “Suggestions from Solid-State Theory Regarding Molecular Calculation” J. Chem. Phys. 43, S228 (1965), https://doi.org/10.1063/1.1701494.

[62] K.H. Johnson, “ “Multiple-Scattering" Model for Polyatomic Molecules”, J. Chem. Phys. 45, 3085–3095 (1966) https://doi.org/10.1063/1.1728065.

[64] J. C. Slater and K. H. Johnson, “Self-Consistent-Field Xα Cluster Method for Polyatomic Molecules and Solids”, Phys. Rev. B 5, 844 (1972).

[65] J. L. Bao, L. Gagliardi, and D. G. Truhlar , “Self-Interaction Error in Density Functional Theory: An Appraisal”, J. Phys. Chem. Lett. 9, 9, 2353–2358 (2018).

[66] O. A. Vydrov, G. E. Scuseria, J. P. Perdew, A. Ruzsinszky, and G. I. Csonka, “Scaling down the Perdew-Zunger self-interaction correction in many-electron regions,” J. Chem. Phys. 124, 094108 (2006).

[67] R. R. Zope, Y. Yamamoto, C. M. Diaz, T. Baruah, J. E. Peralta, K. A. Jackson, B. Santra, and J. P. Perdew, “A step in the direction of resolving the paradox of Perdew-Zunger self-interaction correction,” J. Chem. Phys. 151, 214108 (2019).

[68] Y. Yamamoto, S. Romero, T. Baruah, and R. R. Zope, “Improvements in the orbitalwise scaling down of Perdew–Zunger self-interaction correction in many-electron regions,” J. Chem. Phys. 152, 174112 (2020).

[69] T. Tsuneda, M. Kamiya, and K. Hirao, “Regional self-interaction correction of density functional theory,” J. Comput. Chem. **24**, 1592–1598 (2003).

[70] S. Klüpfel, P. Klüpfel, and H. Jónsson, “The effect of the perdew-zunger self-interaction correction to density functionals on the energetics of small molecules,” J. Chem. Phys. 137, 124102 (2012).

[71] Z. J. Buschmann, “Two Developments for Efficient and Accurate Density Functional Theory Calculations.” Open Access Theses & Dissertations, University of Texas at El Paso. ScholarWorks@UTEP.

CHAPTER 2: COMPLEXITY REDUCTION IN SELF-INTERACTION-FREE DENSITY FUNCTIONAL CALCULATIONS USING THE FERMI-LÖWDIN SELF-INTERACTION CORRECTION METHOD

2.1 ABSTRACT

JCP: 250 words Fermi-Löwdin (FLO) self-interaction-correction (SIC) (FLOSIC) method uses symmetric orthogonalized Fermi orbitals as localized orbitals in one-electron SIC schemes resulting in a formal reduction in the scaling of SIC methods (e.g. Perdew-Zunger method) but requires identifying a set of Fermi orbital descriptors used to define the FLOs which can be computationally taxing. Here, we propose to simplify the SIC calculations using a selective orbital scaling self-interaction correction (SOSIC) by removing SIE from a select set of orbitals that are of interest. We illustrate the approach by choosing a valence set of orbitals as active orbitals in the SOSIC approach. The results obtained using the vSOSIC scheme are compared with those obtained with PZSIC which corrects for all the orbitals. The comparison is made for atomization energies of the AE6 set and a subset of MGAE109, barrier heights of BH6 and WCPT18 sets, ionization energies estimated as absolute HOMO eigenvalues, the polarizability of select molecules, exchange coupling constant and spin densities of Cu containing complexes, and vertical detachment energies (VDE) of water cluster anions. The agreement between the two methods is within a few percent for the majority of the properties. The MAE in the VDE of water cluster anions estimated from the highest occupied eigenvalue with vSOSIC-PBE with respect to benchmark CCSD(T) results is only 15meV making vSOSIC-PBE an excellent alternative to the CCSD(T) to obtain the VDE of water cluster anions. As an illustration of the computational effectiveness, the vSOSIC calculation on $[Cu_2Cl_6]^{2-}$ complex, show that in addition to the cost savings from employing fewer orbitals to account for SIC, the FOD optimization in vSOSIC is also noticeably smoother and faster.

2.2 INTRODUCTION

The low computational expense combined with relatively good accuracy of density functional theory (DFT) [1,2] has made it a quantum mechanical method of choice to study the electronic structure of various types of materials, from atoms and molecules to nanostructures to periodic materials. Practical DFT calculations require approximation to the unknown exchange-correlation functional, and numerous density functional approximations (DFAs) with varying degrees of complexity have been proposed. Many failures of the DFAs have been ascribed to the self-interaction error (SIE) present in the approximate exchange-correlation functionals. The problem arises since the self-Coulomb energy is not completely canceled by the self-exchange energy when the exact, but unknown, exchange-correlation functional is approximated. A few illustrative examples of the failures of DFA are charge delocalization in proteins [3], completely different charge distribution on Kevan structure for the solvated electron [4], spurious charge transfer in organic acid-base cocrystals [5], severe overestimation of hyperpolarizabilities in conjugated molecules [6], structural distortion in the electron polaron model systems [7], a lack of size-intensivity of ionization potential [8] and so on. The self-interaction correction (SIC) methods to remove SIE in an orbital-wise manner were devised long ago [9–17].

The most well-known one-electron SIC method is the Perdew-Zunger SIC (PZSIC) [10,14] method wherein an orbital by orbital correction is applied to the DFA total energy [10]. The PZSIC energy is given by,

$$E^{PZSIC}[\rho_\uparrow, \rho_\downarrow] = E^{DFA}[\rho_\uparrow, \rho_\downarrow] - \Sigma_{i\sigma}^{OCC}\{U[\rho_{i\sigma}] + E_{XC}^{DFA}[\rho_{i\sigma}, 0]\}. \tag{2.1}$$

Here, E^{DFA} is the DFA total energy, $\rho_\uparrow$, $\rho_\downarrow$, and $\rho_{i\sigma}$ are up spin, down spin, and orbital densities, respectively; $U[\rho_{i\sigma}]$ and $E_{XC}^{DFA}[\rho_{i\sigma}, 0]$ are the Coulomb and approximate exchange energies. The PZSIC energy minimization corresponds to finding an optimal unitary transformation of canonical Kohn-Sham orbitals and results in a set of $M(M-1)/2$ conditions (for M occupied orbitals) known as the localization equations [18,19]. These equations are given by

$$\langle \phi_i | V_i - V_j | \phi_j \rangle = 0. \tag{2.2}$$

Here, V_i is the sum of Coulomb and exchange-correlation potential of the i^{th} orbital. Although not as popular as standard gradient-based DFAs, a number of researchers have adopted PZSIC [15,20–55]. Many implementations of the PZSIC use localized orbitals obtained using various criteria [37,56,57]. In 1984, Luken and Culberson observed that properties of the Fermi hole can be used to transform canonical orbitals into a set of localized orbitals [58,59]. As these orbitals are not orthogonal, they proposed a symmetric orthogonalization procedure to obtain a set of orthogonal orbitals. In 2014, Pederson, Ruszinsky and Perdew used these orbitals, which they called Fermi-Löwdin orbitals, to obtain PZSIC energy [60]. This results in a unitary invariant implementation of the PZSIC energy functional (Eq. 2.1). The Fermi orbitals (FO) [58,59] are given by

$$F_{j\sigma}(\vec{r}) = \sum_i^{N_\sigma} \frac{\psi_{i\sigma}(\vec{a}_{j\sigma})\psi_{i\sigma}(\vec{r})}{\sqrt{\rho_\sigma(\vec{a}_{j\sigma})}}. \tag{2.3}$$

Here, the sum of $i\sigma$ represents the sum over Kohn-Sham orbitals ($\psi_{i\sigma}$) and j is the FO index (local orbital), ρ_σ is the total electron spin density, and $\vec{a}_{j\sigma}$ is the so-called Fermi orbital descriptor (FOD) position. The Fermi orbitals are further orthogonalized using the Löwdin method to give the Fermi-Löwdin orbitals (FLOs). The PZSIC energy is minimized by varying the FOD positions in combination with a conjugate gradient or BFGS algorithm [61,62]. The FLOSIC method [60–65] ensures size extensivity, as well as unitary invariance of the total energy. It also simplifies the problem since instead of satisfaction of $N(N-1)/2$ equations only $3N$ variables, where N is the number of orbitals, need to be optimized. This results in a significant reduction in the formal cost of the SIC calculations.

The FLOSIC method has been used to study a wide range of chemical and physical properties [10,34,36,43,66–101]. As mentioned above, obtaining the SIC energy in the PZSIC requires the determination of the optimal FOD positions. In practice, however, the optimization of FOD is a slow process due to the complicated/shallow potential energy surface generated by the FODs, especially for systems containing transition metal (TM) atoms. The FOD optimization of systems with TM atoms is particularly difficult and can often require a few hundred steps. Moreover, the number of steps required grows as the number of FODs increases. Our experience with the FOD

optimizations shows that the difficulties primarily arise from the optimization of core FODs. To alleviate this problem, approaches such as freezing the core FOD for the 1s orbitals or the use of pseudopotential have been adopted in some FLOSIC calculations on transition metal and some organic complexes [79,84,102].

In this work, we propose a simplification of the FLOSIC calculation by selecting a subset of Kohn-Sham orbitals in constructing FLOs for the SIC calculations. Since the physical properties of systems are determined mainly by the valence electrons, we choose this subset to be the valence orbitals. We validate this approach by performing extensive tests on a variety of systems on several different properties. We show that the proposed simplified scheme, which results in a substantial reduction in the number of parameters (FODs) to be optimized, reproduces results of the *full* all-electron FLOSIC method within 1-2 kcal/mol and that for many properties, in fact, provides slightly improved results. We have applied the present approach to the lowest three rungs of functionals, namely, local spin density approximation (LSDA), Perdew-Burke-Ernzerhof generalized gradient approximation (PBE) and r2SCAN meta-GGA functionals. We believe this is the first time SIC-r2SCAN approach has been assessed for a range of electronic properties.

The details about the present approach and its implementation are provided in the next section followed by results and discussion.

2.3 METHODOLOGY

We divide the N occupied KS orbitals into groups of P passive and $(N - P)$ active orbitals such that the corrected exchange-correlation energy can be written as [72]

$$E^{SOSIC-DFA} = E_{XC}^{DFA}[\rho_\uparrow, \rho_\downarrow] - \sum_{i\sigma=1}^{P} X_{i\sigma}^{k}(U[\rho_{i\sigma}] + E_{XC}^{DFA}[\rho_{i\sigma}, 0]) - \sum_{i\sigma=P+1}^{OCC} Y_{i\sigma}^{k}(U[\rho_{i\sigma}] + E_{XC}^{DFA}[\rho_{i\sigma}, 0]) \quad (2.4)$$

Here, $X_{i\sigma}^{k}$ and $Y_{i\sigma}^{k}$ can be considered as scaling factors that can be determined using various criteria [66,74]. The value of P should be chosen carefully. For example, by applying full SIC correction to the orbitals that participate in the stretched bonds and scaling down SIC for other orbitals, Yamamoto and coworkers were able to obtain barrier heights of BH6 dataset within the chemical accuracy [74] using this selective orbital scaling SIC (SOSIC). As our purpose in this work is to simplify the SIC approach to improve its computational efficiency, we choose P to be the core orbitals with the factors $X_{i\sigma}^{k} = 0$ and $Y_{i\sigma}^{k} = 1$. This amounts to applying the full SIC only to the valence electrons. This method of selectively applying SIC to the valence electron will be referred to as vSOSIC hereafter.

We choose the P core electrons as shown in Table 2.1. For example, in the case of manganese which has an electronic configuration $[Ar]4s^2 3d^5$, P is 10, i.e., only the electrons in the $3s$, $3p$, $3d$ and $4s$ are considered for the SIC calculations. Previous calculations indicate that a full shell should be included to allow shell hybridization in the SIC calculations. It is noted that the FOD positions for atoms often follow the shell structure such that four FODs transcribe to the second shell $(2s, 2p)$, 9 for the third shell $(3s, 3p, 3d)$, etc. Therefore, the use of $[Ar]$ core, in this case, is not recommended. The $3d$ transition metal atoms from scandium to zinc are assigned a neon core similar to a small core in effective core potential (SC ECP) schemes. Such a choice considerably simplifies SIC calculations due to reduction in the time-consuming task of calculating orbitalwise SIC potentials. More importantly, it also facilitates the optimization of the FODs since often it is the core FODs that are more difficult to optimize. We note in passing that the proposed scheme also permits the application of SIC in selected regions in space in the spirit of embedding approaches for applications such as, for example, single atom catalysis. Such applications will be pursued in subsequent studies.

Table 2.1. Sets of criteria for determining the value P in Eq. (2.4) for hydrogen up to the barium atom in order to differentiate core and valence electrons.

	Criteria #1 Large core (LC)		Criteria #2 Small core (SC)	
Z	No. core	core-shell	No. core	core-shell
1-4	0		0	
5-12	2	He: $1s^2$	2	He: $1s^2$
13-30	10	Ne: [He] $2s^2 2p^6$	10	Ne: [He] $2s^2 2p^6$
31-48	28	[Ar] $3d^{10}$	10	Ne: [He] $2s^2 2p^6$
49-56	46	[Kr] $4d^{10}$	28	[Ar] $3d^{10}$

[a] Reference 116

In the vSOSIC method, localized Fermi orbitals are constructed from the valence Kohn-Sham orbitals and valence electron density as,

$$F_{j\sigma}(\vec{r}) = \sum_{i=P+1}^{N} \frac{\psi_{i\sigma}(\vec{a}_{j\sigma})\psi_{i\sigma}(\vec{r})}{\sqrt{\rho_{\sigma}^{val}(\vec{a}_{j\sigma})}}. \tag{2.5}$$

Here, $\rho_{\sigma}^{val}(\vec{a}_{j\sigma}) = \sum_{i\sigma=P+1}^{N} |\psi_{i\sigma}(\vec{a}_{j\sigma})|^2$, N is the number of electrons and $\vec{a}_{j\sigma}$ are the Fermi-orbital descriptors. The Fermi-Löwdin orbitals ($\phi_{i\sigma}(\vec{r})$) are obtained after symmetric orthogonalization of the Fermi orbitals from Eq. (2.5). These FLOs are used to compute the SIC potentials and energies. Naturally, vSOSIC requires less number of FODs than the number of occupied orbital. FODs for $[Cu_2Cl_6]^{2-}$ is shown in Fig. 2.1 as an example where 82 FODs are present instead of 162.

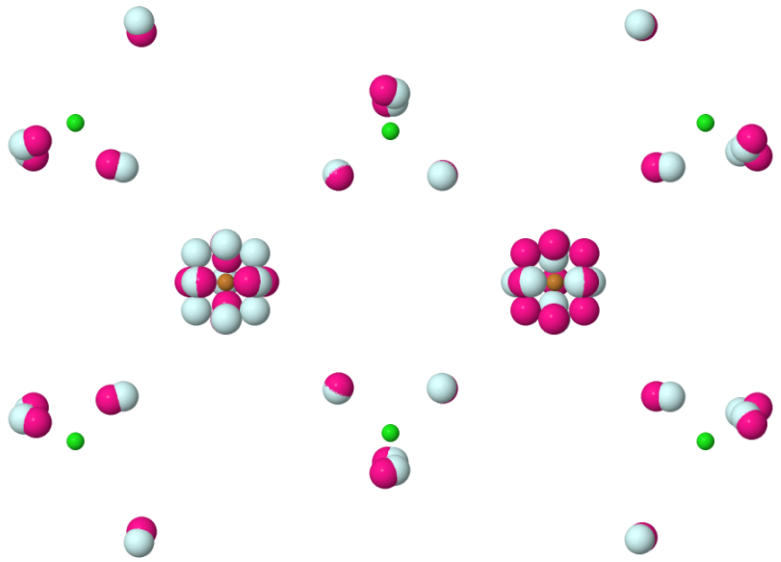

Fig 2.1. [Cu2Cl6]2− SOSIC Fermi orbital descriptors. The magenta (grey) FOD corresponds spin up (down) channel. The orange (green) dots represent copper (chlorine) atom positions. Instread of 162 FODs, vSOSIC uses only 82 FODs.

Self-consistency can be obtained either using optimized effective potential within the Kriger-Li-Ifarate approximation [64] or using the Jacobi update approach [63]. We have used the Jacobi update approach in this work. Fig. 2.2 pictorially presents how the SOSIC Hamiltonian is constructed.

$$\hat{H} = \hat{H}^{DFA} + \hat{H}^{SOSIC}$$

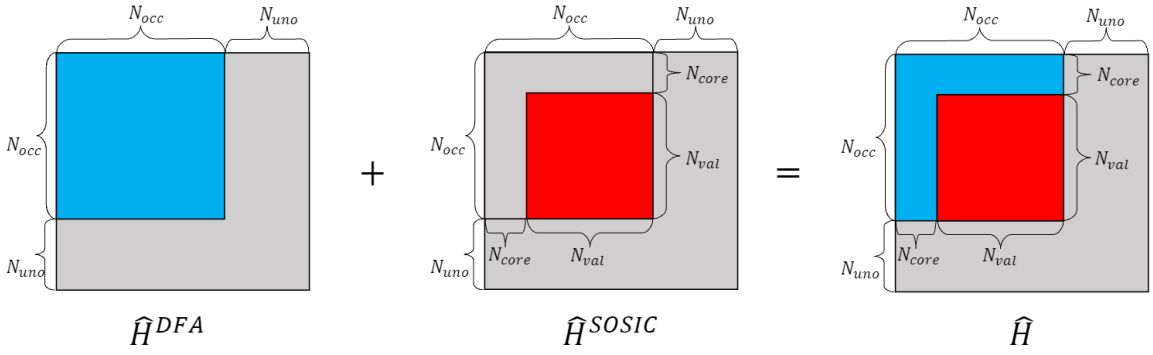

Fig 2.2**.** Visual representation of the DFA+SIC Hamiltonian construction in the SOSIC approach.

We first construct a SIC Hamiltonian as described by Yang *et al.* [63] as

$$H_\sigma = H_\sigma^{DFA} + \sum_{i,j=P+1}^{N_\sigma} \frac{1}{2}\left(V_{ij}^{i\sigma} + V_{ji}^{j\sigma}\right)|\phi_{i\sigma}\rangle\langle\phi_{j\sigma}| \tag{2.6}$$

where, $V_{ij}^{i\sigma} = \langle\phi_{i\sigma}|V^{i\sigma}|\phi_{j\sigma}\rangle$ being the SIC potential for the i^{th} orbital of spin σ. For the vSOSIC case, the SIC part of the Hamiltonian has $M \times M$ non-vanishing elements where $M = N - P$. The Jacobi update approach is used to derive the orthogonal eigenvectors. Once the self-consistency is achieved for a given FOD configuration, the forces on the FODs are calculated [61,62] and the FOD positions are optimized either using the LBFGS or conjugate gradient schemes [103]. We show in Fig. 2.3 the SOSIC algorithm with Jacobi approach.

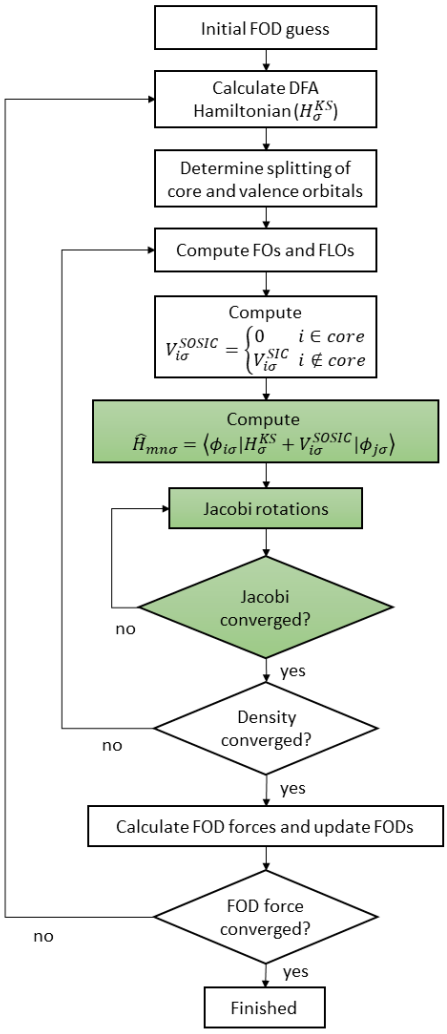

Fig. 2.3. vSOSIC algorithm flowchart for Jacobi rotations approach

The vSOSIC calculations are performed for the *non-empirical* functionals at the three lowest rungs of functional ladder. These are local spin density approximation (LSDA), generalized gradient approximation (GGA), and meta-GGA. We choose PW92 correlation functional [104] for the LSDA, Perdew-Burke-Ernzerhof (PBE) parameterization for the GGA [105,106], and r^2SCAN meta-GGA functionals [107]. For comparison, we have also included PZSIC calculations using FLOs where FLOs are constructed using all Kohn-Sham orbitals as in previous FLOSIC calculations. The PZSIC-LSDA and PZSIC-PBE calculations have been reported earlier while the PZSIC-r^2SCAN results reported herein are new results.

We have modified the FLOSIC code [108] for the work described here. The NRLMOL basis set is used for all calculations in this work [109]. For the vertical detachment energy calculations of water cluster anions, we used the NRLMOL basis set [109] with extra diffused functions to account for the anionic nature of the water clusters [110]. The Gaussian exponents for the extra functions are provided by Yagi *et al*. [111] where their values are 9.87×10^{-3}, 8.57×10^{-3}, and 3.72×10^{-3} for oxygen s and p, and hydrogen s functions, respectively.

As mentioned earlier this is the first work that reports FLOSIC-r2SCAN calculations on a wider range of properties. We therefore briefly comment on the numerical details of SIC calculations with r^2SCAN. In our earlier works [73,87], we have implemented and discussed the performance and numerical sensitivity of the SCAN and rSCAN functionals. The sensitivity of the SCAN functional to the choice of the numerical grid has been noted in a few studies [73,87,112–115]. The numerical instability of SCAN is primarily due to its interpolation function, which is smoothed out in rSCAN and r^2SCAN functionals. The r^2SCAN functional [107] is numerically more stable than the original SCAN and requires a less dense grid. We note that SIC calculations typically require denser numerical grids than the standard DFA calculations as the SIC contributions to the Hamiltonian/Fock matrix elements and SIC energy corrections are evaluated using the orbital densities that can vary far more rapidly than the total spin densities used in evaluating corresponding DFA contributions. Our earlier work has shown that FLOSIC calculations with SCAN functional typically requires very dense grids with about 140000 grid points per atom. We have examined the numerical needs of r^2SCAN in the FLOSIC calculations. We find that FLOSIC-r^2SCAN calculations require a factor of 2-4 times fewer grid points than FLOSIC-SCAN calculations. To describe the energy landscape in covalent bond stretching or reaction pathway, however, it requires a denser mesh than the default mesh of the FLOSIC code. The numerical mesh used in the present SIC-r^2SCAN calculations has roughly 1.1–1.5 times more grid points than the mesh requirements of the SIC-LSDA.

2.3 RESULTS

In this section, we first present the results on energy related properties such as atomization energies, reaction barrier heights, ionization potentials, binding energies of water cluster, and

magnetic exchange coupling parameters followed by polarizabilities which is a density related property using the present vSOSIC approach to assess its performance in comparison to the *all-orbital* PZSIC results in which all canonical KS orbitals are included in the construction of the Fermi-Löwdin orbitals, and SIC energy is calculated by summing SIC energy contribution of all orbitals. We further extend this assessment to include density-related properties such as static dipole polarizabilities of select molecules containing fourth-row elements in the periodic table.

2.3.1 ATOMIZATION ENERGIES

We evaluated the performance of vSOSIC atomization energies (AEs) on the AE6 [117] dataset and a set of 37 molecules from the G2/97 dataset [118]. AE6 consists of the atomization energies of six molecules and is typically used as a small representative benchmark set of the larger main group atomization energy (MGAE109) dataset. We calculated atomization energies as follows, $AE = \sum_i^{N_{atoms}} E_i - E_{mol}$, where E_i is the energy of the atoms and E_{mol} is the energy of the molecule. The mean absolute errors (MAEs) for the AE6 set are derived by comparing against the values from Ref. 117 and are shown in Table 2.2. Since the vSOSIC includes a smaller set of orbitals, we can expect the errors in atomization energies to be between those for DFA and PZSIC-DFA errors. This trend can be seen from Table 2.2.

Additionally, we studied the 37 molecules used in our earlier work (Ref. 87). We experienced SCF convergence issues with the vSOSIC approach for LiBr and NaBr with Jacobi rotation when a large core SOSIC treatment is used on the bromine atom. In such cases, using small core SOSIC can eliminate the issues.

Table 2.2. Mean absolute error (MAE) in kcal/mol and mean absolute percentage error (MAPE) in % of atomization energy for the data sets AE6 and 37 molecules[a,b].

Functional	Method	MAE(kcal/mol)		MAPE(%)	
		AE6	37-molecules	AE6	37-molecules
LSDA	DFA	74.3[a]	64.5	15.9[a]	24.2[b]
LSDA	PZSIC	58.0[a]	46.8[b]	9.4[a]	13.4[b]
LSDA	vSOSIC	66.6	51.1	11.0	13.8
PBE	DFA	13.4[a]	23.7[b]	3.3[a]	8.6[b]
PBE	PZSIC	18.8[a]	20.2[b]	6.8[a]	9.7[b]
PBE	vSOSIC	16.3	22.7	5.3	9.6
r^{2}SCAN	DFA	3.0	16.0	1.9	6.1
r^{2}SCAN	PZSIC	26.3	16.7	6.9	9.9
r^{2}SCAN	vSOSIC	17.2	17.1	5.1	8.9

[a] Reference 119
[b] Reference 87

The qualitative performance of vSOSIC using a small core for the larger atoms is summarized in Table 2.2 compared against Ref. 118. The trends in atomization energies for the AE6 and the larger set are similar for LSDA in that the MAEs are reduced with PZSIC-LSDA compared to DFA-LSDA. With PBE and r^2SCAN functionals, the MAEs for the larger set are comparable with the three approaches. On the other hand, with AE6 set, the application of SIC introduces large errors with r^2SCAN. Since AE6 is a small set, the larger set is more likely to show the general performance of these functionals. Overall, the vSOSIC-DFA MAEs are close to those of PZSIC-DFAs.

2.3.2 BARRIER HEIGHTS

The barrier heights of chemical reactions are difficult to describe correctly with a DFA since the SIE appears in stretched bond situations at the saddle point calculation. DFAs due to SIEs tend to incorrectly provide lower energies for the transition states. Previously, PZSIC performance on the BH76 set was studied [120], and it is reported that both accurate energy functional as well as accurate electron density are important for describing barrier height calculations. Furthermore, previous SOSIC work [74] on the reaction barrier heights of the BH6 dataset [117] showed that SOSIC works well when it includes only the orbitals corresponding to the stretched bonds.

Here, we systematically compare the performance of the vSOSIC methods on reaction barrier heights using the BH6 set. The reactions of BH6 are (a) $OH + CH_4 \rightarrow CH_3 + H_2O$, (b) $H + OH \rightarrow H_2 + O$, and (c) $H + H_2S \rightarrow H_2 + HS$. There are six barrier heights from the combined

forward and reverse reaction pathways. Table 2.3 provides a summary of the results and shows that vSOSIC performance is nearly identical to that of PZSIC with comparable MAEs for the three functionals.

Table 2.3. Mean absolute error (MAE) in kcal/mol for the reaction barrier heights of BH6 and WCPT18 sets.

Functional	Method	MAE(kcal/mol)	
		BH6	WCPT18
LSDA	DFA	17.6[a]	17.7
LSDA	PZSIC	4.9[a]	7.5
LSDA	vSOSIC	5.2	7.6
PBE	DFA	8.0[a]	8.8
PBE	PZSIC	4.2[a]	10.3
PBE	vSOSIC	4.1	9.4
r^{2}SCAN	DFA	7.6	6.2
r^{2}SCAN	PZSIC	2.8	6.0
r^{2}SCAN	vSOSIC	2.6	5.5

[a]Reference 119

Since the BH6 set is a rather small set of reaction barriers, we also additionally used the WCPT18 set [121] to evaluate the vSOSIC performance in comparison to PZSIC. The WCPT18 set consists of 18 reaction barrier heights and requires 28 single-point calculations. The set consists of 9 water-catalyzed proton-transfer reactions that involve zero, one, or two water molecules as a catalyst. The mean absolute errors (MAEs) of the WCPT18 set presented in Table 2.3 for LSDA, PBE and r^2SCAN show that the vSOSIC and PZSIC results agree within 1 kcal/mol. This is expected since the proton transfer reactions involve stretching electron density on the hydrogen atom where SIC is truly needed. This stretching happens on valence orbitals, where vSOSIC and PZSIC have the same SIC effect on these orbitals.

2.3.3 HIGHEST OCCUPIED MOLECULAR ORBITAL (HOMO) EIGENVALUES FOR 38 SELECTED MOLECULES

Janak's theorem relates that the negative of the HOMO eigenvalue in DFT is equivalent to the vertical ionization potential (IP) [122–125]. Since many DFAs do not have a correct asymptotic

potential character, their exchange-correlation potentials tend to be too shallow in the asymptotic region, resulting thereby in absolute HOMO eigenvalues that underestimate the IPs. PZSIC is shown to lower the HOMO energy levels by deepening the exchange-correlation potential and widening the HOMO-LUMO gaps. This usually results in a much-improved agreement between absolute of HOMO eigenvalues with experimental IPs or higher-level theories.

Fig. 2.4 compares the difference of absolute of HOMO eigenvalues of the 38 molecules (the 37 molecules used in the atomization energies plus CN^-) that are a subset of G2/97 set and experimental IP for PZSIC-DFA and vSOSIC-DFA for LSDA, PBE, and r^2SCAN. Although absolute HOMO eigenvalues in PZSIC estimate IPs better than DFA, the absolute HOMO eigenvalues of PZSIC overestimate the experimental IPs by up to 4 eV for the set of molecules studied here. vSOSIC HOMO eigenvalues are in good agreement with PZSIC. The eigenvalue spectra of LiBr and NaBr molecules are shown in Supplementary Materials where it can be seen that SOSIC and PZSIC valence eigenvalues are essentially identical.

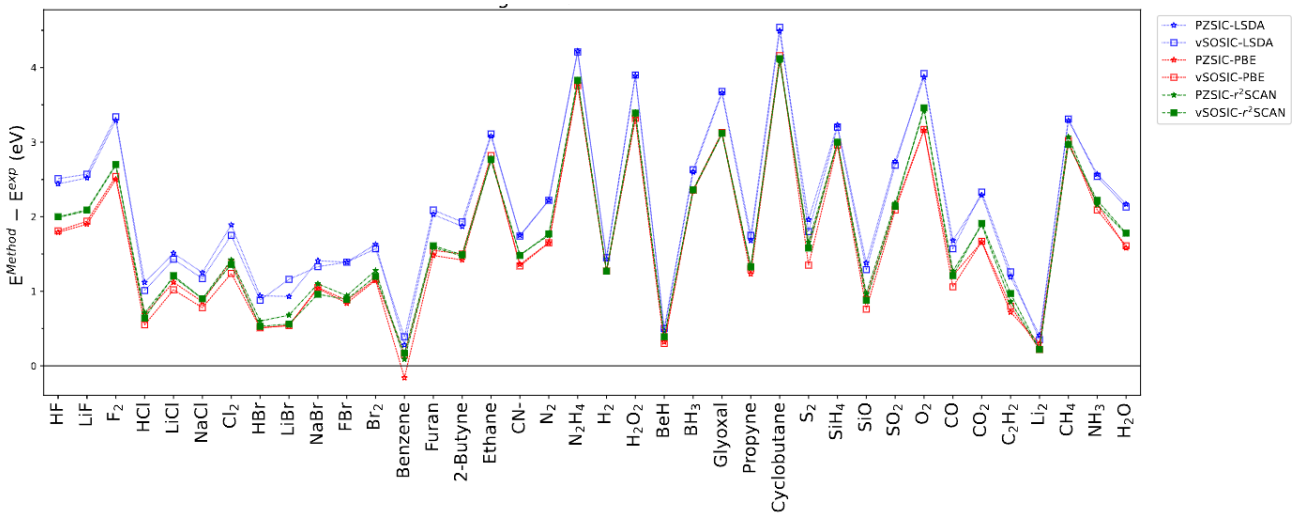

Fig. 2.4. Negative of HOMO eigenvalues of 38 selected molecules, a subset of G2/97 set, compared against experimental ionization potential for three functionals and two SIC methods.

2.3.4 VERTICAL DETATCHMENT ENERGY OF WATER CLUSTER ANIONS

Electron hydration is an important phenomenon in biological processes [126,127]. Modeling such behavior is challenging for the local and semi-local DFA. The semi-local GGA and meta-GGA and B3LYP performance is rather poor for such systems as the electron attached on the water cluster is delocalized over the system. Typically, the extent of the delocalization worsens with increasing water cluster size and consequently post-Hartree-Fock methods are often the methods of choice. Recent studies by Vargas and coworker showed that SIC methods can be a good alternative to MP2 and LC-BOP level of theory for describing the systems of hydrated electrons [97]. An excess electron in water clusters can be dipole-bound, trapped on a cluster surface, solvated internally to a cluster, or bound to dangling OH bonds of a cluster [111]. In all situations, active orbitals play an important role. Earlier studies carried out by this group on electron binding to water clusters have shown that PZSIC-PBE can predict the vertical detachment energies (VDE) in comparable accuracy as the CCSD(T) level of theory when the negative of the HOMO eigenvalues are used to estimate VDE. To assess the present SOSIC approach, we have computed the vertical detachment energies of water clusters from the absolute of the HOMO eigenvalues with only the PBE functional. We consider water dimer, five trimers (3AAa, 3Da, 3I-1a, 3I-2a, and 3La), four tetramers (4AAa, 4Da, 4Ia, and 4La), five pentamers (5AA-1a, 5AA-2a, 5Da, 5Ia, and 5La), and five hexamers (6AA-1a, 6AA-2a, 6Da, 6Ia, and 6La) The same isomer notation is used as in the references 97 and 111.

The calculated VDEs are shown in Table 2.4 where PZSIC-PBE, vSOSIC-PBE, and CCSD(T) values from Ref. 111 are compared. The vSOSIC-PBE performance is very close to PZSIC-PBE with MAEs of 16.9 (PZSIC-PBE) and 15.0 meV (vSOSIC-PBE) when compared to CCSD(T) values, respectively. The differences between the PZSIC-PBE and vSOSIC-PBE VDE values are 20 meV or less for the majority of the isomers except for 6AA-1a for which the difference is 53 meV.

Table. 2.4. Vertical detachment energy of water cluster anions estimated with the negative of HOMO eigenvalues. MAE (in meV) are calculated with respect to CCSD(T).

System	PZSIC-PBE	vSOSIC-PBE	1orb-SOSIC-PBE	CCSD(T)[a]
2La	30	33	18	29
3AAa	180	184	149	187
3Da	14	17	4	6
3I-1a	205	216	107	190
3I-2a	185	188	146	175
3La	148	156	129	146
4AAa	314	319	279	336
4Da	42	62	41	49
4Ia	456	445	314	439
4La	236	246	216	255
5AA-1a	358	385	294	370
5AA-2a	354	357	315	376
5Da	73	77	54	61
5Ia	467	473	372	469
5La	277	282	254	294
6AA-1a	521	574	425	553
6AA-2a	443	456	392	477
6Da	114	118	87	104
6Ia	904	891	671	839
6La	358	367	331	381
MAE	16.9	15.0	56.9	

[a] Reference 111

Typically, the extra electron in water cluster anions is unbound in the standard DFA calculations with positive HOMO eigenvalues. As demonstrated above, the vSOSIC-PBE and PZSIC-PBE can accurately describe electron binding in these clusters. Thus, removal of SIE from the valence orbitals can cure the failure of DFAs. As an interesting application of vSOSIC, here we further examine if removing the SIE for just one orbital (the last orbital with the extra electron) can improve the description of electron binding in these clusters. The results of this one-orbital SOSIC show that the removal of SIE from just one orbital results in electron binding with negative HOMO eigenvalues for all the clusters. In this case, the VDEs obtained from the HOMO eigenvalues

however show a higher MAE of 56.9 meV. Although this MAE is larger compared to the all orbital PZSIC-PBE, it is still comparable to MP2 MAE (44 meV) and far better than that of B3LYP (238 meV) [97]. It is remarkable that the removal of SIE from just one orbital (extra electron) can result in a major improvement in the VDEs of water anions since the cost of this calculation is practically the same as that of PBE functional. Since the SIC is applied only to the extra electron, the FLO in this case is same as the Kohn-Sham orbital. This approach therefore can be readily introduced in most density functional codes.

2.3.5 BINDING ENERGIES OF WATER CLUSTERS

Water is essential in biological systems but has complex intermolecular interactions that include both hydrogen bonds and Van der Waals interactions. Non-local electron correlation is considered necessary for an accurate description of water [128]. There are numerous models for water clusters that account for van der Waals interactions to describe extended water. Here we consider the effect of SIC on the binding energies of water clusters. The binding energies per water cluster are calculated as $BE = \frac{1}{n}[E[(H_2O)n] - nE(H_2O)]$, where n is the cluster size. By this definition, the BE for bound clusters has a negative sign.

Sharkas and coworkers examined the performance of DFA and PZSIC for the binding energy of water clusters from the WATER27 set [129], which included global minimum configuration of water dimer to water pentamer, four low-lying isomers of water hexamer (prism, cage, book, and ring), and the two most stable isomers of water octamer [96]. With the three semi-local DFAs (LSDA, PBE, and SCAN), water clusters are over-bound whose MSEs are −197, −13.2, and −37.9 meV/cluster, in the respective order in functional type. With PZSIC, cluster binding energies are improved but still over-bound for LSDA and SCAN whose MSEs are −128 and −9.5 meV/cluster, respectively. PZSIC-PBE has MSE of 4.2 meV/cluster. Using the DFA@PZSIC-DFA approach (evaluating DFA energy with PZSIC-DFA density), Sharkas and coworkers found that the over-binding behavior is not due to density-driven error but rather a functional (energetic) error as DFA@PZSIC-DFA results are similar to DFA results.

In this subsubsection, we present vSOSIC results on small water clusters of sizes from dimer to hexamers and larger water clusters consisting of twelve, twenty, and thirty water molecules. For

brevity, we refer to the larger clusters as water-12, water-20, and water-30. We have used geometries for water-12 and water-20 optimized using MP2/aug-cc-PVTZ from Ref. 130 and water-30 geometry from Ref. 131 optimized at the M06-2X/6-31++G(d,p) level of theory. MAEs are determined by using the CCSD(T) values [132] for the cluster sizes 2-6 as reference and using the MP2 reference values [130] for the water-12 and water-20. For the larger water-30, we utilized as reference the MP2/aug-cc-pVDZ value [133]. The differences in binding energies calculated in our approach and the reference values are shown in Fig. 2.5. The negative (positive) values of the difference indicate over(under) binding tendency of the given functional.

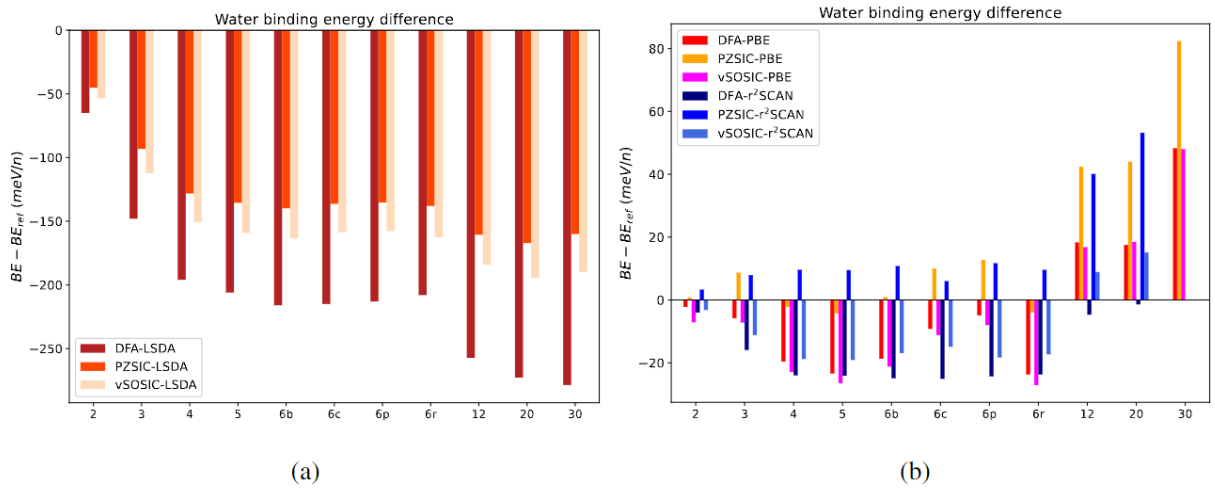

(a) (b)

Fig. 2.5. Relative water cluster binding energy per water cluster of size n (in meV/n) for DFA, PZSIC, and vSOSIC with (a) LSDA and (b) with PBE and r^2SCAN.

As shown in Fig. 2.5(a), the LSDA tends to overbind the water clusters which is reduced by PZSIC and vSOSIC. The vSOSIC errors are close to those of PZSIC but slightly larger. On the other hand, the PZSIC-PBE and vSOSIC-PBE do not perform comparably for the smaller clusters. vSOSIC-PBE tends to overestimate the B.E.s for smaller water clusters and underestimate the B.E.s for large clusters. PZSIC-PBE yields good estimation but does not show a clear trend for the smaller clusters. It, however, significantly overestimates the B.E.s of larger clusters. The signs of the B.E. errors for PZSIC-PBE and vSOSIC-PBE are not always same for the smaller clusters. With r^2SCAN the errors with PZSIC and vSOSIC have opposite signs for all small clusters indicating

vSOSIC-r^2SCAN tends to overbind whereas PZSIC-r^2SCAN underbinds. For the larger clusters, both vSOSIC-PBE and vSOSIC- r^2SCAN underestimate the B.E.s but the errors are smaller than those for PZSIC. The errors for PZSIC-PBE and PZSIC-r^2SCAN are even larger than those for the DFAs only. The comparison between vSOSIC and PZSIC results also shows that the source of the errors in PZSIC lies in the correction for the core orbitals. This is surprising since the core orbitals are unlikely to change significantly going from the water molecule to the cluster. These clusters will be studied in more detail in future.

2.3.6 PERFORMANCE OF STATIC DIPOLE POLARIZABILITIES

In recent years, the effects of SIE on dielectric properties have been investigated [75,76,78]. It is known that SIE noticeably affects dipole moment and static dipole polarizabilities. With DFAs, polarizabilities are, in general, overestimated because of the delocalization in the electron densities arising from SIE. On the other hand, PZSIC polarizabilities tend to be underestimated since the densities may become too compact due to overcorrecting tedency of PZSIC. Since in the vSOSIC approach, the valence (core) electrons are self-interaction corrected (uncorrected), we study how this treatment based on the valence would affect the static dipole polarizabilities. To this end, we chose the heavy molecules from carbon and pnictogen groups where core electrons are excluded from SIC energy evaluations in the vSOSIC approach. The molecules chosen for polarizability are AsH_3, $AsCl_3$, As_4, $GeCl_4$, GeF_4, and GeH_4. We also included benzene in this polarizability calculation.

The polarizability tensor α_{ij} is calculated by taking the derivative of the dipole moments $\vec{\mu}$ with respect to an applied electric field components F_j using finite difference method as:

$$\alpha_{ij} = \frac{\partial \mu_i}{\partial F_j} = \lim_{F_j \to 0} \frac{\mu_i(F_j) - \mu_i(-F_j)}{2F_j}. \tag{2.7}$$

The electric field strength of 0.005 a.u. is used. The average polarizability $\alpha_{avg} = (\alpha_{11} + \alpha_{22} + \alpha_{33})/3$ is calculated from the trace of the polarizability tensor.

In Table 2.5, we show the calculated polarizability of each molecule and the corresponding MAE (MSE) for each method. The LSDA values overestimate experiment with an MAE of 2.44 a_0^3 whereas for PZSIC-LSDA MAE is 4.99 a_0^3. The table clearly shows that LSDA overestimates and PZSIC-LSDA underestimates polarizabilities. This result is consistent with our previous observations on polyacenes and water clusters [75,78]. SOSIC-LSDA results lie between LSDA and PZSIC-LSDA with an MAE of 4.56 a_0^3 which is in slightly better agreement with the experiment than PZSIC but essentially similar to PZSIC. The SOSIC-LSDA, in general, produces the same quality of polarizability as PZSIC-LSDA implying that the amount of density localization is similar. With PBE and r^2SCAN functionals also, it is seen that the PZSIC reduces the polarizabilities compared to the DFA due to the localization of the density. With vSOSIC, the localization of the density is less compared to PZSIC. With LSDA and r^2SCAN a clear trend is seen in that the $\alpha_{DFA} > \alpha_{vSOSIC} > \alpha_{PZSIC}$. This trend is however not clear for PBE in that for some of the systems the vSOSIC polarizabilities are even smaller than those for PZSIC. In the case of PZSIC-PBE, the SI correction for the 1s orbital and for the rest has the opposite sign. By excluding 1s orbital from the correction, vSOSIC likely results in a slightly different electron localization behavior.

Table 2.5. The average polarizability (in a_0^3) of a set of six molecules.

System	Functional	DFA	vSOSIC	PZSIC	Exp[128]
AsH_3	LSDA	37.35	32.74	32.42	36.90
	PBE	34.49	33.87	33.21	
	r^{2}SCAN	35.66	33.71	33.65	
$AsCl_3$	LSDA	78.44	69.27	68.60	76.73
	PBE	78.00	70.72	71.76	
	r^{2}SCAN	75.55	71.96	70.54	
As_4	LSDA	117.02	109.40	111.04	116.70
	PBE	118.03	110.22	117.79	
	r^{2}SCAN	114.73	113.30	110.88	
$GeCl_4$	LSDA	88.61	76.58	73.87	84.29
	PBE	87.59	78.42	81.88	
	r^{2}SCAN	84.52	79.84	78.98	
$GeFl_4$	LSDA	29.58	23.34	23.84	27.33
	PBE	29.51	23.73	24.35	
	r^{2}SCAN	27.85	23.35	22.98	
GeH_4	LSDA	37.52	32.87	30.14	32.19
	PBE	36.61	34.39	32.40	
	r^{2}SCAN	35.35	33.14	32.79	
Benzene	LSDA	70.51	68.39	67.10	67.79
	PBE	70.19	69.23	68.33	
	r^{2}SCAN	69.64	68.05	70.38	
MAE (MSE)	LSDA	2.44 (2.44)	4.56 (-4.19)	4.99 (-4.99)	
	PBE	2.47 (1.78)	4.09 (-3.05)	2.27 (-1.74)	
	r^{2}SCAN	1.45 (0.20)	3.00 (-2.66)	4.02 (-3.10)	

2.3.7 MAGNETIC EXCHANGE COUPLING CONSTANT OF CHLOROCUPRATE

The magnetic exchange interaction between localized spins is another property what is affected by the delocalization error arising from the SIE in the DFAs. The coupling strength

between two magnetic spins is characterized by a quantity known as magnetic exchange coupling constant (J), and its sign and magnitude determine the magnetic nature and strength of materials. The spin Hamiltonian for such interaction is written as

$$\boldsymbol{H}_{spin} = -\boldsymbol{J} \sum_{i,j} \boldsymbol{S_i} \cdot \boldsymbol{S_j} \tag{2.8}$$

By relating the DFT energy of high-spin and low-spin states with a given electron configuration to the $\boldsymbol{H}_{spin}$ of the corresponding spin configuration, we can determine the value of $\boldsymbol{J}$ from the DFT calculations. As an application of the vSOSIC method, we compute magnetic exchange coupling constant of $[Cu_2Cl_6]^{2-}$ system and compare the results with previously SIC results by Mishra *et al*. and other groups [78,80,135,136]. With LSDA and PBE, the coupling strength of this molecule is overestimated by a few orders. Previous PZSIC studies [80] using ECP showed that both the SIC correction to the energy and to the density are needed for accurate descriptions of coupling constants with LSDA and PBE functionals. On the other hand, for the SCAN family of functionals, sometimes only SIC correction to the density may be sufficient [87,95].

The magnetic exchange coupling constant is computed using the spin projection approach of Noodleman [137] given as a formula, $J_{SP} = (E_{BS} - E_{HS})/(2S_AS_B)$, where S_A and S_B are the spins at two magnetic centers, A and B. E_{BS} is the energy of the molecule in broken symmetry spin configuration (↑↓) and E_{HS} is in high-spin spin configuration (↑↑). The vSOSIC calculated magnetic exchange coupling constants are compared with previous results in Table 2.6. It is evident that the two methods (PZSIC and vSOSIC) differ at most by 10 cm−1 for the LSDA and PBE functionals. We note that the magnetic exchange coupling constant is more sensitive to the accuracy in the total energies than other non-magnetic properties, and it requires tighter convergence criteria in FOD optimizations than usual calculations. The density-corrected DFA is a good way to improve the DFA predictions when DFA errors are suspected to be due to density delocalization errors. By comparing both DFA@PZSIC-DFA and DFA@vSOSIC-DFA, we find that the difference is 6 and 14 cm−1 for LSDA and PBE cases, respectively.

Table 2.6. Magnetic exchange coupling constant J_{sp} in cm^{-1} for hexachlorocuprate $[Cu_2Cl_6]^{2-}$ at planar $\theta = 0^\circ$.

Method	J
PZSIC-LSDA	-78[a]
vSOSIC-LSDA	-84
LSDA@PZSIC-LSDA	-131[a]
LSDA@vSOSIC-LSDA	-137
PZSIC-PBE	-94[a]
vSOSIC-PBE	-84
PBE@PZSIC-PBE	-138[a]
PBE@vSOSIC-PBE	-124
PZSIC-r^{2}SCAN	-77[b]
vSOSIC-r^{2}SCAN	-93
Exp.	0 to -40[c]

[a] Reference 80 where the values are calculated with an ECP approach for the PZSIC method.
[b] ECP was used in the calculation.
[c] Reference 138

2.3.8 SPIN CHARGES IN SQUARE PLANAR COPPER COMPLEXES

As the final case study, we applied the vSOSIC method to the square planar copper molecule previously studied by Karanovich *et al*. [84]. They analyzed the electronic configurations for monoanionic $[Cu(C_6H_4S_2)_2]^-$ (Q1) and dianionic $[Cu(C_6H_4S_2)_2]^{2-}$ Cu-based molecules. Similar magnetic square planar structures $[Cu(C_{14}H_20S_2)_2]^z$ $(z = 2-, 1-, 0)$ are synthesized experimentally [139]. Due to its long spin-lattice relaxation times, $[Cu(C_{14}H_20S_2)_2]^{2-}$ complex is considered as a candidate for qubits in the area of quantum information science. There has been a debate about the electronic structures of these square planar metal structures, and it has been suggested beyond-DFT methods such as multireference methods or potentially SIC methods may be required to study these complexes [84,139–141] Use of popular functionals such as PBE or B3LYP results in incorrect electron delocalization for the copper d-electrons. The Mulliken spin population at the Cu site with PBE is 0.32 μB, compared to the EPR experimental value of 0.51

μB. PZSIC-LSDA yields 0.67 μB, which is more similar to the Hartree-Fock and CASSCF estimates (0.79 and 0.70 μB, respectively) [84]. The PZSIC tendency to overestimate the spin population has also been observed in spin-crossover complexes [82]. Within the PBE and B3LYP functionals, the HOMO energy for the Q2 complex is positive, indicating that the additional electron is not bound to the complex. In both complexes, HOMO energy decreases from PBE to PZSIC-LSDA by 4.6 and 5.0 eV for Q1 and Q2 complexes, respectively. We performed the vSOSIC calculations and compared the HOMO and LUMO energy and spin population in Table 2.7. Both the PZSIC-LSDA and vSOSIC-LSDA HOMO energies are negative and agree within 0.1 eV. Similarly, the difference in Mulliken spin population between PZSIC and vSOSIC is 0.120 μB and 0.01 μB for the Cu and S atoms in Q2. Spin population for Q1 is excluded in the table since their spin moment is zero. In this vSOSIC calculation, 100 orbitals are treated with SIC out of 175 total orbitals, reducing the computation time by 57%. The reduced FOD structure for the vSOSIC method is shown in Fig. 2.3. PZSIC calculations on transition metal complexes surrounded by ligands are often computationally costly. These systems demonstrate how vSOSIC can be significantly more computationally efficient than PZSIC.

Table 2.7. he Mulliken population and HOMO and LUMO eigenvalues of (Q1) $[Cu(C_6H_4S_2)_2]^-$ and (Q2) $[Cu(C_6H_4S_2)_2]^{2-}$.

System	Method	Mulliken population (μ_B)		HOMO	LUMO	No. SIC orbitals
		Cu	S	(eV)	(eV)	
Q1	PZSIC-LSDA			-5.9	-1.22	174
	SOSIC-LSDA			-5.9	-1.41	100
Q2	PZSIC-LSDA	0.665	0.334	-2.0	4.35	175
	SOSIC-LSDA	0.551	0.109	-1.9	4.09	101

2.3.9 EFFICIENCY OF VSOSIC METHOD

As a reminder, PZSIC is a one-electron SIC approach wherein self-interaction correction is obtained in an orbital-by-orbital fashion. Thus, a rough estimate of the computational cost of

PZSIC calculation is approximately $N + 1$ times more than a DFA calculation, N being the number of electrons in the system. The actual cost of calculation can be much higher than this estimate since localized orbital densities need to be determined. In the FLOSIC method, this amounts to the optimization of FODs that determine the FLOs used to evaluate SIC terms. Our experience shows that the FOD energy surface is often very shallow with multiple minima, and typically the FODs corresponding to the core orbitals, especially the $1s$ orbital, are harder to optimize. Such problems make the FLOSIC calculations very time-consuming. Thus, by applying SIC to select orbitals, computational costs can be substantially reduced.

vSOSIC can accelerate SIC computations in two ways. As done in this work, if only the valence orbitals the SOSIC calculation for a given set of FOD configurations is $(N + 1)/(N - N_{core} + 1)$ times faster compared to a regular PZSIC calculation. Here N_{core} and N are the number of core orbitals and total orbitals, respectively. This also results in having to optimize $3(N - N_{core})$ FOD parameters in vSOSIC instead the $3N$ in the PZSIC. As mentioned earlier, the optimization of the core FOD parameters is often unsteady, and their removal usually leads to smoother optimization in vSOSIC.

As an illustration of computational savings, we consider a small $[Cu_2Cl_6]^{2-}$ complex and perform vSOSIC and PZSIC with LSDA functional calculations on the NERSC Perlmutter supercomputer that is equipped with AMD EPYC 7763 CPU with base (max) clock speed 2.45GHz (3.5GHz). We utilized two CPU sockets, resulting in a total of 128 cores per node. For conducting the timing test, only one node was used. The number of electrons treated with SIC in PZSIC (vSOSIC) is 160 (80), and a single iteration step takes 343.4 (174.6) seconds with the above setup. This speedup in an SCF from PZSIC to SOSIC is in agreement with the expected speedup of $(N + 1)/(N - Ncore + 1) \approx 2$. In Fig. 2.6 (a) we show the relative energy with respect to their converged energies as a function of FOD update steps for the same system. The FOD optimization in PZSIC requires ≈105 steps to reach the final energy within $10^{-4}\ E_H$ (where the tolerance in the energy derivative is $10^{-2}\ E_H\ /a_0$). In the vSOSIC, the relative energy as well as the energy derivative is almost one order lower than PZSIC at the same FOD update step.

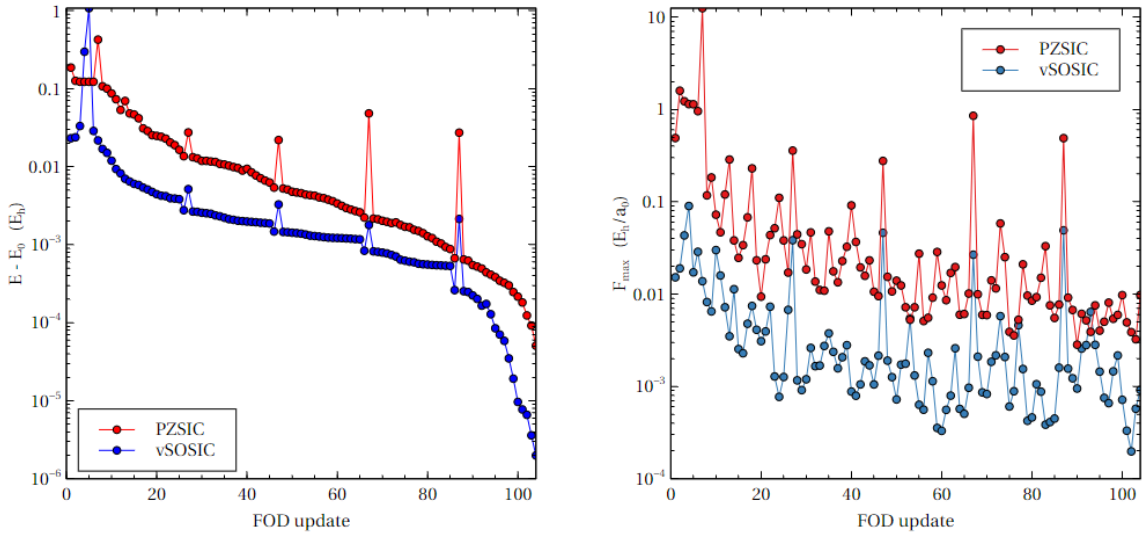

Fig. 2.6. PZSIC and vSOSIC for the relative total energies with respect to their final energies as a function of the FOD update steps (left pane) and the largest FOD force component as a function of the FOD update (right pane).

The largest component of FOD force is plotted as a function of update steps in Fig. 6 (b). While in the PZSIC the force drops below $10^{-2}\ E_H/a_0$ at around 45 steps whereas in vSOSIC it takes only 10 steps. The vSOSIC method is advantageous in FOD optimization.

2.3.9 SCALED DOWN SOSIC

In a previous study [74], we demonstrated that orbital scaling self-interaction correction (OSIC) replaces the asymptotic potential behavior decaying from $-1/r$ to $-X_{HO}/r$, where X_{HO} is the highest orbital scaling factor defined within OSIC [74]. We also demonstrated that SOSIC with $X_{HO} = 1$ reproduces identical HOMO energy as PZSIC for the SCAN functional. Though PZSIC is said to have the $-1/r$ behavior, HOMO energies with PZSIC slightly overestimate IPs from experiments. Therefore, we utilized X_{HO} quantity to enhance the SOSIC HOMO energies compared to the experimental IPs. In Fig. 2.7, we show the vSOSIC HOMO energies in comparison to the experiment. We added a constant orbital scaling factor X within the vSOSIC

method and used it as a tunable parameter. Here we chose two such parameters. First, we apply a linear fitting to the PZSIC HOMO energies vs. experimental IPs plot for the subset molecules from the G2/97 set.

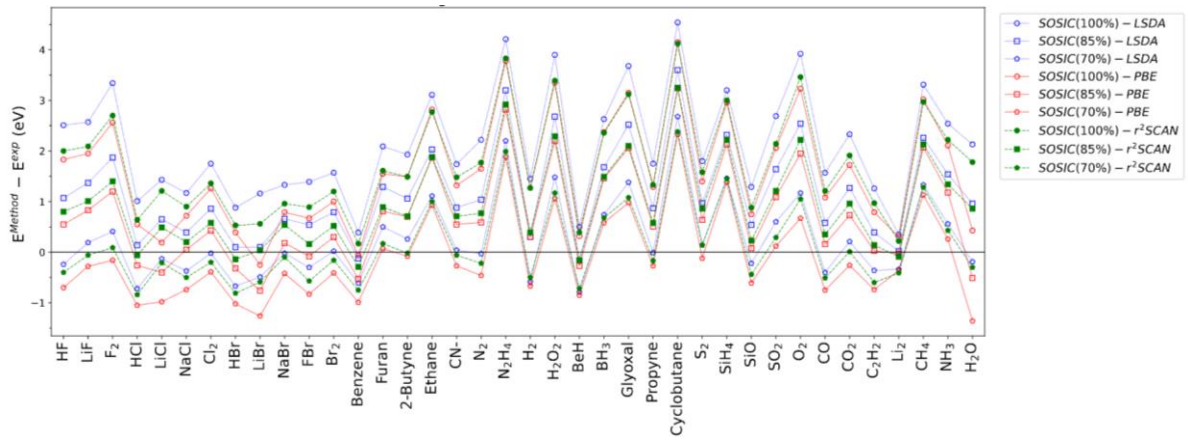

Fig. 2.7. Negative of HOMO eigenvalues of 37 selected molecules, a subset of G2/97 set, compared against experimental ionization potential for vSOSIC scaled.

We have determined the slope of the fitted line to be 0.85 and use this as a choice for X. We also tested another value of X, specifically $X = 0.70$, and found that its corresponding HOMO energies showed good agreement with the experimental data. Hereon, we refer SOSIC with $X = 0.85$ ($X = 0.7$) as vSOSIC(85%) [vSOSIC(70%)]. The scaling process done here is similar in spirit to the scaling approach of the Iceland group [27] where they used 0.5 as the factor for PZSIC calculations. We discuss the performance of vSOSIC(100%), vSOSIC(85%), and vSOSIC(70%) in this section.

The scaled-SOSIC approach changes total atomic energies slightly in comparison to vSOSIC(100%). Table 2.8 presents the total energies of atoms computed using three functionals and three vSOSIC scaling schemes. With vSOSIC(85%), their MAE changes are +11, -16, and -11 mEH for LSDA, PBE, and r^2SCAN, respectively. With vSOSIC(70%), their MAEs change from vSOSIC(100%) by +29, -33, -22 mE_H , respectively. A systematic energy change as varying X is seen for each DFA functional.

Table 2.8. Scaled-vSOSIC mean absolute error (MAE) of the total energy of atoms from hydrogen to argon.

Functional	Method	MAE(E_H)
LSDA	SOSIC-100%	0.607
LSDA	SOSIC-85%	0.618
LSDA	SOSIC-70%	0.636
PBE	SOSIC-100%	0.199
PBE	SOSIC-85%	0.183
PBE	SOSIC-70%	0.166
r^{2}SCAN	SOSIC-100%	0.085
r^{2}SCAN	SOSIC-85%	0.074
r^{2}SCAN	SOSIC-70%	0.063

We have repeated the atomization energy calculation with the AE6 set and G2/97 subset of molecules (cf. Table 2.9). The MAEs in atomization energies are reduced in all vSOSIC(85%) cases and even further for all vSOSIC(70%) cases. The most significant performance shift is observed when scaling vSOSIC on AE6 LSDA (MAE, 66.6 kcal/mol), resulting in a reduction of 7.1 and 12.7 kcal/mol in MAE for vSOSIC(85%) and vSOSIC(70%), respectively. Interestingly, the vSOSIC method on the PBE functional outperformed the bare PBE (with an MAE of 16.3 kcal/mol), where vSOSIC(85%) and vSOSIC(70%) showed an MAE of 13.5 and 11.3 kcal/mol, respectively. Even for r^2SCAN, from 100% to 85% to 70%, the MAE decreases from 17.2 to 15.0 to 12.8 kcal/mol toning down the overcorrecting nature of PZSIC on this functional.

Table 2.9. Scaled-vSOSIC mean absolute error (MAE) and mean absolute percentage error (MAPE) of atomization energy for the AE6 set and the G2/97 subset of data.

		AE6		37 molecules	
Functional	Method	MAE(kcal/mol)	MAPE(%)	MAE(kcal/mol)	MAPE(%)
LSDA	SOSIC-100%	66.6	11.0	51.13	13.75
LSDA	SOSIC-85%	59.5	9.7	48.93	14.55
LSDA	SOSIC-70%	53.9	9.2	47.32	14.94
PBE	SOSIC-100%	16.3	5.3	22.73	9.61
PBE	SOSIC-85%	13.5	4.4	21.31	8.14
PBE	SOSIC-70%	11.3	3.6	20.17	7.07
r^{2}SCAN	SOSIC-100%	17.2	5.1	17.07	8.94
r^{2}SCAN	SOSIC-85%	15.0	4.4	16.10	8.10
r^{2}SCAN	SOSIC-70%	12.8	3.7	15.25	7.29

We have observed mixed performance for scaled-vSOSIC on barrier heights, with changes in performance differing among the three functionals (cf. Table 2.10). However, these changes are relatively less pronounced in comparison to the changes observed in the atomization energies performance. Specifically, we found that scaled-vSOSIC increases the MAE for BH6 when LSDA is used, while we observed a performance improvement for the BH6 set with PBE scaling-vSOSIC. Scaling-vSOSIC has a minimal impact on the BH6 MAE for r^2SCAN, although there are variations in the mean error. In the case of the WCPT18 set, the performance is improved by scaled-vSOSIC in all three functionals where the improvement ranges from 0.46 to 5.07 kcal/mol.

Table 2.10. Scaled-vSOSIC mean absolute error (MAE) reaction barrier heights of BH6 and WCPT18 sets of data.

		BH6		WCPT18
Functional	Method	ME(kcal/mol)	MAE(kcal/mol)	MAE(kcal/mol)
LSDA	SOSIC-100%	-5.2	5.2	7.59
LSDA	SOSIC-85%	-6.0	6.2	
LSDA	SOSIC-70%	-7.1	7.6	7.13
PBE	SOSIC-100%	-0.1	4.1	9.44
PBE	SOSIC-85%	-1.1	3.1	
PBE	SOSIC-70%	-2.2	2.8	4.37
r^{2}SCAN	SOSIC-100%	-0.7	2.6	5.50
r^{2}SCAN	SOSIC-85%	-1.5	2.4	
r^{2}SCAN	SOSIC-70%	-2.4	2.8	3.38

Scaled-vSOSIC with the LSDA functional shows a uniform amount of MSE shift for all water clusters (cf. Fig. 2.8) from vSOSIC(100%) (MSE, -153.3 meV/n) to vSOSIC(70%) (MSE, -169.2 meV/n), where its curve shifts toward the DFA curve whose MSE is -206.9 meV/n. PBE with scaled-vSOSIC shows a similar trend. The MSE of vSOSIC(70%) (-3.9 meV/n) falls in between vSOSIC(100%) (MSE, -4.3 meV/n) and PBE (MSE, -2.1 meV/n). We considered up to water-20 cluster size, and find that scaled-vSOSIC with r^2SCAN shows similar behavior where vSOSIC(70%) -12.6 meV/n falls between SOSIC(100%) MSE of 9.6 meV/n and DFA with -17.2 meV/n.

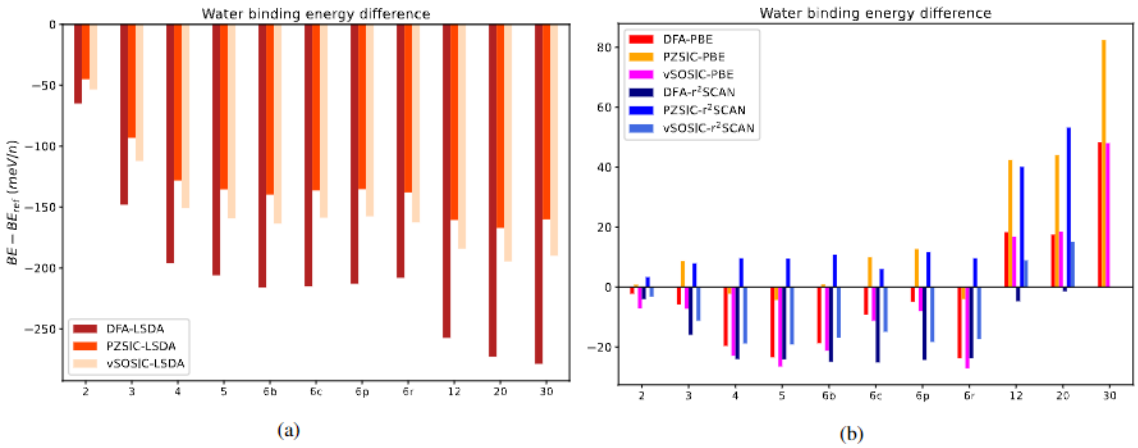

Fig. 2.8. Relative water cluster binding energy per water cluster of size n (in meV/n) for DFA, PZSIC, and vSOSIC with (a) LSDA and (b) with PBE and r^2SCAN.

To summarize this section, we applied the empirically determined scaling factor to vSOSIC to improve agreement between its HOMO energies and IPs from experiments. We have found that scaling factors of 85% and 70% are suitable for constant scaling of the vSOSIC method. The scaling of vSOSIC has an overall beneficial effect, significantly improving atomization energies for the higher functionals, while the performance of barrier heights remains qualitatively the same or improves. Scaled-vSOSIC may be useful for PBE and r^2SCAN, where we observed consistent performance improvement.

2.3 SUMMARY

We have outlined and assessed a simplified one-electron self-interaction-correction scheme where the SIE is removed from a select set of orbitals. In this work, the set chosen is valence orbitals since it is the valence orbitals that define central aspects of the electronic structure and chemical bonding. The approach is, however, more general and can also be used to correct for core states if needed, for example, in the computation of core-electron binding energies. It can also be adapted to apply SIC to a specific region of space, as in the spirit of embedding methods, by

identifying the FLOs that are localized in the region of interest. The present vSOSIC approach differs from the SOSIC method introduced in Ref. 74 in that the Fermi-Löwdin orbitals that are used in evaluating the SIC are constructed from the valence Kohn-Sham orbitals only. This results in a substantial reduction in the computational complexities by reducing the number of Fermi orbital descriptors that need to be optimized thereby providing significant computational speed up. The results obtained using the vSOSIC scheme are compared with those obtained with PZSIC which corrects for all the orbitals. We have studied the performance of vSOSIC on the total energies of atoms, atomization energies, reaction barrier heights, and HOMO eigenvalues of molecules. For the atomization energies of AE6 datasets, with the LSDA functionals MAE with vSOSIC MAE is larger by 7 kcal/mol than the PZSIC, for the PBE functionals vSOSIC MAE is 2 kcal/mol lower while for the r^2SCAN functional vSOSIC MAE is 9 kcal/mol smaller than that of PZSIC. These differences between the performance of vSOSIC and PZSIC diminish for a larger dataset (37 molecules from the MGAE109). The vSOSIC and PZSIC perform similarly within 0.2 kcal/mol in the calculation of the barrier heights of BH6 and WCPT18 datasets. Likewise, the absolute HOMO eigenvalues that approximate the vertical ionization energies, obtained by the vSOSIC and PZSIC are in excellent agreement with each other but they both overestimate the experimental ionization energies. A similar degree of agreement is seen between the two approaches for density-related parameters such as static dipole polarizabilities of select molecules. Furthermore, we applied vSOSIC to vertical detachment energies of water cluster anions, binding energies of water clusters, and magnetic exchange coupling parameters of $[Cu_2Cl_6]^{2-}$ and electronic structure of $[Cu(C_6H_4S_2)_2]^{1-/2-}$ as a test on systems containing transition metals. The vSOSIC and PZSIC predicted exchange coupling constants differ by 6 and 10 cm−1 for the LSDA and PBE functionals, respectively. For the $[Cu(C_6H_4S_2)_2]^{1-/2-}$ molecules, the vSOSIC like PZSIC binds the extra electrons and yields HOMO eigenvalues within 0.1 eV of PZSIC, while for the spin-moment at Cu site, vSOSIC prediction (0.55 μB) agrees with PZSIC (0.67 μB) within 0.1 μB with vSOSIC value being closer to the EPR experimental value of 0.51 μB. The water cluster anions offer an interesting case. Our previous work with PZSIC-PBE showed that the negative of the highest occupied eigenvalue offered an outstanding approximation to the VDE of the water cluster anions, with an MAE of only 17 meV when compared to CCSD(T) values. These results outperformed MP2 method and other hybrid functionals by a wide margin. The vSOSIC technique (with PBE functional) decreases the MAE by another 2 meV, making it an ideal alternative to

CCSDT (T) for determining the vDE of water cluster anions. To determine the vDE of the water anions, an even more straightforward form of SOSIC was explored, in which just the outermost unpaired orbital was corrected for SIE. Interestingly in this scheme, we find that the HOMO eigenvalue is negative indicating electron binding. However, the VDEs derived from the HOMO eigenvalues, in this case, exhibit a higher MAE of 56.9 meV, which is still superior to B3LYP (238 meV) and comparable to MP2 MAE (44 meV). This 1orb-SOSIC is highly encouraging because the computing cost is nearly the same as that of the uncorrected density functional technique and may be useful in molecular dynamics simulations of such complexes. The vSOSIC calculations on the $[Cu_2Cl_6]^{2-}$ complex as an instructive example of the computational efficiency demonstrates that, in addition to the savings from using fewer orbitals to account for SIC, the FOD optimization in vSOSIC is substantially smoother and quicker. Overall, the vSOSIC method involves fewer calculations than the PZSIC method and produces results similar to the PZSIC method. As seen in the computation of the VDE of water anions, the approach may be tailored to the task at hand by selecting relevant orbitals for SIE removal. For example, the properties related to the core orbitals such as core electron binding energies, or Fermi-contact terms will require different choices of the active orbitals in the SOSIC method. The vSOSIC approach can be very useful for studying a large complex composed of heavy elements where SIC effects are expected to be more pronounced due to localized f-electrons.

We applied scaling by a constant factor to SOSIC. The scaling is done in such a way to match SOSIC HOMO energy with known ionization energies from the experiment. The scaled SOSIC shows improvement in atomization energies while slightly changing the barrier height performance. Although this scaled SOSIC method may not retain the exact $-1/r$ asymptotic behavior, this approach has a rationale, and it may be an attractive alternative method to the traditional one-electron SIC method. It is argued that the DFA orbital energy being too high compared to the exact DFT potential is not because of incorrect asymptotic potential or self-interaction error but because LSDA exchange response potentials (also referred non energetic part of KS potential) are too repulsive in the bulk molecular regions [https://doi.org/10.1063/1.495087]. Through the LSDA term, GGA (and likely meta-GGA) functionals inherit the same problem. PZSIC subtracts the orbital density terms, and it gives the XC holes shaped as occupied orbitals and introduces non-locality that is needed for correct Coulombic decay ($-1/r$) in XC potential. From this perspective, we may understand PZSIC and SOSIC as adding a response potential to

(DFA-) KS potential. Particularly, the scaled-vSOSIC can be seen as adjusting the shape of the XC holes and fine-tuning the exchange response potentials. The reason why LSDA does not have the correct $-1/r$ asymptote is that the uniform electron gas of $\rho^{-1/3}$ potential is not meant to describe the density decay outside of the atom or molecule. But at the same time, it was pointed out before that, the asymptotes are a region in space that does not carry any importance for total energy and orbital energy [142]. Hence the focus on any correction to DFA should be on the potential in the bulk regions. In that sense, both scaled and unscaled vSOSIC have a rationale for their approaches.

This work also assessed the performance of the r^2SCAN functional with PZSIC and vSOSIC methods for a range of properties. Our results show that the SIC-r^2SCAN calculations requires

2.4 DATA AVAILABILITY STATEMENT

The data that support the findings of this study are available within the article and its supplementary material.

2.4 ACKNOWLEDGEMENT

This work was supported by the Office of Basic Energy Sciences, U.S. Department of Energy DE-SC0018331.

2.5 REFERENCES

[1] W. Kohn and L. Sham, "Self-consistent equations including exchange and correlation effects," Phys. Rev. 140, A1133–A1138 (1965).

[2] M. Levy, "Universal variational functionals of electron densities, first-order density matrices, and natural spin-orbitals and solution of the v-representability problem," Proceedings of the National Academy of Sciences 76, 6062–6065 (1979).

[3] A. Fouda and U. Ryde, “Does the DFT self-interaction error affect energies calculated in proteins with large QM systems?” J. Chem. Theory Comput. 12, 5667–5679 (2016).
[4] E. R. Johnson, A. Otero-de-la Roza, and S. G. Dale, “Extreme density-driven delocalization error for a model solvated-electron system,” J. Chem. Phys. 139, 184116 (2013), https://doi.org/10.1063/1.4829642.
[5] L. M. LeBlanc, S. G. Dale, C. R. Taylor, A. D. Becke, G. M. Day, and E. R. Johnson, “Pervasive delocalisation error causes spurious proton transfer in organic acid–base Co-crystals,” Angew. Chem. Int. Ed. 130, 15122–15126 (2018).
[6] J. Autschbach and M. Srebro, “Delocalization error and “functional tuning” in Kohn–Sham calculations of molecular properties,” Acc. Chem. Res. 47, 2592–2602 (2014).
[7] B. Rana, M. P. Coons, and J. M. Herbert, “Detection and correction of delocalization errors for electron and hole polarons using density-corrected DFT,” J. Phys.Chem. Lett. 13, 5275–5284 (2022).
[8] X. A. Sosa Vazquez and C. M. Isborn, “Size-dependent error of the density functional theory ionization potential in vacuum and solution,” J. Chem. Phys. 143,244105 (2015).
[9] J. Perdew, “Orbital functional for exchange and correlation: self-interaction correction to the local density approximation,” Chem. Phys. Lett. 64, 127–130 (1979).
[10] J. P. Perdew and A. Zunger, “Self-interaction correction to density-functional approximations for many-electron systems,” Phys. Rev. B 23, 5048–5079 (1981).
[11] I. Lindgren, “A statistical exchange approximation for localized electrons,” Int. J. Quantum Chem. 5, 411–420 (1971).
[12] U. Lundin and O. Eriksson, “Novel method of self-interaction corrections in density functional calculations,” Int. J. Quantum Chem. 81, 247–252 (2001).
[13] M. S. Gopinathan, “Improved approximate representation of the Hartree-Fock potential in atoms,” Phys. Rev. A 15, 2135–2142 (1977).
[14] A. Zunger, J. Perdew, and G. Oliver, “A self-interaction corrected approach to many-electron systems: Beyond the local spin density approximation,” Solid State Commun. 34, 933–936 (1980).
[15] O. Gunnarsson and R. O. Jones, “Self-interaction corrections in the density functional formalism,” Solid State Commun. 37, 249–252 (1981).
[16] S. Manoli and M. Whitehead, “Generalized-exchange local-spin-density functional theory: Self-interaction correction,” Phys. Rev. A 38, 630 (1988).

[17] Y. Guo and M. Whitehead, “An alternative self-interaction correction in the generalized exchange local-density functional theory,” J. Comput. Chem. 12, 803–810 (1991).
[18] M. R. Pederson, R. A. Heaton, and C. C. Lin, “Local-density Hartree-Fock theory of electronic states of molecules with self-interaction correction,” J. Chem. Phys. 80, 1972–1975 (1984), https://doi.org/10.1063/1.446959.
[19] M. R. Pederson, R. A. Heaton, and C. C. Lin, “Density-functional theory with self-interaction correction: Application to the lithium moleculea),” J. Chem. Phys. 82, 2688–2699 (1985), https://doi.org/10.1063/1.448266.
[20] J. Harrison, R. Heaton, and C. Lin, “Self-interaction correction to the local density Hartree-Fock atomic calculations of excited and ground states,” J. PHYS. B-ATMOL. OPT. 16, 2079 (1983).
[21] J. G. Harrison, “An improved self-interaction-corrected local spin density functional for atoms,” J. Chem. Phys. 78, 4562–4566 (1983).
[22] R. A. Heaton and C. C. Lin, “Self-interaction-correction theory for density functional calculations of electronic energy bands for the lithium chloride crystal,” J. Phys. C Solid State Phys. 17, 1853–1866 (1984).
[23] R. A. Heaton and C. C. Lin, “Electronic energy-band structure of the calcium fluoride crystal,” Phys. Rev. B 22, 3629 (1980).
[24] H. Gudmundsdottir, E. Ö. Jónsson, and H. Jonsson, “Calculations of Al dopant in α-quartz using a variational implementation of the Perdew–Zunger self-interaction correction,” New J. Phys. 17, 083006 (2015).
[25] E. Ö. Jónsson, S. Lehtola, and H. Jónsson, “Towards an optimal gradient-dependent energy functional of the PZ-SIC form,” Procedia Comput. Sci. 51,1858–1864 (2015).
[26] S. Lehtola, E. O. Jonsson, and H. Jonsson, “Effect of complex-valued optimal orbitals on atomization energies with the Perdew–Zunger self-interaction correction to density functional theory,” J. Chem. Theory Comput. 12, 4296–4302 (2016).
[27] S. Klüpfel, P. Klüpfel, and H. Jónsson, “The effect of the Perdew-Zunger self-interaction correction to density functionals on the energetics of small molecules,” J. Chem. Phys. 137, 124102 (2012).
[28] S. Lehtola and H. Jónsson, “Variational, self-consistent implementation of the Perdew–

Zunger self-interaction correction with complex optimal orbitals," J. Chem. Theory Comput. 10, 5324–5337 (2014).
[29] O. A. Vydrov and G. E. Scuseria, "Ionization potentials and electron affinities in the perdew–zunger self-interaction corrected density-functional theory," J. Chem. Phys. 122, 184107 (2005).
[30] O. A. Vydrov and G. E. Scuseria, "Effect of the Perdew–Zunger self-interaction correction on the thermochemical performance of approximate density functionals," J. Chem. Phys. 121, 8187–8193 (2004).
[31] S. Lehtola, M. Head-Gordon, and H. Jónsson, "Complex orbitals, multiple local minima, and symmetry breaking in Perdew–Zunger self-interaction corrected density functional theory calculations," J. Chem. Theory Comput. 12, 3195–3207(2016).
[32] B. G. Janesko, "Systematically improvable generalization of self-interaction corrected density functional theory," J. Phys. Chem. Lett. 13, 5698–5702 (2022).
[33] E. J. Bylaska, K. Tsemekhman, and F. Gao, "New development of self-interaction corrected DFT for extended systems applied to the calculation of native defects in 3C–SiC," Phys. Scr. 2006, 86 (2006).
[34] A. Ruzsinszky, J. P. Perdew, G. I. Csonka, O. A. Vydrov, and G. E. Scuseria,"Density functionals that are one- and two- are not always many-electron self-interaction-free, as shown for H+2 , He+2 , LiH+, and Ne+2 ," J. Chem. Phys. 126, 104102 (2007), https://doi.org/10.1063/1.2566637.
[35] A. Ruzsinszky, J. P. Perdew, G. I. Csonka, O. A. Vydrov, and G. E. Scuseria, "Spurious fractional charge on dissociated atoms: Pervasive and resilient self-interaction error of common density functionals," J. Chem. Phys. 125, 194112 (2006), https://doi.org/10.1063/1.2387954.
[36] K. A. Jackson, J. E. Peralta, R. P. Joshi, K. P. Withanage, K. Trepte, K. Sharkas, and A. I. Johnson, "Towards efficient density functional theory calculations without self-interaction: The Fermi-Löwdin orbital self-interaction correction," J. Phys. Conf. Ser. 1290, 012002 (2019).
[37] S. Patchkovskii and T. Ziegler, "Improving "difficult" reaction barriers with self-interaction corrected density functional theory," J. Chem. Phys. 116, 7806–7813 (2002).
[38] S. Kümmel and J. P. Perdew, "Two avenues to self-interaction correction within Kohn—Sham theory: Unitary invariance is the shortcut," Mol. Phys. 101, 1363–1368 (2003).
[39] T. Körzdörfer, S. Kümmel, and M. Mundt, "Self-interaction correction and the optimized effective potential," J. Chem. Phys. 129, 014110 (2008).

[40] T. Baruah, R. R. Zope, A. Kshirsagar, and R. K. Pathak, “Positron binding: A positron-density viewpoint,” Phys. Rev. A 50, 2191–2196 (1994).
[41] V. Polo, E. Kraka, and D. Cremer, “Electron correlation and the self-interaction error of density functional theory,” Mol. Phys. 100, 1771–1790 (2002).
[42] R. A. Heaton, J. G. Harrison, and C. C. Lin, “Self-interaction correction for density-functional theory of electronic energy bands of solids,” Phys. Rev. B 28, 5992–6007 (1983).
[43] S. Goedecker and C. Umrigar, “Critical assessment of the self-interaction-corrected–local-density-functional method and its algorithmic implementation,” Physical Review A 55, 1765 (1997).
[44] A. Svane, “Electronic structure of cerium in the self-interaction-corrected local-spin-density approximation,” Phys. Rev. B 53, 4275–4286 (1996).
[45] A. Svane, W. M. Temmerman, Z. Szotek, J. Lægsgaard, and H. Winter, “Self-interaction-corrected local-spin-density calculations for rare earth materials,” Int. J. Quantum Chem. 77, 799–813 (2000).
[46] M. M. Rieger and P. Vogl, “Self-interaction corrections in semiconductors,” Phys. Rev. B 52, 16567–16574 (1995).
[47] R. R. Zope, M. K. Harbola, and R. K. Pathak, “Atomic compton profiles within different exchange-only theories,” Eur. Phys. J. D-AMOP Phys. 7, 151–155 (1999).
[48] N. Hamada and S. Ohnishi, “Self-interaction correction to the local-density approximation in the calculation of the energy band gaps of semiconductors based on the full-potential linearized augmented-plane-wave method,” Phys. Rev. B 34, 9042 (1986).
[49] M. Biagini, “Self-interaction-corrected density-functional formalism,” Phys. Rev. B 49, 2156 (1994).
[50] Y. Xie, R. Han, and X. Zhang, “Obtaining localized orbitals and band structure in self-interaction-corrected density-functional theory,” Phys. Rev. B 60, 8543 (1999).
[51] M. Arai and T. Fujiwara, “Electronic structures of transition-metal mono-oxides in the self-interaction-corrected local-spin-density approximation,” Phys. Rev. B 51, 1477 (1995).
[52] M. Stengel and N. A. Spaldin, “Self-interaction correction with wannier functions,” Phys. Rev. B 77, 155106 (2008).
[53] D. L. Price, “Application of an on-site self-interaction-corrected method to Ce and the α-Ce surface,” Phys. Rev. B 60, 10588 (1999).

[54] C. Legrand, E. Suraud, and P. Reinhard, "Comparison of self-interaction-corrections for metal clusters," Journal of Physics B: Atomic, Molecular and Optical Physics 35, 1115 (2002).
[55] J. Messud, P. M. Dinh, P.-G. Reinhard, and E. Suraud, "Improved slater approximation to sic–oep," cpl 461, 316–320 (2008).
[56] J. Garza, J. A. Nichols, and D. A. Dixon, "The optimized effective potential and the self-interaction correction in density functional theory: Application to molecules," J. Chem. Phys. 112, 7880–7890 (2000), https://doi.org/10.1063/1.481421.
[57] C. D. Pemmaraju, T. Archer, D. Sánchez-Portal, and S. Sanvito, "Atomic-orbital-based approximate self-interaction correction scheme for molecules and solids," Phys. Rev. B 75, 045101 (2007).
[58] W. L. Luken and D. N. Beratan, "Localized orbitals and the Fermi hole," Theor. Chem. Acc. 61, 265–281 (1982).
[59] W. L. Luken and J. C. Culberson, "Localized orbitals based on the Fermi hole," Theor. Chem. Acc. 66, 279–293 (1984).
[60] M. R. Pederson, A. Ruzsinszky, and J. P. Perdew, "Communication: Self-interaction correction with unitary invariance in density functional theory," J. Chem. Phys. 140, 121103 (2014), https://doi.org/10.1063/1.4869581.
[61] M. R. Pederson and T. Baruah, "Chapter eight - self-interaction corrections within the Fermi-Orbital-based formalism," in Adv. At. Mol. Opt. Phys., Vol. 64, edited by E. Arimondo, C. C. Lin, and S. F. Yelin (Academic Press, 2015) pp. 153–180.
[62] M. R. Pederson, "Fermi orbital derivatives in self-interaction corrected density functional theory: Applications to closed shell atoms," J. Chem. Phys. 142, 064112 (2015), https://doi.org/10.1063/1.4907592.
[63] Z.-h. Yang, M. R. Pederson, and J. P. Perdew, "Full self-consistency in the Fermi-orbital self-interaction correction," Phys. Rev. A 95, 052505 (2017).
[64] C. M. Diaz, T. Baruah, and R. R. Zope, "Fermi-Löwdin-orbital self-interaction correction using the optimized-effective-potential method within the Krieger-Li-Iafrate approximation," Phys. Rev. A 103, 042811 (2021).
[65] C. M. Diaz, P. Suryanarayana, Q. Xu, T. Baruah, J. E. Pask, and R. R. Zope, "Implementation of Perdew–Zunger self-interaction correction in real space using Fermi–Löwdin orbitals," J. Chem. Phys. 154, 084112 (2021).

[66] O. A. Vydrov, G. E. Scuseria, J. P. Perdew, A. Ruzsinszky, and G. I. Csonka, "Scaling down the Perdew-Zunger self-interaction correction in many-electron regions," J. Chem. Phys. 124, 094108 (2006).

[67] J. P. Perdew, A. Ruzsinszky, J. Sun, and M. R. Pederson, "Chapter one - paradox of self-interaction correction: How can anything so right be so wrong?" in Adv. At. Mol. Opt. Phys., Vol. 64 (Academic Press, 2015) pp. 1–14.

[68] G. I. Csonka and B. G. Johnson, "Inclusion of exact exchange for self-interaction corrected h3 density functional potential energy surface," Theor. Chem. Acc. 99, 158–165 (1998).

[69] A. I. Johnson, K. P. K. Withanage, K. Sharkas, Y. Yamamoto, T. Baruah, R. R. Zope, J. E. Peralta, and K. A. Jackson, "The effect of self-interaction error on electrostatic dipoles calculated using density functional theory," J. Chem. Phys. 51, 174106 (2019), https://doi.org/10.1063/1.5125205.

[70] C. M. Diaz, L. Basurto, S. Adhikari, Y. Yamamoto, A. Ruzsinszky, T. Baruah, and R. R. Zope, "Self-interaction-corrected Kohn–Sham effective potentials using the density-consistent effective potential method," J. Chem. Phys. 155, 064109(2021), https://doi.org/10.1063/5.0056561.

[71] P. Bhattarai, B. Santra, K. Wagle, Y. Yamamoto, R. R. Zope, A. Ruzsinszky, K. A. Jackson, and J. P. Perdew, "Exploring and enhancing the accuracy of interior-scaled Perdew–Zunger self-interaction correction," J. Chem. Phys. 154, 094105(2021).

[72] S. Schwalbe, L. Fiedler, J. Kraus, J. Kortus, K. Trepte, and S. Lehtola, "PyFLOSIC: Python-based Fermi–Löwdin orbital self-interaction correction," J. Chem. Phys. 153, 084104 (2020).

[73] Y. Yamamoto, A. Salcedo, C. M. Diaz, M. S. Alam, T. Baruah, and R. R. Zope, "Assessing the effect of regularization on the molecular properties predicted by SCAN and self-interaction corrected SCAN meta-GGA," Phys. Chem. Chem. Phys. 22, 18060–18070 (2020).

[74] Y. Yamamoto, S. Romero, T. Baruah, and R. R. Zope, "Improvements in the orbitalwise scaling down of Perdew–Zunger self-interaction correction in many-electron regions," J. Chem. Phys. 152, 174112 (2020).

[75] S. Akter, Y. Yamamoto, R. R. Zope, and T. Baruah, "Static dipole polarizabilities of polyacenes using self-interaction-corrected density functional approximations," J. Chem. Phys. 154, 114305 (2021), https://doi.org/10.1063/5.0041265.

[76] S. Akter, J. A. Vargas, K. Sharkas, J. E. Peralta, K. A. Jackson, T. Baruah, and R. R. Zope,

"How well do self-interaction corrections repair the overestimation of static polarizabilities in density functional calculations?" Phys. Chem. Chem. Phys. 23, 18678–18685 (2021).
[77] K. P. K. Withanage, S. Akter, C. Shahi, R. P. Joshi, C. Diaz, Y. Yamamoto, R. Zope, T. Baruah, J. P. Perdew, J. E. Peralta, and K. A. Jackson, "Self-interaction-free electric dipole polarizabilities for atoms and their ions using the Fermi-Löwdin self-interaction correction," Phys. Rev. A 100, 012505 (2019).
[78] S. Akter, Y. Yamamoto, C. M. Diaz, K. A. Jackson, R. R. Zope, and T. Baruah, "Study of self-interaction errors in density functional predictions of dipole polarizabilities and ionization energies of water clusters using Perdew–Zunger and locally scaled self-interaction corrected methods," J. Chem. Phys. 153, 164304 (2020), https://doi.org/10.1063/5.0025601.
[79] R. P. Joshi, K. Trepte, K. P. Withanage, K. Sharkas, Y. Yamamoto, L. Basurto, R. R. Zope, T. Baruah, K. A. Jackson, and J. E. Peralta, "Fermi-löwdin orbital self-interaction correction to magnetic exchange couplings," J. Chem. Phys. 149, 164101 (2018).
[80] P. Mishra, Y. Yamamoto, P.-H. Chang, D. B. Nguyen, J. E. Peralta, T. Baruah, and R. R. Zope, "Study of self-interaction errors in density functional calculations of magnetic exchange coupling constants using three self-interaction correction methods," J. Phys. Chem. A 126, 1923–1935 (2022), pMID: 35302373,https://doi.org/10.1021/acs.jpca.1c10354.
[81] P. Mishra, Y. Yamamoto, J. K. Johnson, K. A. Jackson, R. R. Zope, and T. Baruah, "Study of self-interaction-errors in barrier heights using locally scaled and Perdew–Zunger self-interaction methods," J. Chem. Phys. 156, 014306 (2022), https://doi.org/10.1063/5.0070893.
[82] S. Romero, T. Baruah, and R. R. Zope, "Spin-state gaps and self-interaction-corrected density functional approximations: Octahedral Fe(II) complexes as case study," J. Chem. Phys. 158 (2023), 10.1063/5.0133999, 054305, https://pubs.aip.org/aip/jcp/article-pdf/doi/10.1063/5.0133999/16704373/054305_1_online.pdf.
[83] L. Li, K. Trepte, K. A. Jackson, and J. K. Johnson, "Application of self-interaction corrected density functional theory to early, middle, and late transition states," J. Phys. Chem. A 124, 8223–8234 (2020), pMID: 32883077.
[84] A. Karanovich, Y. Yamamoto, K. A. Jackson, and K. Park, "Electronic structure of mononuclear Cu-based molecule from density-functional theory with self-interaction correction," J. Chem. Phys. 155, 014106 (2021).
[85] S. Schwalbe, T. Hahn, S. Liebing, K. Trepte, and J. Kortus, "Fermi-Löwdin orbital self-

interaction corrected density functional theory: Ionization potentials and enthalpies of formation," J. Comput. Chem. 39, 2463–2471 (2018), https://onlinelibrary.wiley.com/doi/pdf/10.1002/jcc.25586.

[86] F. W. Aquino, R. Shinde, and B. M. Wong, "Fractional occupation numbers and self-interaction correction-scaling methods with the Fermi-Löwdin orbital self-interaction correction approach," J. Comput. Chem. 41, 1200–1208 (2020), https://onlinelibrary.wiley.com/doi/pdf/10.1002/jcc.26168.

[87] Y. Yamamoto, C. M. Diaz, L. Basurto, K. A. Jackson, T. Baruah, and R. R. Zope, "Fermi-Löwdin orbital self-interaction correction using the strongly constrained and appropriately normed meta-GGA functional," J. Chem. Phys. 151, 154105 (2019), https://doi.org/10.1063/1.5120532.

[88] K. P. K. Withanage, K. Trepte, J. E. Peralta, T. Baruah, R. Zope, and K. A. Jackson, "On the question of the total energy in the Fermi–Löwdin orbital self-interaction correction method," J. Chem. Theory Comput. 14, 4122–4128 (2018), pMID: 29986131, https://doi.org/10.1021/acs.jctc.8b00344.

[89] D.-y. Kao, K. Withanage, T. Hahn, J. Batool, J. Kortus, and K. Jackson, "Self- consistent self-interaction corrected density functional theory calculations for atoms using Fermi-Löwdin orbitals: Optimized fermi-orbital descriptors for Li–Kr," J. Chem. Phys. 147, 164107 (2017), https://doi.org/10.1063/1.4996498.

[90] K. P. K. Withanage, P. Bhattarai, J. E. Peralta, R. R. Zope, T. Baruah, J. P. Perdew, and K. A. Jackson, "Density-related properties from self-interaction corrected density functional theory calculations," J. Chem. Phys. 154, 024102 (2021).

[91] C. M. Diaz, L. Basurto, S. Adhikari, Y. Yamamoto, A. Ruzsinszky, T. Baruah, and R. R. Zope, "Self-interaction-corrected Kohn–Sham effective potentials using the density-consistent effective potential method," J. Chem. Phys. 155, 064109 (2021).

[92] D. B. Nguyen, M. R. Pederson, J. P. Perdew, K. A. Jackson, and J. E. Peralta, "Initial Fermi orbital descriptors for FLOSIC calculations: The quick-FOD method," Chem. Phys. Lett. 780, 138952 (2021).

[93] S. Schwalbe, K. Trepte, L. Fiedler, A. I. Johnson, J. Kraus, T. Hahn, J. E. Peralta, K. A. Jackson, and J. Kortus, "Interpretation and automatic generation of Fermi-orbital descriptors," J. Comput. Chem. 40, 2843–2857 (2019).

[94] K. Trepte, S. Schwalbe, S. Liebing, W. T. Schulze, J. Kortus, H. Myneni, A. V. Ivanov, and

S. Lehtola, “Chemical bonding theories as guides for self-interaction corrected solutions: Multiple local minima and symmetry breaking,” J. Chem. Phys. 155, 224109 (2021).
[95] K. Wagle, B. Santra, P. Bhattarai, C. Shahi, M. R. Pederson, K. A. Jackson, and J. P. Perdew, “Self-interaction correction in water-ion clusters,” J. Chem. Phys. 154, 094302 (2021).
[96] K. Sharkas, K. Wagle, B. Santra, S. Akter, R. R. Zope, T. Baruah, K. A. Jackson, J. P. Perdew, and J. E. Peralta, “Self-interaction error overbinds water clusters but cancels in structural energy differences,” Proc. Natl. Acad. Sci. 117, 11283–11288 (2020), https://www.pnas.org/content/117/21/11283.full.pdf.
[97] J. Vargas, P. Ufondu, T. Baruah, Y. Yamamoto, K. A. Jackson, and R. R. Zope, “Importance of self-interaction-error removal in density functional calculations on water cluster anions,” Phys. Chem. Chem. Phys. 22, 3789–3799 (2020).
[98] K. Sharkas, L. Li, K. Trepte, K. P. K. Withanage, R. P. Joshi, R. R. Zope, T. Baruah, J. K. Johnson, K. A. Jackson, and J. E. Peralta, “Shrinking self-interaction errors with the Fermi-Löwdin orbital self-interaction-corrected density functional approximation,” J. Phys. Chem. A 122, 9307–9315 (2018).
[99] K. Trepte, S. Schwalbe, T. Hahn, J. Kortus, D.-Y. Kao, Y. Yamamoto, T. Baruah, R. R. Zope, K. P. K. Withanage, J. E. Peralta, and K. A. Jackson, “Analytic atomic gradients in the Fermi-Löwdin orbital self-interaction correction,” J. Comput. Chem. 40, 820–825 (2019), https://onlinelibrary.wiley.com/doi/pdf/10.1002/jcc.25767.
[100] B. Santra and J. P. Perdew, “Perdew-Zunger self-interaction correction: How wrong for uniform densities and large-Z atoms?” J. Chem. Phys. 150, 174106 (2019), https://doi.org/10.1063/1.5090534.
[101] C. Shahi, P. Bhattarai, K. Wagle, B. Santra, S. Schwalbe, T. Hahn, J. Kortus, K. A. Jackson, J. E. Peralta, K. Trepte, S. Lehtola, N. K. Nepal, H. Myneni, B. Neupane, S. Adhikari, A. Ruzsinszky, Y. Yamamoto, T. Baruah, R. R.Zope, and J. P. Perdew, “Stretched or noded orbital densities and self-interaction correction in density functional theory,” J. Chem. Phys. 150, 174102 (2019), https://doi.org/10.1063/1.5087065.
[102] S. Ruan, K. A. Jackson, and A. Ruzsinszky, “Spin-crossover complexes: Self-interaction correction vs density correction,” The Journal of Chemical Physics 158 (2023).
[103] D. C. Liu and J. Nocedal, “On the limited memory BFGS method for large scale optimization,” Math. Program. 45, 503–528 (1989).

[104] J. P. Perdew, J. A. Chevary, S. H. Vosko, K. A. Jackson, M. R. Pederson, D. J. Singh, and C. Fiolhais, “Atoms, molecules, solids, and surfaces: Applications of the generalized gradient approximation for exchange and correlation,” Phys. Rev. B 46, 6671–6687 (1992).
[105] J. P. Perdew, K. Burke, and M. Ernzerhof, “Generalized gradient approximation made simple,” Phys. Rev. Lett. 77, 3865–3868 (1996).
[106] J. P. Perdew, K. Burke, and M. Ernzerhof, “Generalized gradient approximation made simple [Phys. Rev. Lett. 77, 3865 (1996)],” Phys. Rev. Lett. 78, 1396–1396 (1997).
[107] J. W. Furness, A. D. Kaplan, J. Ning, J. P. Perdew, and J. Sun, “Accurate and numerically efficient r2SCAN meta-generalized gradient approximation,” J. Phys. Chem. Lett. 11, 8208–8215 (2020), pMID: 32876454, https://doi.org/10.1021/acs.jpclett.0c02405.
[108] R. R. Zope, T. Baruah, and K. A. Jackson, “FLOSIC 0.2,” Based on the NRLMOL code of M. R. Pederson.
[109] D. Porezag and M. R. Pederson, “Optimization of Gaussian basis sets for density-functional calculations,” Phys. Rev. A 60, 2840–2847 (1999).
[110] J. M. Herbert and M. Head-Gordon, “Calculation of electron detachment energies for water cluster anions: An appraisal of electronic structure methods, with application to (h2o)−
20and (h2o)−24,” J. Phys. Chem. A 109, 5217–5229 (2005).
[111] K. Yagi, Y. Okano, T. Sato, Y. Kawashima, T. Tsuneda, and K. Hirao, “Water cluster anions studied by the long-range corrected density functional theory,” J. Phys. Chem. A 112, 9845–9853 (2008), pMID: 18778041, https://doi.org/10.1021/jp802927d.
[112] J. Doumont, F. Tran, and P. Blaha, “Implementation of self-consistent MGGA functionals in augmented plane wave based methods,” Phys. Rev. B 105, 195138 (2022).
[113] A. P. Bartók and J. R. Yates, “Regularized SCAN functional,” J. Chem. Phys. 150, 161101 (2019), https://doi.org/10.1063/1.5094646.
[114] D. Mejía-Rodríguez and S. B. Trickey, “Comment on "Regularized SCAN functional" [J. Chem. Phys. 150, 161101 (2019)],” J. Chem. Phys. 151, 207101 (2019), https://doi.org/10.1063/1.5120408.
[115] A. P. Bartók and J. R. Yates, “Response to "Comment on ’Regularized SCAN functional’" [J. Chem. Phys. 151, 207101 (2019)],” J. Chem. Phys. 151, 207102 (2019), https://doi.org/10.1063/1.5128484.
[116] P. J. Hay and W. R. Wadt, “Ab initio effective core potentials for molecular calculations.

Potentials for K to Au including the outermost core orbitals," J. Chem. Phys. 82, 299–310 (1985).
[117] B. J. Lynch and D. G. Truhlar, "Small representative benchmarks for thermochemical calculations," J. Phys. Chem. A 107, 8996–8999 (2003), https://doi.org/10.1021/jp035287b.
[118] R. Peverati and D. G. Truhlar, "Communication: A global hybrid generalized gradient approximation to the exchange-correlation functional that satisfies the second-order density-gradient constraint and has broad applicability in chemistry," J. Chem. Phys. 135, 191102 (2011), https://doi.org/10.1063/1.3663871.
[119] R. R. Zope, Y. Yamamoto, C. M. Diaz, T. Baruah, J. E. Peralta, K. A. Jackson, B. Santra, and J. P. Perdew, "A step in the direction of resolving the paradox of Perdew-Zunger self-interaction correction," J. Chem. Phys. 151, 214108 (2019).
[120] P. Mishra, Y. Yamamoto, J. K. Johnson, K. A. Jackson, R. R. Zope, and T. Baruah, "Study of self-interaction-errors in barrier heights using locally scaled and Perdew–Zunger self-interaction methods," J. Chem. Phys. 156, 014306 (2022).
[121] A. Karton, R. J. O'Reilly, and L. Radom, "Assessment of theoretical procedures for calculating barrier heights for a diverse set of water-catalyzed proton-transfer reactions," J. Phys. Chem. A 116, 4211–4221 (2012).
[122] J. F. Janak, "Proof that ∂ e ∂ ni = ε in density-functional theory," Phys. Rev. B 18, 7165–7168 (1978).
[123] M. Levy, J. P. Perdew, and V. Sahni, "Exact differential equation for the density and ionization energy of a many-particle system," Phys. Rev. A 30, 2745–2748 (1984).
[124] M. K. Harbola, "Relationship between the highest occupied Kohn-Sham orbital eigenvalue and ionization energy," Phys. Rev. B 60, 4545–4550 (1999).
[125] J. P. Perdew and M. Levy, "Comment on "Significance of the highest occupied Kohn-Sham eigenvalue"," Phys. Rev. B 56, 16021 (1997).
[126] E. Alizadeh and L. Sanche, "Precursors of solvated electrons in radiobiological physics and chemistry," Chem. Rev. 112, 5578–5602 (2012).
[127] J. M. Herbert and M. P. Coons, "The hydrated electron," Annu. Rev. Phys. Chem. 68, 447–472 (2017).
[128] M. Del Ben, J. Hutter, and J. VandeVondele, "Probing the structural and dynamical properties of liquid water with models including non-local electron correlation," J. Chem. Phys. 143 (2015).

[129] D. Manna, M. K. Kesharwani, N. Sylvetsky, and J. M. L. Martin, "Conventional and explicitly correlated ab initio benchmark study on water clusters: Revision of the BEGDB and WATER27 data sets," J. Chem. Theory Comput. 13, 3136–3152 (2017), pMID: 28530805, https://doi.org/10.1021/acs.jctc.6b01046.

[130] A. Rakshit, P. Bandyopadhyay, J. P. Heindel, and S. S. Xantheas, "Atlas of putative minima and low-lying energy networks of water clusters n = 3-25," J. Chem. Phys. 151 (2019), 10.1063/1.5128378, 214307, https://pubs.aip.org/aip/jcp/article-pdf/doi/10.1063/1.5128378/13361994/214307_1_online.pdf.

[131] A. Malloum, J. J. Fifen, Z. Dhaouadi, S. G. Nana Engo, and J. Conradie, "Structures, relative stability and binding energies of neutral water clusters, (H2O)2˜30," New J. Chem. 43, 13020–13037 (2019).

[132] D. Manna, M. K. Kesharwani, N. Sylvetsky, and J. M. Martin, "Conventional and explicitly correlated ab initio benchmark study on water clusters: Revision of the begdb and water27 data sets," J. Chem. Theory Comput. 13, 3136–3152 (2017).

[133] J. P. Furtado, A. P. Rahalkar, S. Shanker, P. Bandyopadhyay, and S. R. Gadre, "Facilitating minima search for large water clusters at the MP2 level via molecular tailoring," J. Phys. Chem. Lett. 3, 2253–2258 (2012).

[134] National Institute of Standards and Technology, NIST Computational Chemistry Comparison and Benchmark Database NIST Standard Reference Database Number 101 Release 19, April 2018, Editor: Russell D. Johnson III http://cccbdb.nist.gov/ DOI:10.18434/T47C7Z.

[135] J. Miralles, J.-P. Daudey, and R. Caballol, "Variational calculation of small energy differences. The singlet-triplet gap in [Cu2Cl6]2−," Chem. Phys. Lett. 198, 555–562 (1992).

[136] O. Castell, J. Miralles, and R. Caballol, "Structural dependence of the singlet-triplet gap in doubly bridged copper dimers: A variational CI calculation," Chem. Phy. 179, 377–384 (1994).

[137] L. Noodleman, "Valence bond description of antiferromagnetic coupling in transition metal dimers," J. Chem. Phys. 74, 5737–5743 (1981).

[138] R. D. Willett, D. Gatteschi, and O. Kahn, "Magneto-structural correlations in exchange coupled systems," Tech. Rep. (D. Reidel Publishing Co., Hingham, MA, 1985).

[139] K. Ray, T. Weyhermüller, F. Neese, and K. Wieghardt, "Electronic structure of square planar bis (benzene-1, 2-dithiolato) metal complexes [m (l) 2] z (z= 2-, 1-, 0; m= ni, pd, pt, cu, au): An experimental, density functional, and correlated ab initio study," Inorg. Chem. 44, 5345–5360

(2005).
[140] M. S. Fataftah, M. D. Krzyaniak, B. Vlaisavljevich, M. R. Wasielewski, J. M. Zadrozny, and D. E. Freedman, “Metal–ligand covalency enables room temperature molecular qubit candidates,” Chem. Sci. 10, 6707–6714 (2019).
[141] B. K. Maiti, L. B. Maia, K. Pal, B. Pakhira, T. Avilés, I. Moura, S. R. Pauleta, J. L. Nuñez, A. C. Rizzi, C. D. Brondino, et al., “One electron reduced square planar bis (benzene-1, 2-dithiolato) copper dianionic complex and redox switch by o2/ho–,” Inorg. Chem. 53, 12799–12808 (2014).
[142] E. Engel, J. A. Chevary, L. D. Macdonald, and S. H. Vosko, “Asymptotic properties of the exchange energy density and the exchange potential of finite systems: relevance for generalized gradient approximations”, Zeitschrift für Physik D Atoms, Molecules and Clusters volume 23, pages7–14 (1992).

CHAPTER 3: SPIN-STATE GAPS AND SELF-INTERACTION-CORRECTED DENSITY FUNCTIONAL APPROXIMATIONS: OCTAHEDRAL FE(II) COMPLEXES AS CASE STUDY

Reproduced from "Spin-state gaps and self-interaction-corrected density functional approximations: Octahedral Fe(II) complexes as case study", Selim Romero, Tunna Baruah, and Rajendra Rajendra Zope, J. Chem. Phys. 158, 054305 (2023), https://doi.org/10.1063/5.0133999, with the permission of AIP Publishing.

3.1 ABSTRACT

Accurate prediction of spin-state energy difference is crucial for understanding the spin crossover (SCO) phenomena and is very challenging for density functional approximations, especially for local and semi-local approximations due to delocalization errors. Here, we investigate the effect of self-interaction error removal from the local spin density approximation (LSDA) and PBE generalized gradient approximation on the spin-state gaps of Fe(II) complexes with various ligands using recently developed locally scaled self-interaction correction (LSIC) by Zope *et al.* [J. Chem. Phys. **151**, 214108 (2019)]. The LSIC method is exact for one-electron density, recovers uniform electron gas limit of the underlying functional, and approaches the well-known Perdew-Zunger self-interaction correction (PZSIC) as a particular case when the scaling factor is set to unity. Our results, when compared with reference diffusion Monte Carlo (DMC) results, show that the PZSIC method significantly overestimates spin-state gaps favoring low spin states for all ligands, and does not improve upon DFAs. The perturbative LSIC-LSDA using PZSIC densities significantly improves the gaps with a mean absolute error of 0.51 eV but slightly overcorrects for the stronger CO ligands. The quasi self-consistent LSIC-LSDA, like CCSD(T), gives a correct sign of spin-state gaps for all ligands with MAE of 0.56 eV, comparable to that of CCSD(T) (0.49 eV).

3.2 INTRODUCTION

The Kohn–Sham (KS) formulation of the density functional theory (DFT) is an exact theory that is widely used in many areas, such as chemical physics, materials science, and condensed matter physics [1]. Its practical usage requires approximations of the exchange–correlation energy functional, whose complexity determines the accuracy and efficiency of the calculations and system sizes that could be studied. Since there is no systematic way to improve upon the accuracy of exchange–correlation approximations, a large number of density functional approximations (DFAs) with various ingredients have been proposed [2,3]. Semi-local density functionals, in general, offer a good balance of accuracy and efficiency; hence, they are widely used in calculations of large system sizes. While many DFAs perform well for closed-shell systems, they can fail to accurately describe the spin states of the open-shell systems, such as transition metal complexes or organic radicals. Such systems typically have multiple electronic configurations that are close in energy, thereby resulting in several accessible spin states. Prototype examples of such systems are spin-crossover Fe-centered complexes [4-35]. In these systems, the spin-state can change with small temperature/pressure variations. Difficulties of the DFAs in properly describing the *d* electrons in these complexes arise due to inherent self-interaction-error (SIE) in these functionals. SIE can limit their ability to provide a qualitatively accurate description of spin-state ordering in these systems.

The SIE in DFA arises due to the incomplete cancellation of the self-Coulomb energy by the self-exchange energy of the approximate density functionals for one-electron density. The consequences are poor performance for many properties, such as low reaction barrier heights, underestimation of eigenvalues of valence orbitals and unbound atomic anions, overestimation of polarizabilities of molecular chains, and underestimation of bandgaps [36-40]. Perdew and co-workers showed that the density functional total energy of an N-electron system should vary linearly between integer numbers of electrons. However, with the approximate density functionals, the total energy of an N-electron system varies as a convex curve as the electronic charge varies between N and $N + 1$ electrons [41,42]. The DFAs artificially lower the energy of a fractional electron system and thereby produce a convex curve instead of a linear curve between integer electron numbers. This deviation from the linearity is often called *delocalization error* [43-46] or sometimes the *many-electron* SIE [40]. The delocalization error is particularly severe for systems

with *d* or *f* electrons. The SIE can result in incorrect charge states and, consequently, yield erroneous spin-state ordering. Indeed, the elimination of delocalization errors in practical density functional calculations is considered the most outstanding challenge in density functional theory [47].

In this work, we investigate and compare the effect of one-electron self-interaction correction [48] (SIC) on the energy gap between spin-states of single Fe-center complexes using a recently locally scaled self-interaction correction (LSIC) method of Zope and co-workers [49] and compare the results with the well-known Perdew–Zunger SIC (PZSIC) [50] method. The SIC corrections are applied to the simplest local spin density functional (LSDA) and one of the most widely used generalized-gradient-approximations (GGAs) of Perdew, Burke, and Ernzerhof (PBE). Our work shows that the PZSIC performs poorly for the spin-state gaps, favoring low spin states for all cases, while LSIC methods perform significantly better (especially quasi-self-consistent LSIC-LSDA) with a mean absolute error comparable to those of CCSD(T).

In Secs. 2 and 3, we provide brief descriptions of the methods used in this work and the computational details. The results and discussion are presented in Sec. 4.

3.3 THE LOCALLY SCALED SELF-INTERACTION CORRECTION (LSCI) METHOD

LSIC [49] is a one-electron SIC method that is exact for single electron cases, and it employs an orbital-by-orbital correction scheme [48] in which the total energy is given as

$$E^{LSIC}[\rho_\uparrow, \rho_\downarrow] = E^{DFA}[\rho_\uparrow, \rho_\downarrow] + E^{SIC}. \tag{3.1}$$

Here,

$$E^{SIC} = -\Sigma_{i\sigma}^{occ}\{U^{LSIC}[\rho_{i\sigma}] + E_{XC}^{LSIC}[\rho_{i\sigma}, 0]\} \tag{3.2}$$

with

$$U^{LSIC}[\rho_{i\sigma}] = \frac{1}{2}\int d\vec{r}\; z(\vec{r})\rho_{i\sigma}(\vec{r}) \int d\vec{r}\,' \frac{\rho_{i\sigma}(\vec{r}\,')}{|\vec{r}-\vec{r}\,'|}, \tag{3.3}$$

$$E_{XC}^{LSIC}[\rho_{i\sigma}, 0] = \int d\vec{r}\; z(\vec{r})\varepsilon_{XC}^{DFA}([\rho_{i\sigma}, 0], \vec{r}), \tag{3.4}$$

where ε_{XC}^{DFA} is the exchange–correlation energy density per particle. Here, $z_\sigma(\vec{r})$ is the local scaling factor $z_\sigma(\vec{r}) = \tau_\sigma^W(\vec{r})/\tau_\sigma(\vec{r})$, where $\tau_\sigma^W = \left|\vec{\nabla}\rho_\sigma\right|^2/(8\rho_\sigma)$ is the von Weizsäcker kinetic energy density and $\tau_\sigma(\vec{r}) = \frac{1}{2}\Sigma_i\left|\nabla\psi_{i,\sigma}\right|^2$ is the non-interacting kinetic energy density. The scaling factor z_σ is an iso-orbital indicator, which lies between 0 and 1, indicating the nature of the charge for $z_\sigma(\vec{r}) = 1$ as single electron density and for $z_\sigma(\vec{r}) = 0$ as the uniform electron density. Scaling SIC terms with z_σ thus retains the full correction for a one-electron density, making the theory exact in that limit, and eliminates the correction in the limit of uniform density where E_{XC}^{DFA} is already exact by design. The LSIC method can be adapted using any suitable iso-orbital indicator similar to the local hybrid functionals.

The well-known PZSIC method is a special case of the LSIC method when the iso-orbital z_σ in Eqs. (3.3) and (3.4) is set to 1. The total energy in LSIC and in PZSIC not only depends on the density but also on the specific choice of orbitals used to represent that density. Local orbitals are derived from the canonical orbitals through a unitary transformation, and the total energy needs to be minimized with respect to the unitary transformation. Both PZSIC and LSIC total energies are evaluated using the Fermi–Löwdin localized orbitals, as described in subsection 3.3.1.

3.3.1 FERMI-LÖWDIN SELF-INTERACTION-CORRECTION

We use LSIC and PZSIC within the Fermi–Löwdin orbital self-interaction correction (FLOSIC) scheme [51]. In the FLOSIC scheme [51], the SI correction to the total energy in Eq. (3.2) is computed using local orbitals based on Fermi orbitals (FOs) [52]. The Fermi orbitals are obtained from the spin density matrix and spin density as

$$F_{j\sigma}(\vec{r}) = \Sigma_i \frac{\psi_{i\sigma}(\vec{a}_j)\psi_{i\sigma}(\vec{r})}{\sqrt{\rho_\sigma(\vec{a}_j)}}. \quad (3.5)$$

where i and j are the indices of the ith KS orbital and jth FO, respectively, σ is the spin index, and $\vec{a}_j$ are position coordinates referred to as Fermi orbital descriptors (FODs). The FOs are normalized but not orthogonal to each other. Therefore, symmetric orthogonalization is applied to the FOs through the Löwdin [53] scheme to obtain Fermi–Löwdin orbitals (FLOs).

The optimal FLOs are obtained by minimizing *EPZSIC* with respect to the FOD positions [54,55] using a gradient optimization scheme [56]. Further details regarding the FLOSIC methodology and examples of FLOSIC calculations for various properties are available in Refs. 51,54,55, and 57-65.

3.4 COMPUTATIONAL DETAILS

All our calculations were performed using the FLOSIC code [66,67] at the all-electron level and use an extensive Gaussian basis set optimized for the PBE functional [68]. We note that our results for the PBE functional reproduce the literature results [5], validating the choice of the present basis sets. The LSDA functional as parameterized in the PW92 functional [69] is used in SIC-LSDA calculations. LSIC is well-defined for the LSDA functional with no gauge dependency [70]. Our earlier experience, however, shows that LSIC often performs well with the PBE functional [70,71] even though the formal gauge dependency occurs. We applied LSIC with both LSDA and PBE functionals in this study. The self-consistent FLOSIC calculations with $z_\sigma = 1$, i.e., PZSIC, can be performed either using the optimized effective potential within the Krieger–Li–Iafrate approximation [61] or using the Jacobi update approach [57]. Here, we used the latter approach. The quasi-self-consistent LSIC (qLSIC) calculations are performed by ignoring the variation of the scaling factor, as explained in Ref. 71.

In this approach, local scaling is applied to the SIC potential and to the SIC energy density, as shown in Eq. (3.1). We also computed LSIC-DFA total energies using the self-consistent PZSIC densities. A self-consistency tolerance for the total energy of $10^{-6}E_h$ was used in all calculations.

The FOD positions were optimized within PZSIC until the forces [54,55] on the FODs dropped below $10^{-3}E_h/a_0$. All calculations presented herein employed these FOD positions.

Since the self-consistent FLOSIC calculations on the transition metal complexes are not yet very common and are usually challenging, we briefly outline our procedure for the reproducibility of our results. To initiate self-consistent FLOSIC calculation, one needs not only an initial guess of density but also an initial set of FODs that are used to construct initial FLOs. In this work, we use various initial guesses for the density and FOD sets that are compatible with the initial densities. These initial FOD configurations are generated using our recently developed scheme that generates an FOD structure from any single determinantal wave function. We have generated multiple sets of initial FOD configurations using self-consistent densities from various DFAs for each complex. Additionally, we also begin a self-consistent cycle using the superposition of self-interaction-corrected (with LSDA functional) atomic potentials. This procedure usually works. In some cases, the self-interaction-correction can rapidly change the electron density in the self-consistent cycle, resulting in non-compatibility between an initial FOD structure (used at the start of self-consistency) and the electron density at a given self-consistent cycle. This breaks the self-consistent FLOSIC cycle due to small eigenvalues of the overlap matrix during Löwdin orthogonalization, indicating linear dependence of FLOs. This is one of the major difficulties in performing self-consistent FLOSIC calculations. In such cases, we use partially self-interaction-corrected densities from the previous iteration to generate a new set of FODs and restart the calculations. This procedure can be iterated as needed. The details of this method will be published elsewhere. Starting calculations using multiple initial guesses and FOD configurations resulted in the same final energies for all complexes within the tolerances mentioned in Sec. 3.3. The final (optimized) set of FOD positions can be found in the supplementary material (https://aip.scitation.org/doi/suppl/10.1063/5.0133999).

3.5 RESULTS AND DISCUSSION

The octahedral Fe(II) complexes studied in this work are shown in Fig. 3.1. The spin-state ordering of such complexes has been studied earlier by a number of groups to examine the performances of various methods in predicting the spin-state gaps [4-35]. We use the complexes

studied earlier by Wilbraham and co-workers [5] at the double-hybrid levels. These complexes are in octahedral conformation with four different ligands (L), where L = H2O, NH3, NCH, and CO. The ligand field strengths of these four ligands are different. The hexa-aqua and hexa-amine chelated complexes are examples of weak-field limits, while the hexa-carbonyl represents a strong field limit. We used the geometries of Wilbraham and co-workers [5], which are optimized at the PBE0 [72] level of theory, using the modified def2-TZVPP [73] large basis set. The valence electronic configuration of Fe is $3d^6\ 4s^2$. The spin states considered for the Fe(II) complexes are singlet (low spin state) and the quintet (high spin state). In the present calculations, the spin gap between the quintet (HS) and singlet (LS) is defined as

$$\Delta E^{HS-LS} = E(HS) - E(LS) \tag{3.6}$$

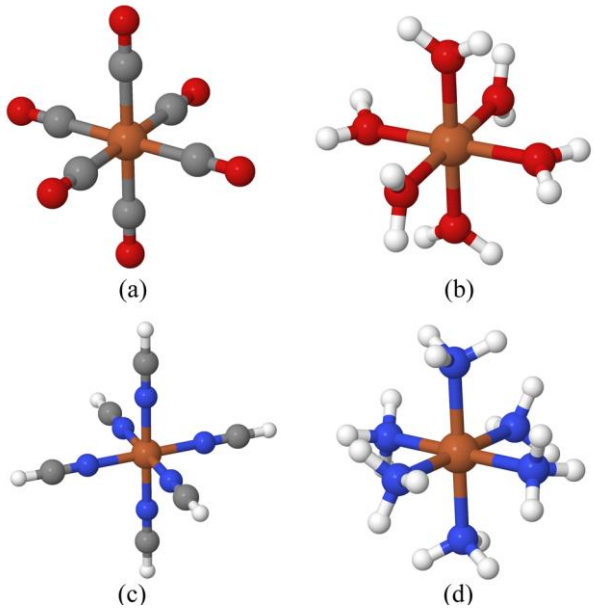

Fig. 3.1. The molecular structures for the systems $[FeL_6]^{2+}$ for $L = CO, H_2O, NCH$ and NH_3.

The spin-state gaps defined as ΔE^{HS-LS} are presented for DFA, PZSIC, LSIC, and qLSIC with LSDA and PBE functionals in Table 3.1. The diffusion Monte Carlo (DMC) spin gap energy values from Ref. 14 are taken as reference. For the sake of comparison, coupled-cluster single double and perturbative triple [CCSD(T)] values are also presented. The positive (negative) values

in Table 3.1 indicate that the LS (HS) state is more stabilized than the HS (LS) state. First, we would like to note that our PBE results are essentially identical to those of Wilbraham and co-workers [5], validating our choices of computational parameters and, especially, of the basis sets. The DFAs, both LSDA and PBE, predict the sign of the spin-state gaps correctly for the weak field ligand H2O and for the strong field ligand CO. However, the errors for the spin gaps are rather large, especially for CO. For the other two ligands, both LSDA and PBE favor low spin states. This is generally known [5,11,12] and has been attributed due to delocalization errors (or self-interaction errors) of these functionals. On the other hand, the Hartree–Fock method that is one electron self-interaction-free and lacks dynamical correlation tends to stabilize high spin states over low spin states. This observation has led to a few studies that explored the reduction of over-stabilization by DFAs by mixing various percentages of HF exchange in the global hybrid functionals [5,26,29]. In general, global hybrid functionals perform better than the local and semi-local functionals. It has also been noted by Song *et al.* that using HF density in the semi-local functional results in improved prediction of the spin-state gaps by the semi-local functionals [14]. Likewise, Propokiou and Kronik reported that correct prediction of the ground spin states of spin-crossover complexes using range separated functionals requires the reduction of the short-range exact exchange fraction to 15% [74]. This observation suggests that one-electron self-interaction correction methods, such as PZSIC or LSIC, might improve spin gaps.

Table 3.1. The spin-state gaps (in eV) calculated with the LSDA and PBE functionals at the DFA, PZSIC, LSIC, and qLSIC levels. MAEs are with respect to diffusion Monte Carlo (DMC). DMC and CCSD(T) values are from Ref. 5.

System	$[Fe(H_2O)_6]^{2+}$	$[Fe(CO)_6]^{2+}$	$[Fe(NCH)_6]^{2+}$	$[Fe(NH_3)_6]^{2+}$	MAE (eV)
LSDA	−0.49	5.24	2.29	0.98	2.90
PBE	−1.17	3.40	0.96	0.08	1.72
PZSIC-LSDA	1.50	2.11	1.81	2.00	2.75
PZSIC-PBE	1.16	0.93	1.27	1.35	2.08
LSIC-LSDA	−1.26	−0.49	−1.15	−0.82	0.51
LSIC-PBE	−1.06	3.40	−1.02	−0.60	1.08
qLSIC-LSDA	−1.08	0.40	−0.54	−0.50	0.56
qLSIC-PBE	−0.94	4.45	−0.44	−0.34	1.58
CCSD(T)	−1.75	1.33	−0.43	−0.78	0.49
DMC	−1.78	0.59	−1.17	−1.23	

The spin-state gaps predicted by the PZSIC method are included in Table 3.1. It is evident that the PZSIC method does not improve upon the bare DFA functionals except for the CO ligand. The mean absolute errors (MAEs) with LSDA, PBE, PZSIC-LSDA, and PZSIC-PBE are 2.90, 1.72, 2.75, and 2.08 eV, respectively. The MAEs show that PZSIC-LSDA barely improves LSDA results, while for PBE functional, PZSIC performs worse than the uncorrected PBE functional. A closer look at the results indicates that PZSIC has a tendency to stabilize the low spin states. Even in the case of a weak field ligand H2O, where uncorrected LSDA and PBE functionals give qualitatively correct results, the PZSIC favors low-spin states, thus worsening the DFA spin gap results qualitatively and quantitatively. It has been known that the PZSIC does not improve upon DFAs (especially semi-local DFAs) for thermochemical properties, but its performance for spin-state gaps has not been known. This failure of the PZSIC method to predict correct spin states is rather surprising and is the most unexpected result of this work. We will return to the discussion of the failure of the PZSIC method toward the end of this section.

The scaling down of the SIC in the many-electron regions using the LSIC method brings the results closer to the DMC results (cf. Table 3.1). This is a perturbative approach that does not change the PZSIC density. The one-shot LSIC method gives results that are in more quantitative agreement with the reference values. The MAE for LSIC-LSDA and LSIC-PBE drops to 0.51 and 1.08 eV from 2.75 and 2.08 eV for PZSIC-LSDA and PZSIC-PBE functionals, respectively. For comparison, the CCSD(T) MAE (0.49 eV) is comparable to LSIC-LSDA MAE. Since the one-shot LSIC is a perturbative approach that does not change the PZSIC density, the improvement comes directly from the LSIC energy functional. The perturbative LSIC significantly reduces the

excessive SIC correction of the PZSIC, thereby improving the results, but it slightly overcorrects in the case of the strong ligand CO. On the other hand, the quasi-LSIC (qLSIC), where the orbital-dependent SIC potentials are scaled, correctly predicts the sign of spin-state gaps for all the complexes studied here. The MAE of the spin gaps in the case of qLSIC-LSDA is 0.56 eV, which is comparable to that of CCSD(T) (0.49 eV). The results also show that both qLSIC and one-shot LSIC perform better with the simpler LSDA than with the PBE functional.

To understand the improved performance of the LSIC method and the failure of the PZSIC method, we analyze the contributions to the spin-state gap from the DFA energy terms, i.e., the first term on the right-hand side (RHS) of Eq. (3.1) and the sum of orbital-wise SIC corrections [i.e., Eq. (3.2)]. Thus, we substitute Eq. (3.1) into Eq. (3.6), resulting in the following expression:

$$\Delta E^{HS-LS} = \Delta E_{DFA}^{HS-LS} + \Delta E_{SIC}^{HS-LS} \tag{3.7}$$

The first term on the RHS is therefore the DFA spin-state gap evaluated using the SIC density, and the second term is the correction due to the energy. This analysis, in some sense, is similar to the HF-DFT approach [75-78]. Unlike the HF-DFT, however, the advantage here is that the E^{DFA} contributions are part of the PZSIC and qLSIC energies and no additional calculations are required. The DFA contribution to the spin-state gaps calculated on self-consistent PZSIC-DFA and qLSIC-DFA densities are shown in Table 3.2. To simplify the discussion below, we use the ΔE_{En}^{Den} notation to convey the calculation scheme where the subscript refers to the energy functional and the superscript refers to the underlying functional for the SIC density. The MAE of $\Delta E_{LSDA}^{PZSIC-LSDA}$ is 1.30 eV. This is significantly better than LSDA (MAE = 2.90 eV). Thus, the density changes due to SIC (to the potential) within the PZSIC method result in a reduction of MAE by about 1.6 eV. An even more spectacular reduction in error is obtained in the case of the PBE functional. $\Delta E_{PBE}^{PZSIC-PBE}$ has a MAE of only 0.23 eV in contrast to 2.08 eV of PZSIC-PBE. This is half the MAE of the CCSD(T) method (0.49 eV). As all self-consistent calculations performed with SIC methods herein generate *self-interaction free* densities, we can use these SIC densities in uncorrected DFAs used in this work to get some idea about error cancellations that play a role in predicting spin-state gaps. It turns out that the PBE functional performs excellently not only with the PZSIC-PBE density but also with PZSIC-LSDA densities (with MAE = 0.34 eV). This suggests that more sophisticated meta-GGA functionals may also perform well for spin-state gaps,

but that discussion is beyond the scope of this work. The use of qLSIC densities in the uncorrected DFAs, however, does not show a similar level of improvement in the spin-state gaps. For example, $\Delta E_{LSDA}^{qLSIC-LSDA}$ has an MAE of 2.48 eV comparable to that of LSDA. Similarly, $\Delta E_{PBE}^{qLSIC-PBE}$ has an MAE of 1.37 eV. These results are not very surprising. It is apparent from Eq. (3.7) that any method that performs well with ΔE_{DFA}^{HS-LS} for spin-state gaps must yield a small contribution from the SIC term (ΔE_{SIC}^{HS-LS}). This gives a hint that the poor performance of PZSIC is due to its excessive SIC to the energy. Indeed, such a tendency of PZSIC to excessively correct has also been seen in earlier studies [49,60,71,79]. This excessive correcting tendency of PZSIC results in somewhat greater localization of density, which might be beneficial for use in uncorrected DFAs for removing delocalization errors as done in the HF-DFT or density-corrected DFT and also seen in the present results.

Table 3.2. The spin-state gap values (in eV) for $[FeL_6]^{2+}$ calculated with LSDA and PBE from the DFA part in PZSIC and qLSIC calculations [that is, the first term on the right-hand side of Eq. (3.7)]. MAEs are computed against DMC. DMC and CCSD(T) reference values are from Ref. 5.

System	$[Fe(H_2O)_6]^{2+}$	$[Fe(CO)_6]^{2+}$	$[Fe(NCH)_6]^{2+}$	$[Fe(NH_3)_6]^{2+}$	MAE (eV)
$\Delta E_{LSDA}^{PZSIC-LSDA}$	−1.06	2.55	0.28	−0.17	1.30
$\Delta E_{PBE}^{PZSIC-LSDA}$	−1.55	0.93	−0.76	−0.86	0.34
$\Delta E_{LSDA}^{PZSIC-PBE}$	−1.08	2.31	0.11	−0.20	1.18
$\Delta E_{PBE}^{PZSIC-PBE}$	−1.56	0.69	−0.92	−0.88	0.23
$\Delta E_{LSDA}^{qLSIC-LSDA}$	−0.67	4.71	1.69	0.59	2.48
$\Delta E_{PBE}^{qLSIC-PBE}$	−1.29	2.99	0.42	−0.24	1.37
CCSD(T)	−1.75	1.33	−0.43	−0.78	0.49
DMC	−1.78	0.59	−1.17	−1.23	

As discussed below, among all the self-consistent SIC methods used here, the PZSIC density is the most localized. The density differences between the PZSIC and LSDA and between qLSIC and LSDA are plotted in Fig. 3.2 for [Fe(NCH)6]2+. The red iso-surface shows the regions where DFA density is larger than the qLSIC/PZSIC density. The LSDA density is higher in the interatomic region around the Fe center compared to the SIC density. This plot also shows that

although the density differences with PZSIC and qLSIC are similar, with qLSIC, the differences are smaller, particularly near the Fe center. To obtain additional evidence about the (greater) localizing tendency of PZSIC, we compute the spin charges at Fe(II) in the complex by integrating the spin densities within atomic spheres centered at Fe and with a radius equal to the Van der Waals radius of Fe. Likewise, we also compute spin charges using Löwdin's population analysis. These results are presented in Table 3.3. It is evident from Table 3.3 that the uncorrected LSDA and PBE functionals have the smallest values of spin charges consistent with the known delocalization tendency of density within these methods. On the other hand, PZSIC has the largest values of spin charges among all methods, suggesting its spin density to be the most localized among all methods. This is consistent with the above discussion. In addition, the qLSIC spin charges are intermediate between the PZSIC and uncorrected DFA spin charges. The less localized qLSIC density is not favorable for uncorrected DFAs for the density-corrected DFT calculations. The qLSIC-LSDA provides the most balanced description of the spin-state gaps [comparable to CCSD(T)] wherein both the terms in Eq. (3.6) contribute to the gap. The qLSIC-LSDA also predicts the correct sign for spin-state gaps for all ligands. The qLSIC-PBE does not perform as well as qLSIC-LSDA possibly due to gauge-dependence [70].

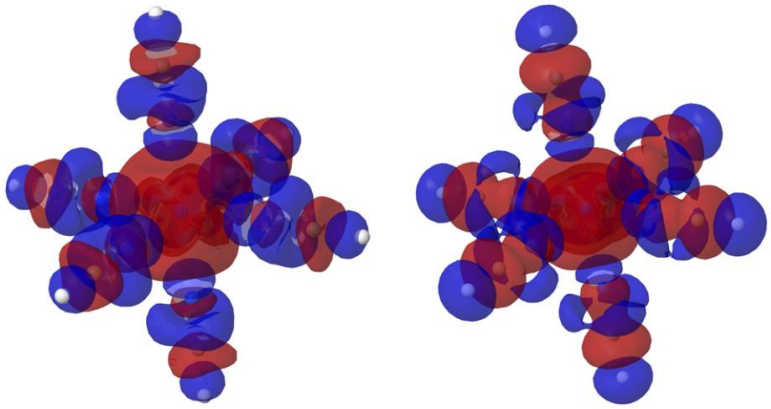

Fig. 3.2. Total density difference of (a) PZSIC-LSDA and LSDA and (b) qLSIC-LSDA and LSDA for the $[Fe(NCH)_6]^{2+}$ complex in the LS state. The isosurface value used for both images is 0.0005e, and the red (blue) surface shows regions where LSDA density is larger (smaller)

Table 3.3. Spin charges (in e) at the Fe site for the high spin-state in various approximations. Spin charges are obtained from Löwdin population analysis and by integrating spin density using atomic sphere (see the text for details).

	H_2O				CO			
	LSDA		PBE		LSDA		PBE	
Population analysis	Atomic sphere	Löwdin	Atomic sphere	Löwdin	Atomic sphere	Löwdin	Atomic sphere	Löwdin
DFA	3.607	3.648	3.637	3.674	3.509	3.665	3.554	3.695
PZSIC	3.768	3.799	3.764	3.793	3.734	3.792	3.708	3.797
qLSIC	3.686	3.724	3.703	3.737	3.587	3.715	3.608	3.727

Another possible explanation for the improved performance of LSIC (that scales down SIC) relative to PZSIC is because scaling down of SIC restores the DFA description in the many-electron region, leading to improved treatment of correlation effects. As noted by Cremer and co-workers [80], the exchange SIE mimics long-range (static) correlation effects, which can be important for spin-crossover systems. The study of spin-crossover systems using hybrid functionals and range-separated functionals with various fractions of the Hartree–Fock exchange shows that the correct prediction of the ground state in these compounds requires a smaller fraction of (short-range in the case of the range separated) exact exchange as including a larger fraction of DFA exchange helps in capturing some static correlation [74,81,82]. However, detailed studies on a large number of transition metal complexes are needed to better understand the error cancellations (balancing of the correlation effects) in the LSIC method.

3.6 CONCLUSIONS

In summary, we have examined the effect of SIC on the spin-state gaps of octahedral [FeL6]2+ complexes with L = CO, NCH, NH3, and H2O using the LSIC and PZSIC methods. One surprising result is that the PZSIC fails to improve upon the DFA results for weak field ligands and has a propensity to stabilize low spin states. Analysis of the results shows that the PZSIC energy functional provides too much SI correction to the energy. In fact, no PZSIC energy correction is needed as the DFA part of the PZSIC functional alone is sufficient to provide good spin gaps. The analysis of the results shows that the PZSIC produces more localized density than

the quasi-self-consistent LSIC method. The more localized density is favorable for use in the uncorrected functional as in the HF-DFT or density-corrected DFT. Indeed, the spin-state gaps obtained using the DFA functional on PZSIC densities are significantly improved compared to those of self-consistent PZSIC or DFA results. This improvement is spectacular for the PBE functional. The perturbative LSIC results evaluated on the PZSIC densities predict accurate spin-state gaps, and its performance is comparable to that of the CCSD(T) method, even with the simplest DFA. Likewise, qLSIC-LSDA predicts the correct sign for spin gaps for all ligands with a mean absolute error comparable to that of CCSD(T). LSIC does not work that well with the PBE functional, especially for the CO ligand possibly due to gauge dependency. Still, it is very gratifying that the simplest (LSDA) density functional when corrected for SIE using the LSIC method accurately predicts spin-state gaps of Fe(II) complexes and predicts correct spin states as the most stable states. It remains unclear if the LSIC method will perform to the same degree of excellence for other SCO complexes. We will be undertaking a large-scale study to address this question.

3.7 SUPPLEMENTAL MATERIAL

The supplementary material (https://aip.scitation.org/doi/suppl/10.1063/5.0133999) contains the optimized FOD positions (X = up FOD, Z = down FOD) for each SCO system (H2O, NH3, NCH, and CO) for HS (quintet) and LS (singlet) states with LSDA and PBE functionals and separate plots of spin densities of [Fe(NCH)6)]2+ (cf. Fig. 3.2 in the text) with the qLSIC and PZSIC methods.

3.8 ACKNOWLEDGMENTS

The authors thank Dr. Yoh Yamamoto for discussions. This work was supported by the U.S. Department of Energy, Office of Science, Office of Basic Energy Sciences, as part of the Computational Chemical Sciences Program under Award No. DE-SC0018331. Support for the computational time at the Texas Advanced Computing Center and at NERSC is gratefully

acknowledged. S.R. acknowledges the Mexican National Council for Science and Technology (CONACYT) for financial support.

3.9 AUTHOR DECLARATIONS

3.9.1 CONFLICT OF INTEREST

The authors have no conflicts to disclose.

3.9.2 AUTHOR CONTRIBUTIONS

Selim Romero: Data curation (equal); Formal analysis (equal); Investigation (equal); Software (equal); Validation (equal); Visualization (equal); Writing – original draft (equal). **Tunna Baruah**: Formal analysis (equal); Funding acquisition (equal); Investigation (equal); Methodology (equal); Project administration (equal); Resources (equal); Supervision (equal); Validation (equal); Writing – review & editing (equal). **Rajendra R. Zope**: Conceptualization (equal); Formal analysis (equal); Funding acquisition (equal); Investigation (equal); Methodology (equal); Project administration (equal); Resources (equal); Supervision (equal); Validation (equal); Writing – review & editing (equal).

3.10 DATA AVAILABILITY

The data that support the findings of this study are available within the article.

3.11 REFERENCES

[1] R. O. Jones, “Density functional theory: Its origins, rise to prominence, and future,” Rev. Mod. Phys. **87**, 897 (2015).

[2] J. P. Perdew and K. Schmidt, “Jacob’s ladder of density functional approximations for the exchange-correlation energy,” AIP Conf. Proc. **577**, 1–20 (2001).

[3] M. A. L. Marques, M. J. T. Oliveira, and T. Burnus, “Libxc: A library of exchange and correlation functionals for density functional theory,” Comput. Phys. Commun. **183**, 2272–2281 (2012).

[4] Y. Cytter, A. Nandy, A. Bajaj, and H. J. Kulik, “Ligand additivity and divergent trends in two types of delocalization errors from approximate density functional theory,” J. Chem. Phys. **13**, 004549–4555 (2022).

[5] L. Wilbraham, C. Adamo, and I. Ciofini, “Communication: Evaluating nonempirical double hybrid functionals for spin-state energetics in transition-metal complexes,” J. Chem. Phys. **148**, 041103 (2018).

[6] M. Radon, “Benchmarking quantum chemistry methods for spin-state energetics ′of iron complexes against quantitative experimental data,” Phys. Chem. Chem. Phys. **21**, 4854–4870 (2019).

[7] H. J. Kulik, “Making machine learning a useful tool in the accelerated discovery of transition metal complexes,” Wiley Interdiscip. Rev.: Comput. Mol. Sci. **10**, e1439 (2020).

[8] A. Nandy, D. B. K. Chu, D. R. Harper, C. Duan, N. Arunachalam, Y. Cytter, and H. J. Kulik, “Large-scale comparison of 3d and 4d transition metal complexes illuminates the reduced effect of exchange on second-row spin-state energetics,” Phys. Chem. Chem. Phys. **22**, 19326–19341 (2020).

[9] M. Alipour and T. Izadkhast, “Appraising spin-state energetics in transition metal complexes using double-hybrid models: Accountability of SOS0-PBESCAN0-2(a) as a promising paradigm,” Phys. Chem. Chem. Phys. **22**, 9388–9404 (2020).

[10] S. Vela, M. Fumanal, J. Cirera, and J. Ribas-Arino, “Thermal spin crossover in Fe(II) and Fe(III). Accurate spin state energetics at the solid state,” Phys. Chem. Chem. Phys. **22**, 4938–4945 (2020).

[11] L. A. Mariano, B. Vlaisavljevich, and R. Poloni, “Biased spin-state energetics of Fe(II) molecular complexes within density-functional theory and the linear-response Hubbard *U* correction,” J. Chem. Theory Comput. **16**, 6755–6762 (2020).

[12] L. A. Mariano, B. Vlaisavljevich, and R. Poloni, “Improved spin-state energy differences of

Fe(II) molecular and crystalline complexes via the Hubbard *U*-corrected density," J. Chem. Theory Comput. **17**, 2807–2816 (2021).
[13] B. M. Flöser, Y. Guo, C. Riplinger, F. Tuczek, and F. Neese, "Detailed pair natural orbital-based coupled cluster studies of spin crossover energetics," J. Chem. Theory Comput. **16**, 2224–2235 (2020).
[14] S. Song, M.-C. Kim, E. Sim, A. Benali, O. Heinonen, and K. Burke, "Benchmarks and reliable DFT results for spin gaps of small ligand Fe(II) complexes," J. Chem. Theory Comput. **14**, 2304–2311 (2018).
[15] A. Patra, H. Peng, J. Sun, and J. P. Perdew, "Rethinking CO adsorption on transition-metal surfaces: Effect of density-driven self-interaction errors," Phys. Rev. B **100**, 035442 (2019).
[16] A. Droghetti, D. Alfè, and S. Sanvito, "Assessment of density functional theory for iron(II) molecules across the spin-crossover transition," J. Chem. Phys. **137**, 124303 (2012).
[17] G. Ganzenmüller, N. Berkaïne, A. Fouqueau, M. E. Casida, and M. Reiher, "Comparison of density functionals for differences between the high- (5*T*2*g*) and low- (1*A*1*g*) spin states of iron(II) compounds. IV. Results for the ferrous complexes [Fe (*L*)('NHS4')]," J. Chem. Phys. **122**, 234321 (2005).
[18] D. N. Bowman and E. Jakubikova, "Low-spin vs high-spin ground state in pseudo-octahedral iron complexes," Inorg. Chem. **51**, 6011–6019 (2012).
[19] A. Fouqueau, S. Mer, M. E. Casida, L. M. Lawson Daku, A. Hauser, T. Mineva, and F. Neese, "Comparison of density functionals for energy and structural differences between the high- [5T 2g:(t2g)4(eg)2] and low- [1A1g:(t2g)6(eg)0] spin states of the hexaquoferrous cation [Fe(H2O)6]2+," J. Chem. Phys. **120**, 9473–9486 (2004).
[20] A. Fouqueau, M. E. Casida, L. M. L. Daku, A. Hauser, and F. Neese, "Comparison of density functionals for energy and structural differences between the high- [5T2g:(t2g)4(eg)2] and low- [1A1g:(t2g)6(eg)0] spin states of iron(II) coordination compounds. II. More functionals and the hexaminoferrous cation, [Fe(NH3)6]2+," J. Chem. Phys. **122**, 044110 (2005).
[21] K. Pierloot and S. Vancoillie, "Relative energy of the high- (5*T*2*g*) and low- (1*A*1*g*) spin states of [Fe(H2O)6]2+, [Fe(NH3)6]2+, and [Fe(bpy)3]2+: CASPT2 vs density functional theory," J. Chem. Phys. **125**, 124303 (2006).
[22] K. Pierloot and S. Vancoillie, "Relative energy of the high- (5*T*2*g*) and low- (1*A*1*g*) spin states of the ferrous complexes [Fe(*L*)(NHS4)]: CASPT2 vs density functional theory," J. Chem. Phys.

128, 034104 (2008).
[23] L. Wilbraham, P. Verma, D. G. Truhlar, L. Gagliardi, and I. Ciofini, "Multiconfiguration pair-density functional theory predicts spin-state ordering in iron complexes with the same accuracy as complete active space second-order perturbation theory at a significantly reduced computational cost," J. Phys. Chem. Lett. **8**, 2026–2030 (2017).
[24] P. Verma, Z. Varga, J. E. M. N. Klein, C. J. Cramer, L. Que, and D. G. Truhlar, "Assessment of electronic structure methods for the determination of the ground spin states of Fe(II), Fe(III) and Fe(IV) complexes," Phys. Chem. Chem. Phys. **19**, 13049–13069 (2017).
[25] S. Ye and F. Neese, "Accurate modeling of spin-state energetics in spin-crossover systems with modern density functional theory," Inorg. Chem. **49**, 772–774 (2010).
[26] E. I. Ioannidis and H. J. Kulik, "Towards quantifying the role of exact exchange in predictions of transition metal complex properties," J. Chem. Phys. **143**, 034104 (2015).
[27] A. Rudavskyi, C. Sousa, C. de Graaf, R. W. A. Havenith, and R. Broer, "Computational approach to the study of thermal spin crossover phenomena," J. Chem. Phys. **140**, 184318 (2014).
[28] M. Fumanal, L. K. Wagner, S. Sanvito, and A. Droghetti, "Diffusion Monte Carlo perspective on the spin-state energetics of [Fe(NCH)6]2+," J. Chem. Theory Comput. **12**, 4233–4241 (2016).
[29] B. Pinter, A. Chankisjijev, P. Geerlings, J. N. Harvey, and F. De Proft, "Conceptual insights into DFT spin-state energetics of octahedral transition-metal complexes through a density difference analysis," Chem. Eur. J. **24**, 5281–5292 (2018).
[30] S. R. Mortensen and K. P. Kepp, "Spin propensities of octahedral complexes from density functional theory," J. Phys. Chem. A **119**, 4041–4050 (2015).
[31] L. M. Lawson Daku, F. Aquilante, T. W. Robinson, and A. Hauser, "Accurate spin-state energetics of transition metal complexes. 1. CCSD(T), CASPT2, and DFT study of [M(NCH)6]2+(M = Fe, Co)," J. Chem. Theory Comput. **8**, 4216–4231 (2012).
[32] M. Kepenekian, V. Robert, B. Le Guennic, and C. De Graaf, "Energetics of [Fe(NCH)6]2+ via CASPT2 calculations: A spin-crossover perspective," J. Comput. Chem. **30**, 2327–2333 (2009).
[33] A. Domingo, M. Àngels Carvajal, and C. De Graaf, "Spin crossover in Fe(II) complexes: An *ab initio* study of ligand σ-donation," Int. J. Quantum Chem. **110**, 331–337 (2010).
[34] B. G. Janesko, "Reducing density-driven error without exact exchange," Phys. Chem. Chem. Phys. **19**, 4793–4801 (2017).

[35] M. Swart, “Accurate spin-state energies for iron complexes,” J. Chem. Theory Comput. **4**, 2057–2066 (2008).
[36] J. P. Perdew, “Accurate density functional for the energy: Real-space cutoff of the gradient expansion for the exchange hole,” Phys. Rev. Lett. **55**, 2370 (1985).
[37] L. J. Sham and M. Schlüter, “Density-functional theory of the energy gap,” Phys. Rev. Lett. **51**, 1888–1891 (1983).
[38] S. Patchkovskii and T. Ziegler, “Improving “difficult” reaction barriers with self-interaction corrected density functional theory,” J. Chem. Phys. **116**, 7806–7813 (2002).
[39] J. Gräfenstein, E. Kraka, and D. Cremer, “The impact of the self-interaction error on the density functional theory description of dissociating radical cations: Ionic and covalent dissociation limits,” J. Chem. Phys. **120**, 524–539 (2004).
[40] A. Ruzsinszky, J. P. Perdew, G. I. Csonka, O. A. Vydrov, and G. E. Scuseria, “Spurious fractional charge on dissociated atoms: Pervasive and resilient self-interaction error of common density functionals,” J. Chem. Phys. **125**, 194112 (2006).
[41] P. Mori-Sánchez, A. J. Cohen, and W. Yang, “Localization and delocalization errors in density functional theory and implications for band-gap prediction,” Phys. Rev. Lett. **100**, 146401 (2008).
[42] A. J. Cohen, P. Mori-Sánchez, and W. Yang, “Insights into current limitations of density functional theory,” Science **321**, 792–794 (2008).
[43] X. Zheng, M. Liu, E. R. Johnson, J. Contreras-García, and W. Yang, “Delocalization error of density-functional approximations: A distinct manifestation in hydrogen molecular chains,” J. Chem. Phys. **137**, 214106 (2012).
[44] A. D. Dwyer and D. J. Tozer, “Dispersion, static correlation, and delocalization errors in density functional theory: An electrostatic theorem perspective,” J. Chem. Phys. **135**, 164110 (2011).
[45] C. Li, X. Zheng, N. Q. Su, and W. Yang, “Localized orbital scaling correction for systematic elimination of delocalization error in density functional approximations,” Natl. Sci. Rev. **5**, 203–215 (2018).
[46] E. R. Johnson, A. Otero-de-la-Roza, and S. G. Dale, “Extreme density-driven delocalization error for a model solvated-electron system,” J. Chem. Phys. **139**, 184116 (2013).
[47] K. R. Bryenton, A. A. Adeleke, S. G. Dale, and E. R. Johnson, “Delocalization error: The

greatest outstanding challenge in density-functional theory," Wiley Interdiscip. Rev.: Comput. Mol. Sci. (published online, 2022).
[48] I. Lindgren, "A statistical exchange approximation for localized electrons," Int. J. Quantum Chem. **5**, 411–420 (1971).
[49] R. R. Zope, Y. Yamamoto, C. M. Diaz, T. Baruah, J. E. Peralta, K. A. Jackson, B. Santra, and J. P. Perdew, "A step in the direction of resolving the paradox of Perdew-Zunger self-interaction correction," J. Chem. Phys. **151**, 214108 (2019).
[50] J. P. Perdew and A. Zunger, "Self-interaction correction to density-functional approximations for many-electron systems," Phys. Rev. B **23**, 5048–5079 (1981).
[51] M. R. Pederson, A. Ruzsinszky, and J. P. Perdew, "Communication: Self-interaction correction with unitary invariance in density functional theory," J. Chem. Phys. **140**, 121103 (2014).
[52] W. L. Luken and D. N. Beratan, "Localized orbitals and the Fermi hole," Theor. Chim. Acta **61**, 265–281 (1982).
[53] P. O. Löwdin, "On the non-orthogonality problem connected with the use of atomic wave functions in the theory of molecules and crystals," J. Chem. Phys. **18**, 365–375 (1950).
[54] M. R. Pederson, "Fermi orbital derivatives in self-interaction corrected density functional theory: Applications to closed shell atoms," J. Chem. Phys. **142**, 064112 (2015).
[55] M. R. Pederson and T. Baruah, "Chapter eight - self-interaction corrections within the fermi-orbital-based formalism," in *Advances in Atomic, Molecular, and Optical Physics*, edited by E. Arimondo, C. C. Lin, and S. F. Yelin (Academic Press, 2015), Vol. 64, pp. 153–180.
[56] D. C. Liu and J. Nocedal, "On the limited memory BFGS method for large scale optimization," Math. Program. **45**, 503–528 (1989).
[57] Z.-h. Yang, M. R. Pederson, and J. P. Perdew, "Full self-consistency in the fermiorbital self-interaction correction," Phys. Rev. A **95**, 052505 (2017).
[58] M. R. Pederson, T. Baruah, D.-y. Kao, and L. Basurto, "Self-interaction corrections applied to Mg-porphyrin, C60, and pentacene molecules," J. Chem. Phys. **144**, 164117 (2016).
[59] S. Schwalbe, T. Hahn, S. Liebing, K. Trepte, and J. Kortus, "Fermi-Löwdin orbital self-interaction corrected density functional theory: Ionization potentials and enthalpies of formation," J. Comput. Chem. **39**, 2463–2471 (2018).
[60] Y. Yamamoto, C. M. Diaz, L. Basurto, K. A. Jackson, T. Baruah, and R. R. Zope, "Fermi-

Löwdin orbital self-interaction correction using the strongly constrained and appropriately normed meta-GGA functional," J. Chem. Phys. **151**, 154105 (2019).
[61] C. M. Diaz, T. Baruah, and R. R. Zope, "Fermi-Löwdin-orbital self-interaction correction using the optimized-effective-potential method within the Krieger-LiIafrate approximation," Phys. Rev. A **103**, 042811 (2021).
[62] C. M. Diaz, L. Basurto, S. Adhikari, Y. Yamamoto, A. Ruzsinszky, T. Baruah, and R. R. Zope, "Self-interaction-corrected Kohn–Sham effective potentials using the density-consistent effective potential method," J. Chem. Phys. **155**, 064109 (2021).
[63] F. W. Aquino, R. Shinde, and B. M. Wong, "Fractional occupation numbers and self-interaction correction-scaling methods with the Fermi-Löwdin orbital self-interaction correction approach," J. Comput. Chem. **41**, 1200–1208 (2020).
[64] P. Mishra, Y. Yamamoto, J. K. Johnson, K. A. Jackson, R. R. Zope, and T. Baruah, "Study of self-interaction-errors in barrier heights using locally scaled and Perdew–Zunger self-interaction methods," J. Chem. Phys. **156**, 014306 (2022).
[65] P. Mishra, Y. Yamamoto, P.-H. Chang, D. B. Nguyen, J. E. Peralta, T. Baruah, and R. R. Zope, "Study of self-interaction errors in density functional calculations of magnetic exchange coupling constants using three self-interaction correction methods," J. Phys. Chem. A **126**, 1923–1935 (2022).
[66] R. R. Zope, T. Baruah, and K. A. Jackson, FLOSIC 0.2, Based on the NRLMOL code of M. R. Pederson.
[67] Y. Yamamoto, L. Basurto, C. M. Diaz, R. R. Zope, and T. Baruah, "Self-interaction correction to density functional approximations using Fermi-Löwdin orbitals: methodology and parallelization" (Unpublished).
[68] D. Porezag and M. R. Pederson, "Optimization of Gaussian basis sets for density-functional calculations," Phys. Rev. A **60**, 2840–2847 (1999).
[69] J. P. Perdew and Y. Wang, "Accurate and simple analytic representation of the electron-gas correlation energy," Phys. Rev. B **45**, 13244–13249 (1992).
[70] P. Bhattarai, K. Wagle, C. Shahi, Y. Yamamoto, S. Romero, B. Santra, R. R. Zope, J. E. Peralta, K. A. Jackson, and J. P. Perdew, "A step in the direction of resolving the paradox of Perdew–Zunger self-interaction correction. II. gauge consistency of the energy density at three levels of approximation," J. Chem. Phys. **152**, 214109 (2020).

[71] S. Akter, Y. Yamamoto, C. M. Diaz, K. A. Jackson, R. R. Zope, and T. Baruah, "Study of self-interaction errors in density functional predictions of dipole polarizabilities and ionization energies of water clusters using Perdew–Zunger and locally scaled self-interaction corrected methods," J. Chem. Phys. **153**, 164304 (2020).
[72] C. Adamo and V. Barone, "Toward reliable density functional methods without adjustable parameters: The PBE0 model," J. Chem. Phys. **110**, 6158–6170 (1999).
[73] F. Weigend, "Accurate coulomb-fitting basis sets for H to Rn," Phys. Chem. Chem. Phys. **8**, 1057–1065 (2006).
[74] G. Prokopiou and L. Kronik, "Spin-state energetics of Fe complexes from an optimally tuned range-separated hybrid functional," Chem. - Eur. J. **24**, 5173–5182 (2018).
[75] P. Verma, A. Perera, and R. J. Bartlett, "Increasing the applicability of DFT I: Non-variational correlation corrections from Hartree-Fock DFT for predicting transition states," Chem. Phys. Lett. **524**, 10–15 (2012).
[76] M.-C. Kim, E. Sim, and K. Burke, "Understanding and reducing errors in density functional calculations," Phys. Rev. Lett. **111**, 073003 (2013).
[77] S. Vuckovic, S. Song, J. Kozlowski, E. Sim, and K. Burke, "Density functional analysis: The theory of density-corrected DFT," J. Chem. Theory Comput. **15**, 6636–6646 (2019).
[78] B. G. Janesko, "Replacing hybrid density functional theory: Motivation and recent advances," Chem. Soc. Rev. **50**, 8470 (2021).
[79] O. A. Vydrov and G. E. Scuseria, "Effect of the Perdew-Zunger self-interaction correction on the thermochemical performance of approximate density functionals," J. Chem. Phys. **121**, 8187–8193 (2004).
[80] J. Gräfenstein and D. Cremer, "The self-interaction error and the description of non-dynamic electron correlation in density functional theory," Theor. Chem. Acc. **123**, 171–182 (2009).
[81] M. Reiher, O. Salomon, and B. Artur Hess, "Reparameterization of hybrid functionals based on energy differences of states of different multiplicity," Theor. Chem. Acc. **107**, 48–55 (2001).
[82] M. Reiher, "Theoretical study of the Fe(phen)2(NCS)2 spin-crossover complex with reparametrized density functionals," Inorg. Chem. **41**, 6928–6935 (2002).

CHAPTER 4: SELF-CONSISTENT IMPLEMENTATION OF LOCALLY SCALED SELF-INTERACTION CORRECTION METHOD

Reproduced from "Self-consistent implementation of locally scaled self-interaction-correction method", Yoh Yamamoto, Tunna Baruah, Po-Hao Chang, Selim Romero, and Rajendra Zope, J. Chem. Phys. 158, 064114 (2023), https://doi.org/10.1063/5.0130436, with the permission of AIP Publishing.

4.1 ABSTRACT

Recently proposed local self-interaction correction (LSIC) method [Zope *et al.*, *J. Chem. Phys.* **151**, 214108 (2019)] is a one-electron self-interaction-correction (SIC) method that uses an iso-orbital indicator to apply the SIC at each point in space by scaling the exchange–correlation and Coulomb energy densities. The LSIC method is exact for the one-electron densities, also recovers the uniform electron gas limit of the uncorrected density functional approximation, and reduces to the well-known Perdew–Zunger SIC (PZSIC) method as a special case. This article presents the self-consistent implementation of the LSIC method using the ratio of Weizsäcker and Kohn–Sham kinetic energy densities as an iso-orbital indicator. The atomic forces as well as the forces on the Fermi-Löwdin orbitals are also implemented for the LSIC energy functional. Results show that LSIC with the simplest local spin density functional predicts atomization energies of the AE6 dataset better than some of the most widely used generalized-gradient-approximation (GGA) functional [e.g., Perdew–Burke–Ernzerhof (PBE)] and barrier heights of the BH6 database better than some of the most widely used hybrid functionals (e.g., PBE0 and B3LYP). The LSIC method [a mean absolute error (MAE) of 0.008 Å] predicts bond lengths of a small set of molecules better than the PZSIC-LSDA (MAE 0.042 Å) and LSDA (0.011 Å). This work shows that accurate results can be obtained from the simplest density functional by removing the self-interaction-errors using an appropriately designed SIC method.

4.2 INTRODUCTION

The Kohn–Sham formulation of density functional theory (DFT) [1,2] with suitable density functional approximations (DFA) is a powerful tool in many-body quantum physics, but its predictive capabilities are often limited by notorious self-interaction error (SIE) that arises from an incomplete cancellation of self-Hartree energy with self-exchange–correlation energy. The Kohn–Sham DFT is an exact theory, but the approximation required for its practical implementation suffers from the SIE. Many failures of DFAs have been attributed to the SIEs [3]. The self-interaction correction (SIC) methods to remove SIE in an orbitalwise fashion have been devised long ago [4-12]. Besides the one-electron SIC methods that remove SIE in an orbitalwise fashion, several other approaches, such as von Weizsäcker kinetic energy density-based SICs (an exchange functional by Becke and Roussel derived from Taylor expansion of exchange hole,[13,14] regional SIC,[15,16] and local hybrid functional [17-19]), long-range asymptotic corrections [20], Koopmans compliant functionals [21,22], atomic SIC (ASIC) [23], multiconfiguration pair-DFT (MC-PDFT)[24], and DFT+U approach [25,26], have been proposed to remove or mitigate SIE. One of the most widely used approaches to mitigate the effects of SIE is to mix DFAs with the Hartree–Fock exchange using various criteria [17,27-29]. Among the one-electron SIC methods, the Perdew and Zunger (PZSIC) [7] method is the most well-known method. In fact, PZSIC has become synonymous with SIC. Although not as widely used as standard gradient-based DFAs, a number of researchers have adopted the PZSIC method [10,30-63]. PZSIC improves the description of stretched bonds [44] and gives significant improvement over DFA for barrier heights [64], atomic anions [7], etc. It is, however, well known that PZSIC tends to overcorrect, particularly for the equilibrium properties, resulting in errors of the opposite sign to those from semilocal functionals [65,66]. PZSIC predicts bond lengths that are too short [53,65,67,68] and provides little improvement for reaction energies [69].

Early efforts in the development and application of SIC methods are reviewed in the classic article by Perdew and Zunger [7]. Another perspective on SIC methods is by Perdew and Pederson [70]. In recent years, a unitary invariant implementation [48] of PZSIC was proposed that uses orthogonalized Fermi orbitals (FOs) [71,72]. The resultant Fermi–Löwdin orbital SIC (FLOSIC) method [73-78] has been used by a few research groups to study wide areas of electronic structure

properties, such as atomization energies [69,78-84], static dipole polarizability of molecules [85-88], magnetic exchange coupling [89,90], chemical reaction energies and barriers [64,91,92], transition metal ions and molecules [93], ionization energy [94-98], electrostatic dipole moments [68,99], photoelectron spectra [100], interpretation of Fermi orbital descriptor [101-103], water and water–ion cluster [104-106], dissociation energies [46,107], and bond lengths of molecules [108].

Recently, Zope and co-workers [84] introduced the locally scaled SIC method (LSIC), which uses a pointwise iso-orbital indicator to identify the one-electron self-interaction regions in the many-electron system (see Sec. 4.3.1) and to determine the magnitude of SIC in the many-electron regions. LSIC was conceptualized while pruning dense numerical grids required for SIC calculations with meta-generalized-gradient-approximation (meta-GGA) functionals [82,96] and was inspired by the regional SIC [15] and the functionals that use iso-orbital indicators to identify single electron regions. LSIC works well for both equilibrium properties as well as for properties that involve a stretched bond, and it provides improved performance with respect to the standard PZSIC method for a wide range of electronic structure properties [69,79,85,86,88].

Early LSIC calculations [69,80,90,91] made use of self-consistent PZSIC densities obtained from the PZSIC method with Fermi–Löwdin orbitals (FLOs) as localized orbitals [73]. The perturbative LSIC method using the simplest DFA, such as LSDA, predicted several properties more accurately than those obtained by the widely used Perdew–Burke–Ernzerhof (PBE) generalized-gradient approximation (GGA) [109,110]. It simultaneously provides good estimates of atomization energies of the AE6 dataset of molecules [111] (better than the PBE-GGA) and the barrier heights of BH6 database molecules (better than popular hybrids, such as B3LYP and PBE0), which is difficult for the most DFAs. The barrier heights of the BH6 database were predicted within the chemical accuracy. The barrier heights of a more diverse BH76 database are predicted within a few kcal/mol [91]. Likewise, the dissociation curve of the positively charged helium dimer using the LSIC method was qualitatively in line with the CCSD(T) dissociation curve [69]. Self-consistent implementation of the LSIC method at the time was not possible as our code lacked the ability to compute the Coulomb potential due to the charge density scaled by the iso-orbital indicator, which is needed when the variation of LSIC self-Hartree energy term is taken. A simplified *quasi*-self-consistent (quasi-SCF) scheme was instead employed in the LSIC studies of

electron density-related properties, such as dipole moments and polarizabilities [85,86,88]. The quasi-SCF approach ignores the variation of the local scaling factor and is valid when the variation of the local scaling factor is negligible. To gauge the full potential of the LSIC method, a fully self-consistent implementation is needed. In this work, we present the outline of the scheme for the self-consistent LSIC method and describe its implementation using the Fermi–Löwdin orbitals in the FLOSIC code [112,113]. We subsequently assess the performance of self-consistent LSIC by computing atomic total energies, atomization energies, reaction barrier heights, bond lengths, and the highest occupied molecular orbital (HOMO) eigenvalues. These results are compared against accurate reference values along with previous one-shot and quasi-SCF results of LSIC. The results of this work show that the self-consistent LSIC method, similar to one-shot LSIC, performs well for the properties studied in this work.

4.3 THEORY AND COMPUTATIONAL DETAILS

Both PZSIC and LSIC are one-electron SIC methods that remove SIE in an orbital-by-orbital manner. We first briefly outline the PZSIC method [7] and then describe the LSIC method in Sec. 2.3.1. The PZSIC total energy is given by

$$E^{PZSIC}[\rho_\uparrow, \rho_\downarrow] = E^{DFA}[\rho_\uparrow, \rho_\downarrow] - \Sigma_{i\sigma}^{occ}(U[\rho_{i\sigma}] + E_{XC}^{DFA}[\rho_{i\sigma}, 0]). \quad (4.1)$$

Here, the self-Coulomb $U[\rho_{i\sigma}]$ and self-exchange–correlation energies $E_{XC}^{DFA}[\rho_{i\sigma}, 0]$ are subtracted from DFA energy for each occupied orbital. PZSIC is exact for all one-electron density and nearly many-electron SIE-free [44]. The size extensivity requirement necessitates the use of local orbitals in the PZSIC method. In this work, we use FLOs as local orbitals [71,72]. In particular, we used the FLOSIC approach of Pederson *et al.* [73,75] FLOSIC is an FLO implementation of PZSIC where the SIC energies are obtained with FLOs. FLOs are localized orbitals and can be obtained from KS orbitals using what is called Fermi orbital descriptor (FOD) positions. Using FODs, FOs are obtained from KS orbitals as

$$\phi_i^{FO}(\vec{r}) = \sum_j^{N_{occu}} \frac{\psi_j(\vec{a}_i)\psi_j(\vec{r})}{\sqrt{\rho(\vec{a}_i)}}. \quad (4.2)$$

FOs are then orthogonalized with the Löwdin's orthogonalization scheme to form a set of FLOs. ρ_σ in Eq. (2.1) are the square of the *i*th FLO. FLOs are used in both the PZSIC and LSIC calculations presented in this work. We note that in some early articles on FLOSIC, the term FLOSIC was occasionally used interchangeably with the term PZSIC. However, other one-electron SIC methods, such as orbital scaling SIC (OSIC) [65,83,114] or LSIC, can also be implemented using FLOs, and these may be referred to a FLOSIC implementation of OSIC or LSIC equations. In the FLOSIC approach, the optimal set of FLOs is obtained by minimizing the total energy with respect to the FOD positions using a gradient-based algorithm. The expressions for the FOD forces have been derived earlier for the PZSIC energy functional [74,75]. In this work, we follow these earlier works to obtain the FOD force expression by minimizing the LSIC energy expression.

4.3.1 LOCAL SCALING SELF-INTERACTION-CORRECTION METHOD

Like the PZSIC method, the LSIC is also a one-electron SIC method in which the exchange–correlation energy is obtained as

$$E_{XC}^{LSIC-DFA} = E_{XC}^{DFA}[\rho_\uparrow, \rho_\downarrow] - \Sigma_{i\sigma}^{occ}\{U^{LSIC}[\rho_{i\sigma}] + E_{XC}^{LSIC}[\rho_{i\sigma}, 0]\}. \quad (4.3)$$

Here,

$$U^{LSIC}[\rho_{i\sigma}] = \frac{1}{2}\int d\vec{r}\, z(\vec{r})\rho_{i\sigma}(\vec{r}) \int d\vec{r}\,' \frac{\rho_{i\sigma}(\vec{r}\,')}{|\vec{r}-\vec{r}\,'|} \quad (4.4)$$

and

$$E_{XC}^{LSIC}[\rho_{i\sigma}, 0] = \int d\vec{r}\, z(\vec{r})\varepsilon_{XC}^{DFA}([\rho_{i\sigma}, 0], \vec{r}). \quad (4.5)$$

$z_\sigma(\vec{r})$ is the local scaling factor or an iso-orbital indicator that is used to identify one-electron self-interaction regions. LSIC offers flexibility in that any suitable choice of an iso-orbital indicator can be used to distinguish between many-electron and one-electron-like regions.

In this work, we use $z_\sigma(\vec{r})$ as the ratio of kinetic energy densities $\tau_\sigma^W(\vec{r})/\tau_\sigma(\vec{r})$. The total kinetic energy density $\tau_\sigma(\vec{r})$ and Weizsäcker kinetic energy density $\tau_\sigma^W(\vec{r})$ are defined as follows [115]:

$$\tau_\sigma(\vec{r}) = \frac{1}{2}\sum_i \left|\vec{\nabla}\psi_{i\sigma}(\vec{r})\right|^2, \tag{4.6}$$

$$\tau_\sigma^W(\vec{r}) = \frac{\left|\vec{\nabla}\rho_\sigma(\vec{r})\right|^2}{8\rho_\sigma(\vec{r})}, \tag{4.7}$$

$z_\sigma(\vec{r})$ approaches unity in the single electron regions and becomes vanishingly small in the uniform density regions. Thus, LSIC corrects SIEs in the single electron region and reduces to DFA in uniform density regions, recovering the uniform gas limit of parent semilocal DFA violated by the PZSIC method [69,116].

The functional derivative of E^{LSIC} with respect to variation in density is written as follows:

$$\begin{aligned}\frac{\delta E^{LSIC}}{\delta\rho(\vec{r})} = v^{DFA}(\vec{r}) &- \frac{1}{2}\int \frac{z_\sigma(\vec{r}')\rho_{i\sigma}(\vec{r}')}{|\vec{r}-\vec{r}'|}d\vec{r}' - \frac{1}{2}z_\sigma(\vec{r})\int \frac{\rho_{i\sigma}(\vec{r}')}{|\vec{r}-\vec{r}'|}d\vec{r}' \\ &- z_\sigma(\vec{r})v_{XC}^{i\sigma}(\vec{r}) - \frac{1}{2}\sum_j^{N_\sigma}\frac{\delta z_\sigma(\vec{r})}{\delta\rho}\rho_{j\sigma}(\vec{r})\int \frac{\rho_{j\sigma}(\vec{r}')}{|\vec{r}-\vec{r}'|}d\vec{r}' \\ &- \sum_j^{N_\sigma}\frac{\delta z_\sigma(\vec{r})}{\delta\rho}\epsilon_{XC}^{i\sigma}(\vec{r})\end{aligned} \tag{4.8}$$

It is straightforward to construct the Fock matrix corresponding to the first four terms in the above equation. To obtain the contribution to the Fock matrix from the last two terms, we use the so-called ODDM approach [117] and obtain the Fock matrix elements as follows:

$$H_{\mu\nu}^{\sigma} = -\sum_{j}^{N_\sigma} \int \left(\varepsilon_{coul}^{j\sigma}(\vec{r}) + \varepsilon_{XC}^{j\sigma}(\vec{r})\right) \frac{\partial z_\sigma(\vec{r})}{\partial \rho(\vec{r})} \phi_\mu(\vec{r}) \phi_\nu(\vec{r}) d\vec{r}$$
$$-\sum_{j}^{N_\sigma} \int \left(\varepsilon_{coul}^{j\sigma}(\vec{r}) + \varepsilon_{XC}^{i\sigma}(\vec{r})\right) \frac{\partial z_\sigma(\vec{r})}{\partial \vec{\nabla}\rho(\vec{r})} \cdot \vec{\nabla}\left(\phi_\mu(\vec{r}) \phi_\nu(\vec{r})\right) d\vec{r}$$
$$-\sum_{j}^{N_\sigma} \frac{1}{2} \int \left(\varepsilon_{coul}^{j\sigma}(\vec{r}) + \varepsilon_{XC}^{j\sigma}(\vec{r})\right) \frac{\partial z_\sigma(\vec{r})}{\partial \tau_\sigma(\vec{r})} \vec{\nabla}\phi_\mu(\vec{r}) \cdot \vec{\nabla}\phi_\nu(\vec{r}) d\vec{r}. \quad (4.9)$$

Here, $\varepsilon_{coul}^{j\sigma}(\vec{r})$ and $\varepsilon_{XC}^{j\sigma}(\vec{r})$ are one-electron energy densities such that

$$\varepsilon_{coul}^{j\sigma}(\vec{r}) = \frac{1}{2} \rho_{j\sigma}(\vec{r}) \int \frac{\rho_{j\sigma}(\vec{r}')}{|\vec{r} - \vec{r}'|} d\vec{r}', \quad (4.10)$$

And for the LSDA,

$$\varepsilon_{XC}^{j\sigma}(\vec{r}) = -\frac{3}{4}\left(\frac{6}{\pi}\right)^{\frac{1}{3}} \rho_{j\sigma}^{\frac{4}{3}}(\vec{r}) + \varepsilon_C\left(r_s(\vec{r}) = \left(\frac{3}{4\pi\rho_{j\sigma}(\vec{r})}\right)^{\frac{1}{3}}, \zeta(\vec{r}) = 1\right), \quad (4.11)$$

Where ζ is the relative spin polarization.

4.3.1.1 NUMERICAL POISSOM SOLVER

The analytical evaluation of the second term on the right-hand side of Eq. (2.8) is not straightforward. We have therefore developed a numerical Poisson solver [118] based on the multi-center grid originally proposed by Becke [119]. A brief description of the implementation is as follows: First, a spherical mesh is constructed by multiplying the Lebedev spherical mesh [120] onto radial quadrature [121] for each atomic center. Due to the overlap between the spherical meshes from different atomic centers, a special type of integration weight function $w_n(\vec{r})$ [122-124] that satisfies the condition $\sum_n w_n(\vec{r}) = 1$ is also constructed on each grid point to scale down

the charge density as $\rho_n(\vec{r}) = w_n(\vec{r})\rho(\vec{r})$ to eliminate double counting in the mesh overlapping region. As a result, the entire space is partitioned into small regions, where each of these regions confines a portion of charge ρ_n and can be treated independently.

The advantage of this approach is that it allows each $\rho_n(\vec{r})$ to be expressed in spherical coordinates for efficient integration. By applying multipolar expansion on both the charge distribution ρ_n and its corresponding Coulomb potential V_n, the radial and the angular degrees of freedom become separable and the Poisson equation becomes a set of 1D differential equations for the radial parts of the potential $V_{lm}(r)$. The final full Coulomb potential due to $\rho_n(\vec{r})$ can be reconstructed on any given mesh using the following expression:

$$V_n(\vec{r}) = \sum_{l=0} \sum_{m=-l}^{l} V_{lm}(r) Y_{lm}(\theta, \phi\,), \tag{4.12}$$

with interpolation of $V_{lm}(r)$ onto any given r.

To solve for the radial solutions $V_{lm}(r)$, common approaches are either to use a finite-difference method to solve the differential equation directly [119] or to integrate the Green's function (GF) solution to the Laplacian [123]. For the former approach, it uses the differential equations of the following form:

$$\big(1 + p(r)\big)\frac{\partial^2}{\partial r^2} U_{lm}(r) - q(r) U_{lm}(r) = f(r), \tag{4.13}$$

with $V_{lm}(r) = U_{lm}(r)/r$ and $p(r)$ and $q(r)$ being the coefficient functions whose values depend on the radial quadrature in use. For the latter approach, the GF solution to Laplacian is written as

$$I_{lm}(r) = \frac{1}{r^{l+1}} \int_0^r r'^{l+2} \rho_{lm}(r') dr' + r^l \int_r^\infty \frac{\rho_{lm}(r')}{r'^{l-1}} dr', \tag{4.14}$$

with $V_{lm}(r) = \frac{4\pi}{2l+1} I_{lm}(r)$.

Most of the latest implementations are based on the GF approach [125,126] often combined with screening charge and Dunlap correction [123,125-127]. In an orbital-by-orbital SIC calculation

where the Coulomb potentials need to be evaluated for each occupied orbital, the technique mentioned above is performed repeatedly for each orbital density. By analyzing the sources of errors and accuracy in the two approaches, we put forth a hybrid method to optimize the radial solutions. More details of this hybrid approach can be found in Ref. 118.

4.3.2 QUASI-SELF-CONSISTENT LSIC

A simplified *quasi*-self-consistent procedure can be obtained if one ignores the variation of the iso-orbital (scaling factor) in Eq. (2.8) and replaces $z_\sigma(\vec{r}')$ in the second term with $z_\sigma(\vec{r})$, which is mathematically valid only when $z_\sigma(\vec{r})$ is constant. Since the iso-orbital indicator $z_\sigma(\vec{r})$ varies substantially in space, the resulting Hamiltonian is not equivalent to Eq. (2.8) except for one-electron systems. The resultant *quasi*-self-consistent Hamiltonian is given by

$$H_{i\sigma}^{quasi-LSIC} = H^{DFA} - z_\sigma(\vec{r}) \int \frac{\rho_{j\sigma}(\vec{r}')}{|\vec{r} - \vec{r}'|} d\vec{r}' - z_\sigma(\vec{r}) v_{XC}^{i\sigma}(\vec{r}). \tag{4.15}$$

This Hamiltonian can be viewed as local scaling applied to orbital dependent SIC potential instead of SIC energy densities. As mentioned in the Introduction, a few applications, such as static dipole polarizabilities and dipole moments of water clusters and polyacenes, have been carried out using the *quasi*-self-consistent LSIC approach [85,88]. Good results obtained in these studies show that the *quasi*-self-consistent LSIC approach can be useful to study some (especially density-related) properties.

4.3.2 FOD FORCE AND ATOMIC FORCE

The optimal FLOs in the standard FLOSIC implementation are obtained by minimizing the energy with respect to FOD positions, in which determination of Fermi orbital derivative terms is needed. The expression for the FOD force (energy derivative) [74] can be simplified as follows:

$$\frac{dE^{SIC}}{da_m} = \sum_{kl} \epsilon_{kl}^{k} \left\{ \left\langle \frac{d\phi_k}{da_m} | \phi_l \right\rangle - \left\langle \frac{d\phi_l}{da_m} | \phi_k \right\rangle \right\}, \tag{4.16}$$

$$\epsilon_{kl}^{k} = \langle \phi_l | V_k^{SIC} | \phi_k \rangle. \tag{4.17}$$

Since the term ϵ_{kl}^{k} here is the Lagrange multiplier matrix, we substitute this term with equivalent terms constructed from Eqs. (2.8) and (2.9) for LSIC-LSDA. In our case, FOD optimizations are performed using this implementation.

The Pulay atomic force [128] for PZSIC-LSDA is given in Ref. 108 as follows:

$$F_v^{Pulay} = -2 \sum_{i}^{M} \sum_{kl}^{N} c_k^i c_l^i \left\langle \frac{\partial \chi_k}{\partial \vec{R}_v} | H_i^{DFA-SIC} | \chi_l \right\rangle + 2 \sum_{ij}^{M} \Lambda_{ij} \sum_{kl}^{N} c_k^i c_l^j \left\langle \frac{\partial \chi_k}{\partial \vec{R}_v} | \chi_l \right\rangle, \tag{4.18}$$

where M is the number of occupied orbitals, N is the size of the basis set, χ_k is the local basis function, $\Lambda_{ij} = \frac{1}{2} \left(\lambda_{ij} - \lambda_{ji} \right)$ is an element of the symmetrized Lagrange multiplier matrix, and $\vec{R}$ is the nuclear position. Here, to obtain atomic forces in the LSIC, we modify the terms $\langle \frac{\partial \chi_k}{\partial R_v} | H_i^{SIC} | \chi_l \rangle$ and Λ_{ij} to accommodate the LSIC Hamiltonian. This modification allows simultaneous optimization of FODs and nuclei positions, in principle, but, in practice, requires care as it adds more degrees of freedom to the FOD optimization processes, and the FOD energy landscape is quite complicated. We have verified both the FOD forces and atomic forces by comparing them against the forces obtained numerically using finite difference methods.

4.3.3 COMPUTATIONAL DETAILS

Both PZSIC and LSIC methods are implemented in the developmental version of the FLOSIC code [112.113]. FLOSIC code is based on the UTEP-NRLMOL code, which itself is a modernized version of legacy NRLMOL (FORTRAN 77) code [128,129] with many additional new capabilities. We consider the LSDA functional, since LSIC applied to LSDA is free from the gauge problem [84]. Application of LSIC to GGAs and particularly to SCAN metaGGA [130] provides little improvement compared to the PZSIC-SCAN except for the reaction barriers that are

improved. The cause for this shortcoming has been identified as a gauge problem as their exchange–correlation potentials and energy densities are not in the Hartree gauge and, therefore, require a gauge transformation [84,131] or inclusion of a calibration function [132,133]. For the LSIC-LSDA calculations in this work, the LSDA correlation functional parameterized as PW92 [134] is used. The Gaussian basis sets of triple zeta quality [135] are used. The basis sets used in this work are available at https://github.com/FLOSIC/NRLMOL_basis_set. The NRLMOL basis set is also accessible at Basis Set Exchange [136] as DFO(+)-NRLMOL. The matrix elements are obtained numerically using variational mesh [137]. Although the LSIC energy functional depends on the kinetic energy densities, we have found that for the properties studied in this work, standard numerical grids used for SIC calculations are sufficiently accurate, and no numerical instabilities were found. Generally, a kinetic energy density-dependent (meta-GGA) functional requires a denser mesh for numerical integration than needed for GGAs because the derivative terms arising from the iso-orbital indicator may oscillate abruptly in space. The numerical problems with meta-GGA functionals have been reported by a few groups [82,96,138-140]. However, $z_\sigma(\vec{r})$ and its partial derivatives are smooth, and these quantities alone do not cause numerical instabilities. The self-consistent FLOSIC calculations can be performed either using optimized effective potential within the Krieger–Li–Iafrate approximation [77] or using the Jacobi update approach [76]. In this work, we used the Jacobi update approach. The SCF convergence tolerance of $10^{-6}E_h$ for the total energy is used. For FOD optimizations, force criteria with $10^{-3}E_h/a0$ are used. For all LSIC calculations, we used the converged densities and optimized FODs from PZSIC-LSDA as the starting point for perturbative, quasi-SCF, and full SCF calculations. Both potential mixing and Hamiltonian mixing can be used with LSICLSDA to accelerate the self-consistence convergence, since the DFA Fock matrix does not depend on integration by parts and the Jacobi update approach applies the mixing algorithm to the DFA Fock matrix only. The molecular structures and their optimal FOD coordinates for selected systems are made available at http://github.com/FLOSIC/si_LSIC_SCF.

The real orbital implementation of SIC is used in this work. Alternatively, complex orbitals can be used with SIC. SIC with complex orbitals was previously used by Klüpfel *et al.* for variation with respect to the orbitals [141] and by Hofmann *et al.* for variation with respect to the density [142,143]. PZSIC with complex orbitals provides a slight performance improvement in the total energies of atoms for PBE and TPSS and a notable improvement in the atomization energies for

PBEsol over their DFA performances, whereas PZSIC with real orbitals worsens them [36]. Additionally, the FLOSIC approach has recently adapted complex FLOs and found the energy shift of the same order as in previously found results [144].

4.4 RESULTS

In this section, we present the results for atomic total energies, atomization energies, barrier heights, HOMO eigenvalues, and equilibrium bond lengths.

4.4.1 TOTAL ENERGY OF ATOMS

We have calculated the self-consistent LSIC total energies of atoms from hydrogen through argon. The deviations of total energies from accurate reference values reported in Ref. 145 are shown in Fig. 2.1. The mean absolute errors (MAE) of the LSIC-LSDA method with respect to the reference values are summarized in Table 2.1. For comparison, the PBE and SCAN [130] and their PZSIC values [96] are included in the table. We have also included the MAE of the perturbative and *quasi*-self-consistent LSIC-LSDA calculations to make the effect of full self-consistency evident. As previously found, the perturbative LSIC-LSDA shows an MAE of 0.041 E_h and performs intermediate between the PBE and SCAN functionals. The self-consistency, on average, lowers the energies of atoms by 2.4 mE_h. The optimization of the FODs further lowers the atomic energies by 1.7 mE_h on average. Due to these very small energy gains, the MAEs of quasi-SCF, SCF, and SCF with FOD optimization are 0.040 E_h in all three cases. These results show that self-consistency and the FOD optimization do not alter the performance of LSIC significantly for the atomic energies and that the perturbative LSIC-LSDA is sufficient to get good estimates of atomic energies.

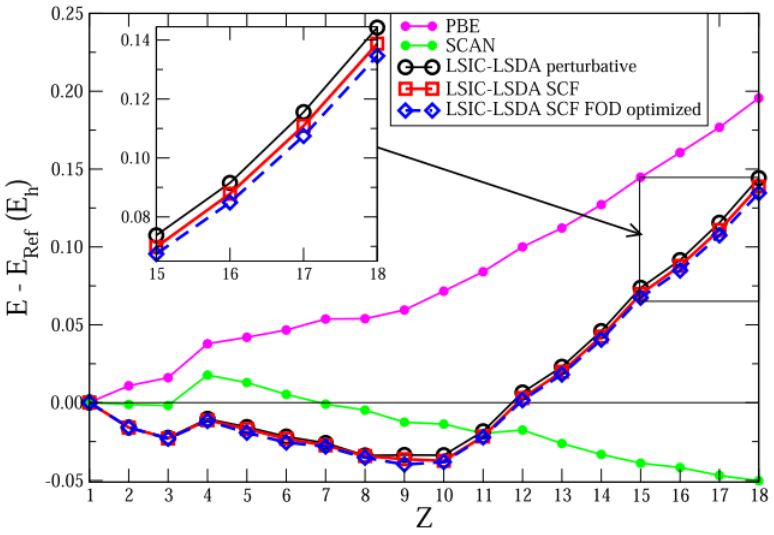

Fig. 4.1. Total energies of atoms (in E_h) compared against the reference values of Ref. 145

Table 4.1. MAE of atomic total energies (in E_h) with respect to the reference atomic energies from Ref. 145.

Method	MAE (E_h)
LSDA[a]	0.726
PBE[a]	0.083
SCAN[a]	0.019
PZSIC-LSDA[a]	0.381
PZSIC-PBE[a]	0.159
PZSIC-SCAN[a]	0.147
LSIC-LSDA, perturbative	0.041
LSIC-LSDA, quasi-SCF	0.040
LSIC-LSDA, SCF	0.040
LSIC-LSDA, SCF FOD optimized	0.040

[a]Reference 96.

4.4.2 ATOMIZATION ENERGIES

We studied the performance of LSIC on atomization energies using the AE6 set [111] of molecules. The AE6 set is part of the Minnesota Database and is often used for benchmarking the performance of density functional approximations for atomization energies. The AE6 set is composed of six molecules: SiH4, S2, SiO, C3H4 (propyne), HCOCOH (glyoxal), and C4H8 (cyclobutane). The atomization energy E_A is obtained as the energy difference of the sum of fragment atomic energies $E^i_{fragment}$ and the complex energy $E_{complex}$ as follows:

$$E_A = \sum_i E^i_{fragment} - E_{complex} \tag{4.19}$$

The MAEs are summarized in Table 2.2. For the sake of comparison, we also included our previous results for atomization energies of two widely used semi-local functionals PBE-GGA and SCAN meta-GGA and their self-interaction-corrected counterparts. As previously shown, perturbative LSIC-LSDA with an MAE of 9.94 kcal/mol displays better performance than PZSIC for three different kinds of functionals (PZSIC-LSDA, PZSIC-PBE, and PZSICSCAN). It is, to our knowledge, the first real orbital one-electron SIC scheme that gives atomization energies better than the PBE-GGA. LSIC-LSDA, however, falls short of the bare SCAN functional. While there are meta-GGA and hybrid functionals (e.g., VSXC, B3LYP, and PBE0) that perform better than LSIC-LSDA for atomization energies, many of these functionals do not always provide good performance for barrier heights and dissociation energies.

The atomization energy of individual molecules in the AE6 set changes by up to 4 kcal/mol when self-consistency is introduced. The MAE (9.53 kcal/mol), however, decreases very slightly by 0.41 kcal/mol compared to the perturbative LSIC. The self-consistency lowers molecular energies by about 2–6 kcal/mol. This energy lowering is about the same order of magnitude as in the case of atoms. Since atomization energies are obtained from the energy differences between atoms and complexes, the energy shift due to self-consistency is canceled out, and as a result, self-consistent LSIC performance remains close to the perturbative LSIC approach. The MAE difference between the two approaches is under 1 kcal/mol.

Table 4.2. MAE of the AE6 set of atomization energies.

Method	MAE (kcal/mol)
LSDA[a]	74.26
PBE[a]	13.43
SCAN[a]	2.85
PZSIC-LSDA[a]	57.97
PZSIC-PBE[a]	18.83
PZSIC-SCAN[b]	26.52
LSIC-LSDA, perturbative	9.94
LSIC-LSDA, quasi-SCF	6.57
LSIC-LSDA, SCF	9.53
LSIC-LSDA, SCF FOD optimized	8.66
B3LYP/MG3S[c]	3.2
PBE0/MG3S[c]	5.4

[a]Reference 69.
[b]Reference 83.
[c]Reference 146.

We repeated the atomization energy calculations for the LSIC using the quasi-SCF approach. We find that quasi-SCF shows a smaller MAE of 6.57 kcal/mol. In quasi-SCF, energy shifts with respect to the perturbative LSIC energies are positive, and larger molecules tend to experience larger energy shifts (+32.1 kcal/mol for cyclobutane) than the smaller molecules (+5.5 kcal/mol for SiO), resulting thereby in a decrease in the MAE of atomization energies. Finally, relaxation of the FODs results in further decrease in MAE of self-consistent LSIC by roughly 1 kcal/mol (MAE 8.66 kcal/mol). Overall performance remained unchanged from the perturbative approach to SCF to FOD optimized SCF. To summarize the results of this section, the performance of self-consistent LSIC with and without FOD optimization remains similar to that of perturbative LSIC that uses PZSIC orbital densities.

4.4.3 BARRIER HEIGHTS

We used the BH6 set [111] of reactions to study the LSIC performance on barrier heights. BH6 is a set of three hydrogen transfer reactions: (1) OH + CH4 → CH3 + H2O, (2) OH + H →

O + H2, and (3) H + H2S → HS + H2. For each reaction, single point energies of the left- and right-hand side and saddle point of the reactions were calculated, and then forward and reverse barrier heights were computed. Simultaneous accurate description of barrier heights and atomization is challenging not only for uncorrected DFAs but also for self-interaction correction methods [147]. Improvements in barrier heights usually occur at the expense of the accuracy of atomization energies. Our previous results of perturbative LSIC showed that it goes beyond this paradoxical behavior of the well-known PZSIC method and can provide a good description of both barrier heights and atomization energies. The performance of the LSIC method(s) is summarized in Table 2.3. All three DFAs in Table 2.3 underestimate barrier heights, where the transition state energies are predicted too low due to SIE in the energy functional. As such, LSDA show an MAE of 17.6 kcal/mol. All PZSIC calculations improve the barrier heights for semilocal functionals with the MAE ranging from 3.0 kcal/mol of PZSIC-SCAN to 4.9 kcal/mol of PZSIC-LSDA. Application of LSIC-LSDA raises the barriers and further reduces MAE down to 1.3 kcal/mol. We note that LSIC barrier heights are not necessarily between those predicted by the bare DFA and PZSICDFA since energy shifts vary for reactant, product, and transition states. The MAE of self-consistent LSIC is 1.1 kcal/mol. Once again, we see that full self-consistency performs similarly to perturbative LSIC (MAE 1.3 kcal/mol). This holds true even after FODs are optimized (MAE 1.2 kcal/mol). Although quasi-SCF also gives a smaller MAE of 1.5 kcal/mol, deviation in barrier heights from molecule to molecule is far more compared to perturbative LSIC and self-consistent LSIC. It is likely that the performance of quasi-SCF would deviate from the others for a more diverse dataset. For a larger BH76 dataset, perturbative LSIC showed an MAE of 3.7 kcal/mol [91].

Table 4.3. MAE of the BH6 set of barrier height.

Method	MAE (kcal/mol)
LSDA[a]	17.6
PBE[b]	9.6
SCAN[a]	7.9
PZSIC-LSDA[a]	4.9
PZSIC-PBE[a]	4.2
PZSIC-SCAN[a]	3.0
LSIC-LSDA, perturbative[a]	1.3
LSIC-LSDA, quasi-SCF	1.5
LSIC-LSDA, SCF	1.1
LSIC-LSDA, SCF FOD optimized	1.2
B3LYP/MG3S[c]	4.7
PBE0/MG3S[c]	4.6
HF/MG3S[d]	12.3

[a]Reference 69.
[b]Reference 84.
[c]Reference 146.
[d]Reference 111.

4.4.3 HOMO EIGENVALUES

In DFT, the negative of the HOMO eigenvalue equals the first ionization potential [148-152]. The validity of this relation in the approximate density functional calculations depends on the quality of the asymptotic description of the effective potential, which is affected by the SIE. In most DFAs, the absolute of the HOMO eigenvalue underestimates the first ionization potential substantially due to the shallow asymptotic nature of the approximate exchange potential. Correcting for the long-range description of the DFA exchange potential improves the accuracy of HOMO [153] and can result in bound atomic anions [154]. PZSIC can improve the HOMO eigenvalues over those from DFAs by improving the asymptotic description of the exchange potential. Earlier perturbative LSIC calculations could not assess the quality of (negative of) HOMO eigenvalues in approximating the first ionization energies. We compare the PZSIC and LSIC HOMO eigenvalues of a set of molecules and compare them against the experimental ionization energies reported in the NIST database. We present the deviations in Fig. 2.2. As expected, the semilocal functionals PBE and SCAN underestimate the ionization energies with MAEs of 4.02 and 3.70 eV, respectively. On the other hand, PZSIC-LSDA overestimates with an MAE of 2.10 eV, where the majority of the values deviate between 0 and 4 eV above the experimental values. The valence electrons in the PZSIC are too strongly bound. We find that

LSIC HOMO eigenvalues fall between the DFA and PZSIC HOMO eigenvalues. LSIC HOMO eigenvalues exhibit a trend that is opposite to the PZSIC eigenvalues. They are underestimated with a MAE 1.04 eV, which is roughly half the MAE of PZSIC-LSDA. Interestingly, quasi-SCF LSIC shows even better agreement with the experiment (MAE 0.77 eV) than the full SCF case. As quasi-LSIC can be viewed as local scaling applied to the potential instead of energy, this suggests that for some properties, scaling the potential rather than the energy density can be beneficial.

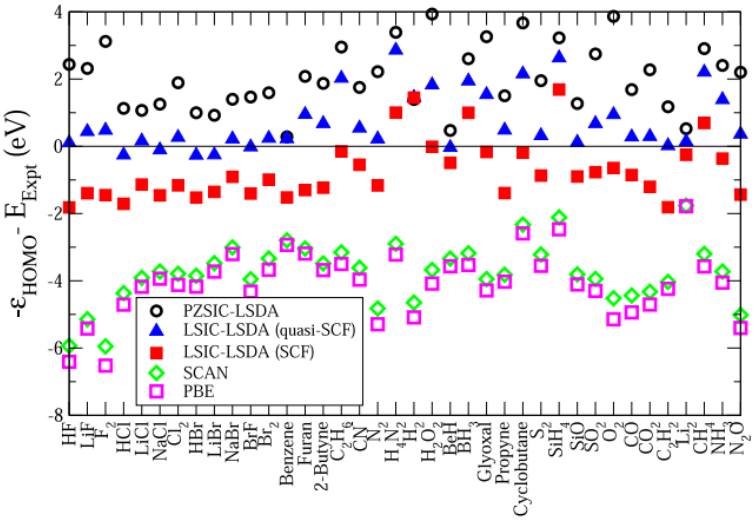

Fig. 4.2. The deviation of $-\varepsilon_{HOMO}$ against the experimental IP (in eV).

4.4.4 BOND LENGTHS

We investigated how well LSIC performs for bond lengths. The uncorrected LSDA performs fairly well in predicting bond lengths. On the other hand, PZSIC is known to predict bond lengths of molecules that are too short in comparison to the experiments [53,65,67,68]. For this reason, PZSIC is not suited for determining an optimal geometry, and in many cases, PZSIC calculations are commonly performed on geometries obtained using PBE, PBE0, or B3LYP functionals or using geometries from beyond Hartree–Fock methods. Vydrov and Scuseria

investigated [114] the equilibrium bond lengths of 12 small molecules and found mean errors of -0.045 Å for PZSIC-LSDA and -0.024 Å for PZSIC-PBE against experimentally found values. Those 12 molecules are LiH, BeH, BH, CH4, CO, NH, NO, N2, OH, O2, HF, and F2. This short bond length behavior is partly because PZSIC provides excessive corrections along bonding regions. Here, we examined how well LSIC performs in determining bond lengths using the same set of 12 molecules used in Vydrov and Scuseria's study. In the FLOSIC formalism, the geometry optimization and the FOD optimization can be, in principle, performed simultaneously [108]. However, our experience is that the FLOs (and FODs) are very sensitive to small changes in the geometry, which makes simultaneous optimization of FODs and atomic positions difficult. To obtain the equilibrium bond lengths, we perform PZSIC and LSIC calculations at five geometries around the experimental bond lengths. This range of geometries covers minima in all three DFA, PZSIC, and LSIC cases. We subsequently used the fitting function $f(x) = a + b(x-c)^2 + d(x-c)^3$ to determine the equilibrium bond lengths. During the fitting, the cubic term was introduced to reduce the fitting errors, and the parameter *d* was initially set to a very small value. The comparisons against the experimental values reported in Ref. 155 were made and shown in Fig. 2.3. We report the MAE of each method. LSDA shows a reasonable estimate with an MAE of 0.011 Å, whereas PZSIC-LSDA shows apparent underestimation (MAE 0.044 Å). The LSIC bond lengths (MAE 0.008 Å) in comparison to PZSIC-LSDA are longer and are in better agreement with experimental bond lengths than the PZSICLSDA and LSDA for this set of molecules. In most cases, SCF and FOD optimization have a small effect on the bond length. However, optimizing FODs tends to slightly improve bond lengths, especially for BH and OH.

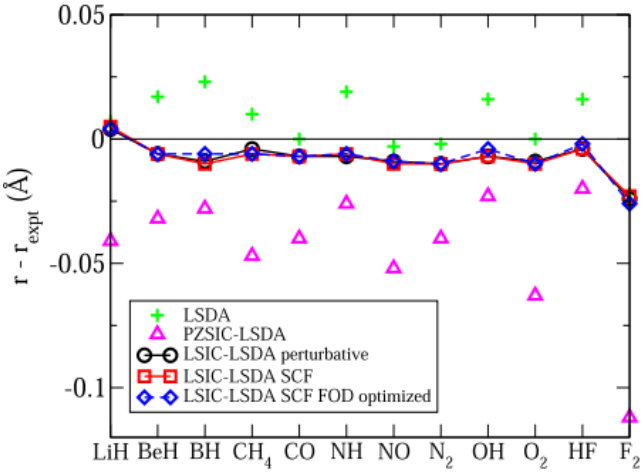

Fig. 4.3. Equilibrium bond lengths (in Å) compared against experimental values from Ref. 155.

Additionally, the parameter b used in the fitting function can be used to estimate harmonic frequency ω of the set of diatomic molecules. The values of ω obtained from LSDA show better agreement with the experiment than both the PZSIC and LSIC values (cf. Fig. 2.4). PZSIC frequencies ω are about 13% higher than the LSDA. The chemical bonds in PZSIC are *vibrationally blueshifted* compared to bonds in the LSDA. As seen for many other properties, LSIC corrects the PZSIC frequencies and predicts ω values that are intermediate between the LSDA and PZSIC.

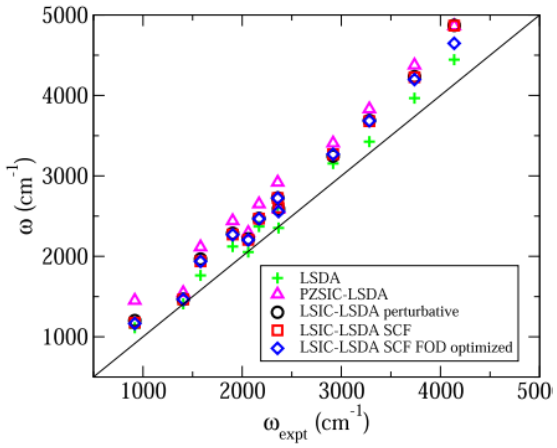

Fig. 4.4. Harmonic frequency obtained from the fitting function (in cm^{-1}) compared against the experimental values from Refs. 156 and 157.

4.5 CONCLUSIONS

To summarize, in this work, we present the self-consistent implementation of the LSIC method. We have presented the pertinent equations and details of the code implementation using the integration-by-part approach. The performance of the self-consistent LSIC method for atomic energies, atomization energies, and reaction barrier heights is assessed using standard benchmark databases. The results are compared with PZSIC-LSDA, the perturbative one-shot LSIC using PZSIC densities, as well as the *quasi*-self-consistent approach. In most cases, the *quasi*-self-

consistent approach provides results comparable to the full self-consistent LSIC method. In addition, we have obtained the ionization energies from the HOMO eigenvalues and the bond lengths of a set of molecules with the full self-consistent LSIC method. The HOMO eigenvalues of LSIC fall between those of LSDA and PZSIC-LSDA. Interestingly, a simpler quasi-SCF LSIC provides better agreements between HOMO eigenvalues and experimental ionization energies, indicating that LSIC applied to the potential may be a more useful approach for certain properties. Finally, we investigated the equilibrium bond lengths of dimers. PZSIC-LSDA tends to shorten the bond lengths, which is corrected by the LSIC. The bond lengths of a chosen set of molecules obtained with the LSIC method are somewhat shorter than those predicted by the LSDA but are in slightly better agreement with experimental values. From perturbative LSIC to self-consistent LSIC, energy as a function of bond length is a uniform shift, and there is no significant change in the estimated bond lengths. The present results show that perturbative LSIC on top of PZSIC and the self-consistent LSIC approaches perform similarly for the properties considered in this work. The cost of perturbative LSIC is insignificant if PZSIC densities are available. The self-consistent results of this work confirm our previous conclusions that the LSIC method provides superior results than the well-known PZSIC method for all properties studied here, thus providing an attractive approach to eliminate self-interaction-errors that pervade most density functional studies. Further improvements in the performance of the LSIC method may be possible by designing better iso-orbital indicators that work with LSIC or by designing more sophisticated density functionals for the LSIC method than the simple LSDA functional considered in this work. The vdW and nonlocal corrections can also be included in LSIC-DFA to improve its performance for the weakly bonded systems. The self-consistent implementation of the LSIC method presented in this work also opens up its applications beyond energetic properties. Such studies will be carried out in the future.

The results of this work and previous one-shot LSIC results show that an accurate description of several electronic properties can be obtained from the simplest local spin density functional by removing the self-interaction errors using an appropriately designed self-interaction correction method. The one-electron SIC method(s) is often considered synonymous with the PZSIC method, and the success and failures of PZSIC have often been misinterpreted as those of the one-electron SIC method(s). We hope that the present LSIC results along with those in earlier works with the perturbative or quasi-self-consistent LSIC method help remove this general misconception. More

studies, especially in cases where the effect of SIE is pronounced, such as the transition metals, lanthanides, and actinides complexes, or ions in solution, are needed to obtain a comprehensive picture of the scope of the LSIC method.

4.6 SUPPLEMENTARY MATERIAL

See the supplementary material (https://aip.scitation.org/doi/suppl/10.1063/5.0130436) for the detailed results of atomic and molecular properties computed with the local self-interaction correction method.

4.7 ACKNOWLEDGMENTS

The authors dedicate this work to Dr. Brett Dunlap on his 75th birthday and acknowledge discussions with Dr. Carlos Diaz and Dr. Luis Basurto. This work was supported by the U.S. Department of Energy, Office of Science, Office of Basic Energy Sciences, as part of the Computational Chemical Sciences Program under Award No. DE-SC0018331. Support for computational time at the Texas Advanced Computing Center (TACC), the Extreme Science and Engineering Discovery Environment (XSEDE), and the National Energy Research Scientific Computing Center (NERSC) is gratefully acknowledged.

4.8 AUTHOR DECLARATIONS

4.8.1 CONFLICT OF INTEREST

The authors have no conflicts to disclose.

4.8.2 AUTHOR CONTRIBUTIONS

Yoh Yamamoto: Data curation (equal); Formal analysis (equal); Investigation (equal); Software (equal); Validation (equal); Writing – original draft (equal). **Tunna Baruah**: Conceptualization (equal); Funding acquisition (equal); Methodology (equal); Project administration (equal); Resources (equal); Supervision (equal); Writing – review & editing (equal). **Po-Hao Chang**: Software (equal); Writing – review & editing (equal). **Selim Romero**: Data curation (equal); Validation (equal); Writing – review & editing (equal). **Rajendra R. Zope**: Conceptualization (equal); Funding acquisition (equal); Methodology (equal); Project administration (equal); Supervision (equal); Writing – review & editing (equal).

4.9 DATA AVAILABILITY

The data that support findings in this article is provided within the manuscript and supplementary information.

4.11 REFERENCES

[1] W. Kohn and L. J. Sham, "Self-consistent equations including exchange and correlation effects," Phys. Rev. **140**, A1133–A1138 (1965).

[2] M. Levy, "Universal variational functionals of electron densities, first-order density matrices, and natural spin-orbitals and solution of the v-representability problem," Proc. Natl. Acad. Sci. U. S. A. **76**, 6062–6065 (1979).

[3] K. R. Bryenton, A. A. Adeleke, S. G. Dale, and E. R. Johnson, "Delocalization error: The greatest outstanding challenge in density-functional theory," Wiley Interdiscip. Rev.: Comput. Mol. Sci. e1631 (2022).

[4] I. Lindgren, "A statistical exchange approximation for localized electrons," Int. J. Quantum Chem. **5**, 411–420 (1971).

[5] J. P. Perdew, "Orbital functional for exchange and correlation: Self-interaction correction to

the local density approximation," Chem. Phys. Lett. **64**, 127–130 (1979).
[6] M. S. Gopinathan, "Improved approximate representation of the Hartree-Fock potential in atoms," Phys. Rev. A **15**, 2135–2142 (1977).
[7] J. P. Perdew and A. Zunger, "Self-interaction correction to density-functional approximations for many-electron systems," Phys. Rev. B **23**, 5048–5079 (1981).
[8] U. Lundin and O. Eriksson, "Novel method of self-interaction corrections in density functional calculations," Int. J. Quantum Chem. **81**, 247–252 (2001).
[9] A. Zunger, J. P. Perdew, and G. L. Oliver, "A self-interaction corrected approach to many-electron systems: Beyond the local spin density approximation," Solid State Commun. **34**, 933–936 (1980).
[10] O. Gunnarsson and R. O. Jones, "Self-interaction corrections in the density functional formalism," Solid State Commun. **37**, 249–252 (1981).
[11] S. Manoli and M. A. Whitehead, "Generalized-exchange local-spin-densityfunctional theory: Self-interaction correction," Phys. Rev. A **38**, 630–635 (1988).
[12] Y. Guo and M. A. Whitehead, "An alternative self-interaction correction in the generalized exchange local-density functional theory," J. Comput. Chem. **12**, 803–810 (1991).
[13] A. D. Becke and M. R. Roussel, "Exchange holes in inhomogeneous systems: A coordinate-space model," Phys. Rev. A **39**, 3761–3767 (1989).
[14] A. D. Becke, "Hartree-Fock exchange energy of an inhomogeneous electron gas," Int. J. Quantum Chem. **23**, 1915–1922 (1983).
[15] T. Tsuneda, M. Kamiya, and K. Hirao, "Regional self-interaction correction of density functional theory," J. Comput. Chem. **24**, 1592–1598 (2003).
[16] T. Tsuneda and K. Hirao, "Self-interaction corrections in density functional theory," J. Chem. Phys. **140**, 18A513 (2014).
[17] J. Jaramillo, G. E. Scuseria, and M. Ernzerhof, "Local hybrid functionals," J. Chem. Phys. **118**, 1068–1073 (2003).
[18] M. Kaupp, H. Bahmann, and A. V. Arbuznikov, "Local hybrid functionals: An assessment for thermochemical kinetics," J. Chem. Phys. **127**, 194102 (2007).
[19] T. Schmidt, E. Kraisler, A. Makmal, L. Kronik, and S. Kümmel, "A selfinteraction-free local hybrid functional: Accurate binding energies vis-á-vis accurate ionization potentials from Kohn-Sham eigenvalues," J. Chem. Phys. **140**, 18A510 (2014).

[20] R. Latter, “Atomic energy levels for the Thomas-Fermi and Thomas-FermiDirac potential,” Phys. Rev. **99**, 510–519 (1955).

[21] I. Dabo, A. Ferretti, and N. Marzari, “Piecewise linearity and spectroscopic properties from Koopmans-compliant functionals,” in *First Principles Approaches to Spectroscopic Properties of Complex Materials*, edited by C. Di Valentin, S. Botti and M. Cococcioni (Springer Berlin Heidelberg, Berlin, Heidelberg, 2014), pp. 193–233.

[22] G. Borghi, A. Ferretti, N. L. Nguyen, I. Dabo, and N. Marzari, “Koopmanscompliant functionals and their performance against reference molecular data,” Phys. Rev. B **90**, 075135 (2014).

[23] C. D. Pemmaraju, T. Archer, D. Sánchez-Portal, and S. Sanvito, “Atomicorbital-based approximate self-interaction correction scheme for molecules and solids,” Phys. Rev. B **75**, 045101 (2007).

[24] G. Li Manni, R. K. Carlson, S. Luo, D. Ma, J. Olsen, D. G. Truhlar, and L. Gagliardi, “Multiconfiguration pair-density functional theory,” J. Chem. Theory Comput. **10**, 3669–3680 (2014).

[25] V. I. Anisimov, J. Zaanen, and O. K. Andersen, “Band theory and Mott insulators: Hubbard U instead of Stoner I,” Phys. Rev. B **44**, 943 (1991).

[26] A. I. Liechtenstein, V. I. Anisimov, and J. Zaanen, “Density-functional theory and strong interactions: Orbital ordering in Mott-Hubbard insulators,” Phys. Rev. B **52**, R5467–R5470 (1995).

[27] A. D. Becke, “A new mixing of Hartree-Fock and local density-functional theories,” J. Chem. Phys. **98**, 1372–1377 (1993).

[28] H. Iikura, T. Tsuneda, T. Yanai, and K. Hirao, “A long-range correction scheme for generalized-gradient-approximation exchange functionals,” J. Chem. Phys. **115**, 3540–3544 (2001).

[29] B. G. Janesko, “Replacing hybrid density functional theory: Motivation and recent advances,” Chem. Soc. Rev. **50**, 8470 (2021).

[30] J. G. Harrison, R. A. Heaton, and C. C. Lin, “Self-interaction correction to the local density Hartree-Fock atomic calculations of excited and ground states,” J. Phys. B: At. Mol. Phys. **16**, 2079–2091 (1983).

[31] J. G. Harrison, “An improved self-interaction-corrected local spin density functional for

atoms," J. Chem. Phys. **78**, 4562–4566 (1983).
[32] R. A. Heaton and C. C. Lin, "Self-interaction-correction theory for density functional calculations of electronic energy bands for the lithium chloride crystal," J. Phys. C: Solid State Phys. **17**, 1853–1866 (1984).
[33] R. A. Heaton and C. C. Lin, "Electronic energy-band structure of the calcium fluoride crystal," Phys. Rev. B **22**, 3629 (1980).
[34] H. Gudmundsdóttir, E. Ö. Jónsson, and H. Jónsson, "Calculations of Al dopant in α-quartz using a variational implementation of the Perdew–Zunger self-interaction correction," New J. Phys. **17**, 083006 (2015).
[35] E. Ö. Jónsson, S. Lehtola, and H. Jónsson, "Towards an optimal gradientdependent energy functional of the PZ-SIC form," Procedia Comput. Sci. **51**, 1858–1864 (2015).
[36] S. Lehtola, E. Ö. Jónsson, and H. Jónsson, "Effect of complex-valued optimal orbitals on atomization energies with the Perdew-Zunger self-interaction correction to density functional theory," J. Chem. Theory Comput. **12**, 4296–4302 (2016).
[37] S. Klüpfel, P. Klüpfel, and H. Jónsson, "The effect of the Perdew-Zunger self-interaction correction to density functionals on the energetics of small molecules," J. Chem. Phys. **137**, 124102 (2012).
[38] S. Lehtola and H. Jónsson, "Variational, self-consistent implementation of the Perdew-Zunger self-interaction correction with complex optimal orbitals," J. Chem. Theory Comput. **10**, 5324–5337 (2014).
[39] O. A. Vydrov and G. E. Scuseria, "Ionization potentials and electron affinities in the Perdew-Zunger self-interaction corrected density-functional theory," J. Chem. Phys. **122**, 184107 (2005).
[40] O. A. Vydrov and G. E. Scuseria, "Effect of the Perdew-Zunger self-interaction correction on the thermochemical performance of approximate density functionals," J. Chem. Phys. **121**, 8187–8193 (2004).
[41] S. Lehtola, M. Head-Gordon, and H. Jónsson, "Complex orbitals, multiple local minima, and symmetry breaking in Perdew-Zunger self-interaction corrected density functional theory calculations," J. Chem. Theory Comput. **12**, 3195–3207 (2016).
[42] B. G. Janesko, "Systematically improvable generalization of self-interaction corrected density functional theory," J. Phys. Chem. Lett. **13**, 5698–5702 (2022).
[43] E. J. Bylaska, K. Tsemekhman, and F. Gao, "New development of self-interaction corrected

DFT for extended systems applied to the calculation of native defects in 3C–SiC," Phys. Scr. **T124**, 86–90 (2006).

[44] A. Ruzsinszky, J. P. Perdew, G. I. Csonka, O. A. Vydrov, and G. E. Scuseria, "Density functionals that are one- and two- are not always many-electron selfinteraction-free, as shown for, LiH+, and H+ 2 , He+ 2 Ne+ 2 ," J. Chem. Phys. **126**, 104102 (2007).

[45] A. Ruzsinszky, J. P. Perdew, G. I. Csonka, O. A. Vydrov, and G. E. Scuseria, "Spurious fractional charge on dissociated atoms: Pervasive and resilient selfinteraction error of common density functionals," J. Chem. Phys. **125**, 194112 (2006).

[46] K. A. Jackson, J. E. Peralta, R. P. Joshi, K. P. Withanage, K. Trepte, K. Sharkas, and A. I. Johnson, "Towards efficient density functional theory calculations without self-interaction: The Fermi-Löwdin orbital self-interaction correction," J. Phys.: Conf. Ser. **1290**, 012002 (2019).

[47] S. Patchkovskii and T. Ziegler, "Improving "difficult" reaction barriers with selfinteraction corrected density functional theory," J. Chem. Phys. **116**, 7806–7813 (2002).

[48] S. Kümmel and J. P. Perdew, "Two avenues to self-interaction correction within Kohn-Sham theory: Unitary invariance is the shortcut," Mol. Phys. **101**, 1363–1368 (2003).

[49] T. Körzdörfer, S. Kümmel, and M. Mundt, "Self-interaction correction and the optimized effective potential," J. Chem. Phys. **129**, 014110 (2008).

[50] T. Baruah, R. R. Zope, A. Kshirsagar, and R. K. Pathak, "Positron binding: A positron-density viewpoint," Phys. Rev. A **50**, 2191–2196 (1994).

[51] V. Polo, E. Kraka, and D. Cremer, "Electron correlation and the self-interaction error of density functional theory," Mol. Phys. **100**, 1771–1790 (2002).

[52] R. A. Heaton, J. G. Harrison, and C. C. Lin, "Self-interaction correction for density-functional theory of electronic energy bands of solids," Phys. Rev. B **28**, 5992 (1983).

[53] S. Goedecker and C. J. Umrigar, "Critical assessment of the self-interactioncorrected–local-density-functional method and its algorithmic implementation," Phys. Rev. A **55**, 1765 (1997).

[54] A. Svane, "Electronic structure of cerium in the self-interaction-corrected localspin-density approximation," Phys. Rev. B **53**, 4275 (1996).

[55] A. Svane, W. M. Temmerman, Z. Szotek, J. Lægsgaard, and H. Winter, "Selfinteraction-corrected local-spin-density calculations for rare earth materials," Int. J. Quantum Chem. **77**, 799–813 (2000).

[56] M. M. Rieger and P. Vogl, "Self-interaction corrections in semiconductors," Phys. Rev. B **52**,

16567 (1995).
[57] R. R. Zope, M. K. Harbola, and R. K. Pathak, “Atomic Compton profiles within different exchange-only theories,” Eur. Phys. J. D **7**, 151–155 (1999).
[58] N. Hamada and S. Ohnishi, “Self-interaction correction to the local-density approximation in the calculation of the energy band gaps of semiconductors based on the full-potential linearized augmented-plane-wave method,” Phys. Rev. B **34**, 9042 (1986).
[59] M. Biagini, “Self-interaction-corrected density-functional formalism,” Phys. Rev. B **49**, 2156 (1994).
[60] Y. Xie, R. Han, and X. Zhang, “Obtaining localized orbitals and band structure in self-interaction-corrected density-functional theory,” Phys. Rev. B **60**, 8543 (1999).
[61] M. Arai and T. Fujiwara, “Electronic structures of transition-metal mono-oxides in the self-interaction-corrected local-spin-density approximation,” Phys. Rev. B **51**, 1477 (1995).
[62] M. Stengel and N. A. Spaldin, “Self-interaction correction with Wannier functions,” Phys. Rev. B **77**, 155106 (2008).
[63] D. L. Price, “Application of an on-site self-interaction-corrected method to Ce and the α-Ce surface,” Phys. Rev. B **60**, 10588 (1999).
[64] C. Shahi, P. Bhattarai, K. Wagle, B. Santra, S. Schwalbe, T. Hahn, J. Kortus, K. A. Jackson, J. E. Peralta, K. Trepte, S. Lehtola, N. K. Nepal, H. Myneni, B. Neupane, S. Adhikari, A. Ruzsinszky, Y. Yamamoto, T. Baruah, R. R. Zope, and J. P. Perdew, “Stretched or noded orbital densities and self-interaction correction in density functional theory,” J. Chem. Phys. **150**, 174102 (2019).
[65] O. A. Vydrov, G. E. Scuseria, J. P. Perdew, A. Ruzsinszky, and G. I. Csonka, “Scaling down the Perdew-Zunger self-interaction correction in many-electron regions,” J. Chem. Phys. **124**, 094108 (2006).
[66] J. P. Perdew, A. Ruzsinszky, J. Sun, and M. R. Pederson, “Paradox of selfinteraction correction: How can anything so right be so wrong?” Adv. At., Mol., Opt. Phys. **64**, 1–14 (2015).
[67] G. I. Csonka and B. G. Johnson, “Inclusion of exact exchange for self-interaction corrected H3 density functional potential energy surface,” Theor. Chem. Acc. **99**, 158–165 (1998).
[68] A. I. Johnson, K. P. K. Withanage, K. Sharkas, Y. Yamamoto, T. Baruah, R. R. Zope, J. E. Peralta, and K. A. Jackson, “The effect of self-interaction error on electrostatic dipoles calculated using density functional theory,” J. Chem. Phys. **151**, 174106 (2019).

[69] R. R. Zope, Y. Yamamoto, C. M. Diaz, T. Baruah, J. E. Peralta, K. A. Jackson, B. Santra, and J. P. Perdew, "A step in the direction of resolving the paradox of Perdew-Zunger self-interaction correction," J. Chem. Phys. **151**, 214108 (2019).
[70] M. R. Pederson and J. P. Perdew, "5 scientific highlight of the month selfinteraction correction in density functional theory: The road less traveled," Psi-k Newsletter **109**, 77 (2012).
[71] W. L. Luken and D. N. Beratan, "Localized orbitals and the Fermi hole," Theor. Chem. Acc. **61**, 265–281 (1982).
[72] W. L. Luken and J. C. Culberson, "Localized orbitals based on the Fermi hole," Theor. Chem. Acc. **66**, 279–293 (1984).
[73] M. R. Pederson, A. Ruzsinszky, and J. P. Perdew, "Communication: Selfinteraction correction with unitary invariance in density functional theory," J. Chem. Phys. **140**, 121103 (2014).
[74] M. R. Pederson, "Fermi orbital derivatives in self-interaction corrected density functional theory: Applications to closed shell atoms," J. Chem. Phys. **142**, 064112 (2015).
[75] M. R. Pederson and T. Baruah, "Chapter eight—Self-interaction corrections within the Fermi-orbital-based formalism," Adv. At., Mol., Opt. Phys. **64**, 153–180 (2015).
[76] Z.-h. Yang, M. R. Pederson, and J. P. Perdew, "Full self-consistency in the fermiorbital self-interaction correction," Phys. Rev. A **95**, 052505 (2017).
[77] C. M. Diaz, T. Baruah, and R. R. Zope, "Fermi-Löwdin-orbital self-interaction correction using the optimized-effective-potential method within the Krieger-LiIafrate approximation," Phys. Rev. A **103**, 042811 (2021).
[78] C. M. Diaz, P. Suryanarayana, Q. Xu, T. Baruah, J. E. Pask, and R. R. Zope, "Implementation of Perdew–Zunger self-interaction correction in real space using Fermi–Löwdin orbitals," J. Chem. Phys. **154**, 084112 (2021).
[79] P. Bhattarai, B. Santra, K. Wagle, Y. Yamamoto, R. R. Zope, A. Ruzsinszky, K. A. Jackson, and J. P. Perdew, "Exploring and enhancing the accuracy of interiorscaled Perdew-Zunger self-interaction correction," J. Chem. Phys. **154**, 094105 (2021).
[80] S. Romero, Y. Yamamoto, T. Baruah, and R. R. Zope, "Local self-interaction correction method with a simple scaling factor," Phys. Chem. Chem. Phys. **23**, 2406–2418 (2021).
[81] S. Schwalbe, L. Fiedler, J. Kraus, J. Kortus, K. Trepte, and S. Lehtola, "PyFLOSIC: Python-based Fermi–Löwdin orbital self-interaction correction," J. Chem. Phys. **153**, 084104 (2020).

[82] Y. Yamamoto, A. Salcedo, C. M. Diaz, M. S. Alam, T. Baruah, and R. R. Zope, "Assessing the effect of regularization on the molecular properties predicted by SCAN and self-interaction corrected SCAN meta-GGA," Phys. Chem. Chem. Phys. **22**, 18060–18070 (2020).
[83] Y. Yamamoto, S. Romero, T. Baruah, and R. R. Zope, "Improvements in the orbitalwise scaling down of Perdew-Zunger self-interaction correction in manyelectron regions," J. Chem. Phys. **152**, 174112 (2020).
[84] P. Bhattarai, K. Wagle, C. Shahi, Y. Yamamoto, S. Romero, B. Santra, R. R. Zope, J. E. Peralta, K. A. Jackson, and J. P. Perdew, "A step in the direction of resolving the paradox of Perdew–Zunger self-interaction correction. II. Gauge consistency of the energy density at three levels of approximation," J. Chem. Phys. **152**, 214109 (2020).
[85] S. Akter, Y. Yamamoto, R. R. Zope, and T. Baruah, "Static dipole polarizabilities of polyacenes using self-interaction-corrected density functional approximations," J. Chem. Phys. **154**, 114305 (2021).
[86] S. Akter, J. A. V. Tellez, K. Sharkas, J. Peralta, K. Jackson, T. Baruah, and R. Zope, "How well do self-interaction corrections repair the over-estimation of molecular polarizabilities in density functional calculations?" Phys. Chem. Chem. Phys. **23**, 18678 (2021).
[87] K. P. K. Withanage, S. Akter, C. Shahi, R. P. Joshi, C. Diaz, Y. Yamamoto, R. Zope, T. Baruah, J. P. Perdew, J. E. Peralta, and K. A. Jackson, "Selfinteraction-free electric dipole polarizabilities for atoms and their ions using the Fermi-Löwdin self-interaction correction," Phys. Rev. A **100**, 012505 (2019).
[88] S. Akter, Y. Yamamoto, C. M. Diaz, K. A. Jackson, R. R. Zope, and T. Baruah, "Study of self-interaction errors in density functional predictions of dipole polarizabilities and ionization energies of water clusters using Perdew–Zunger and locally scaled self-interaction corrected methods," J. Chem. Phys. **153**, 164304 (2020).
[89] R. P. Joshi, K. Trepte, K. P. K. Withanage, K. Sharkas, Y. Yamamoto, L. Basurto, R. R. Zope, T. Baruah, K. A. Jackson, and J. E. Peralta, "Fermi-Löwdin orbital self-interaction correction to magnetic exchange couplings," J. Chem. Phys. **149**, 164101 (2018).
[90] P. Mishra, Y. Yamamoto, P.-H. Chang, D. B. Nguyen, J. E. Peralta, T. Baruah, and R. R. Zope, "Study of self-interaction errors in density functional calculations of magnetic exchange coupling constants using three self-interaction correction methods," J. Phys. Chem. A **126**, 1923–1935 (2022).

[91] P. Mishra, Y. Yamamoto, J. K. Johnson, K. A. Jackson, R. R. Zope, and T. Baruah, "Study of self-interaction-errors in barrier heights using locally scaled and Perdew-Zunger self-interaction methods," J. Chem. Phys. **156**, 014306 (2022).

[92] L. Li, K. Trepte, K. A. Jackson, and J. K. Johnson, "Application of self-interaction corrected density functional theory to early, middle, and late transition states," J. Phys. Chem. A **124**, 8223–8234 (2020).

[93] A. Karanovich, Y. Yamamoto, K. A. Jackson, and K. Park, "Electronic structure of mononuclear Cu-based molecule from density-functional theory with self-interaction correction," J. Chem. Phys. **155**, 014106 (2021).

[94] S. Schwalbe, T. Hahn, S. Liebing, K. Trepte, and J. Kortus, "Fermi-Löwdin orbital self-interaction corrected density functional theory: Ionization potentials and enthalpies of formation," J. Comput. Chem. **39**, 2463–2471 (2018).

[95] F. W. Aquino, R. Shinde, and B. M. Wong, "Fractional occupation numbers and self-interaction correction-scaling methods with the Fermi-Löwdin orbital selfinteraction correction approach," J. Comput. Chem. **41**, 1200–1208 (2020).

[96] Y. Yamamoto, C. M. Diaz, L. Basurto, K. A. Jackson, T. Baruah, and R. R. Zope, "Fermi-Löwdin orbital self-interaction correction using the strongly constrained and appropriately normed meta-GGA functional," J. Chem. Phys. **151**, 154105 (2019).

[97] K. P. K. Withanage, K. Trepte, J. E. Peralta, T. Baruah, R. Zope, and K. A. Jackson, "On the question of the total energy in the Fermi-Löwdin orbital self-interaction correction method," J. Chem. Theory Comput. **14**, 4122–4128 (2018).

[98] D.-y. Kao, K. Withanage, T. Hahn, J. Batool, J. Kortus, and K. Jackson, "Selfconsistent self-interaction corrected density functional theory calculations for atoms using Fermi-Löwdin orbitals: Optimized Fermi-orbital descriptors for Li–Kr," J. Chem. Phys. **147**, 164107 (2017).

[99] K. P. K. Withanage, P. Bhattarai, J. E. Peralta, R. R. Zope, T. Baruah, J. P. Perdew, and K. A. Jackson, "Density-related properties from self-interaction corrected density functional theory calculations," J. Chem. Phys. **154**, 024102 (2021).

[100] C. M. Diaz, L. Basurto, S. Adhikari, Y. Yamamoto, A. Ruzsinszky, T. Baruah, and R. R. Zope, "Self-interaction-corrected Kohn–Sham effective potentials using the density-consistent effective potential method," J. Chem. Phys. **155**, 064109 (2021).

[101] D. B. Nguyen, M. R. Pederson, J. P. Perdew, K. A. Jackson, and J. E. Peralta, "Initial Fermi

orbital descriptors for FLOSIC calculations: The quick-FOD method," Chem. Phys. Lett. **780**, 138952 (2021).
[102] S. Schwalbe, K. Trepte, L. Fiedler, A. I. Johnson, J. Kraus, T. Hahn, J. E. Peralta, K. A. Jackson, and J. Kortus, "Interpretation and automatic generation of Fermi-orbital descriptors," J. Comput. Chem. **40**, 2843–2857 (2019).
[103] K. Trepte, S. Schwalbe, S. Liebing, W. T. Schulze, J. Kortus, H. Myneni, A. V. Ivanov, and S. Lehtola, "Chemical bonding theories as guides for self-interaction corrected solutions: Multiple local minima and symmetry breaking," J. Chem. Phys. **155**, 224109 (2021).
[104] K. Wagle, B. Santra, P. Bhattarai, C. Shahi, M. R. Pederson, K. A. Jackson, and J. P. Perdew, "Self-interaction correction in water-ion clusters," J. Chem. Phys. **154**, 094302 (2021).
[105] K. Sharkas, K. Wagle, B. Santra, S. Akter, R. R. Zope, T. Baruah, K. A. Jackson, J. P. Perdew, and J. E. Peralta, "Self-interaction error overbinds water clusters but cancels in structural energy differences," Proc. Natl. Acad. Sci. U. S. A. **117**, 11283–11288 (2020).
[106] J. Vargas, P. Ufondu, T. Baruah, Y. Yamamoto, K. A. Jackson, and R. R. Zope, "Importance of self-interaction-error removal in density functional calculations on water cluster anions," Phys. Chem. Chem. Phys. **22**, 3789–3799 (2020).
[107] K. Sharkas, L. Li, K. Trepte, K. P. K. Withanage, R. P. Joshi, R. R. Zope, T. Baruah, J. K. Johnson, K. A. Jackson, and J. E. Peralta, "Shrinking self-interaction errors with the Fermi-Löwdin orbital self-interaction-corrected density functional approximation," J. Phys. Chem. A **122**, 9307–9315 (2018).
[108] K. Trepte, S. Schwalbe, T. Hahn, J. Kortus, D.-Y. Kao, Y. Yamamoto, T. Baruah, R. R. Zope, K. P. K. Withanage, J. E. Peralta, and K. A. Jackson, "Analytic atomic gradients in the Fermi-Löwdin orbital self-interaction correction," J. Comput. Chem. **40**, 820–825 (2019).
[109] J. P. Perdew, K. Burke, and M. Ernzerhof, "Generalized gradient approximation made simple," Phys. Rev. Lett. **77**, 3865–3868 (1996).
[110] J. P. Perdew, K. Burke, and M. Ernzerhof, "Generalized gradient approximation made simple [Phys. Rev. Lett. 77, 3865 (1996)]," Phys. Rev. Lett. **78**, 1396 (1997).
[111] B. J. Lynch and D. G. Truhlar, "Small representative benchmarks for thermochemical calculations," J. Phys. Chem. A **107**, 8996–8999 (2003).
[112] R. R. Zope, T. Baruah, and K. A. Jackson, "FLOSIC 0.2," Based on the NRLMOL code of M. R. Pederson.

[113] Y. Yamamoto, L. Basurto, C. M. Diaz, R. R. Zope, and T. Baruah, "FLOSIC software public release," Based on the NRLMOL code of M. R. Pederson.
[114] O. A. Vydrov and G. E. Scuseria, "A simple method to selectively scale down the self-interaction correction," J. Chem. Phys. **124**, 191101 (2006).
[115] C. v. Weizsäcker, "Zur theorie der kernmassen," Z. Phys. **96**, 431–458 (1935).
[116] B. Santra and J. P. Perdew, "Perdew-Zunger self-interaction correction: How wrong for uniform densities and large-Z atoms?" J. Chem. Phys. **150**, 174106 (2019).
[117] F. Zahariev, S. S. Leang, and M. S. Gordon, "Functional derivatives of meta-generalized gradient approximation (meta-GGA) type exchange-correlation density functionals," J. Chem. Phys. **138**, 244108 (2013).
[118] P.-H. Chang, Z. Buschmann, and R. R. Zope, A hybrid approach to basis set independent Poisson solver for an arbitrary charge distribution (2022).
[119] A. D. Becke and R. M. Dickson, "Numerical solution of Poisson's equation in polyatomic molecules," J. Chem. Phys. **89**, 2993–2997 (1988).
[120] V. I. Lebedev, "Quadratures on a sphere," USSR Comput. Math. Math. Phys. **16**, 10–24 (1976).
[121] M. E. Mura and P. J. Knowles, "Improved radial grids for quadrature in molecular density-functional calculations," J. Chem. Phys. **104**, 9848–9858 (1996).
[122] A. D. Becke, "A multicenter numerical integration scheme for polyatomic molecules," J. Chem. Phys. **88**, 2547–2553 (1988).
[123] B. Delley, "An all-electron numerical method for solving the local density functional for polyatomic molecules," J. Chem. Phys. **92**, 508–517 (1990)
[124] R. E. Stratmann, G. E. Scuseria, and M. J. Frisch, "Achieving linear scaling in exchange-correlation density functional quadratures," Chem. Phys. Lett. **257**,213–223 (1996).
[125] M. Franchini, P. H. T. Philipsen, and L. Visscher, "The Becke fuzzy cells integration scheme in the Amsterdam density functional program suite," J. Comput. Chem. **34**, 1819–1827 (2013).
[126] V. Blum, R. Gehrke, F. Hanke, P. Havu, V. Havu, X. Ren, K. Reuter, and M. Scheffler, "*Ab initio* molecular simulations with numeric atom-centered orbitals," Comput. Phys. Commun. **180**, 2175–2196 (2009).
[127] B. I. Dunlap, "Fitting the Coulomb potential variationally in Xα molecular calculations," J. Chem. Phys. **78**, 3140–3142 (1983).

[128] K. Jackson and M. R. Pederson, "Accurate forces in a local-orbital approach to the local-density approximation," Phys. Rev. B **42**, 3276–3281 (1990).
[129] M. R. Pederson, D. V. Porezag, J. Kortus, and D. C. Patton, "Strategies for massively parallel local-orbital-based electronic structure methods," Phys. Status Solidi B **217**, 197–218 (2000).
[130] J. Sun, A. Ruzsinszky, and J. P. Perdew, "Strongly constrained and appropriately normed semilocal density functional," Phys. Rev. Lett. **115**, 036402 (2015).
[131] J. Tao, V. N. Staroverov, G. E. Scuseria, and J. P. Perdew, "Exact-exchange energy density in the gauge of a semilocal density-functional approximation," Phys. Rev. A **77**, 012509 (2008).
[132] A. V. Arbuznikov and M. Kaupp, "Towards improved local hybrid functionals by calibration of exchange-energy densities," J. Chem. Phys. **141**, 204101 (2014).
[133] T. M. Maier, M. Haasler, A. V. Arbuznikov, and M. Kaupp, "New approaches for the calibration of exchange-energy densities in local hybrid functionals," Phys. Chem. Chem. Phys. **18**, 21133–21144 (2016).
[134] J. P. Perdew, J. A. Chevary, S. H. Vosko, K. A. Jackson, M. R. Pederson, D. J. Singh, and C. Fiolhais, "Atoms, molecules, solids, and surfaces: Applications of the generalized gradient approximation for exchange and correlation," Phys. Rev. B **46**, 6671–6687 (1992).
[135] D. Porezag and M. R. Pederson, "Optimization of Gaussian basis sets for density-functional calculations," Phys. Rev. A **60**, 2840–2847 (1999).
[136] B. P. Pritchard, D. Altarawy, B. Didier, T. D. Gibson, and T. L. Windus, "A new basis set exchange: An open, up-to-date resource for the molecular sciences community," J. Chem. Inf. Model. **59**, 4814–4820 (2019).
[137] M. R. Pederson and K. A. Jackson, "Variational mesh for quantum-mechanical simulations," Phys. Rev. B **41**, 7453–7461 (1990).
[138] A. P. Bartók and J. R. Yates, "Regularized SCAN functional," J. Chem. Phys. **150**, 161101 (2019).
[139] J. W. Furness and J. Sun, "Enhancing the efficiency of density functionals with an improved iso-orbital indicator," Phys. Rev. B **99**, 041119 (2019).
[140] J. W. Furness, A. D. Kaplan, J. Ning, J. P. Perdew, and J. Sun, "Accurate and numerically efficient r2SCAN meta-generalized gradient approximation," J. Phys. Chem. Lett. **11**, 8208–8215 (2020).
[141] S. Klüpfel, P. Klüpfel, and H. Jónsson, "Importance of complex orbitals in calculating the

self-interaction-corrected ground state of atoms," Phys. Rev. A **84**, 050501 (2011).
[142] D. Hofmann, T. Körzdörfer, and S. Kümmel, "Kohn-Sham self-interaction correction in real time," Phys. Rev. Lett. **108**, 146401 (2012).
[143] D. Hofmann, S. Klüpfel, P. Klüpfel, and S. Kümmel, "Using complex degrees of freedom in the Kohn-Sham self-interaction correction," Phys. Rev. A **85**, 062514 (2012).
[144] K. P. K. Withanage, K. A. Jackson, and M. R. Pederson, "Complex FermiLöwdin orbital self-interaction correction," J. Chem. Phys. **156**, 231103 (2022).
[145] S. J. Chakravorty, S. R. Gwaltney, E. R. Davidson, F. A. Parpia, and C. F. p Fischer, "Ground-state correlation energies for atomic ions with 3 to 18 electrons," Phys. Rev. A **47**, 3649–3670 (1993).
[146] Y. Zhao, J. Pu, B. J. Lynch, and D. G. Truhlar, "Tests of second-generation and third-generation density functionals for thermochemical kinetics," Phys. Chem. Chem. Phys. **6**, 673–676 (2004).
[147] B. G. Janesko and G. E. Scuseria, "Hartree–Fock orbitals significantly improve the reaction barrier heights predicted by semilocal density functionals," J. Chem. Phys. **128**, 244112 (2008).
[148] J. F. Janak, "Proof that $\partial\partial nei = \epsilon$ in density-functional theory," Phys. Rev. B **18**, 7165–7168 (1978).
[149] J. P. Perdew, R. G. Parr, M. Levy, and J. L. Balduz, Jr, "Density-functional theory for fractional particle number: Derivative discontinuities of the energy," Phys. Rev. Lett. **49**, 1691 (1982).
[150] M. Levy, J. P. Perdew, and V. Sahni, "Exact differential equation for the density and ionization energy of a many-particle system," Phys. Rev. A **30**, 2745–2748 (1984).
[151] J. P. Perdew and M. Levy, "Comment on "Significance of the highest occupied Kohn-Sham eigenvalue"," Phys. Rev. B **56**, 16021 (1997).
[152] M. K. Harbola, "Relationship between the highest occupied Kohn-Sham orbital eigenvalue and ionization energy," Phys. Rev. B **60**, 4545–4550 (1999)
[153] L. Gallandi, N. Marom, P. Rinke, and T. Körzdörfer, "Accurate ionization potentials and electron affinities of acceptor molecules II: Non-empirically tuned long-range corrected hybrid functionals," J. Chem. Theory Comput. **12**, 605–614 (2016).
[154] R. Baer and D. Neuhauser, "Density functional theory with correct long-range asymptotic behavior," Phys. Rev. Lett. **94**, 043002 (2005).

[155] D. R. Lide, *CRC Handbook of Chemistry and Physics* (CRC Press, 2004), Vol. 85.

[156] K. K. Irikura, "Experimental vibrational zero-point energies: Diatomic molecules," J. Phys. Chem. Ref. Data **36**, 389–397 (2007).

[157] T. Shimanouchi, "Tables of molecular vibrational frequencies. Consolidated volume II," J. Phys. Chem. Ref. Data **6**, 993–1102 (1977).

CHAPTER 5: LOCAL SELF-INTERACTION CORRECTION METHOD WITH ASIMPLE SCALING FACTOR

Reproduced from Ref. “Local self-interaction correction method with a simple scaling factor,” Phys. Chem. Chem. Phys., 2021,23, 2406-2418, DOI https://doi.org/10.1039/D0CP06282K, with permission from the Royal Society of Chemestry Owner Societies.

5.1 ABSTRACT

A recently proposed local self-interaction correction (LSIC) method [Zope et al., J. Chem. Phys., 2019, 151, 214108] when applied to the simplest local density approximation provides a significant improvement over standard Perdew–Zunger SIC (PZSIC) for both equilibrium properties such as total or atomization energies as well as properties involving stretched bond such as barrier heights. The method uses an iso-orbital indicator to identify the single-electron regions. To demonstrate the LSIC method, Zope *et al*. used the ratio zs of von Weizsa¨cker tW s and total kinetic energy densities ts, (zs = tW s /ts) as a scaling factor to scale the self-interaction correction. The present work further explores the LSIC method using a ratio of orbital and spin densities as a simpler scaling factor in place of the ratio of kinetic energy densities. We compute a wide array of both, equilibrium and non-equilibrium properties using LSIC and orbital scaling methods using this simple scaling factor and compare them with previously reported results. Our study shows that LSIC with the simple scaling factor performs better than PZSIC, with results comparable to those obtained by LSIC(zs) for most properties, but has slightly larger errors than LSIC(zs). Furthermore, we study the binding energies of small water clusters using both scaling factors. Our results show that LSIC with zs has limitations in predicting the cluster binding energies of weakly bonded systems due to the inability of zs to distinguish weakly bonded regions from slowly varying density regions. LSIC when used with the density ratio as a scaling factor, on the other hand, provides a good description of water cluster binding energies, thus highlighting the appropriate choice of the iso-orbital indicator.

5.2 INTRODUCTION

The Kohn–Sham (KS) formulation of density functional theory (DFT) [1-3] is widely used to study electronic structures of atoms, molecules, and solids because of its low computational cost and its availability in easy to use software packages. The practical application of DFT requires an approximation to the exchange–correlation (XC) functional. The simplest form of the XC functional is the local spin density approximation (LSDA) [1,4] which belongs to the lowest rung of Jacob's ladder of XC functionals [5]. The higher rungs of the ladder contain more complex and more accurate functionals-generalized gradient approximation (GGA), meta-GGA, hybrid functionals, and functionals that include virtual orbitals. The majority of the density functional approximations (DFAs) suffer from self-interaction errors (SIE) though the magnitude of error can vary from one class of functionals to another or from one parameterization to another in a given class of functionals. The SIE occurs as a result of incomplete cancellation of self-Coulomb energy by the self-exchange energy of the approximate XC functional.

Many failures of DFAs have been attributed to SIE. SIE causes the potential to decay asymptotically as $-exp(-r)$ instead of the correct $-1/r$ decay for finite neutral systems. As a result, DFAs produce errors such as overly shallow eigenvalues of valence orbitals, inaccurate chemical reaction barriers, electron delocalization errors, incorrect charges on dissociated fragments, incorrect binding energies for anions, etc. [4,6–8]. The $-1/r$ asymptotic behavior is also important for the computation of electronic properties that are sensitive to virtual orbitals and long-range density such as excited states, for example.

Several approaches to remove SIEs have been proposed [9–20]. Early approaches [9,10] used orbitalwise schemes to eliminate SIE but used functionals related to Slater's Xa method [21]. The most widely used approach to remove SIE is the one proposed by Perdew and Zunger (PZ) [4]. Their approach is commonly referred to as PZ self-interaction correction (PZSIC) where the one-electron SIE due to both exchange and correlation are removed from a DFA calculation on an

orbital-by-orbital basis. PZSIC provides exact cancellation for one-electron self-interaction (SI), but not necessarily for many-electron SI [22]. It has been applied to study properties of atoms, molecules, clusters, and solids [4,8,12,15,16,23-101].

PZSIC is an orbital dependent theory and when used with KS orbitals results in the size-extensivity problem. In PZSIC, local orbitals are used to keep the corrections size-extensive. Traditionally, PZSIC requires solving the so-called Pederson or localization equations (LE) [23,25] to find the set of local orbitals that minimizes the total energy. Solving the LE and finding the optimal orbitals compliant with these conditions is computationally expensive since it requires solving the LE for each pair of orbitals. Pederson *et al*. in 2014 used Fermi–Löwdin orbitals [102,103] (FLOs) to solve the PZSIC equations. This approach is known as FLO-SIC [104,105]. FLOs are a Löwdin orthogonalized set of Fermi orbitals (FOs) [102,103] that can be obtained from the KS orbitals. The FOs depend on the density matrix and spin density. The FLOs are the local orbitals that make FLOSIC total energy unitarily invariant. For the construction of FLOs, Fermi orbital descriptor (FOD) positions are used as $3N$ parameters in space that can be optimized analogously to the optimization of atomic positions in molecular structure optimization. Unlike the traditional PZSIC implementation which requires determination of N^2 parameters, the FLOSIC method requires determination of only $3N$ parameters.

Earlier applications of FLO-SIC with LSDA showed significant improvements in atomic and molecular properties over SI-uncorrected LSDA performance [51,74,106,107]. Naturally, FLOSIC was later also applied to more sophisticated XC functionals, such as Perdew–Burke–Ernzerhof (PBE) and Strongly Constrained and Appropriately Normed (SCAN), to see whether SIC improves the performance of those functionals in the higher rungs [17,52,66,67,69,70,75-78,108-113]. PZSIC when applied to semilocal functionals such as PBE GGA and SCAN meta-GGA provides a good description of stretched bond situations and predicts bound atomic anions, but this improvement occurs at the expense of worsening [36,109,110,114-116] the performance for properties where SI-uncorrected DFA performs well. Shahi *et al*. [109] recently attributed the poor performance of PZSIC with GGAs and higher rung functionals to the nodality of the local orbital densities. The use of complex localized orbitals with nodeless densities in PZSIC calculations by Klüpfel, Klüpfel, and Jónsson [115] and by Lethola *et al*. [117] show that complex orbital densities ameliorate the worsening of atomization energies when used with PBE. This

conflicting performance of PZSIC is called the paradox of SIC by Perdew and coworkers [118]. The worsening of energetics pertaining to equilibrium regions primarily is a result of the overcorrecting tendency of PZSIC. A few methods have been proposed to mitigate this overcorrection by scaling down the SIC contribution. Jónsson group simply scaled the SIC by a constant scaling factor [114]. In a similar spirit, Vydrov *et al*. proposed a method to scale down the SIC according to an orbital dependent scaling factor (OSIC) [38]. This method however does not provide a significant improvement for all properties. It improved over PZSIC atomization energies but worsened barrier heights. Moreover, the scaling approach by Vydrov *et al*. results in a worsening of the asymptotic description of the effective potential, causing atomic anions to be unbound. Ruzsinszky *et al*. [119] found that many-electron SIE and fractional-charge dissociation behavior of positively charged dimers reappear in the OSIC of Vydrov *et al*. Yamamoto and coworkers [112] implemented a new 'selective OSIC' method (SOSIC), that selectively scales down the SIC in many-electron regions. SOSIC overcomes the deficiencies of the OSIC method and predicts stable atomic anions as well as improved total atomic energies. It also improves the barrier heights over the OSIC method. Very recently, Zope *et al*. [17] proposed a new SIC method which identifies single-electron regions using iso-orbital indicators and corrects for SIE in a pointwise fashion by scaling down the SIC. The iso-orbital indicator serves as a weight in numerical integration and identifies both the single-orbital regions where full correction is needed and the uniform density regions where the DFAs are already accurate and correction is not needed. They called the new SIC method local-SIC (LSIC)17 and assessed its performance for a wide array of properties using LSDA. Unlike PZSIC, LSIC performed remarkably for both equilibrium properties like atomization energies and stretched bond situations that occur in barrier height calculation.

The LSIC method makes use of an iso-orbital indicator to identify one-electron regions. It offers an additional degree of freedom in that a suitable iso-orbital can be used or designed to identify one-electron regions or tune the SIC contribution in a pointwise manner. In the original LSIC work, Zope *et al*. used a ratio of von Weiszäcker and total kinetic energy densities as a choice for the local scaling factor. This iso-orbital indicator has been used in the construction of self-correlation free meta-GGAs, in the regional SIC [15] and also in local hybrid functionals [120,121]. Several different choices for the local scaling factors are already available in the literature. Alternatively, new iso-orbital indicators particularly suitable for LSIC can be

constructed. In this work, we explore the performance of the LSIC method using a simple ratio of the orbital density and spin density as the weight of SIC correction at a given point in space. This is the same scaling factor used by Slater to average the Hartree–Fock exchange potential in his classic work that introduced the Hartree–Fock–Slater method [21]. We refer to this choice of scaling factor as LSIC(w) for the remainder of this manuscript and use LSIC(z) to refer to the first LSIC application where the scaling factor is the ratio of von Weiszäcker kinetic energy and kinetic energy densities. We investigate the performance of LSIC(w) for a few atomic properties: total energy, ionization potentials, and electron affinities. For molecules, we calculate the total energies, atomization energies, and dissociation energies of a few selected systems. We find that LSIC(w) provides comparable results to LSIC(z). We also show a case where LSIC(w) performs better than the original LSIC(z). Additionally, we examine the performance of the scaling factor w based on the density ratio with the OSIC scheme.

In the following section, brief descriptions of the PZSIC, OSIC, and LSIC methods are presented. These methods are implemented using FLOs. Therefore, very brief definitions pertaining to FLOs are also presented. The results and discussion are presented in section 5.4.

5.3 THEORY AND COMPUTATIONS

5.3.1 PERDEW-ZUNGER AND FERMI-LÖWDIN SELF-INTERACTION CORRECTION

In the PZSIC method,4 SIE is removed on an orbital-by-orbital basis from the DFA energy as,

$$E^{PZSIC-DFA}[\rho_\uparrow, \rho_\downarrow] = E^{DFA}[\rho_\uparrow, \rho_\downarrow] - \Sigma_{i\sigma}^{OCC}\{U[\rho_{i\sigma}] + E_{XC}^{DFA}[\rho_{i\sigma}, 0]\}. \quad (5.1)$$

where i is the orbital index, σ is the spin index, $\rho_{i\sigma}$ is the electron density (local orbital density), $U[\rho_{i\sigma}]$ is the exact self-Coulomb energy and $E_{XC}^{DFA}\ [\rho_{i\sigma}, 0]$ is the self-exchange–correlation energy for a given DFA XC functional. Perdew and Zunger applied this scheme to atoms using KS orbitals. For larger systems, KS orbitals can be delocalized which would result in a violation of

size extensivity. Therefore, local orbitals are required. This was recognized long ago by Slater and Wood [122] in 1971 and was also emphasized by Gopinathan [10] in the context of SIC of the Hartree–Slater method and later by Perdew and Zunger in the context of approximate Kohn–Sham calculations. Subsequent PZSIC calculations by the Wisconsin group [23-25,80] used local orbitals in a variational implementation. It was shown by Pederson and coworkers [23,25] that local orbitals used in Eq. (5.1) must satisfy LEs for variational minimization of energy. The LE for the orbitals $\phi_{i\sigma}$ is a pairwise condition and is given as

$$\langle \phi_{i\sigma} | V_{i\sigma}^{SIC} - V_{j\sigma}^{SIC} | \phi_{j\sigma} \rangle = 0. \tag{5.2}$$

These equations are sometimes called symmetry conditions [59]. In the FLOSIC approach, FLOs are used instead of directly solving Eq (5.2). First, FOs ϕ^{FO} are constructed with the density matrix and spin density at special positions in space called Fermi orbital descriptor (FOD) positions as

$$\phi_i^{FO}(\vec{r}) = \sum_j^{N_{occ}} \frac{\psi_j(\vec{a}_i)\psi_j(\vec{r})}{\sqrt{\rho(\vec{a}_i)}}. \tag{5.3}$$

Here i and j are the orbital indexes, ψ_j is the KS orbital, ρ is the electron spin density and $\vec{a}_i$ is the FOD position. The FOs are then orthogonalized with Löwdin's scheme to form the FLOs. The FLOs are used for the calculation of the SIC energy and potential. In this method, the optimal set of FLOs is obtained by minimizing the total SIC energy by adjusting the corresponding FODs. The optimization of FOD positions is similar to the optimization of atomic (ionic) positions in standard structure optimization. We emphasize that FLOs can be used in all three SIC (PZSIC, OSIC, and LSIC) methods.

5.3.2 ORBITALWISE SCALING OF SIC (OSIC)

As mentioned in section 5.2, PZSIC tends to overcorrect the DFA energies, and several modifications to PZISC were proposed to scale down the PZSIC correction. In the OSIC method of Vydrov *et al*. [38] mentioned in the Introduction, Eq (5.1) is modified to

$$E^{OSIC-DFA} = E_{XC}^{DFA}[\rho_\uparrow, \rho_\downarrow] - \sum_{i\sigma}^{OCC} X_{i\sigma}^{k}(U[\rho_{i\sigma}] + E_{XC}^{DFA}[\rho_{i\sigma}, 0]), \tag{5.4}$$

where each local orbitalwise scaling factor $X_{i\sigma}^{k}$ is defined as

$$X_{i\sigma}^{k} = \int z_\sigma^k(\vec{r})\rho_{i\sigma}(\vec{r})d\vec{r} \tag{5.5}$$

Here, i indicates the orbital index, σ is the spin index, z_σ is the iso-orbital indicator and k is an integer. The quantity z_σ is used to interpolate the single-electron regions ($z_\sigma = 1$) and uniform density regions ($z_\sigma = 0$). In their original work, Vydrov *et al*. used $z_\sigma = \tau_\sigma^W/\tau_\sigma$ to study the performance of OSIC with various XC functionals, where $\tau_\sigma^W(\vec{r}) = \left|\vec{\nabla}\rho_\sigma(\vec{r})\right|^2/(8\rho_\sigma(\vec{r}))$ is the von Weiszäcker kinetic energy density and $\tau_\sigma(\vec{r}) = \frac{1}{2}\sum_i\left|\vec{\nabla}\psi_{i\sigma}(\vec{r})\right|^2$ is the non-interacting kinetic energy density. Satisfying the gradient expansion in ρ requires $k \geq 1$ for LSDA, $k \geq 2$ for GGAs, and $k \geq 3$ for meta-GGAs. Vydrov *et al*., however, used various values of k to study its effect on the OSIC performance.

In their subsequent work, Vydrov and Scuseria [16] used

$$w_{i\sigma}^{k}(\vec{r}) = \left(\frac{\rho_{i\sigma}(\vec{r})}{\rho_\sigma(\vec{r})}\right)^k, \tag{5.6}$$

the weight used by Slater [21] in averaging Hartree-Fock potential, as a scaling factor instead of kinetic energy density ratio. They repeated the OSIC calculations using wis in place of z_σ in Eq. (5.5). Notice that Eq. (5.6) contains a local orbital index, this weight is thus an orbital dependent quantity. $w_{i\sigma}$ approaches unity at single orbital regions since $\rho_\sigma(\vec{r}) = \rho_{i\sigma}(\vec{r})$ at this limit. Similarly, $w_{i\sigma}$ approaches zero at the many-electron region since $\rho_\sigma(\vec{r}) \gg \rho_{i\sigma}$ at this condition. It was reported by Vydrov and Scuseria [16] that OSIC with Eq. (5.6) showed comparable performance as $z_\sigma = \tau^W/\tau_\sigma$ despite its simpler form.

5.3.3 LOCAL SCALING OF SIC (LSIC)

Though OSIC had some success in improving the performance with SIC, the approach leads to parameter k dependent performance. Also, it gives $-X_{HO}/r$ asymptotic potential instead of $-1/r$ for finite neutral systems and results in an inaccurate description of dissociation behavior [22]. In addition, many electron SIE and fractional-charge dissociation behavior of positively charged dimers reemerge with OSIC [119]. The recent LSIC method by Zope *et al*.[123] applies the SIC in a different way than OSIC [38] and PZSIC [4]. It retains desirable beneficial features of PZSIC. In LSIC, the SIC energy density is scaled down locally as follows,

$$E^{LSIC-DFA}[\rho_\uparrow, \rho_\downarrow] = E^{DFA}[\rho_\uparrow, \rho_\downarrow] - \Sigma_{i\sigma}^{occ}\{U^{LSIC}[\rho_{i\sigma}] + E_{XC}^{LSIC}[\rho_{i\sigma}, 0]\}, \tag{5.7}$$

where

$$U^{LSIC}[\rho_{i\sigma}] = \frac{1}{2}\int d\vec{r}\; z_\sigma^k(\vec{r})\rho_{i\sigma}(\vec{r}) \int d\vec{r}\,' \frac{\rho_{i\sigma}(\vec{r}\,')}{|\vec{r}-\vec{r}\,'|}, \tag{5.8}$$

$$E_{XC}^{LSIC}[\rho_{i\sigma}, 0] = \int d\vec{r}\; z_\sigma^k(\vec{r})\varepsilon_{XC}^{DFA}([\rho_{i\sigma}, 0], \vec{r}), \tag{5.9}$$

LSIC uses an iso-orbital indicator to apply SIC pointwise in space. An ideal choice of the iso-orbital indicator should be such that LSIC reduces to DFA in the uniform gas limit and reduces to PZSIC in the pure one-electron limit. To demonstrate the LSIC concept, Zope *et al*. [17] used $z_\sigma = \tau^W/\tau_\sigma$ as an iso-orbital indicator. In this study, however, we $w_{i\sigma}(\vec{r}) = \rho_{i\sigma}(\vec{r})/\rho_\sigma$ in place of z_σ in Eq. (5.8) and (5.9).

5.3.3 COMPUTATIONAL DETAILS

All calculations were performed using the developmental version of the FLOSIC code [107,124], a software based on the UTEP-NRLMOL code. The PZSIC, OSIC, and LSIC methods using FLOs are implemented in this code. For brevity, hereafter we will refer FLO-PZSIC, FLO-OSIC, and FLO-LSIC calculations as PZSIC, OSIC, and LSIC. The FLOSIC/NRLMOL code uses

Gaussian type orbitals [125]. We used the NRLMOL default basis sets throughout our calculations. For calculations of atomic anions, long range s, p, and d single Gaussian orbitals are added to give a better description of the extended nature of anions. The exponents β of these added single Gaussians were obtained using the relation $\beta(N\ +\ 1) = \beta(N)^2/\beta(N-1)$, where N is the N-th exponent. The FLOSIC code uses an adaptive integration mesh [126] that provides accurate numerical integration.

In this work, we use LSIC with the PW92 LSDA functional [127]. LSIC applied to LSDA is free from the gauge problem [123] unlike GGAs and meta-GGAs where a gauge transformation is needed since their XC potentials are not in the Hartree gauge. The geometries used in our calculations are the same as in the respective databases and no further optimizations were performed. We used the SCF energy convergence criteria of $10^6\ E_h$ for the total energy and an FOD force tolerance of $10^3 E_h$ per Bohr for FOD optimizations [105,128] in FLOSIC calculations. The self-consistency in the PZSIC calculations is obtained using Jacobi-like iterative procedure [129]. For OSIC and LSIC calculations, we used the respective PZSIC densities and FODs as a starting point and performed one-shot (non-self-consistent) calculation of energy on the PZSIC densities. The self-interaction correction effects are included in these densities at the PZSIC level. To assess the effect of self-consistency we have calculated the atomization energies, barrier heights, etc. by performing self-consistent OSIC(w) calculations. The results from the table show that mean absolute errors in total energies of atoms, atomization energies, and barrier heights in the OSIC($w, k = 1$) method changed only slightly ($0.1\ -\ 0.7 kcal\ mol^{-1}$) after selfconsistency. We expect similar differences in the LSIC method and therefore think that the present work provides the general picture of the performance of LSIC(w) method. The present results can alternatively be viewed as the performance of LSIC(w) energy functional in the spirit of density corrected DFT by Kim, Sim, and Burke [130]. Several values for the scaling power k are used in the LSIC(w) and OSIC(w) calculations. The additional computational cost of the scaling factor in OSIC and LSIC is small compared to standard PZSIC calculation.

5.4 RESULTS AND DISCUSSION

We assessed the performance of LSIC(w) vis-a`-vis LSIC(z) and OSIC(w) using the wide array of electronic properties. We consider total energies, ionization potentials, and electron affinities for atoms and atomization energies, reaction barrier heights and dissociation energies for molecules.

5.4.1 ATOMS

In this section, we present our results for total energies, ionization potentials, and electron affinities for atoms.

5.4.1.1 TOTAL ENERGY OF ATOMS

We compared the total atomic energies of the atoms $Z = 1 - 18$ against accurate non-relativistic values reported by Chakravorty *et al*. [131] Various integer values of k were used for LSIC(w) and OSIC(w). The differences between our calculated total energies with $k = 1$ and the reference values are plotted in Fig. 5.1. The plot clearly shows the effect of scaling on the total energies of atoms. Consistent with reported results, the LSDA total energies are too high compared to accurate reference values [131] whereas PZSIC consistently underestimates the total energies due to its over correcting tendency. The LSIC method, where both scaling factors perform similarly, provides the total energies closer to the reference values than LSDA and the PZSIC. Likewise, the OSIC method also reduces the overcorrection, bringing the total energies into close agreement with the reference values. The mean absolute errors (MAEs) in total energy with respect to the reference for various k values are shown in Table 5.1. The MAE of PZSIC is $0.381\ E_h$ whereas LSIC(w) and OSIC(w) show MAEs of 0.061 and $0.074\ E_h$, respectively, with $k = 1$. LSIC(z) shows a better performance than OSIC(w) and LSIC(w). The LSIC(w) MAE is in the same order of magnitude as the earlier reported MAE of LSIC(z) of $0.041\ E_h$ [17]. As the value of k increases, the magnitude of SI-correction is reduced. This results in MAEs become larger for $k > 1$ eventually approaching the LSDA numbers.

Table 5.1 Mean absolute error of the total atomic energy (in Eh) for atoms Z = 1–18 with respect to accurate nonrelativistic estimates [132].

Table 1 Mean absolute error of the total atomic energy (in E_h) for atoms Z = 1–18 with respect to accurate nonrelativistic estimates[132]

Method	MAE
PZSIC	0.381
LSIC(z,k = 1)	0.041
LSIC(w,k = 1)	0.061
LSIC(w,k = 2)	0.196
LSIC(w,k = 3)	0.277
LSIC(w,k = 4)	0.332
OSIC(w,k = 1)	0.074
OSIC(w,k = 2)	0.070
OSIC(w,k = 3)	0.135

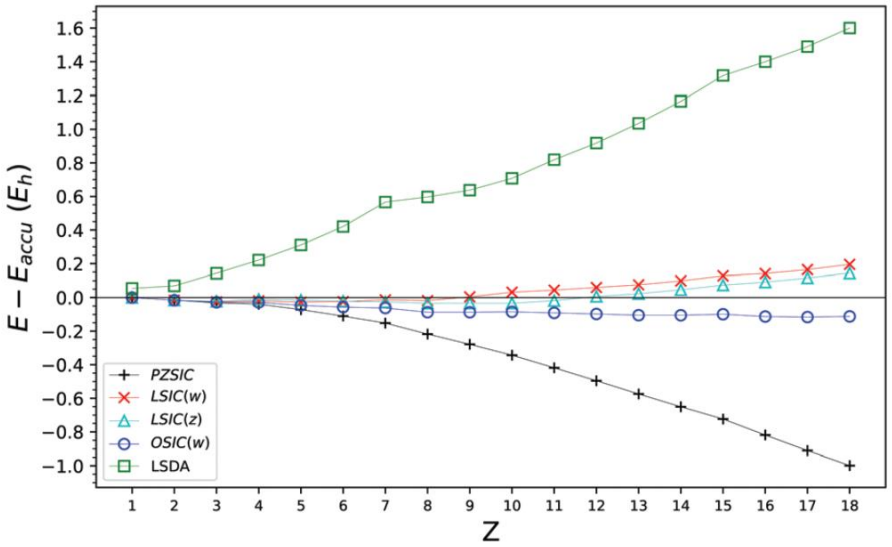

Fig. 5.1 Total energy difference (in E_h) of atoms $Z = 1-18$ with respect to accurate nonrelativistic estimates [131].

For $k = 0$ the scaled methods correctly produce the PZSIC results. The scaling is optimal for $k = 1$ which results in an optimal magnitude of SI-correction for LSIC(w) and an almost right magnitude for OSIC(w). The magnitude of the SIC energy of each orbital is compared among different methods. It is found that the SIC energy in LSIC(w) is larger (i.e. less scaling down) for the core orbitals than in LSIC(z). This trend is reversed for the valence orbitals (cf. Table 5.2). It can be seen from Table 5.2 that total SIC energy in both methods is essentially similar in magnitude. However, the way scaling factors behave affects the orbitalwise contribution to the total SIC energy. This changes the SIC potentials and results in the two methods performing differently for cations and anions. For OSIC(w), we find the smallest MAE for $k = 2$ of $0.070\ E_h$, a value slightly smaller than that for $k = 1$.

Table 5.2 Magnitude of SIC energy (in E_h) per orbital type in Ar atom for each method with $k = 1$.

Orbital	PZSIC	LSIC(z)	LSIC(w)	OSIC(w)
1s	−0.741	−0.387	−0.490	−0.584
$2sp^3$	−0.126	−0.070	−0.050	−0.062
$3sp^3$	−0.016	−0.017	−0.006	−0.008
Total SIC	−2.616	−1.473	−1.421	−1.729

5.4.1.2 IONIZATION POTENTIAL

The ionization potential (IP) is the energy required to remove an electron from the outermost orbital. Since electron removal energy is related to the asymptotic shape of the potential, one can expect SIC plays an important role in determining IPs. We calculated the IPs using the DSCF method defined as

$$E_{IP} = E_{cat} - E_{neut} \tag{5.10}$$

where E_{cat} is the total energy in the cationic state and E_{neut} is the total energy at the neutral state. The calculations were performed for atoms from helium to krypton, and we compared the computed IPs against experimental ionization energies [132]. FODs were relaxed both for neutral

atoms and for their cations. Fig. 5.2 shows the difference of calculated IPs with respect to the reference values. MAEs with different methods are shown in Table 5.3 for a subset $Z = 2 - 18$ as well as for the entire set $Z = 2 - 36$ to facilitate comparison against literature. For the smaller subset, $Z = 2 - 18$, the MAEs are 0.248 and 0.206 eV for PZSIC and LSIC(z), respectively. The MAE for OSIC($w, k = 1$) is 0.223 eV, showing an improvement over PZSIC. LSIC($w, k = 1$) shows MAE of 0.251 eV, a comparable error with PZSIC. MAEs increase for LSIC($w, k \geq 2$) and OSIC($w, k \geq 2$) in comparison to their respective $k = 1$ MAEs. Interestingly, however, when we considered the entire set of atoms ($Z = 2 - 36$), LSIC(w) has MAEs of 0.238 and 0.216 eV for $k = 1$ and $k = 2$ respectively showing smaller errors than PZSIC (MAE, 0.364 eV), but LSIC(w) falls short of LSIC(z) which has the smallest error (MAE, 0.170 eV). For this case, OSIC($w, k = 1 - 3$) shows better performance than PZSIC but not as well as LSIC(w) for a given k. LSIC(z) performs better than both LSIC(w) and OSIC(w). The difference in performance between LSIC(z) and LSIC(w) implies that scaling of SIC for the cationic states is more sensitive to the choice of a local scaling factor than for the neutral atoms.

Table 3 Mean absolute error of ionization potentials (in eV) for set of atoms $Z = 2 - 18$ and $Z = 2 - 36$ with respect to experiment [132].

Method	Z = 2–18 (17-IPs)	Z = 2–36 (35-IPs)
PZSIC	0.248	0.364
LSIC(z,k = 1)	0.206	0.170
LSIC(w,k = 1)	0.251	0.238
LSIC(w,k = 2)	0.271	0.216
LSIC(w,k = 3)	0.297	0.247
LSIC(w,k = 4)	0.324	0.284
OSIC(w,k = 1)	0.223	0.267
OSIC(w,k = 2)	0.247	0.247
OSIC(w,k = 3)	0.255	0.259

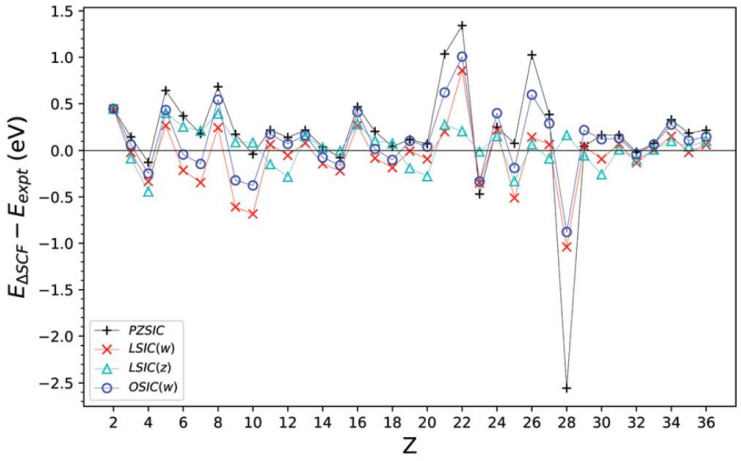

Fig. 2 Energy difference in ionization potential (in eV) for a set of atoms $Z = 2 - 36$ with respect to experimental values [132].

5.4.1.3 ELECTRON AFFINITY

The electron affinity (EA) is the energy released when an electron is added to the system. We studied EAs for 20 atoms that are experimentally found to bind an electron.133 They are H, Li, B, C, O, F, Na, Al, Si, P, S, Cl, K, Ti, Cu, Ga, Ge, As, Se, and Br atoms. The EAs were calculated using the DSCF method $E_{EA} = E_{neut} - E_{anion}$ and values were compared against the experimental EAs [133].

Fig. 5.3 shows the deviation of EA from reference experimental values for various methods. The MAEs are summarized in Table 5.4. We have presented the MAEs in two sets, the smaller subset which contains hydrogen through chlorine (12 EAs) and for the complete set, hydrogen to bromine (20 EAs).

Table 5.4 Mean absolute error in electron affinities (in eV) for 12 EAs and 20 EAs set of atoms with respect to experiment [133].

Method	(12 EAs) MAE	(20 EAs) MAE
PZSIC	0.152	0.190
LSIC(z,k = 1)	0.097	0.102
LSIC(w,k = 1)	0.235	0.224
LSIC(w,k = 2)	0.229	0.205
LSIC(w,k = 3)	0.215	0.189
LSIC(w,k = 4)	0.202	0.176
OSIC(w,k = 1)	0.152	0.172
OSIC(w,k = 2)	0.150	0.164
OSIC(w,k = 3)	0.145	0.155

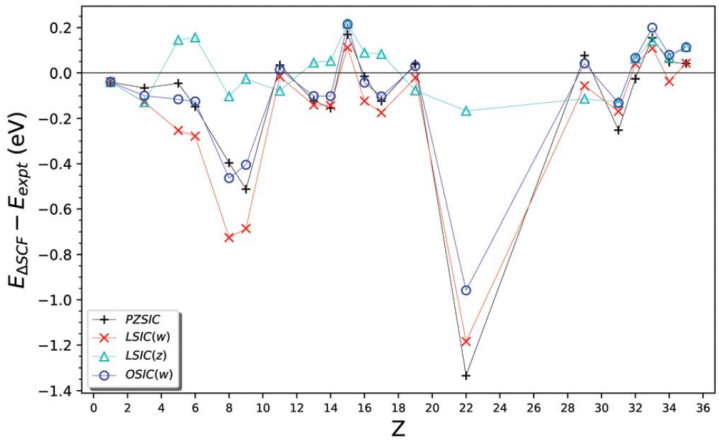

Fig. 5.3 Electron affinity (eV) difference for atoms $Z = 2 - 36$ with respect to experiment [133].

For 12 EAs, MAEs for PZSIC and LSIC(z) are 0.152 and 0.097 eV, respectively. OSIC(w) shows MAE of 0.152 eV for $k = 1$, the same performance as PZSIC. LSIC(w), however, does not perform as well as PZSIC, giving the MAEs of 0.235 eV for $k = 1$. In both cases, the error decreases slightly for $k \geq 2$ but there is no significant impact on their performance.

For 20 EAs, a similar trend persists. PZSIC and LSIC(z) have MAEs of 0.190 and 0.102 eV, respectively. The MAEs of LSIC(w) are in the range 0.176–0.224 eV for $k = 1 - 4$ and those of OSIC(w) are between 0.155-0.172 eV for $k = 1 - 3$. Again, a decrease in error is observed as k increases. In particular, a larger discrepancy between LSIC($w, k = 1$) and experiment is seen for O, F, and Ti atoms. This is due to LSIC(w) raising the anion energies more than their neutral state energies.

5.4.2 ATOMIZATION ENERGIES

To study the performance of LSIC(w) for molecules, first, we calculated the atomization energies (AEs) of 37 selected molecules. Many of these molecules are a subset of the G2/97 test set [134]. The 37 molecules include systems from the AE6 set [135], a small but good representative subset of the main group atomization energy (MGAE109) set [136]. The AEs were calculated by taking the energy difference of fragment atoms and the complex, that is, $AE = \sum_i^{N_{atom}} E_i - E_{mol}$. E_i is the total energy of an atom, E_{mol} is the total energy of the molecule and N_{atom} is the number of atoms in the molecule. The calculated AEs were compared to the non-spin–orbit coupling reference values [136] for the AE6 set and to experimental values [133] for the entire set of 37 molecules. The percentage errors obtained through various methods are shown in Fig. 5.4. The overestimation of AEs with PZSIC–LSDA due to overcorrection is rectified in LSIC(w). We have summarized MAEs and mean absolute percentage errors (MAPEs) of AE6 and 37 molecules from the G2 set in Table 5.5. For the AE6 set, MAEs for PZSIC, LSIC(z), LSIC($w, k = 1$), and OSIC($w, k = 1$) are 57.9, 9.9, 13.8, and 33.7 $kcal/mol$ respectively. The MAE in LSIC($w, k = 1$) is about 4 7 $kcal/mol$ larger than LSIC(z) but substantially better than the PZSICs or OSIC(w). For the larger k in LSIC(w), however, the performance starts to degrade with a consistent increase in the MAE of 33.5 7 $kcal/mol$ for $k = 4$. This is in contrast to OSIC where the performance improves for $k = 2$ and 3 compared to $k = 1$. The scaling thus differently affects the two methods. OSIC($w, k = 1$) tends to slightly underestimate total energies. By increasing k, total energies shift toward the LSDA total energies, and performance is improved for a moderate increase in k. On the contrary, total energies are slightly overestimated for LSIC($w, k = 1$), and increasing k makes the energies deviate away from the accurate estimates. OSIC($w, k = 3$) and LSIC($w, k = 1$) have a similar core orbital SIC energy. In their study of OSIC(w), Vydrov and Scuseria [16] used values of k up to 5 and found the smallest error of $k = 5$ (MAE, 11.5 $kcal/mol$). But we expect the OSIC performance to degrade eventually for large k since an increase in k results in an increase in quenching of the SIC, thus the results will eventually approach those of DFA, in this LSDA case. For the full set of 37 molecules, PZSIC, LSIC(z), LSIC($w, k = 1$), and OSIC($w, k = 1$) show the MAPEs of 13.4, 6.9, 9.5, and 11.9 %, respectively. OSIC(w) shows a slight improvement in MAPE for $k = 2$ and 3. For the larger set, LSIC(w)

consistently shows smaller MAPEs than OSIC(w) for $k = 1 - 3$. All four values of k with the LSIC(w) in this study showed better performance than PZSIC for the 37 molecules set.

Table 5.5 Mean absolute error (in $kcal/mol$) and mean absolute percentage error (in %) of atomization energy for AE6 set of molecules [136] and for the set of 37 molecules from G2 set with respect to experiment [133].

Method	AE6 MAE (kcal mol^{-1})	AE6 MAPE (%)	37 molecules MAPE (%)
PZSIC	57.9	9.4	13.4
LSIC(z,k = 1)	9.9	3.2	6.9
LSIC(w,k = 1)	13.8	3.9	9.5
LSIC(w,k = 2)	18.6	4.8	9.1
LSIC(w,k = 3)	26.9	5.8	9.2
LSIC(w,k = 4)	33.5	6.7	9.7
OSIC(w,k = 1)	33.7	6.3	11.9
OSIC(w,k = 2)	24.1	5.1	11.3
OSIC(w,k = 3)	17.8	4.3	10.9

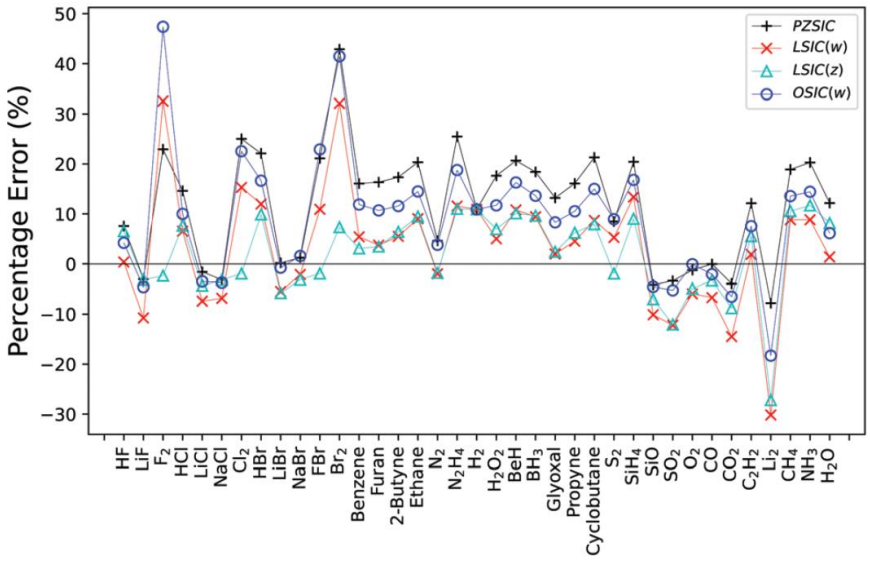

Fig. 5.4 Percentage errors of atomization energy (%) for a set of 37 molecules with respect to experimental values133 using different scaling methods.

5.4.3 BARRIER HEIGHTS

An accurate description of chemical reaction barriers is challenging for DFAs since it involves the calculation of energies in nonequilibrium situations. In most cases, the saddle point energies are underestimated since DFAs do not perform well for a nonequilibrium state that involves a stretched bond. This shortcoming of DFAs in a stretched bond case arises from SIE; when an electron is shared and stretched out, SIE incorrectly lowers the energy of transition states. SIC handles the stretched bond states accurately and provides a correct picture of chemical reaction paths. We studied the reaction barriers using the BH6 [135] set of molecules for the LSIC(w) method. BH6 is a representative subset of the larger BH24 [137] set consisting of three reactions $OH + CH4 \rightarrow CH3 + H2O$, $H + OH \rightarrow H_2 + O$, and $H + H_2S \rightarrow H_2 + HS$. We calculated the total energies of the left- and right-hand sides and at the saddle point of these chemical reactions.

The barrier heights for the forward (f) and reverse (r) reactions were obtained by taking the energy differences of their corresponding reaction states.

The mean errors (MEs) and MAEs of computed barrier heights are compared against the reference values [135] in Table 5.6. MAEs for PZSIC, LSIC(z), LSIC($w, k = 1$), and OSIC($w, k = 1$) are 4.8, 1.3, 3.6, and 3.6 $kcal/mol$, respectively. PZSIC significantly improves MAE compared to LSDA (MAE, 17.6 $kcal/mol$), LSIC($w, k = 1$) further reduces the error from PZSIC. Its ME and MAE indicate that there is no systematic underestimation or overestimation. LSIC($w, k = 1$) also further improves upon PZSIC, but not to the same extent as LSIC(z). For $k \geq 2$, MAEs increases systematically for LSIC($w, k \geq 2$) though small MEs are seen for LSIC($w, k = 2,3$). The performance deteriorates for $k > 2$ beyond that of PZSIC. OSIC(w) shows marginally better performance than PZSIC. Vydrov and Scuseria16 showed that the best performance is achieved with $k = 1$ (MAE, 3.5 $kcal/mol$). The performance improvement with OSIC is not as dramatic as that with LSIC where the rather large MEs are seen with OSIC. Overall LSIC(w) performs better than OSIC(w) for barrier heights.

Table 5.6 Mean error (in $kcal/mol$) and mean absolute error (in $kcal/mol$) of BH6 sets of chemical reactions [135].

Method	ME (kcal mol^{-1})	MAE (kcal mol^{-1})
PZSIC	−4.8	4.8
LSIC(z,k = 1)	0.7	1.3
LSIC(w,k = 1)	−1.0	3.6
LSIC(w,k = 2)	−0.1	4.6
LSIC(w,k = 3)	0.3	5.0
LSIC(w,k = 4)	0.6	5.5
OSIC(w,k = 1)	−3.4	3.6
OSIC(w,k = 2)	−3.1	4.1
OSIC(w,k = 3)	−3.0	4.6

5.4.4 DISSOCIATION AND REACTION ENERGIES

A pronounced manifestation of SIE is seen in the dissociation of positively charged dimers X_2^+. SIE causes the system to dissociate into two fractionally charged cations instead of X and X^+. Here we use the SIE4x4 [138] and SIE11 [139] sets to study the performance of LSIC(w) and OSIC(w) in correcting the SIEs. The SIE4x4 set consists of dissociation energy calculations of four positively charged dimers at varying bond distances R from their equilibrium distance R_e such that $R/R_e = 1.0$, 1.25, 1.5, and 1.75. The dissociation energy E_D is calculated as

$$E_D = E(X) + E(X^+) - E(X_2^+) \tag{5.11}$$

The SIE11 set consists of eleven reaction energy calculations: five cationic reactions and six neutral reactions. These two sets are commonly used for studying SIE related problems. The calculated dissociation and reaction energies are compared against the CCSD(T) reference values [138,139], and MAEs are summarized in Table 5.7. For the SIE4x4 set, PZSIC, LSIC(z), LSIC($w, k = 1$), and OSIC($w, k = 1$) show MAEs of 3.0, 2.6, 4.7, and 5.2 $kcal/mol$. LSIC(z) provides a small improvement in equilibrium energies while keeping the accurate behavior of PZSIC at the dissociation limit, resulting in marginally better performance. LSIC(w) shows errors a few $kcal/mol$ larger than PZSIC. This increase in error arises because LSIC(w) alters the $(NH_3)_2^+$ and $(H_2O)_2^+$ dissociation curves. In LSIC(z) the scaling of SIC occurs mostly for the core orbitals (cf. Table 5.2), whereas LSIC(w) also includes some noticeable scaling down effects from valence orbitals. This different scaling behavior seems to contribute to different dissociation curves. Lastly, OSIC(w) has a slightly larger error than LSIC(w).

For the SIE11 set, MAEs are 11.5, 4.5, 8.3, and 11.1 $kcal/mol$ for PZSIC, LSIC(z), LSIC($w, k = 1$), and OSIC($w, k = 1$), respectively All scaled-down approaches we considered, LSIC(z) and LSIC(w) and OSIC(w) showed a performance improvement over PZSIC. LSIC(z) shows the largest error reduction by 60%, while LSIC($w, k = 1$) shows 28% decrease in error with respect to PZSIC. OSIC(w) with $k = 1 - 3$ has slightly smaller MAEs within 1 $kcal/mol$ of PZSIC. The LSIC(z) method improves cationic reactions more than neutral reactions with respect to PZSIC. An increase in k beyond 2 results in over suppression of SIC and leads to an increase in error for

LSIC($w, k \geq 2$). LSIC(w) yielded consistently smaller MAEs than OSIC(w), but larger than LSIC(z) for all SIE11 reactions.

Table 5.7 Mean absolute error for dissociation and reaction energies (in $kcal/mol$) of SIE4x4 and SIE11 sets of chemical reactions with respect to CCSD(T) [138,139].

Reaction	SIE4x4	SIE11	SIE11 5 cationic	SIE11 6 neutral
PZSIC	3.0	11.5	14.9	8.7
LSIC(z)	2.6	4.5	2.3	6.3
LSIC(w) (k = 1)	4.7	8.3	8.6	8.0
LSIC(w) (k = 2)	5.5	8.3	8.3	8.3
LSIC(w) (k = 3)	5.8	8.8	8.2	9.3
LSIC(w) (k = 4)	5.9	9.3	8.2	10.2
OSIC(w) (k = 1)	5.2	11.1	13.7	9.0
OSIC(w) (k = 2)	6.0	11.0	13.5	9.0
OSIC(w) (k = 3)	6.4	10.9	13.3	8.8

Finally, we show the ground-state dissociation curves for H_2^+ and He_2^+ in Fig. 5.5. As previously discussed in literature [140]. DFAs at large separation cause the complexes to dissociate into two ionic fragments. PZSIC restores the correct dissociation behavior at large separations. When LSIC is applied, the behavior of PZSIC at the dissociation limit is preserved in both LSIC(z) and present LSIC(w). For H_2^+, a one-electron system, LSIC reproduces the identical behavior as PZSIC [Fig. 5.5(a)]. For He_2^+, a three-electron system, LSIC applies the correction to PZSIC only near-equilibrium regime [Fig. 5.5(b)]. LSIC brings the equilibrium energy qualitatively closer to the CCSD(T) energy compared to PZSIC. The implication of Fig. 5.5 is that the scaling factor w performs well in differentiating the single orbital-like regions and many-electron-like regions.

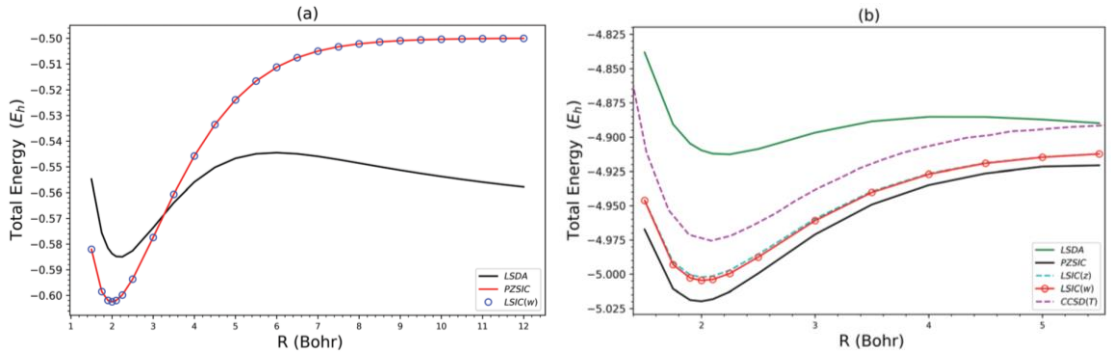

Fig. 5.5 Dissociation curves of (a) H_2^+ and (b) He_2^+ using various methods. The CCSD(T) curve from ref. 22 is plotted for comparison.

5.4.4 DISSOCIATION AND REACTION ENERGIES

Sharkas *et al*. [78] recently studied binding energies of small water clusters using the PZSIC method in conjunction with FLOs to examine the effect of SIC on the binding energies of these systems. Water clusters are bonded by weaker hydrogen bonds and provide a different class of systems to test the performance of the LSIC method. Earlier studies using LSIC(z) on the water clusters of their polarizabilities and IPs have shown that LSIC(z) provides excellent descriptions of these properties when compared to CCSD(T) results [67,141]. Here, we study the binding energies of the water clusters and find that the choice of iso-orbital indicator plays a critical role. The structures considered in this work are $(H_2O)_n$ $(n = 1 - 6)$ whose geometries are from the WATER27 set [142] optimized at the B3LYP/6-311++G(2d,2p) theory. The hexamer structure has a few known isomers, and we considered the book (b), cage (c), prism (p), and ring (r) isomers. The results are compared against the CCSD(T)-F12b values from ref. 143 in Table 5.8. We obtained the MAEs of 118.9, 172.1, and 46.9 meV per H_2O for PZSIC, LSIC(z), and LSIC(w), respectively. Thus, LSIC(z) underestimates binding energies of water clusters by a roughly similar magnitude as LSDA (MAE, 183.4 meV per H_2O). This is one of few cases where LSIC(z) does not improve over PZSIC. A simple explanation for this behavior of LSIC(z) is that although z_σ can detect the weak bond regions, it cannot differentiate the slow-varying density regions from weak bond regions. $z_\sigma \to 0$ in both situations, causing the weak bound regions to be improperly treated. Fig. 5.6(a) shows z_σ for the water dimer where both slow-varying density and weak interaction regions are detected but not differentiated. As a result, the total energies of the complex shift too much in comparison to the individual water molecules. Thus, the underestimation of water cluster binding energies is due to the choice of z and not necessarily of the LSIC method. Indeed, by choosing w as a scaling parameter, the binding energies are much improved. Fig. 5.6(b) shows that there is no discontinuity of w between the two water molecules (w_i's of two FLOs along the hydrogen bond are plotted together in the figure). Hence, unlike in LSIC(z), the weakly interacting region is not improperly scaled-down with LSIC(w). LSIC(w) shows an MAE of 46.9 meV per

H_2O, comparable to SCAN (MAE, 35.2 meV per H_2O). This result is interesting as SCAN uses a function that can identify weak bond interaction. So LSIC(w)–LSDA may be behaving qualitatively similar to the detection function in SCAN in weak bond regions. The study of water cluster binding energies is one of few cases where the original LSIC(z) performed poorly. A recent study by Bhattarai et al. [144] examined the performance of LSIC(z) for interaction energies of noncovalently bonded complexes from the S22 data set and found that LSIC(z) performed poorly for the interaction energies of the weakly bonded complexes. A full understanding of how well LSIC performs for the binding energies of such complexes would require full self-consistency. The LSIC method may be improved by using a different iso-orbital indicator. These cases serve as motivation for identifying an appropriate iso-orbital indicator that would work for all bonding regions in LSIC.

Table 5.8 The binding energy of water clusters (in meV per H_2O)

n	PZSIC	LSIC(z)	LSIC(w)	CCSD(T)[a]
2	−153.7	−34.9	−82.7	−108.6
3	−321.6	−73.9	−183.0	−228.4
4	−425.2	−125.0	−248.6	−297.0
5	−446.9	−142.7	−264.8	−311.4
6b	−467.1	−133.6	−275.0	−327.3
6c	−466.8	−113.9	−274.8	−330.5
6p	−467.7	−104.8	−276.2	−332.4
6r	−458.1	−150.5	−275.5	−320.1
MAE	118.9	172.1	46.9	

[a] Ref. 143.

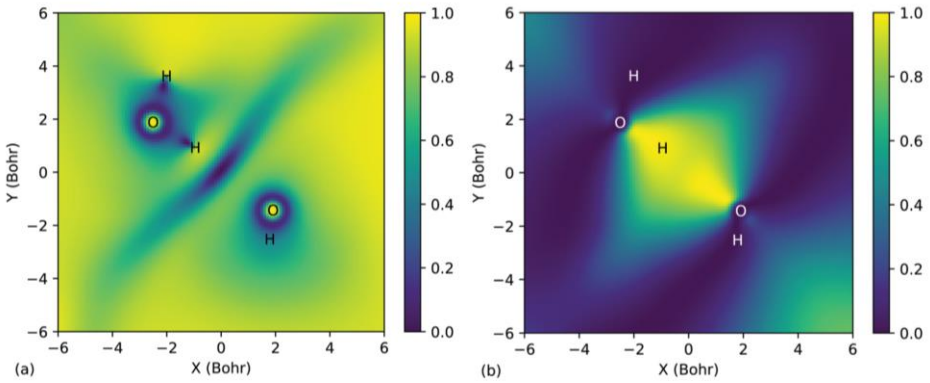

Fig. 5.6 Cross sectional plots of the iso-orbital indicators for water cluster dimer: (a) τ^W/τ and (b) ρ_i/ρ's from the two FLOs along the hydrogen bond.

We now provide a qualitative explanation of why LSIC(w) gives improved results over PZSIC. This reasoning is along the same line as offered by Zope et al [17]. As mentioned in section 5.2, when SIE is removed using PZSIC, an improved description of barrier heights which involve stretched bonds is obtained, but the equilibrium properties like total energies, atomization energies, etc. are usually deteriorated compared to the uncorrected functional. This is especially so for the functionals that go beyond the simple LSDA. Typically this is because of the overcorrecting tendency of PZSIC. The non-empirical semilocal DFAs are designed to be exact in the uniform electron gas limit, this exact condition is no longer satisfied when PZSIC is applied to the functionals [145]. This can be seen from the exchange energies of noble gas atoms and the extrapolation using the large-Z expansion of E_X as shown in Fig. 5.7. Following Ref. 145, we plot atomic exchange energies as a function of $Z^{-1/3}$. Thus, the region near the origin corresponds to the uniform gas limit. The plot was obtained by fitting the exchange energies (E_X) of Ne, Ar, Kr, and Xe atoms (within LSIC(w)–LSDA, LSIC(z)–LSDA, and LSDA) to the curve using the following fitting function [145].

$$\frac{E_X^{approx} - E_X^{exact}}{E_X^{exact}} * 100\% = a + bx^2 + cx^3, \tag{5.12}$$

where $x = Z^{-1/3}$ and a, b, and c are the fitting parameters. The LSDA is exact in the uniform gas limit. So also is LSIC(z) since the scaling factor z_σ approaches zero as the gradient of electron

density vanishes while the kinetic energy density in the denominator remains finite. The small deviation from zero seen near the origin (in Fig. 5.7) for LSIC(z) is due to the fitting error (due to limited data point). This error is 0.62% for LSIC(z). Thus, correcting LSDA using PZSIC introduces a large error in the uniform gas limit. The scaling factor w used here identifies single-electron regions since the density ratio approaches one in this limit. Fig. 5.7 shows that LSIC(w) also recovers the lost uniform gas limit. This partly explains the success of LSIC(w). Though the performance of LSIC(w) is substantially better than PZSIC–LSDA, it falls short of LSIC(z). On the other hand, unlike LSIC(z) it provides a good description of weak hydrogen bonds highlighting the need to identify suitable iso-orbital indicators or scaling factor(s) to apply pointwise SIC using the LSIC method. One possible choice may be scaling factors that are functions of a used in the construction of SCAN meta-GGA and the recently proposed [146] β parameter. A scaling factor containing β recently used by Yamamoto and coworkers with the OSIC scheme showed improved results [112]. Future work would involve designing suitable scaling factors involving β for use in the LSIC method.

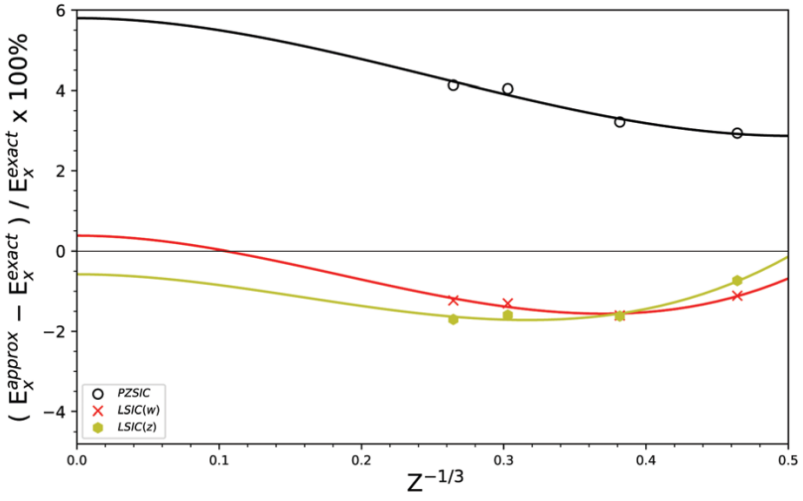

Fig. 5.7 Plot of percentage error of the approximated exchange energy compared to the exact exchange energy as a function of $Z^{-1/3}$.

5.5 CONCLUSION

To recapitulate, we investigated the performance of LSIC with a simple scaling factor, w, that depends only on orbital and spin densities. Performance assessment has been carried out on atomic energies, atomization energies, ionization potentials, electron affinities, barrier heights, dissociation energies, and binding energies on standard data sets of molecules. The results show that LSIC(w) performs better than PZSIC for all properties with exception of electron affinity and a SIE4x4 subset of dissociation energies. We also compared the performance of LSIC(w) against the OSIC method of Vydrov *et al*. Results indicate that although OSIC overall performs better than PZSIC, the improvement over PZSIC is somewhat limited. On the other hand, LSIC(w) is consistently better than OSIC(w). We have also studied the binding energies of small water clusters which are bonded by weak hydrogen bonds. Here, LSIC(w) performs very well compared to both PZSIC and LSIC(z), with performance comparable to SCAN. The present work shows the promise of the LSIC method and also demonstrates its limitation in describing weak hydrogen bonds if used with kinetic energy density ratio, z_σ, as an iso-orbital indicator. This limitation is due to the inability of zs to distinguish weak bonding regions from slowly varying density regions. The scaling factor w works differently than the scaling factor z, hence LSIC(w) provides a good description of weak hydrogen bonds in water clusters. The work thus highlights the importance of designing suitable iso-orbital indicators for use with LSIC that can detect weak bonding regions.

5.6 DATA AVAILABILITY

The data that supports the findings of this study are available within the article and the ESI.

5.7 CONFLICT OF INTEREST

There are no conflicts of interest to declare.

5.8 AKNOWLEDGMENTS

Authors acknowledge Drs Luis Basurto, Carlos Diaz, Jorge Vargas, and Po-Hao Chang for discussions and technical supports. Authors also acknowledge Mr Zachary Buschmann for proof-reading the manuscript. This work was supported by the US Department of Energy, Office of Science, Office of Basic Energy Sciences, as part of the Computational Chemical Sciences Program under Award No. DE-SC0018331. Support for the computational time at the Texas Advanced Computing Center through NSF Grant No. TG-DMR090071, and at NERSC is gratefully acknowledged.

5.9 REFERENCES

[1] W. Kohn and L. Sham, Phys. Rev., 1965, 140, A1133–A1138.

[2] R. O. Jones, Rev. Mod. Phys., 2015, 87, 897.

[3] R. O. Jones and O. Gunnarsson, Rev. Mod. Phys., 1989, 61, 689–746.

[4] J. P. Perdew and A. Zunger, Phys. Rev. B: Condens. Matter Mater. Phys., 1981, 23, 5048–5079.

[5] J. P. Perdew and K. Schmidt, AIP Conf. Proc., 2001, 577, 1–20.

[6] E. R. Johnson, P. Mori-Sánchez, A. J. Cohen and W. Yang, J. Chem. Phys., 2008, 129, 204112.

[7] E. R. Johnson, A. Otero-de-la Roza and S. G. Dale, J. Chem. Phys., 2013, 139, 184116.

[8] J. Gräfenstein, E. Kraka and D. Cremer, J. Chem. Phys., 2004, 120, 524–539.

[9] I. Lindgren, J. Quantum Chem., 1971, 5, 411–420.

[10] M. S. Gopinathan, Phys. Rev. A: At., Mol., Opt. Phys., 1977, 15, 2135–2142.

[11] J. P. Perdew, R. G. Parr, M. Levy and J. L. Balduz Jr, Phys. Rev. Lett., 1982, 49, 1691.

[12] U. Lundin and O. Eriksson, J. Quantum Chem., 2001, 81, 247–252.

[13] P. Mori-Sánchez, A. J. Cohen and W. Yang, J. Chem. Phys., 2006, 125, 201102.

[14] N. I. Gidopoulos and N. N. Lathiotakis, J. Chem. Phys., 2012, 136, 224109.

[15] T. Tsuneda, M. Kamiya and K. Hirao, J. Comput. Chem., 2003, 24, 1592–1598.

[16] O. A. Vydrov and G. E. Scuseria, J. Chem. Phys., 2006, 124, 191101.

[17] R. R. Zope, Y. Yamamoto, C. M. Diaz, T. Baruah, J. E. Peralta, K. A. Jackson, B. Santra and J. P. Perdew, J. Chem. Phys., 2019, 151, 214108.
[18] D.-K. Seo, Phys. Rev. B: Condens. Matter Mater. Phys., 2007, 76, 033102.
[19] G. Borghi, C.-H. Park, N. L. Nguyen, A. Ferretti and N. Marzari, Phys. Rev. B: Condens. Matter Mater. Phys., 2015, 91, 155112.
[20] T. Tsuneda and K. Hirao, J. Chem. Phys., 2014, 140, 18A513.
[21] J. C. Slater, Phys. Rev., 1951, 81, 385.
[22] A. Ruzsinszky, J. P. Perdew, G. I. Csonka, O. A. Vydrov and G. E. Scuseria, J. Chem. Phys., 2007, 126, 104102.
[23] M. R. Pederson, R. A. Heaton and C. C. Lin, J. Chem. Phys., 1985, 82, 2688–2699.
[24] J. G. Harrison, R. A. Heaton and C. C. Lin, J. Phys. B: At. Mol. Phys., 1983, 16, 2079–2091.
[25] M. R. Pederson, R. A. Heaton and C. C. Lin, J. Chem. Phys., 1984, 80, 1972–1975.
[26] J. Garza, J. A. Nichols and D. A. Dixon, J. Chem. Phys., 2000, 112, 7880–7890.
[27] J. Garza, R. Vargas, J. A. Nichols and D. A. Dixon, J. Chem. Phys., 2001, 114, 639–651.
[28] S. Patchkovskii, J. Autschbach and T. Ziegler, J. Chem. Phys., 2001, 115, 26–42.
[29] M. K. Harbola, Solid State Commun., 1996, 98, 629–632.

[30] S. Patchkovskii and T. Ziegler, J. Chem. Phys., 2002, 116, 7806–7813.
[31] S. Patchkovskii and T. Ziegler, J. Phys. Chem. A, 2002, 106, 1088–1099.
[32] S. Goedecker and C. J. Umrigar, Phys. Rev. A, 1997, 55, 1765–1771.
[33] V. Polo, E. Kraka and D. Cremer, Mol. Phys., 2002, 100,1771–1790.
[34] V. Polo, J. Gräfenstein, E. Kraka and D. Cremer, Theor. Chem. Acc., 2003, 109, 22–35.
[35] J. Gra ¨fenstein, E. Kraka and D. Cremer, Phys. Chem. Chem. Phys., 2004, 6, 1096–1112.
[36] O. A. Vydrov and G. E. Scuseria, J. Chem. Phys., 2004, 121, 8187–8193.
[37] O. A. Vydrov and G. E. Scuseria, J. Chem. Phys., 2005, 122, 184107.
[38] O. A. Vydrov, G. E. Scuseria, J. P. Perdew, A. Ruzsinszky and G. I. Csonka, J. Chem. Phys., 2006, 124, 094108.
[39] J. Chen, J. B. Krieger, Y. Li and G. J. Iafrate, Phys. Rev. A, 1996, 54, 3939–3947.
[40] R. R. Zope, M. K. Harbola and R. K. Pathak, Eur. Phys. J. D, 1999, 7, 151–155.
[41] R. R. Zope, Phys. Rev. A: At., Mol., Opt. Phys., 2000, 62, 064501.
[42] E. S. Fois, J. I. Penman and P. A. Madden, J. Chem. Phys., 1993, 98, 6352–6360.

[43] J. B. Krieger, Y. Li and G. J. Iafrate, Phys. Rev. A, 1992, 45, 101–126.
[44] J. B. Krieger, Y. Li and G. J. Iafrate, Phys. Rev. A, 1992, 46, 5453–5458.
[45] Y. Li, J. B. Krieger and G. J. Iafrate, Phys. Rev. A, 1993, 47, 165–181.
[46] S. Lehtola, M. Head-Gordon and H. Jónsson, J. Chem. Theory Comput., 2016, 12, 3195–3207.
[47] G. I. Csonka and B. G. Johnson, Theor. Chem. Acc., 1998, 99, 158–165.
[48] L. Petit, A. Svane, M. Lüders, Z. Szotek, G. Vaitheeswaran, V. Kanchana and W. Temmerman, J. Phys.: Condens. Matter, 2014, 26, 274213.
[49] S. Kümmel and L. Kronik, Rev. Mod. Phys., 2008, 80, 3.
[50] T. Schmidt, E. Kraisler, L. Kronik and S. Kümmel, Phys. Chem. Chem. Phys., 2014, 16, 14357–14367.
[51] D.-y. Kao, M. Pederson, T. Hahn, T. Baruah, S. Liebing and J. Kortus, Magnetochemistry, 2017, 3, 31.
[52] S. Schwalbe, T. Hahn, S. Liebing, K. Trepte and J. Kortus, J. Comput. Chem., 2018, 39, 2463–2471.
[53] H. Jónsson, K. Tsemekhman and E. J. Bylaska, Abstracts of Papers of the American Chemical Society, 2007, pp. 120–120.
[54] M. M. Rieger and P. Vogl, Phys. Rev. B: Condens. Matter Mater. Phys., 1995, 52, 16567–16574.
[55] W. Temmerman, A. Svane, Z. Szotek, H. Winter and S. Beiden, Electronic Structure and Physical Properies of Solids, Springer, 1999, pp. 286–312.
[56] M. Daene, M. Lueders, A. Ernst, D. Ködderitzsch, W. M. Temmerman, Z. Szotek and W. Hergert, J. Phys.: Condens. Matter, 2009, 21, 045604.
[57] Z. Szotek, W. Temmerman and H. Winter, Phys. B, 1991, 172, 19–25.
[58] J. Messud, P. M. Dinh, P.-G. Reinhard and E. Suraud, Phys. Rev. Lett., 2008, 101, 096404.
[59] J. Messud, P. M. Dinh, P.-G. Reinhard and E. Suraud, Chem. Phys. Lett., 2008, 461, 316–320.
[60] M. Lundberg and P. E. M. Siegbahn, J. Chem. Phys., 2005, 122, 224103.
[61] C. D. Pemmaraju, T. Archer, D. Sa ´nchez-Portal and S. Sanvito, Phys. Rev. B: Condens. Matter Mater. Phys., 2007, 75, 045101.

[62] T. Körzdörfer, M. Mundt and S. Kümmel, Phys. Rev. Lett., 2008, 100, 133004.
[63] T. Körzdörfer, S. Kümmel and M. Mundt, J. Chem. Phys., 2008, 129, 014110.
[64] I. Ciofini, C. Adamo and H. Chermette, Chem. Phys., 2005, 309, 67–76.
[65] T. Baruah, R. R. Zope, A. Kshirsagar and R. K. Pathak, Phys. Rev. A, 1994, 50, 2191–2196.
[66] A. I. Johnson, K. P. K. Withanage, K. Sharkas, Y. Yamamoto, T. Baruah, R. R. Zope, J. E. Peralta and K. A. Jackson, J. Chem. Phys., 2019, 151, 174106.
[67] J. Vargas, P. Ufondu, T. Baruah, Y. Yamamoto, K. A. Jackson and R. R. Zope, Phys. Chem. Chem. Phys., 2020, 22, 3789–3799.
[68] N. Poilvert, G. Borghi, N. L. Nguyen, N. D. Keilbart, K. Wang and I. Dabo, Advances in Atomic, Molecular, and Optical Physics, Elsevier, 2015, vol. 64, pp. 105–127.
[69] K. Trepte, S. Schwalbe, T. Hahn, J. Kortus, D.-Y. Kao, Y. Yamamoto, T. Baruah, R. R. Zope, K. P. K. Withanage, J. E. Peralta and K. A. Jackson, J. Comput. Chem., 2019, 40, 820–825.
[70] K. P. K. Withanage, K. Trepte, J. E. Peralta, T. Baruah, R. Zope and K. A. Jackson, J. Chem. Theory Comput., 2018, 14, 4122–4128.
[71] S. Lehtola and H. Jo ´nsson, J. Chem. Theory Comput., 2014, 10, 5324–5337.
[72] M. R. Pederson, T. Baruah, D.-y. Kao and L. Basurto, J. Chem. Phys., 2016, 144, 164117.
[73] S. Schwalbe, L. Fiedler, T. Hahn, K. Trepte, J. Kraus and J. Kortus, PyFLOSIC – Python based Fermi–Lo¨wdin orbital self-interaction correction, 2019.
[74] D.-y. Kao, K. Withanage, T. Hahn, J. Batool, J. Kortus and K. Jackson, J. Chem. Phys., 2017, 147, 164107.
[75] R. P. Joshi, K. Trepte, K. P. K. Withanage, K. Sharkas, Y. Yamamoto, L. Basurto, R. R. Zope, T. Baruah, K. A. Jackson and J. E. Peralta, J. Chem. Phys., 2018, 149, 164101.
[76] K. Sharkas, L. Li, K. Trepte, K. P. K. Withanage, R. P. Joshi, R. R. Zope, T. Baruah, J. K. Johnson, K. A. Jackson and J. E. Peralta, J. Phys. Chem. A, 2018, 122, 9307–9315.
[77] K. A. Jackson, J. E. Peralta, R. P. Joshi, K. P. Withanage, K. Trepte, K. Sharkas and A. I. Johnson, J. Phys.: Conf. Ser., 2019, 1290, 012002.
[78] K. Sharkas, K. Wagle, B. Santra, S. Akter, R. R. Zope, T. Baruah, K. A. Jackson, J. P. Perdew and J. E. Peralta, Proc. Natl. Acad. Sci. U. S. A., 2020, 117, 11283–11288.
[79] H. Gudmundsdóttir, E. O. Jónsson and H. Jónsson, New J. Phys., 2015, 17, 083006.
[80] R. A. Heaton, J. G. Harrison and C. C. Lin, Phys. Rev. B: Condens. Matter Mater. Phys., 1983, 28, 5992–6007.

[81] R. A. Heaton and C. C. Lin, J. Phys. C: Solid State Phys., 1984, 17, 1853–1866.

[82] A. Svane and O. Gunnarsson, Europhys. Lett., 1988, 7, 171–175.

[83] A. Svane and O. Gunnarsson, Phys. Rev. B: Condens. Matter Mater. Phys., 1988, 37, 9919–9922.

[84] S. C. Erwin and C. C. Lin, J. Phys. C: Solid State Phys., 1988, 21, 4285–4309.

[85] Z. Szotek, W. Temmerman and H. Winter, Solid State Commun., 1990, 74, 1031–1033.

[86] Z. Szotek, W. Temmerman and H. Winter, Phys. B, 1990, 165–166, 275–276.

[87] A. Svane and O. Gunnarsson, Phys. Rev. Lett., 1990, 65, 1148–1151.

[88] A. Svane, Phys. Rev. Lett., 1992, 68, 1900–1903.

[89] D. Vogel, P. Krüger and J. Pollmann, Phys. Rev. B: Condens. Matter Mater. Phys., 1995, 52, R14316–R14319.

[90] M. Arai and T. Fujiwara, Phys. Rev. B: Condens. Matter Mater. Phys., 1995, 51, 1477–1489.

[91] D. Vogel, P. Krüger and J. Pollmann, Phys. Rev. B: Condens. Matter Mater. Phys., 1996, 54, 5495–5511.

[92] A. Svane, Phys. Rev. B: Condens. Matter Mater. Phys., 1996, 53, 4275–4286.

[93] A. Svane, W. M. Temmerman, Z. Szotek, J. Lægsgaard and H. Winter, Int. J. Quantum Chem., 2000, 77, 799–813.

[94] A. Filippetti and N. A. Spaldin, Phys. Rev. B: Condens. Matter Mater. Phys., 2003, 67, 125109.

[95] E. Bylaska, K. Tsemekhman and H. Jonsson, APS March Meeting Abstracts, 2004.

[96] M. Lüders, A. Ernst, M. Däne, Z. Szotek, A. Svane, D. Ködderitzsch, W. Hergert, B. L. Györffy and

W. M. Temmerman, Phys. Rev. B: Condens. Matter Mater. Phys., 2005, 71, 205109.

[97] E. J. Bylaska, K. Tsemekhman and F. Gao, Phys. Scr., 2006, T124, 86–90.

[98] B. Hourahine, S. Sanna, B. Aradi, C. Ko¨hler, T. Niehaus and T. Frauenheim, J. Phys. Chem. A, 2007, 111, 5671–5677.

[99] M. Stengel and N. A. Spaldin, Phys. Rev. B: Condens. Matter Mater. Phys., 2008, 77, 155106.

[100] M. Da ¨ne, M. Lüders, A. Ernst, D. Ködderitzsch, W. M. Temmerman, Z. Szotek and W. Hergert, J. Phys.: Condens. Matter, 2009, 21, 045604.

[101] N. L. Nguyen, N. Colonna, A. Ferretti and N. Marzari, Phys. Rev. X, 2018, 8, 021051.

[102] W. L. Luken and D. N. Beratan, Theor. Chem. Acc., 1982, 61, 265–281.

[103] W. L. Luken and J. C. Culberson, Theor. Chem. Acc., 1984, 66, 279–293.
[104] M. R. Pederson, A. Ruzsinszky and J. P. Perdew, J. Chem. Phys., 2014, 140, 121103.
[105] M. R. Pederson and T. Baruah, in Advances In Atomic, Molecular, and Optical Physics, ed. E. Arimondo, C. C. Lin and S. F. Yelin, Academic Press, 2015, vol. 64, pp. 153–180.
[106] R. P. Joshi, J. J. Phillips and J. E. Peralta, J. Chem. Theory Comput., 2016, 12, 1728–1734.
[107] R. R. Zope, T. Baruah and K. A. Jackson, FLOSIC 0.2, https://http://flosic.org/, based on the NRLMOL code of M. R. Pederson.
[108] K. P. K. Withanage, S. Akter, C. Shahi, R. P. Joshi, C. Diaz, Y. Yamamoto, R. Zope, T. Baruah, J. P. Perdew, J. E. Peralta and K. A. Jackson, Phys. Rev. A, 2019, 100, 012505.
[109] C. Shahi, P. Bhattarai, K. Wagle, B. Santra, S. Schwalbe, T. Hahn, J. Kortus, K. A. Jackson, J. E. Peralta, K. Trepte, S. Lehtola, N. K. Nepal, H. Myneni, B. Neupane, S. Adhikari, A. Ruzsinszky, Y. Yamamoto, T. Baruah, R. R. Zope and J. P. Perdew, J. Chem. Phys., 2019, 150, 174102.
[110] Y. Yamamoto, C. M. Diaz, L. Basurto, K. A. Jackson, T. Baruah and R. R. Zope, J. Chem. Phys., 2019, 151, 154105.
[111] M. R. Pederson and T. Baruah, unpublished.
[112] Y. Yamamoto, S. Romero, T. Baruah and R. R. Zope, J. Chem. Phys., 2020, 152, 174112.
[113] S. Schwalbe, L. Fiedler, J. Kraus, J. Kortus, K. Trepte and S. Lehtola, J. Chem. Phys., 2020, 153, 084104.
[114] S. Klüpfel, P. Klüpfel and H. Jónsson, J. Chem. Phys., 2012, 137, 124102.
[115] S. Klüpfel, P. Klüpfel and H. Jónsson, Phys. Rev. A, 2011, 84, 050501.
[116] E. O¨. Jónsson, S. Lehtola and H. Jónsson, Proc. Comput. Sci., 2015, 51, 1858–1864.
[117] S. Lehtola, E. O¨. Jónsson and H. Jónsson, J. Chem. Theory Comput., 2016, 12, 4296–4302.
[118] J. P. Perdew, A. Ruzsinszky, J. Sun and M. R. Pederson, Advances In Atomic, Molecular, and Optical Physics, Academic Press, 2015, vol. 64, pp. 1–14.
[119] A. Ruzsinszky, J. P. Perdew, G. I. Csonka, O. A. Vydrov and G. E. Scuseria, J. Chem. Phys., 2006, 125, 194112.
[120] J. Jaramillo, G. E. Scuseria and M. Ernzerhof, J. Chem. Phys., 2003, 118, 1068–1073.
[121] T. Schmidt, E. Kraisler, A. Makmal, L. Kronik and S. Kummel, J. Chem. Phys., 2014, 140, 18A510.
[122] J. C. Slater and J. H. Wood, Int. J. Quantum Chem., 1970, 5, 3–34.

[123] P. Bhattarai, K. Wagle, C. Shahi, Y. Yamamoto, S. Romero, B. Santra, R. R. Zope, J. E. Peralta, K. A. Jackson and
J. P. Perdew, J. Chem. Phys., 2020, 152, 214109.
[124] Y. Yamamoto, L. Basurto, C. M. Diaz, R. R. Zope and T. Baruah, Self-interaction correction to density functional
approximations using Fermi–Löwdin orbitals: methodology and parallelization, unpublished.
[125] D. Porezag and M. R. Pederson, Phys. Rev. A, 1999, 60, 2840–2847.
[126] M. R. Pederson and K. A. Jackson, Phys. Rev. B: Condens. Matter Mater. Phys., 1990, 41, 7453–7461.
[127] J. P. Perdew, J. A. Chevary, S. H. Vosko, K. A. Jackson, M. R. Pederson, D. J. Singh and C. Fiolhais, Phys. Rev. B: Condens. Matter Mater. Phys., 1992, 46, 6671–6687.
[128] M. R. Pederson, J. Chem. Phys., 2015, 142, 064112.
[129] Z.-h. Yang, M. R. Pederson and J. P. Perdew, Phys. Rev. A, 2017, 95, 052505.
[130] M.-C. Kim, E. Sim and K. Burke, Phys. Rev. Lett., 2013, 111, 073003.
[131] S. J. Chakravorty, S. R. Gwaltney, E. R. Davidson, F. A. Parpia and C. F. p Fischer, Phys. Rev. A, 1993, 47, 3649–3670.
[132] A. Kramida, Yu. Ralchenko, J. Reader and NIST ASD Team, NIST Atomic Spectra Database (ver. 5.6.1), [Online]. Available: https://physics.nist.gov/asd [2018, July 25]. National Institute of Standards and Technology, Gaithersburg, MD,
2018.
[133] National Institute of Standards and Technology, NIST Computational Chemistry Comparison and Benchmark
Database NIST Standard Reference Database Number 101 Release 19, April 2018, Editor: Russell D. Johnson III, http://cccbdb.nist.gov/, DOI: 10.18434/T47C7Z.
[134] L. A. Curtiss, K. Raghavachari, G. W. Trucks and J. A. Pople, J. Chem. Phys., 1991, 94, 7221–7230.
[135] B. J. Lynch and D. G. Truhlar, J. Phys. Chem. A, 2003, 107, 8996–8999.
[136] R. Peverati and D. G. Truhlar, J. Chem. Phys., 2011, 135, 191102.
[137] J. Zheng, Y. Zhao and D. G. Truhlar, J. Chem. Theory Comput., 2007, 3, 569–582.
[138] L. Goerigk, A. Hansen, C. Bauer, S. Ehrlich, A. Najibi and S. Grimme, Phys. Chem. Chem. Phys., 2017, 19, 32184–32215.

[139] L. Goerigk and S. Grimme, J. Chem. Theory Comput., 2010, 6, 107–126.
[140] A. Ruzsinszky, J. P. Perdew and G. I. Csonka, J. Phys. Chem. A, 2005, 109, 11006–11014.
[141] S. Akter, Y. Yamamoto, C. M. Diaz, K. A. Jackson, R. R. Zope and T. Baruah, J. Chem. Phys., 2020, 153, 164304.
[142] V. S. Bryantsev, M. S. Diallo, A. C. T. van Duin and W. A. Goddard, J. Chem. Theory Comput., 2009, 5, 1016–1026.
[143] D. Manna, M. K. Kesharwani, N. Sylvetsky and J. M. L. Martin, J. Chem. Theory Comput., 2017, 13, 3136–3152.
[144] P. Bhattarai, B. Santra, K. Wagle, Y. Yamamoto, R. R. Zope, K. A. Jackson and J. P. Perdew, unpublished.
[145] B. Santra and J. P. Perdew, J. Chem. Phys., 2019, 150, 174106.
[146] J. W. Furness and J. Sun, Phys. Rev. B, 2019, 99, 041119.

APPENDIX

LIST OF PUBLICATIONS

1. "Local self-interaction correction method with a simple scaling factor", **Selim Romero**, Yoh Yamamoto, Tunna Baruah and Rajendra Zope, Phys. Chem. Chem. Phys. 23, 2406 (2021), DOI: https://doi.org/10.1039/D0CP06282K
2. "Complexity reduction for more efficient Fermi-Löwdin Self-interaction-correction calculations", **Selim Romero**, Yoh Yamamoto, Tunna Baruah, Rajendra Zope [in submission to Journal of Chemical Physics (JCP)]
3. "Spin-state gaps and self-interaction-corrected density functional approximations: Octahedral Fe(II) complexes as case study", **Selim Romero**, Tunna Baruah and Rajendra Zope, *J. Chem. Phys.* 158, 054305 (2023), https://doi.org/10.1063/5.0133999
4. "Improvements in the orbitalwise scaling down of Perdew–Zunger self-interaction correction in many-electron regions", Yoh Yamamoto, **Selim Romero**, Tunna Baruah and Rajendra R. Zope, J. Chem. Phys. 152, 174112 (2020), DOI: https://doi.org/10.1063/5.0004738
5. "Assessing self-interaction errors in NOx reactions in zeolites using the FLOSIC method", Priyanka Shukla, **Selim Romero**, et al [manuscript in preparation]
6. "A Step in the Direction of Resolving the Paradox of Perdew-Zunger Self-interaction Correction. II. Gauge Consistency of the Energy Density at Three Levels of Approximation", Puskar Bhattarai, Kamal Wagle, Chandra Shahi, Yoh Yamamoto, **Selim Romero**, Biswajit Santra, Rajendra R. Zope, Juan E. Peralta, Koblar A. Jackson, and John P. Perdew, J. Chem. Phys. 152, 214109 (2020); https://doi.org/10.1063/5.0010375 [not included in the thesis]
7. "A GEANT4 Study of a Gamma-ray Collimation Array", J. A. Lopez, **S. S. Romero**, O. Hernandez Rodriguez, J. Holmes and R. Alarcon, Journal of Nuclear Physics, Material Sciences, Radiation and Applications, 7(2), 217-221., 2020, DOI: https://doi.org/10.15415/jnp.2020.72028 [unrelated work to this field]

VITA

My name is Selim Romero. I began my graduate studies at the University of Texas at El Paso (UTEP) in 2016. I earned an M.S. in Physics degree from UTEP between 2016 and 2018 under the supervision of Jorge Lopez. During this period, my primary focus was on a project titled "GEANT4 STUDY OF A GAMMA RAY COLLIMATOR FOR PROTON THERAPY." Subsequently, I embarked on the M.S. and Ph.D. program in Computational Science at UTEP, under the guidance of Rajendra Zope from 2018 to 2023. My current work revolves around this manuscript. I specialize in programming languages such as C, C++, Fortran90, MATLAB, bash scripting, and Python. I have actively contributed to the publication of five research works and have two ongoing publications. My expertise lies in computational methods, specifically finite difference methods and first principles approaches in physics, including density functional theory (DFT), Hartree-Fock (HF), and self-interaction correction (SIC) methods. Much of my experience involves translating mathematical equations for first principles approaches into Fortran within the FLOSIC code. Moreover, I possess proficiency in parallelizing numerical integrations across mesh-wise properties like density, wavefunction, and energy using the Message Passing Interface (MPI) for high-performance computing (HPC). I have hands-on experience operating supercomputers such as TACC Lonestar and NERSC Perlmutter. Throughout my academic journey, I have had the privilege of serving as a teacher and research assistant (TA/RA). In these roles, I had the opportunity to tutor students in calculus, algebra, and linear algebra. Additionally, I provided guidance on understanding quantum electronic interactions within the framework of first principle approaches.

Contact info: selimiles52@gmail.com